Covalently Bound Organic Monolayers on Silicon Surfaces

Visible Light Attachment, Characterization, and Electrical Properties

Promotor

Prof. dr. E. J. R. Sudhölter, hoogleraar in de organische chemie, Wageningen Universiteit

Co-promotor

Dr. H. Zuilhof, universitair hoofddocent, Laboratorium voor Organische Chemie, Wageningen Universiteit

Samenstelling promotiecommissie

Dr. B. R. Horrocks	University of Newcastle upon Tyne, UK
Prof. dr. ir. P. Bergveld	Universiteit Twente
Prof. dr. L. W. Jenneskens	Universiteit Utrecht
Prof. dr. ir. W. Norde	Wageningen Universiteit / Rijksuniversiteit Groningen

Covalently Bound Organic Monolayers on Silicon Surfaces

Visible Light Attachment, Characterization, and Electrical Properties

Louis C. P. M. de Smet

Proefschrift
ter verkrijging van de graad van doctor
op gezag van de rector magnificus
van Wageningen Universiteit
prof. dr. M. J. Kropff,
in het openbaar te verdedigen
op woensdag 15 februari 2006
des namiddags te half twee in de Aula.

de Smet, Louis C. P. M.
Covalently Bound Organic Monolayers on Silicon Surfaces. Visible Light Attachment, Characterization, and Electrical Properties
Thesis Wageningen University – with summaries in English and Dutch

Cover: Schematic representation of drops of water on silicon oxide, hydrogen-terminated silicon and an alkyl monolayer on silicon, respectively.

ISBN 90-8504-367-0

Contents

1 General Introduction 1

1.1 Introduction 2
1.2 Hydrogen-Terminated Crystalline and Porous Silicon 3
1.3 Intrinsic and Doped Silicon 5
1.4 Requirements for the Design of Functional Monolayers for Sensor Applications 6
1.5 Outline of this Thesis 8

2 Covalently Attached Monolayers on Hydrogen-Terminated Si(100): Extremely Mild Visible Light Attachment 11

2.1 Introduction 12
2.2 Experimental 14
2.2.1 General Information 14
2.2.2 Synthesis of Esters 14
2.2.3 Monolayer Preparation 16
2.2.4 Monolayer Characterization 17
2.2.4.1 Contact Angle Measurements 17
2.2.4.2 Attenuated Total Reflection Infrared Spectroscopy 17
2.2.4.3 Angle-resolved X-ray Photoelectron Spectroscopy 17
2.3 Results and Discussion 18
2.4 Conclusions 24

3 Visible Light Attachment of Monolayers on Hydrogen-Terminated Si(100) and Si(111): Effect of Wavelength and Doping 27

3.1 Introduction 28
3.2 Experimental 28
3.2.1 General Information 28
3.2.2 Purification and Analysis of Synthesized Compounds 29
3.2.3 Synthesis of 11-Fluoro-1-Undecene 29
3.2.4 Sample Cleaning and Etching 30
3.2.5 Monolayer Preparation 31
3.2.5.1 Photochemical Method 31
3.2.5.2 Thermal Method 31
3.2.6 Monolayer Characterization 31
3.3 Results and Discussion 32
3.3.1 Formation of Organic Monolayers on Si(100) and Si(111) using 447 nm Light 32

3.3.2 Effect of Irradiation Wavelength 35
3.3.3 Infrared Reflection-Absorption Spectroscopy 37
3.3.4 Effect of the Type of Silicon: Doping Type, Doping Concentration, and Orientation 41
3.3.5 Mixed Monolayers 45
3.4 Conclusions 48

4 Covalently Attached Carbohydrates on Silicon Surfaces 51

4.1 Introduction 52
4.2 Experimental 53
4.2.1 General Information 53
4.2.2 Synthesis of Carbohydrate Derivatives 54
4.3 Results and Discussion 58
4.3.1 Synthesis of Alkenylated Carbohydrate Derivatives 58
4.3.2 Characterization of Covalently Attached Carbohydrates on Silicon Surfaces 61
4.4 Conclusions 64

5 Fibrinogen Adsorption on Hexa(Ethylene Glycol)-Terminated Monolayers on Silicon Surfaces 67

5.1 Introduction 68
5.1.1 Bio-resistant Materials 68
5.1.2 Mechanism of Protein Resistance 68
5.1.3 Oligo(Ethylene Glycol) Derivatives on H-Terminated Silicon 70
5.1.4 Aim of the Research 71
5.2 Experimental Section 73
5.2.1 General Information 73
5.2.2 Organic Synthesis of Alkenylated Hexa(Ethylene Glycol) Derivatives 73
5.2.3 Monolayer Preparation using Visible Light 74
5.2.4 Monolayer Characterization 75
5.2.5 Adsorption Studies 76
5.3 Results and Discussion 76
5.3.1 Monolayer Characterization 76
5.3.2 Bio-resistant Properties 84
5.3.2.1 Effect of Exposure to Buffer on Wettability and Layer Thickness 84
5.3.2.2 Effect of Exposure to Fibrinogen on Wettability and Layer Thickness 84
5.4 Conclusions 87

6 Electrical Properties of Organic Monolayers on Crystalline Silicon Surfaces 91

6.1 General Introduction 92

6.2 Theoretical Background 93
6.2.1 Energy Band Diagrams of a Metal-Semiconductor Junction 93
6.2.2 Current-Voltage Behavior 95
6.2.3 Capacitance-Voltage Behavior 97
6.2.4 Extraction of Parameters from *J-V* and *C-V* Measurements 98
6.2.5 Interface States and Fixed Charges 99
6.3 Molecular Tuning of Metal–Insulator–Silicon (MIS) Diodes 100
6.3.1 Introduction 100
6.3.2 Results and Discussion 101
6.3.2.1 Plots Derived from *J-V* and *C-V* Measurements 101
6.3.2.2 Barrier Height and Series Resistance 104
6.3.2.3 Dielectric Properties 106
6.3.2.4 Insulator Charges 106
6.3.2.5 Tunneling Constants 107
6.3.3 Conclusions 108
6.4 Improved Electrical Monolayer Properties: 1-Alkenes versus 1-Alkynes 108
6.4.1 Introduction 108
6.4.2 Experimental Section 111
6.4.3 Results and Discussion 111
6.4.3.1 Plots Derived from *J-V* and *C-V* Measurements 111
6.4.3.2 Barrier Height and Series Resistance 112
6.4.3.3 Flatband Potential and Insulator Charges 114
6.4.3.4 X-ray Photoelectron Spectroscopy 117
6.4.4 Conclusions 118

7 Mechanism of the Hydrosilylation Reaction of Alkenes at Porous Silicon: Experimental and Computational Deuterium Labeling Studies 123

7.1 Introduction 124
7.2 Experimental Section 127
7.2.1 Materials 127
7.2.2 Porous Silicon 127
7.2.3 Formation of Monolayers 129
7.2.4 Infrared Spectroscopy 130
7.2.5 NMR Spectroscopy 130
7.2.6 Computational Methods 130
7.3 Results and Discussion 131
7.3.1 Comparison of Deuterium-Terminated (PS–D) versus Hydrogen-Terminated (PS–H) Porous Silicon 132
7.3.2 Isotopic H/D Exchange Experiments in Toluene and Benzene 135
7.3.3 Thermal Reaction of 1-Alkenes with PS–H in Toluene and Benzene 135
7.3.4 Thermal Reaction of 1-Alkenes with PS–H in Deuterated Solvents 137
7.3.5 Thermal Reaction of 1-Alkenes with PS–D 138
7.3.6 Thermal Reaction of Styrene with PS–D 140

7.3.7 Source of Radicals in Thermal Hydrosilylation of PS–H and PS–D 142
7.3.8 Lewis Acid-Catalyzed Reaction of Undec-1-ene with PS-D 143
7.3.9 Ab Initio and Density Functional Theory (DFT) Calculations 145
7.3.9.1 Ratio between A_n(Si–H) and A_n(Si–D) 145
7.3.9.2 Ratio between A_n(C–H) and A_n(C–D) and Estimation of A(2100) 146
7.3.9.3 Interaction between C–D and Si–H 148
7.4 Conclusions 151

Appendix: Field Effect Transistors **155**

1 Introduction 156
2 Ion-Sensitive Field Effect Transistor 156
3 Chemically Sensitive Field Effect Transistor 158
4 Hybrid Organic Semiconductor Field Effect Transistor 159
5 Applications of Field Effect Transistors 160

Summary & 'Samenvatting voor Niet-Chemici' **163**

Curriculum Vitae **169**

List of Publications **170**

Dankwoord **172**

Chapter 1

General Introduction

Abstract – This chapter gives a brief introduction to the thesis. After an introduction into the attachment chemistry of alkenes and alkynes onto hydrogen-terminated silicon surfaces, the different types of hydrogen-terminated silicon substrates are described in some more detail. Next, the influence of doping on the electrical properties of semiconductors is illustrated. The requirements of the properties of functional monolayers for sensor applications are discussed. Finally, the contents of the thesis are outlined.

1.1 Introduction

The full control over surface properties is a 'Holy Grail' in materials science. Organic monolayers are a strong candidate to achieve this highly desired control and therefore have been investigated for many years.[1] Much of the research on organic monolayers is based on monolayers prepared by the Langmuir-Blodgett technique, the self-assembly of monolayers of thiols on gold, and the chemisorption of organosilicon derivatives on silicon oxide.

An important step forward in the area of organic monolayers includes the covalent attachment of 1-alkenes and 1-alkynes onto hydrogen-terminated silicon surfaces (Figure 1.1). This presented the first case of organic monolayers that are highly stable, also at elevated temperatures and under highly acidic conditions. This type of monolayers has continued to attract attention ever since the first reports of Linford and Chidsey in 1993 and 1995 (Figure 1.2).[2,3] This thesis presents our recent contributions to the further development of this reaction and the characterization of the obtained monolayers.

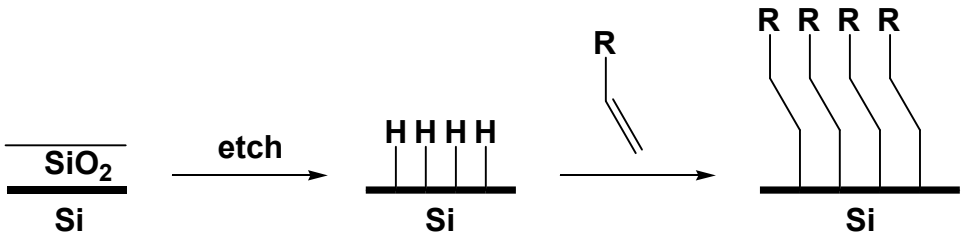

Figure 1.1 Schematic representation of the etching of a native oxide-covered silicon surface yielding an oxide-free hydrogen-terminated surface, followed by the reaction with 1-alkenes, resulting in the formation of a Si–C linked monolayer.

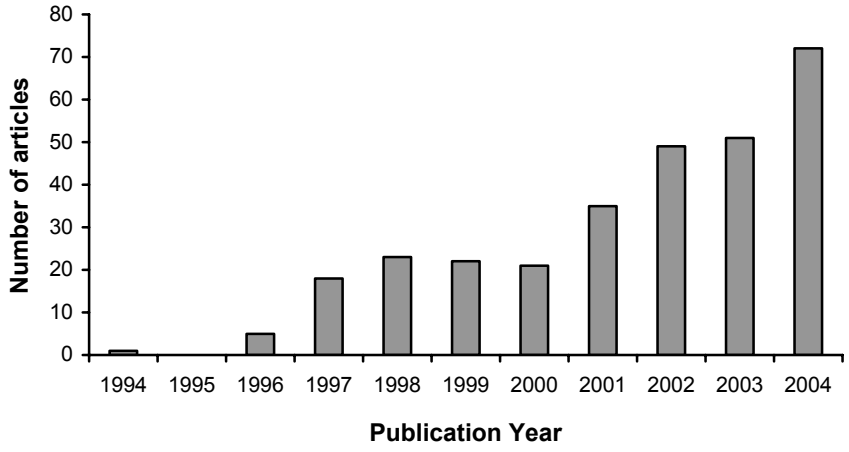

Figure 1.2 Number of articles (297 in total) per publication year that cite at least one of the two papers that cover the pioneering work on covalently attached monolayers on silicon surface.[4]

Over the past five years several reviews have been published on the preparation of organic monolayers on oxide-free hydrogen-terminated silicon surfaces.[5-9] The resulting monolayers do not only provide a tremendous flexibility in tuning the surface properties, but also allow the integration of biomolecules or (bio-)functional groups with monolayers on the silicon surface (Figure 1.3). In this manner the (bio)organic chemistry of the monolayers can be linked to the inorganic chemistry and physical properties of silicon.

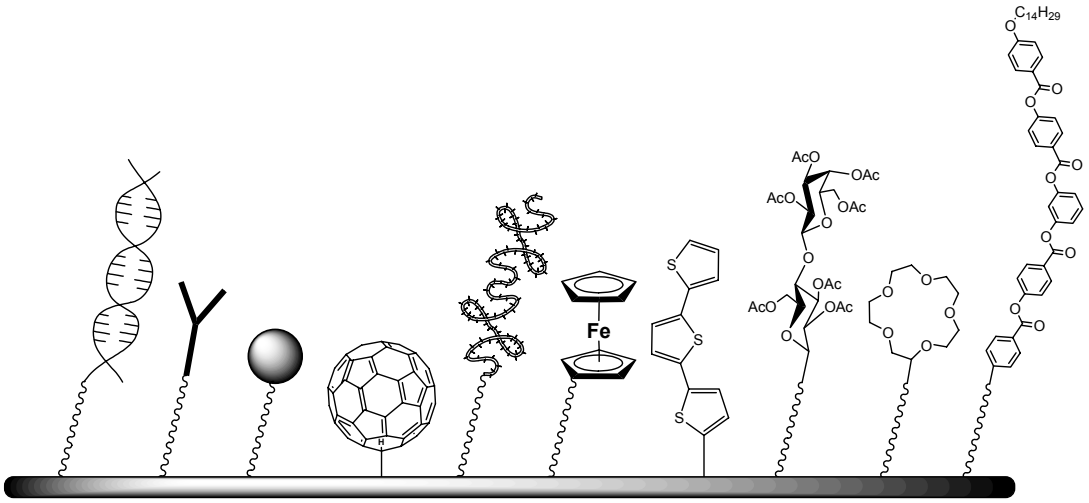

Figure 1.3 A selected number of functional groups that have been covalently attached to hydrogen-terminated silicon surfaces (from left to right): DNA,[10] antibodies,[11] Au nanoparticles,[12] fullerenes,[13] proteins,[14] ferrocene groups,[15] oligothiophenes,[16] carbohydrates,[17] crown ethers,[18] and banana-shaped liquid crystals.[19]

1.2 Hydrogen-Terminated Crystalline and Porous Silicon

The most common surface orientations of silicon are the Si(100) and Si(111) facets. Upon exposure to air single-crystalline silicon surfaces readily oxidize, resulting in the formation of a thin native oxide layer. Oxide-free, hydrogen-terminated silicon surfaces can be obtained by the adsorption of atomic hydrogen under ultra-high vacuum conditions. A rapid and efficient alternative method involves the dissolution of the native oxide layer in fluoride-containing aqueous sources. Interfacial Si atoms on the Si(100) surface are occupied with two hydrogen atoms (SiH_2), while the Si(111) surface is mainly occupied with Si–H groups (Figure 1.4). In the case of Si(111) an atomically flat surface is formed with terraces on the scale of ~10^2 by ~10^4 nm^2.[8,20] The H-terminated Si(100) surface is not atomically flat. Figure 1.5 depicts a Scanning Tunneling Microcopy (STM) image of the Si(111)–H surface.

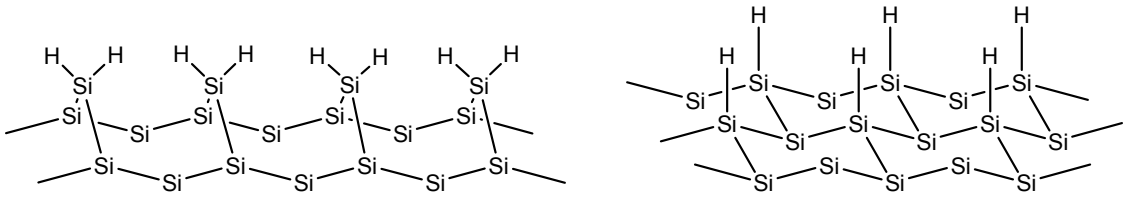

Figure 1.4 Schematic representations of the hydrogen-terminated Si(100) (left) and Si(111) (right) surface.

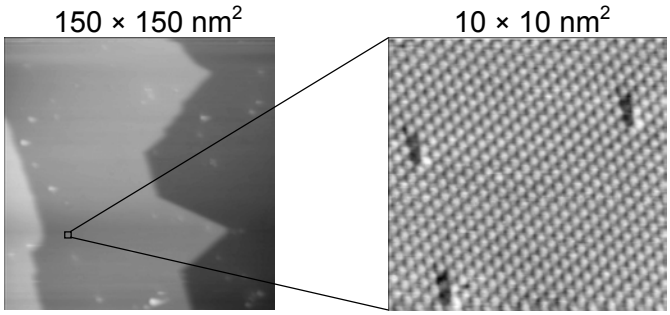

Figure 1.5 (left) STM image of 150 × 150 nm^2 of the Si(111)–H surface visualizing three terraces. (right) The enlargement (10 × 10 nm^2) shows a part of the surface on one terrace (courtesy of dr. Greg Lopinski, NRC, Ottawa, Canada).

Apart from flat single-crystalline silicon also porous silicon is of high interest. The discovery of Canham that porous silicon has luminescent properties[21,22] opened additional possibilities for applications of silicon in optoelectronic technology. In addition, the high surface area of porous silicon and its ability to produce tailored porous silicon makes this material especially attractive for bio- and chemical sensing applications. The preparation of porous silicon can be accomplished from crystalline silicon substrates either chemically or electrochemically. Porous silicon is covered with SiH_3, SiH_2 and SiH groups and is black (Figure 1.6).

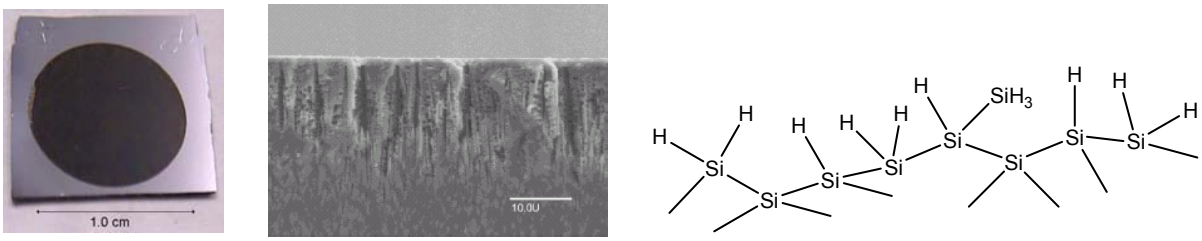

Figure 1.6 From left to right: a photograph of a typical porous silicon sample, prepared electrochemically, where the circular black part is porous silicon and the remaining shiny area is crystalline silicon; a cross-sectional SEM of a porous silicon surface (taken from literature),[23] and a schematic representation of the hydrogen-terminated porous silicon surface.

The pore dimensions in porous silicon can range from several microns in width to only a few nanometers. Cross-sectional scanning electron micrographs (SEMs) of porous silicon revealed the anisotropic nature of the material (Figure 1.6, center).[23,24]

To summarize, where crystalline surfaces offer a superior structural homogeneity that is extremely useful for controlled reactivity studies, porous silicon is of high interest because of its luminescent properties and its high surface area.

1.3 Intrinsic and Doped Silicon

In Figure 1.1 it is suggested that only the surface atoms are involved in the reaction between H-terminated silicon surfaces and 1-alkenes or 1-alkynes. However, results described in Chapter 3 show an unexpected and significant effect on the monolayer formation by different types of dopants and their concentration.

It is well known that the addition of a very small percentage of dopants to intrinsic silicon produces dramatic changes in its electrical properties. The addition of pentavalent dopants such as antimony (Sb), arsenic (As) or phosphorous (P) all add extra electrons to the conduction band of silicon and produces n-type silicon. The addition of trivalent dopants such as boron (B), aluminum (Al) or gallium (Ga) to silicon creates a lack of valence electrons (holes) and produces p-type silicon. Figure 1.7 (top) depicts schematic representations of two-dimensional crystal lattices of intrinsic silicon, Sb-doped (n-type) silicon and B-doped (p-type) silicon.

In addition, the energy diagrams of intrinsic silicon and two types of doped silicon are given (Figure 1.7, bottom). The difference between the energy level of the conduction and valence band is the band gap (E_g), which amounts 1.12 eV (~1107 nm) for silicon at 300 K.[25] The Fermi level (E_F) is an energy level that is located between the energy levels of the valence and conduction band. In the case of intrinsic silicon, the Fermi level is located exactly halfway between these bands. Due to the presence of dopants the Fermi level will change. In n-type silicon there are additional electron energy levels near the top of the band gap. The extra electrons can easily be thermally excited into the conduction band, leaving fixed donor cations near the top of the band gap and producing mobile electrons in the conduction band (majority charge carriers). As a result there are more electrons in the conduction band of silicon than holes in the valence band and the Fermi level increases with respect to intrinsic silicon. In p-type silicon, electrons from the valence band can easily be thermally excited into the holes of the doping level, located near the bottom of the band gap. This results in the formation of fixed donor anions and the presence of mobile holes in the

valence band (majority charge carriers). Consequently, the number of holes in the valence band is higher than the number of electrons in the conducting band. The Fermi level of p-type silicon is therefore decreased with respect to the Fermi level of intrinsic silicon.

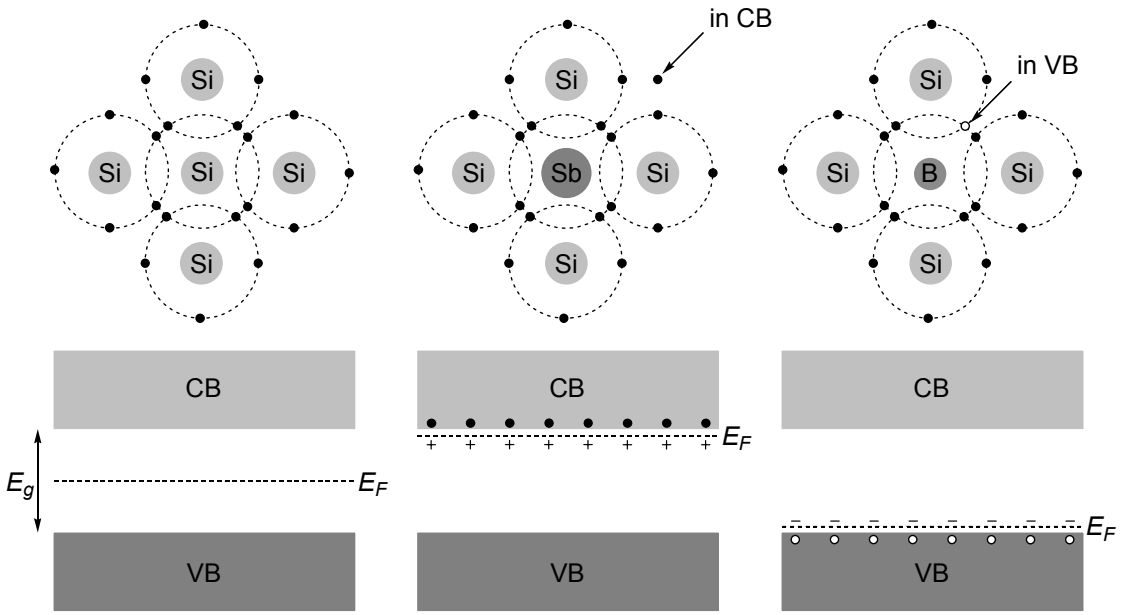

Figure 1.7 Schematic 2-dimensional representations of crystal lattices (top) and energy diagrams[26,27] (bottom) of intrinsic silicon (left), n-type silicon (center) and p-type silicon (right). CB, VB, E_F, and E_g are the conduction band, the valence band, the Fermi level, and band gap, respectively. The dots and open circles represent electrons and holes, respectively. The positive and negative charges represent the fixed donor ions (Sb^+) and fixed acceptor ions (B^-), respectively.

The conductivity of semiconductors is usually reported in terms of the resistivity, which is equal to the reciprocal of the conductivity. The resistivity of intrinsic silicon is 230 kΩcm.[25] However, this is the theoretical limit. Upon the addition of dopants, the resistivity can decrease spectacularly. The resistivity does not only depend on the dopant concentration, but also on the type of dopant as the mobilities of electrons and holes are different. To give an example, the addition of only 1 phosphorus or boron atom to 5×10^{10} Si atoms reduces the resistivity of the semiconductor at 296 K with a factor of ~60 and ~18, respectively. In this thesis we used silicon substrates with resistivities of ~0.01 and ~1-2 Ωcm, which are referred to as highly doped and lowly doped, respectively.

1.4 Requirements for the Design of Functional Monolayers for Sensor Applications

Hybrid structures that consist of organic materials on inorganic surfaces are of particular interest in sensor technology, since it allows one to combine the bioorganic world of, e.g.,

molecular recognition to the one of semi-conductor technology. One possible strategy to realize the desired transduction of the molecular recognition process into an electrical output is based on field-effect transistors (FETs) in which the conventional SiO_2 layer is replaced by an organic monolayer.[28] The basic structure of a FET and a historical overview on FET technology are outlined in the appendix (page 155). Briefly, a FET measures changes in the electric surface potential on an activated area that occur when a (bio)molecular recognition occurs at that Si surface.

The ideal modified surface applicable for FET technology has to meet requirements in different areas. First, functional groups (receptors) that have the ability to detect specific molecules or ions should be attached to the surface or the organic layer. This can be realized via the direct attachment of (bio-)functionalized alkenes or via indirect attachment schemes. The first approach requires mild surface modifications conditions, while the latter ideally involves a multi-step procedure for a well-defined monolayer functionalization.

In addition, since a linear response between the ligand concentration and the sensor output is desirable, the ideal functionalized monolayer probably contains isolated receptor structures in combination with moieties that prevent any nonspecific interaction with ligands or other ions/molecules present in the solution. In the case of monolayers designed for the detection of antibodies one can think of receptor molecules combined with molecules that have bio-resistant properties.

Thirdly, the organic monolayers should be electrically insulating as the sensor is supposed to record only specific receptor-ligand interactions. Figure 1.8 summarizes the different desired properties and characteristics of the monolayer in order to make it a feasible sensor interface.

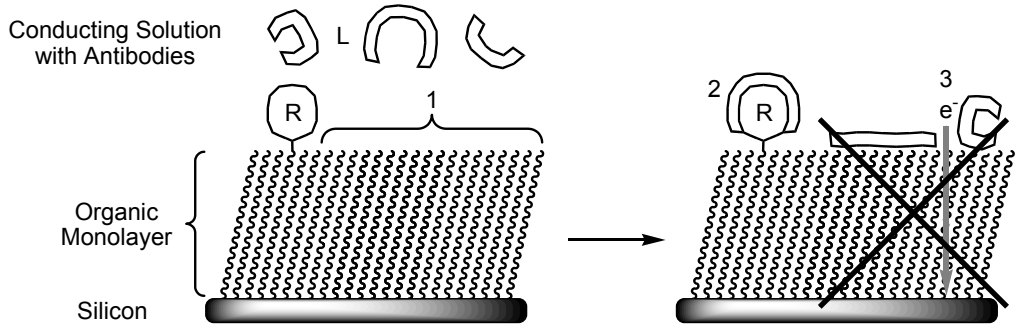

Figure 1.8 Schematic representation of an organic monolayer attached to a surface in order to visualize the desired properties and characteristics of the monolayer. The receptor (R) should specifically bind (2) to only one of the ligands (L), and none of the ligands should complex to other regions (1) of the organic monolayer due to bio-resistant properties. Finally, the monolayer should be electrically insulating (3).

1.5 Outline of this Thesis

All chapters in this thesis deal with different aspects of the preparation and characterization of (functionalized) organic monolayers on hydrogen-terminated silicon surfaces, in order to make the resulting modified surfaces suitable for sensing purposes. In Chapters 2 to 6 crystalline silicon surfaces are described, whereas Chapter 7 deals with porous silicon.

Chapter 2 describes the development of an easy and extremely mild and practical method using visible light (447 nm) to attach organic monolayers on flat Si(100) surfaces. Properties of the resulting monolayers were compared with those of monolayers that were prepared via the established method of thermal modification.

In Chapter 3 the visible light method is studied in more detail and we address the effect of the irradiation wavelength on the monolayer quality, as well as the effect of substrate doping on the rate of the monolayer formation. In addition, we evaluate the applicability of infrared reflection-absorption spectroscopy (IRRAS) in the analysis of organic monolayers on the planer silicon surface.

Chapter 4 covers the work on the synthesis of different alkenylated monosaccharide derivatives and the preparation and characterization of carbohydrate-containing monolayers on silicon. Fragile sugar derivatives are attached to silicon, showing the value of the visible-light attachment.

Chapter 5 describes the preparation and characterization of monolayers containing hexa(ethylene glycol) units. Subsequently we report on their ability to reduce the adsorption of fibrinogen.

The electrical properties of monolayers derived from 1-alkenes and 1-alkynes are studied via the construction of metal–insulator–silicon structures, which is described in Chapter 6.

Experimental and computational deuterium labeling studies that probe the mechanism of the hydrosilylation reaction of 1-alkenes at porous silicon are presented in Chapter 7.

References and Notes

[1] Ulman, A. *An Introduction to Ultrathin Organic Films*, Academic Press: Boston, MA, USA, 1991.

[2] Linford, M. R.; Chidsey, C. E. D. *J. Am. Chem. Soc.* **1993**, *115*, 12631-12632.

[3] Linford, M. R.; Fenter, P. E.; Eisenberger, P. M.; Chidsey, C. E. D. *J. Am. Chem. Soc.* **1995**, *117*, 3145-3155.

[4] ISI Web of Knowledge.

[5] Shirahata, N.; Hozumi, A.; Yonezawa, T. *Chem. Rec.* **2005**, *5*, 145-159.

[6] Bent, S. F. *Surf. Sci.* **2002**, *500*, 879-903.
[7] Buriak, J. M. *Chem. Rev.* **2002**, *102*, 1271-1308.
[8] Wayner, D. D. M.; Wolkow, R. A. *J. Chem. Soc., Perkin Trans. 2* **2002**, 23-34.
[9] Sieval, A. B.; Linke, R.; Zuilhof, H.; Sudhölter, E. J. R. *Adv. Mat.* **2000**, *12*, 1457-1460.
[10] Strother, T.; Cai, W.; Zhao, X.; Hamers, R. J.; Smith, L. M. *J. Am. Chem. Soc.* **2000**, *122*, 1205-1209.
[11] Liao, W.; Wei, F.; Qian, M. X.; Zhao, X. S. *Sens. Actuators B* **2004**, *101*, 361-367.
[12] Yamanoi, Y.; Yonezawa, T.; Shirahata, N.; Nishihara, H. *Langmuir* **2004**, *20*, 1054-1056.
[13] Feng, W.; Miller, B. *Langmuir* **1999**, *15*, 3152-3156.
[14] Guo, D.-J.; Xiao, S.-J.; Xia, B.; Wei, S.; Pei, J.; Pan, Y.; You, X.-Z.; Gu, Z.-Z.; Lu, Z. *J. Phys. Chem. B.* **2005**, *109*, 20620-20628.
[15] Eagling, R. D.; Bateman, J. E.; Goodwin, N. J.; Henderson, W.; Horrocks, B. R.; Houlton, A. *J. Chem. Soc., Dalton Trans.* **1998**, 1273-1275.
[16] He, J.; Patitsas, S. N.; Preston, K. F.; Wolkow, R. A.; Wayner, D. D. M. *Chem. Phys. Lett.* **1998**, *286*, 508-514.
[17] de Smet , L. C. P. M.; Pukin, A. V.; Sun, Q.-Y.; Eves, B. J.; Lopinski, G. P.; Visser, G. M.; Zuilhof, H.; Sudhölter, E. J. R. *Appl. Surf. Sci.* **2005**, *252*, 24-30.
[18] de Smet, L. C. P. M.; Zuilhof, H; Sudhölter, E. J. R. - unpublished results.
[19] Achten, R; de Smet, L. C. P. M.; Giesbers, M.; Zuilhof, H; Marcelis, A. T. M.; Sudhölter, E. J. R. - unpublished results.
[20] Higashi, G. S.; Becker, R. S.; Chabal, Y. J.; Becker, A. J. *Appl. Phys. Lett.* **1991**, *58*, 1656-1658.
[21] Canham, L. T. *Appl. Phys. Lett.* **1990**, *57*, 1046-1048.
[22] Cullis, A. G.; Canham, L. T.; Calcott, P. D. J. *J. Appl. Phys.* **1997**, *82*, 909-965.
[23] Stewart, M. P.; Buriak, J. M. *Adv. Mat.* **2000**, *12*, 859-869.
[24] Sailor, M. J., Heinrich, J. L., Lauerhaas, J. M. in *Semiconductor Nanoclusters* (Eds: Kamat, P.V., Meisel, D.), Elsevier, Amsterdam, 1997, pp 209-235.
[25] Zhang, X. G. *Electrochemistry of Silicon and its Oxide*, New York: Kluwer Academic/Plenum Publishers, 2001.
[26] Based on figures from the website of C. R. Nave, Department of Physic and Astronomy at the Georgia State University (http://hyperphysics.phy-astr.gsu.edu/hbase/hph.html).
[27] Sze, S. M. *Semiconductor Devices: Physics and Technology*, Wiley: New York, 1985, pp 21-24.
[28] Sudhölter, E. J. R.; Zuilhof, H.; Sieval, A. B.; de Smet, L. C. P. M.; Visser, G. M.; Bergveld, P.; Olthuis, W.; Faber, E. J. patent *WO 03098204 (A1)*, **2003**.

Chapter 2

Covalently Attached Monolayers on Hydrogen-Terminated Si(100): Extremely Mild Visible Light Attachment*

Abstract – An extremely mild and practical method using visible light (447 nm) to attach organic monolayers on flat Si(100) surfaces was developed. High water contact angles were obtained for alkyl monolayers indicating a high monolayer quality. With high-resolution angle-resolved XPS (ARXPS) depth profiles of the elements in the monolayer (~2 nm thickness) were obtained.

* This chapter is based on:

- Sun, Q.-Y.; de Smet, L. C. P. M.; van Lagen, B.; Wright, A.; Zuilhof, H.; Sudhölter, E. J. R. *Angew. Chem., Int. Ed. Engl.* **2004**, *43*, 1352-1355.
- de Smet, L. C. P. M.; Pukin, A. V.; Sun, Q.-Y.; Eves, B. J.; Lopinski, G. P.; Visser, G. M.; Zuilhof, H., Sudhölter, E. J. R. *Appl. Surf. Sci.* **2005**, *252*, 24-30.

2.1 Introduction

In the field of covalently bonded organic monolayers on oxide-free silicon surfaces, a variety of preparative hydrosilylation methods have been developed over the past 12 years.[1-3] Si–C bond attached monolayers have been prepared by making use of high temperatures,[3-7] UV irradiation,[8-11] electrochemistry,[12-14] hydrosilylation catalysts,[15-18] and chemomechanical scribing.[19-21] These studies have allowed a proper characterization of such monolayers, and now allow a focus on the integration of functional groups or biomolecules in monolayers on the silicon surface. Although thermal conditions and UV irradiation yield stable,[5,6] and densely packed monolayers,[22,23] they are too harsh to allow the use of labile bioactive materials. This situation has two ways out (Scheme 2.1). In the first route (Scheme 2.1, bottom) one makes use of a protected precursor (R) that can stand such harsh conditions. Subsequently, this precursor is deprotected and transformed into the bioactive monolayer. Such an approach has been used by several groups to obtain functional monolayers, ranging from the attachment and deprotection of useful precursors, like esters,[6,24,25] and amides[26] to the attachment of DNA[10,27-30] and proteins/antibodies.[31-33]

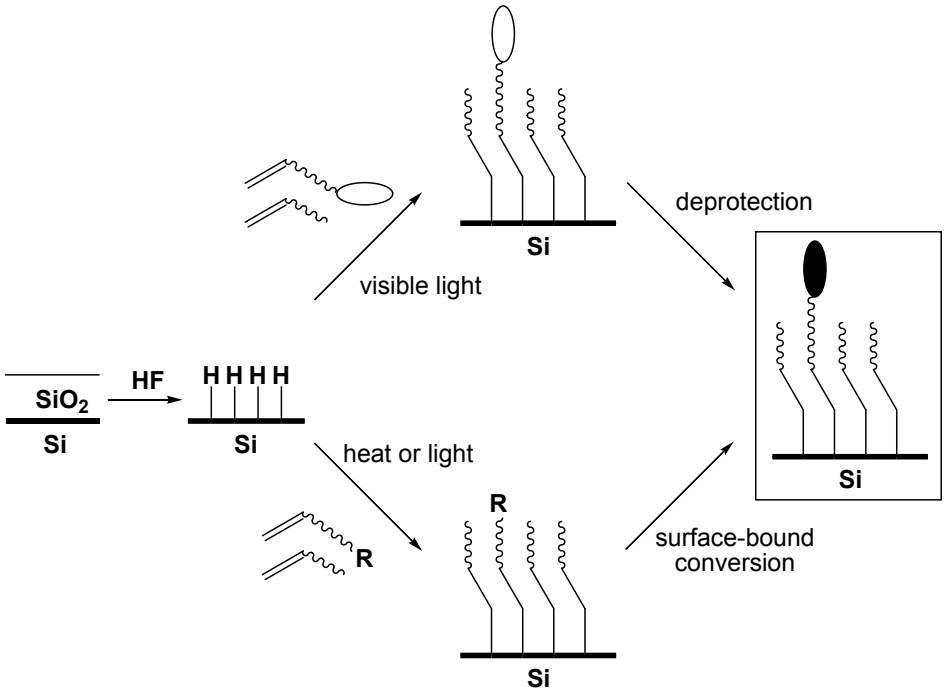

Scheme 2.1 Schematic representation of (top) a direct method with protected functionalities (open oval) and (bottom) an indirect method via precursors (R), both yielding a biofunctional monolayer (in box).

The second route (Scheme 2.1, top) would make use of mild reaction conditions that are compatible with bioactive moieties. In the case of porous silicon such an approach has been

taken by Buriak et al. through either the use of a white light-promoted reaction[34] or a hydride-abstracting agent.[35] It was demonstrated that excitons generated through illumination of the surface of photoluminescent porous silicon with white light (400 nm) are capable of driving a surface hydrosilylation reaction on hydride-terminated porous silicon, producing Si–C bonds, also in line with recent computational studies.[36] On the basis of the bond strength of the Si–H bond, a minimum energy of 3.5 eV (<350 nm) is required to perform Si–H bond cleavage. Since Stewart and Buriak used wavelengths ≥400 nm, they concluded that the mechanism of hydrosilylation on porous silicon does not start with a homolytic cleavage of the Si–H bonds. For this reason a radical chain mechanism[5] (Scheme 2.2, top), as operative in the case of thermal and UV hydrosilylation, was rejected, and a new mechanism was proposed that involves attack by a 1-alkene or 1-alkyne on a surface-localized positive charge (the hole) in a nucleophilic fashion, resulting in Si–C bond formation (Scheme 2.2, bottom).[34] It was thought that quantum confinement effects were crucial for this attachment reaction, which was thus thought to be limited to porous silicon. This was in line with observations by Effenberger and co-workers,[9] who used 380 nm light for the modification of flat hydrogen-terminated Si(111) with 1-octadecene, but the reported water contact angles (only ~95°) indicated a poor monolayer quality. To circumvent this limitation, Hamers studied partially iodinated Si(111) and Si(100) surfaces, and reported visible light (514 nm) initiated modification thereof.[37] This reaction works well, but requires an extra step, and involves a somewhat poorly defined substrate due to the fact that the iodination is only partial.

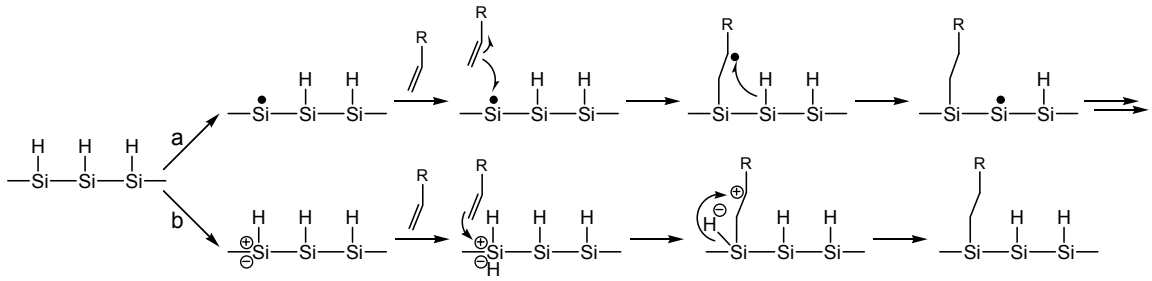

Scheme 2.2 Representation of the proposed (a) radical chain mechanism[5] under thermal and UV conditions and (b) electron/hole pair mechanism[34] for visible light-initiated hydrosilylation on porous silicon.

In this chapter we further develop this second route by the first formation of densely packed covalently attached monolayers using a variety of unsaturated compounds on well-defined Si(100)–H (i.e. hydrogen-terminated) surfaces by visible light (447 nm) at room temperature. Angle-resolved X-ray photoelectron spectroscopy (ARXPS) and contact angle measurements were used to evaluate the monolayers in detail.

2.2 Experimental

2.2.1 General Information

Single-polished Si(100): n-type, 500-550 µm thick, resistivity 1-2 Ωcm (Seltec Silicon, Mitsubishi Silicon America), p-type, 375 µm thick, resistivity 1-2 Ωcm (Bayer Solar Freiberg, Germany), p-type, 475 µm thick, resistivity 0.015-0.025 Ωcm (Okmetic Inc., USA).

Petroleum ether of the bp 40-60 °C fraction (hereafter: PE 40/60), CH_2Cl_2, MeOH and EtOH were distilled. THF was distilled over Na/benzophenone. Benzene (Janssen Chimica, 99%) was dried over sodium wires and pyridine (Merck, 99%) was dried over KOH. 2,2,2-Trifluoroethanol (Aldrich, 99+%), 10-undecenoyl chloride (Fluka, ≥97%), 16-bromohexadecanoic acid (99+%, Aldrich), CBr_4 (99%, Aldrich), *t*-BuOK (95%, Aldrich), CF_3CH_2OH (99+%, Aldrich), 4-(dimethylamino)pyridine (DMAP, 99%, Aldrich) and dicyclohexylcarbodiimide (DCC, 99%, Acros) were used as received. HF (Fluka, 50% p.a.-plus) was diluted with demineralized H_2O.

Thin layer chromatography (TLC) was performed on Merck silica gel 60F254 plastic sheets and detection was realized by charring with an aqueous solution of $KMnO_4$. Column chromatography was conducted by elution of a column of Merck Kieselgel silica (230-400 Mesh) using eluents as specified below. NMR spectra were recorded on a Bruker AC200 FT-NMR spectrometer or a Bruker DPX 400 spectrometer in $CDCl_3$ at room temperature.

10-Undecylenic acid methyl ester (**2.1**) was prepared and purified according to literature.[6] The synthesis of the 1-alykenes is described elsewhere.[38]

2.2.2 Synthesis of Esters

10-Undecenoic Acid, 2,2,2-Trifluoroethanol Ester (2.2)

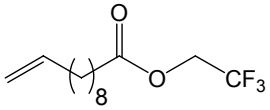

2.2

10-Undecylenic chloride (20.00 g, 98.7 mmol) in 20 mL of benzene was added to a stirring solution of 2,2,2-trifluoroethanol (10 mL, 137 mmol) in pyridine (10 mL) under a nitrogen atmosphere at 0 °C over a period of 3 h. The reaction mixture was allowed to warm to room temperature, left over night, and water (75 mL) and ether (100 mL) were added. The layers were separated and the aqueous layer was extracted with ether until TLC showed the absence of product in the organic layer. The combined organic layers were washed with 0.5 M HCl until pyridine was removed, washed with saturated $NaHCO_3$ (100 mL), water (100 mL), and brine (100 mL). The organic layer was dried over Na_2SO_4. After filtration, the solvent was removed

under reduced pressure at 40 °C, yielding 25.01 g of crude product. Purification by column chromatography (PE 40/60:CH_2Cl_2 = 2:1) yielded 24.24 g (91.0 mmol, 92%) of compound **2.2**.

TLC R_f (PE 40/60:CH_2Cl_2 = 2:1) = 0.39. **^{1}H NMR** (200 MHz, $CDCl_3$) δ 5.89-5.69 (m, 1H), 5.01-4.89 (m, 2H), 4.51-4.38 (q, 2H, *J* ~8.5 Hz), 2.39 (t, 2H, *J* ~7.5 Hz), 2.0-1.9 (q, 2H, *J* 6.8 Hz), 1.7-1.6 (m, 2H), 1.28 (bs, 10H); **^{13}C NMR** (50 MHz, $CDCl_3$) δ 173.09, 140.09, 123.96 (q, *J* 275 Hz), 115.09, 61.04 (q, *J* 36 Hz), 34.73, 34.56, 30.18, 30.06, 29.96, 29.88, 29.82, 25.62; **IR** (film between NaCl windows, cm^{-1}): 3080 (w, vinyl–H), 2929 (m-s, C–H), 2857 (m, C–H), 1762 (s, C=O), 1641 (w-m, C=C), 1283-1170 (s-vs, C–O).

16-Bromohexadecanoic Acid, Methyl Ester

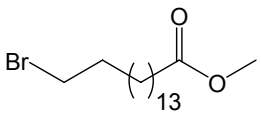

The following procedure is according to Lee et al.[39] 2.50 g (7.46 mmol) of 16-bromohexadecanoic acid was dissolved in 75 mL of freshly distilled MeOH. 2.5 mL of this solution was added to a quartz cuvette, which contained 124 mg (0.37 mmol) of CBr_4. The cuvette was irradiated directly by 254 nm light at room temperature under stirring. After 30 minutes the contents of the cuvette was added to the solution of the carboxylic acid in MeOH. The solution was stirred overnight at room temperature. The organic solvent was removed under reduced pressure. Column chromatography (CH_2Cl_2) yielded 2.54 g (7.26 mmol) of the title compound (97%) as a white solid.

TLC R_f (CH_2Cl_2) = 0.59; **^{1}H NMR** (400 MHz, $CDCl_3$): δ 3.69 (s, 3H), 3.43 (t, 2H, *J* 6.9 Hz), 2.32 (t, 2H, *J* 7.5 Hz), 1.91-1.84 (m, 2H), 1.67-1.60 (m, 2H), 1.46-1.40 (m, ~2H), 1.27 (bs, 20H); **^{13}C NMR** (100 MHz, $CDCl_3$): δ 174.77, 51.85, 34.53, 34.48, 33.25, 33.25, 30.02, 29.99, 29.94, 29.84, 29.66, 29.56, 29.18, 28.59, 28.35, 27.46, 25.37.

15-Hexadecenoic Acid, 2,2,2-Trifluoroethyl Ester (2.3)

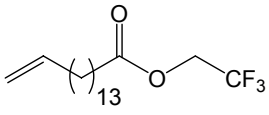

2.3

This procedure is based on a method described by Hostetler et al.[40] a) 50 mL of freshly distilled THF was added to 2.52 g (7.22 mmol) of 16-bromohexadecanoic acid, methyl ester and 4.05 g (36 mmol) of *t*-BuOK. The suspension was refluxed for 42 h under a stream of nitrogen. The solvent was removed under reduced pressure. 100 mL of ether, 150 mL of water and 10 mL of 37% HCl were added. The layers were separated and the water layer was extracted twice again (2 × 50 mL). The organic layers were combined and dried over Na_2SO_4. The solvent was removed under reduced pressure yielding a white-yellow solid (mixture A). ^{1}H NMR showed

traces of the starting material, but since most of the derivatives were hydrolyzed, there was hardly any difference in polarity, which made purification by column chromatography difficult. For that reason, the crude product was used directly for the esterification with CF_3CH_2OH.

b) 190 mg (1.56 mmol) of DMAP and 25 mL of freshly distilled CH_2Cl_2 were added to mixture A. Subsequently 1.32 mL (1.81 g, 18.05 mmol) of CF_3CH_2OH was added and the solution was stirred at 0 °C. 2.00 g (9.69 mmol) of DCC in 5 mL of freshly distilled CH_2Cl_2 were added and the reaction mixture was stirred for 22h. The solution was filtered over a glass filter to remove the precipitate. The solvent was removed under reduced pressure, yielding 3.61 g of crude product. Flash column chromatography (PE 40/60:CH_2Cl_2 = 4:1) yielded 1.44 g (4.29 mmol) of compound **2.3** (59%).

TLC R_f (PE 40/60:CH_2Cl_2 = 4:1) = 0.45; **^{1}H NMR** (400 MHz, $CDCl_3$): δ 5.88-5.78 (m, 1H), 5.03-4.93 (m, 2H), 4.48 (q, 2H, *J* 8.5 Hz), 2.43 (t, 2H, *J* 7.5 Hz), 2.09-2.03 (m, 2H), 1.71-1.63 (m, 2H), 1.28 (bs, 20H); **^{13}C NMR** (100 MHz, $CDCl_3$): δ 172.54, 139.63, 123.41 (q, *J* 275 Hz), 114.45, 60.50 (q, *J* 36 Hz), 34.22, 34.02, 33.73, 30.02, 30.00, 29.95, 29.90, 29.80, 29.56, 29.56, 29.35, 29.35, 25.08. **MS** $[M]^{+\bullet}$ observed: 336.2279 amu, calculated for $C_{18}H_{31}O_2F_3$: 336.2276 amu.

2.2.3 Monolayer Preparation

Si(100) samples were cleaned in piranha solution (H_2SO_4:35% H_2O_2 = 2:1 (v/v)) at ~85 °C for 2 h, and subsequently etched using 2.5% HF for 2 min. The alkene solution was flushed with N_2 for 30 min before and 30 min after adding the fresh Si(100)–H wafer to the solution, before the light was turned on. The reaction took place in a special vessel with a rectangular bottom part (Figure 2.1).

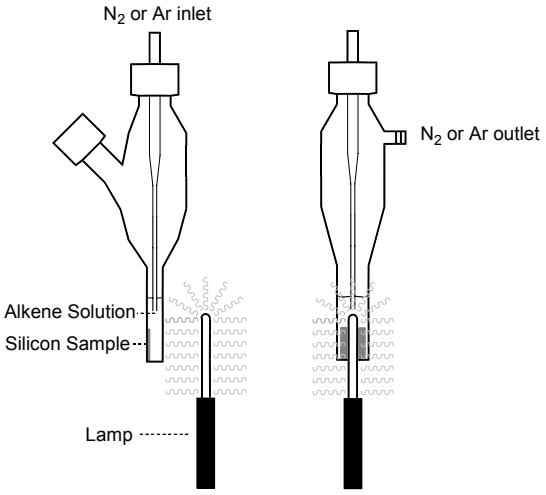

Figure 2.1 Schematic representation of the set-up used for the photochemical modification of crystalline silicon samples (front and side view).

The visible light-initiated reaction was performed by irradiation of a wafer-containing 0.1 M solution of 1-alkene/1-alkyne in mesitylene with monochromatic 447 nm light (phosphor-coated pen lamp from Jelight Company, model 84-247-2, 32 nm bandwidth, ~3 mW/cm^2 intensity at 2 cm) from 0.5 cm for 15 h under a N_2 atmosphere. Afterwards, the surface was excessively rinsed with PE 40/60, EtOH and CH_2Cl_2.

Freshly etched double-polished Si(100) attenuated total reflection (ATR) crystals (see §2.2.4.2) were irradiated simultaneously on both sides by making use of two 447 nm pen lamps.

2.2.4 Monolayer Characterization

2.2.4.1 Contact Angle Measurements

Static water contact angles were obtained using an Erma G-1 contact angle meter (volume of the drop of ultrapure water, 3.5 μL). Contact angles of two or three drops were measured. The error of the contact angles is ± 1°.

2.2.4.2 Attenuated Total Reflection Infrared Spectroscopy

Attenuated total reflection infrared (ATR-IR) spectra of the monolayers were recorded on a Perkin Elmer 1725X FT-IR spectrometer equipped with a liquid nitrogen-cooled MCT-detector using a fixed angle multiple reflection attachment (Harrick Scientific). The infrared light was incident on one of the 45° edges of the ATR-plate. Spectra (512 scans) were recorded with p-polarized light and collected using a spectral resolution of 4 cm^{-1}. Before each measurement the compartment was flushed with dry air. An ATR crystal was oxidized in 'piranha' (H_2SO_4:35% H_2O_2 = 2:1 (v/v)) at ~85 °C for 2 h. *Caution: the acidic solutions of hydrogen peroxide described in this procedure are dangerous, strong oxidants, and should be handled with great care.* The crystal was removed from the solution and rinsed extensively with water and further cleaned for 2 min in a plasma cleaner/sterilizer (Harrick PDC-32G).[41] ATR-IR spectra of monolayers were obtained by the spectral subtraction of the modified ATR crystal with the (same) cleaned native oxide-covered ATR-crystal without any further data manipulation.

2.2.4.3 Angle-resolved X-ray Photoelectron Spectrocopy

Angle-resolved X-ray photoelectron spectrocopy (ARXPS) makes use of a 2-dimensional micro-channel detector (MCD) to simultaneously measure the intensity of the photoelectron

emission as a function of emission angle (16 detection segments of 3.75° each, Figure 2.2). Large detection angles – with respect to the surface normal – yield surface-sensitive signals, while photoelectrons captured at small detection angles reflect more bulk-sensitive signals. Analysis of these signals provides a relative depth profile, which is basically a cross section of the monolayer per element. The MCD allows ARXPS experiments without tilting the sample, and with a concomitantly constant analysis area for all detection angles. As a result, unparalleled resolution can be acquired with respect to the depth distribution of elements on the surface.

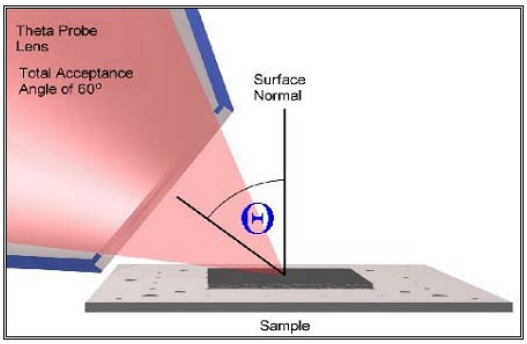

Figure 2.2 Schematic representation of the two-dimensional detection system.

The ARXPS analysis was performed on a Theta Probe (Thermo VG Scientific, UK) using a monochromatic AlKα X-ray source with a spot size of 400 µm in diameter at 100 W under UHV conditions. The snapshot mode of acquisition was used for the ARXPS data. This acquires spectral data across the full detector width at a fixed analyzer energy. The ARXPS snapshot spectra were acquired from 500 × 1 s frames at a pass energy of 150 eV. 16 Angles were measured in the range of 23-83°. The relative surface sensitivity for a particular chemical species was determined by calculating the ratio of the sum of the relevant peak areas at three bulk-sensitive angles (23-35°) and the sum of the equivalent peak areas at three surface-sensitive angles (65-75°).

The XPS data presented in Figure 2.5 were obtained on a Quantera SXM from Physical Electronics, equipped with monochromator and an AlKα X-ray source of 1486.6 eV. The spot size was 100 μm in diameter.

2.3 Results and Discussion

Figure 2.3 shows the gradual formation of a hexadecyl monolayer upon irradiation of Si(100)–H wafers in the presence of 1-hexadecene. The water contact angle obtained after ≥ 10 h is 110°, which is comparable with the best literature values.[38]

Table 2.1 lists the static water contact angle of the surfaces modified by a variety of 1-alkenes, 1-alkynes and two ω-esterified-1-alkenes (compounds **2.1**, and **2.2**) using this mild procedure, together with the corresponding results of the thermal radical reaction.[38] These results indicate that visible light attachment yields monolayers with similar properties as those obtained from thermal radical reactions,[7] without the disadvantage of requiring a high temperature (165 °C).

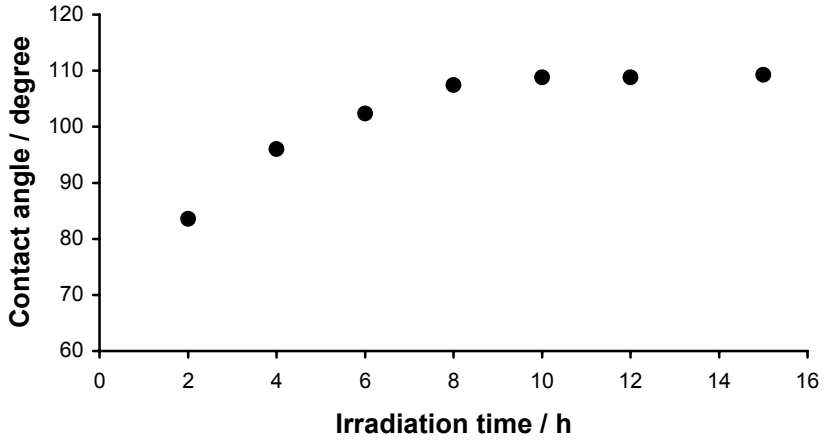

Figure 2.3 Static water contact angle of a hexadecyl monolayer on a hydrogen-terminated Si(100) surface as function of irradiation time (447 nm).

Table 2.1 Static water contact angles (degrees) of monolayers on Si(100) surfaces prepared via the visible light-initiated and thermal method.[a]

Reactants	Photochemical reaction	Thermal reaction
$CH{\equiv}C{-}C_{10}H_{21}$	108	108[b]
$CH{\equiv}C{-}C_{12}H_{25}$	110	110[b]
$CH{\equiv}C{-}C_{14}H_{29}$	110	110[b]
$CH_2{=}CH{-}C_{10}H_{21}$	109	108[c]
$CH_2{=}CH{-}C_{12}H_{25}$	108	108[c]
$CH_2{=}CH{-}C_{14}H_{29}$	109	108[c]
$CH_2{=}CH{-}C_8H_{16}COOCH_3$ (**2.1**)	78	77[d]
$CH_2{=}CH{-}C_8H_{16}COOCH_2CF_3$ (**2.2**)	85	88[d]

[a] All experiments at least duplicates; experimental error is ± 1°; [b] Data taken from reference 38; [c] Data taken from reference 6; [d] Value obtained using conditions as described in literature.[38]

This has also been confirmed using ATR-IR spectroscopy, which provided clear peaks for, e.g., the antisymmetric and symmetric CH_2 stretching vibrations (Figure 2.4). The precise position of the antisymmetric CH_2 stretching vibration (2921.7 ± 0.1 cm^{-1} for monolayers derived from 1-hexadecene, and 2921.5 ± 0.1 cm^{-1} for those obtained photochemically from 1-hexadecyne) suggests a comparable quality as was obtained for thermally prepared monolayers (~2920-2922 cm^{-1}).

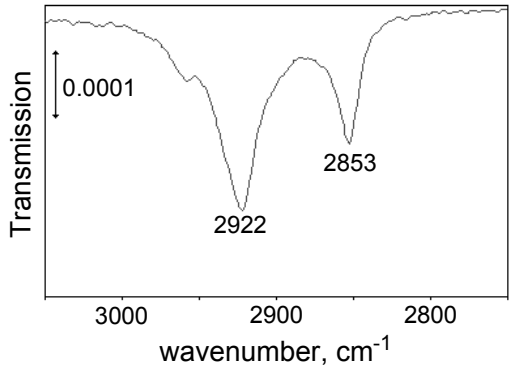

Figure 2.4 C–H stretching vibration region of an ATR-IR spectrum of 1-hexadecene-derived monolayer on Si(100) using 447 nm light.

Up to now, photo-induced hydrosilylation of unsaturated hydrocarbons onto H-terminated flat silicon surfaces had only been reported using UV light. The mechanism for UV-induced hydrosilylation involves photolytic homolysis of a surface Si–H bond, e.g., a radical-induced reaction. Based on the Si–H bond dissociation energy on a silicon surface, a wavelength of shorter than 350 [8,15,42,43] - 380 nm [9] is necessary to obtain surface silicon radicals on H-terminated flat Si(111). This implies that a radical-based initiation is not in operation during the visible light-promoted hydrosilylation reaction described here. Stewart and Buriak proposed an alternative mechanism to explain the white light-promoted hydrosilylation of photoluminescent nanocrystalline silicon.[34,35] We hypothesize that this mechanism, perhaps rephrased in terms of surface plasmons,[44] depicted in Scheme 2.3, is also active here.[45] If this mechanism is operative, it is expected – based on findings of Hamers et al. for the photo attachment of alkenes on partly iodine-terminated Si(111) and Si(001)[37] – that the required reaction time to obtain densely packed monolayers depends on the dopant concentration. This has indeed been found: after 5 h Si(100)–H with low dopant concentration (p- or n-type) yields contact angles of ~100°. However, heavily doped p-type Si(100)–H is much harder to modify, and yields after 5 h a contact angle of ~90°, and after 10 h of only 104°, in line with the effects of the dopant on the band bending.

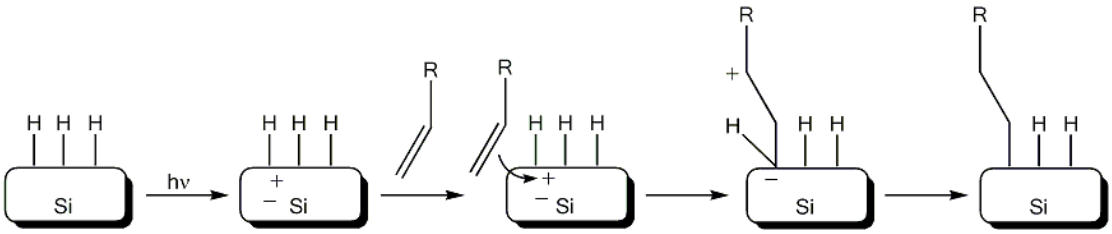

Scheme 2.3 Proposed mechanism for the hydrosylilation of Si(100)–H with 447 nm light.[45]

Monolayers of 1-hexadecene and 1-hexadecyne Si(100)–H were analyzed by X-ray photoelectron spectroscopy (XPS), a very useful tool for the study of covalently attached monolayers on silicon.[8,10,15,19,26,28,37,46-52] Figure 2.5 shows the C_{1s} and Si_{2p} regions of the XPS spectra. For both reagents, the C_{1s}/Si_{2p} ratios are comparable, indicating that the amount of attached molecules is roughly the same. In addition, for both the surfaces only a small amount of fully oxidized silicon can be observed at 103-104 eV, which points to the reduced tendency for oxidation of these surfaces.[3] Detailed observation (insert in Figure 2.5, right) shows that the degree of oxidation for the 1-alkyne-derived monolayer is even slightly lower than that observed for the 1-alkene-derived monolayer. As 1-alkynes can in principle react with two silicon atoms,[38] such a tandem reaction would reduce the number of unreacted sites at the silicon surface. As a result, a smaller number of these sites can yield oxidized surface sites at the later stage, which could explain the displayed observation. Additional XPS studies on monolayers derived from 1-octadecene and 1-octadecyne combined with Mott Schottky measurements are presented in §6.3. The results indeed show more oxide for monolayers derived from 1-alkenes as compared to monolayers from 1-alkynes.

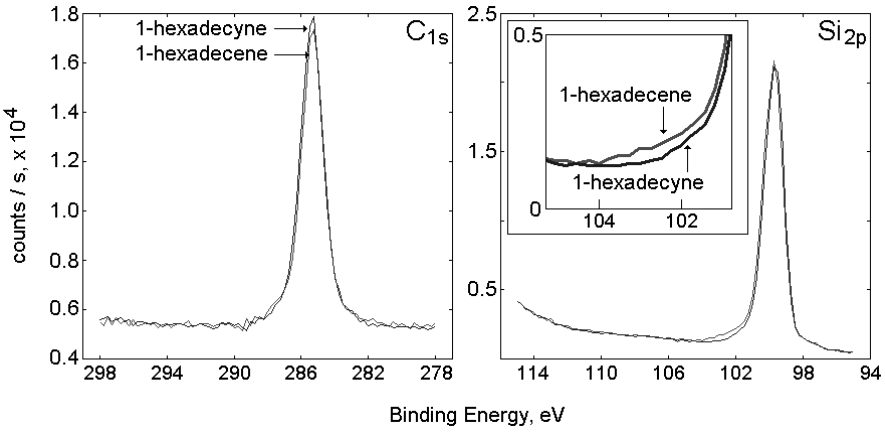

Figure 2.5 C_{1s} (left) and Si_{2p} (right) region of XPS spectra of monolayers on Si(100) prepared via the visible-light method (447 nm, 15 h) using 1-hexadecene and 1-hexadecyne. The inset depicts a 2.5-fold enlargement of the Si–O region.

In order to obtain more information about the composition of monolayers derived from ω-functionalized 1-alkenes, 15-hexadecylenic acid, trifluoroethyl ester (**2.3**) was synthesized (Scheme 2.4) and photoattached to Si(100)–H wafers. Figure 2.6 shows the C_{1s}, F_{1s}, and Si_{2p} regions of the resulting XPS spectrum. The C_{1s} region spectrum shows peaks from 288 to 294 eV, which can be assigned to the different carbons in the trifluoroethyl ester moiety.[10] The presence of C_{1s}d (294 eV) and F_{1s} (689 eV) signals indicates that a trifluoroethyl ester-terminated monolayer was formed on the Si(100)–H surface. Additionally, the silicon spectrum shows very little oxidation of the surface as evidenced by the small signal in the 101-103 eV region. The results are comparable to those obtained with UV light (254 nm) to attach the trifluoroethyl ester of undecylenic acid onto the Si(111)–H surface.[10]

An important issue in the preparation of surfaces for the application in sensor technology is the control over the amount and depth distribution of sensing functionalities in mixed monolayers. In order to study the relation between the ratio of two 1-alkenes in the solution and their relative amounts in the resulting mixed monolayer, mixed monolayers of compounds **2.1** and **2.2** were prepared.

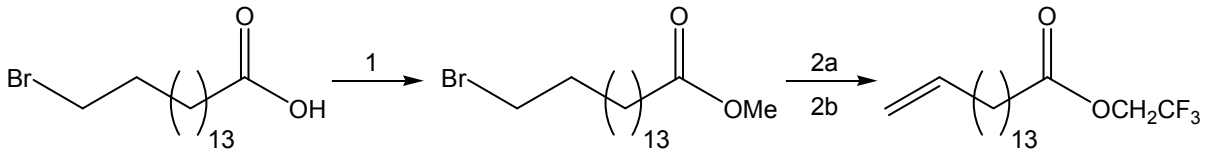

2.3

Scheme 2.4 Synthesis of 15-hexadecenoic acid, 2,2,2-trifluoroethyl ester (**2.3**). (1) CBr_4/MeOH (5%/5 mL), $h\nu$ (30 min), stir overnight at rt (97%), (2a) *t*-BuOK in dry THF (rt and N_2 atmosphere, 42 h) and (2b) CF_3CH_2OH, DMAP and DCC in dry CH_2Cl_2 (step 2: 59%).

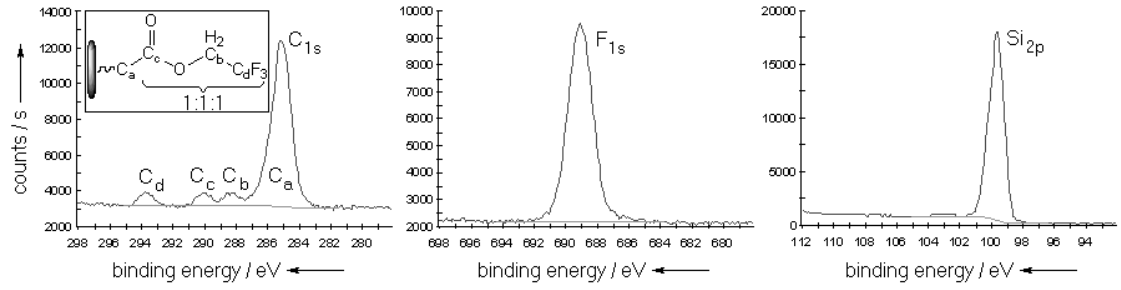

Figure 2.6 X-ray photoelectron region spectra of a monolayer of compound **2.3** on Si(100)–H prepared via the method of visible light-induced hydrosilylation.

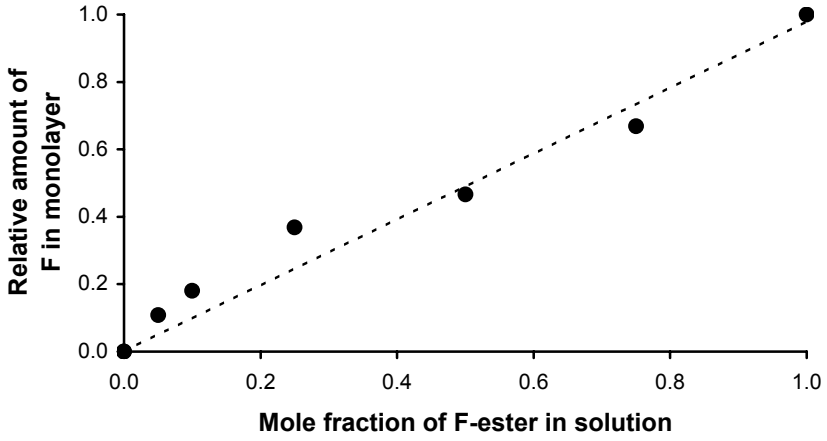

Figure 2.7 Linear correlation of the amount of F atoms in the photochemically prepared monolayers as function of the mole fraction of trifluoroethyl ester **2.2** in mixed solutions.

Figure 2.7 shows that the amount of F (as measured by XPS) of the mixed monolayers increases linearly with increasing molar fraction of compound **2.2** in the alkene solution from which the samples were prepared. This implies that one can obtain a surface that can easily be defined via solution properties. Such a relation has previously been proposed based on indirect fluorescence labeling.[53] Since the diameter of the probe molecule – rhodamine – is larger than that of an alkyl spacer, it is unlikely that the observed linearity from a 0% to a 100% rhodamine-substituted monolayer can be attributed to a linearly changing composition of constant monolayer thickness/packing density of a densely packed monolayer. In addition, ATR-IR has been used to study to the ratio of the ester carbonyl stretch to the total methylene asymmetric stretch as a function of the mole fraction of ethyl undec-1-enylate in 1-decene.[54] Although qualitatively in line with the present finding, quantification of monolayer IR data is harder than that of XPS data. The value of XPS was, e.g., shown by detailed analysis of mixed monolayers of compound **2.3** with 1-hexadecene. The fluorine probe works well since quantitative XPS allows one to obtain the amount of F of the surface *directly* for the *total* concentration range, while the constant packing density of the monolayer of both thermally and photochemically prepared monolayers could be ascertained via the C_{1s}a signal.

Apart from with conventional XPS, the monolayers were also studied with parallel angle-resolved XPS (ARXPS) using a 2-dimensional micro channel detector (MCD) that measures the intensity of the photoelectron emission as a function of emission angle (see §2.2.4.3 for more detailed information about this technique). Figure 2.8 depicts a relative depth profile of such a mixed monolayer of compound **2.3**, for a monolayer of only 1.4 nm total thickness. To

the best of our knowledge, this is the first report of an ARXPS-based relative depth profile on an ultra-thin organic monolayer. The relative depth profile locates bulk Si at the bottom (Si_{2p}), subsequently the Si peak of Si atoms bound to O ($Si_{2p}Ox$), and the corresponding O atoms ($O_{1s}a$). Then the alkyl spacer carbon signals and the ester oxygen atoms are found ($C_{1s}a$ and $O_{1s}b$), while on top the signals are found for $C_{1s}d$ and F_{1s} that belong to the CF_3 group (data for intermediate $C_{1s}b$ & $C_{1s}c$ are not shown).

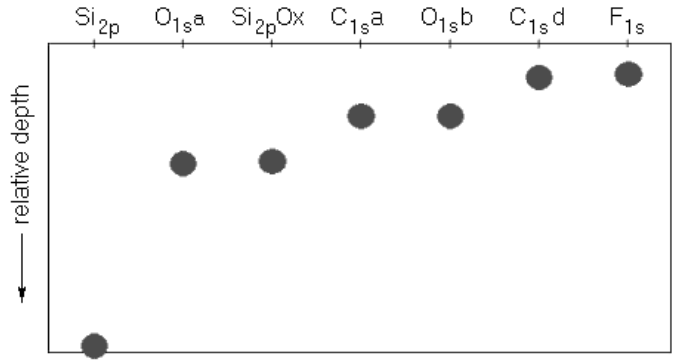

Figure 2.8 A relative depth profile of the elements of a Si(100) sample modified by compound **2.3**.

2.4 Conclusions

We reported for the first time a visible-light induced reaction for attaching functional monolayers onto the Si(100)–H surface. According to the water contact angle the quality of monolayers derived in this way is as good as that of monolayers obtained via the thermal reaction. High-resolution ARXPS was used to provide detailed information about the depth distribution of the elements in the monolayer. Further, it was shown by quantitative XPS that for appropriately sized functional groups, the surface composition can be easily defined via the solution composition. The combination of these techniques opens an attractive avenue for the attachment and characterization of (bio-)active functionalization of monolayers on Si, including a variety of lithographic techniques.

Acknowledgment

Cees Heijboer and dr. Richard White (Thermo Electron) and dr. Klaus Simon (ASML) are thanked for stimulating discussions.

References and Notes

[1] Buriak, J. M. *Chem. Rev.* **2002**, *102*, 1271-1308.
[2] Wayner, D. D. M.; Wolkow, R. A. *J. Chem. Soc. Perkin Trans.* **2002**, *2*, 23-34.
[3] Sieval, A. B.; Linke, R.; Zuilhof, H.; Sudhölter, E. J. R. *Adv. Mater.* **2000**, *12*, 1457-1460.
[4] Linford, M. R.; Chidsey, C. E. D. *J. Am. Chem. Soc.* **1993**, *115*, 12631-12632.

[5] Linford, M. R.; Fenter, P. E.; Eisenberger, P. M.; Chidsey, C. E. D. *J. Am. Chem. Soc.* **1995**, *117*, 3145-3155.

[6] Sieval, A. B.; Demirel, A. L.; Nissink, J. W. M.; Linford, M. R.; van der Maas, J. H.; de Jeu, W. H.; Zuilhof, H.; Sudhölter, E. J. R. *Langmuir* **1998**, *14*, 1759-1768.

[7] Sieval, A. B.; Vleeming, V.; Zuilhof, H.; Sudhölter, E. J. R. *Langmuir* **1999**, *15*, 8288-8291.

[8] Cicero, R. I.; Linford, M. R.; Chidsey, C. E. D. *Langmuir* **2000**, *16*, 5688-5695.

[9] Effenberger, F.; Gotz, G.; Bidlingmaier, B.; Wezstein, M. *Angew. Chem. Int. Ed. Engl.* **1998**, *37*, 2462-2464.

[10] Strother, T.; Cai, W.; Zhao, X. S.; Hamers, R. J.; Smith, L. M. *J. Am. Chem. Soc.* **2000**, *122*, 1205-1209.

[11] Strother, T.; Hamers, R. J.; Smith, L. M. *Nucleic Acid Res.* **2000**, *28*, 3535-3541.

[12] deVilleneuve, C. H.; Pinson, J.; Bernard, M. C.; Allongue, P. M. *J. Phys. Chem. B.* **1997**, *101*, 2415-2420.

[13] Gurtner, C.; Wun, A. W.; Sailor, M. J. *Angew. Chem. Intl. Ed. Engl.* **1999**, *38*, 1966-1968.

[14] Robins, E. G.; Stewart, M. P.; Buriak, J. M. *Chem. Commun.* **1999**, 2479-2480.

[15] Boukherroub, R.; Morin, S.; Bensebaa, F.; Wayner, D. D. M. *Langmuir* **1999**, *15*, 3831-3835.

[16] Buriak, J. M.; Allen, M. J. *J. Am. Chem. Soc.* **1998**, *120*, 1339-1340.

[17] Buriak, J. M.; Stewart, M. P.; Geders, T. W.; Allen, M. J.; Choi, H. C.; Smith, J.; Raftery, D.; Canham, L. T. *J. Am. Chem. Soc.* **1999**, *121*, 11491-11502.

[18] Holland, J. M.; Stewart, M. P.; Allen, M. J.; Buriak, J. M. *J. Solid State Chem.* **1999**, *147*, 251-258.

[19] Niederhauser, T. L.; Jiang, G. L.; Lua, Y. Y.; Dorff, M. J.; Woolley, A. T.; Asplund, M. C.; Berges, D. A.; Linford, M. R. *Langmuir* **2001**, *17*, 5889-5900.

[20] Niederhauser, T. L.; Lua, Y.-Y.; Sun, Y.; Jiang, G.; Strossman, G. S.; Pianetta, P.; Linford, M. R. *Chem. Mater.* **2002**, *14*, 27-29.

[21] Niederhauser, T. L.; Lua, Y.-Y.; Jiang, G.; Davis, S. D.; Matheson, R.; Hess, D. A.; Mowat, I. A.; Linford, M. R. *Angew. Chem. Int. Ed.* **2002**, *41*, 2353-2356.

[22] Sieval, A. B.; van den Hout, B.; Zuilhof, H.; Sudhölter, E. J. R. *Langmuir* **2000**, *16*, 2987-2990.

[23] Sieval, A. B.; van den Hout, B.; Zuilhof, H.; Sudhölter, E. J. R. *Langmuir* **2001**, *17*, 2172-2181.

[24] Wojtyk, J. T. C.; Morin, K. A.; Boukherroub, R.; Wayner, D. D. M. *Langmuir* **2002**, *18*, 6081-6087.

[25] Liu, Y.-J.; Navasero, N. M.; Yu, H.-Z. *Langmuir* **2004**, *20*, 4039-4050.

[26] Sieval, A. B.; Linke, R.; Heij, G.; Meijer, G.; Zuilhof, H.; Sudhölter, E. J. R. *Langmuir* **2001**, *17*, 7554-7559.

[27] Wagner, P.; Nock, S.; Spudich, J. A.; Volkmuth, W. D.; Chu, S.; Cicero, R. I.; Wade, C. P.; Linford, M. R.; Chidsey, C. E. D. *J. Structural Biology* **1997**, *119*, 189-201.

[28] Lin, Z.; Strother, T.; Cai, W.; Cao, X. P.; Smith, L. M.; Hamers, R. J. *Langmuir* **2002**, *18*, 788-796.

[29] Pike, A. R.; Lie, L. H.; Eagling, R. A.; Ryder, L. C.; Patole, S. N.; Connolly, B. A.; Horrocks, B. R.; Houlton, A. *Angew. Chem. Int. Ed. Engl.* **2002**, *41*, 615-617.

[30] Wei, F.; Sun, B.; Guo, Y.; Zhao, X. S. *Biosens. Bioelectron.* **2003**, *18*, 1157-1163.

[31] More, S. D.; Hudecek, J.; Urisu, T. *Surf. Sci.* **2003**, *532*, 993-998.

[32] Liao, W.; Wei, F.; Qian, M. X.; Zhao, X. S. *Sens. Actuators B: Chem.* **2004**, *101*, 361-367.

[33] Dancil, K.-P. S.; Greiner, D. P.; Sailor, M. J. *J. Am. Chem. Soc.* **1999**, *121*, 7925-7930.

[34] Stewart, M. P.; Buriak, J. M. *J. Am. Chem. Soc.* **2001**, *123*, 7821-7830.
[35] Schmeltzer, J. M.; Porter, L. A.; Stewart, M. P.; Buriak, J. M. *Langmuir* **2002**, *18*, 2971-2974.
[36] Reboredo, F. A.; Schwegler, E.; Galli, G. *J. Am. Chem. Soc.* **2003**, *125*, 15243-15249.
[37] Cai, W.; Lin, Z.; Strother, T.; Smith, L. M.; Hamers, R. J. *J. Phys. Chem. B* **2002**, *106*, 2656-2664.
[38] Sieval, A. B.; Opitz, R.; Maas, H. P. A.; Schoeman, M. G.; Meijer, G.; Vergeldt, F. J.; Zuilhof, H.; Sudhölter, E. J. R. *Langmuir* **2000**, *16*, 10359-10368.
[39] Lee, A. S.-Y.; Yang, H. C.; Su, F. Y. *Tetrahedron Lett.* **2001**, *42*, 301-303.
[40] Hostetler, E. D.; Fallis, S.; McCarthy, T. J.; Welch, M. J.; Katzenellenbogen, J. A. *J. Org. Chem* **1998**, *63*, 1348-1351.
[41] The cleaning procedure of silicon samples in our laboratory has been adapted over the past four years. Initially piranha solutions were used to clean silicon surfaces before etching. In a later stage we started using a plasma cleaning process by which the use of piranha solutions could be circumvented for regular silicon samples. However, for the regeneration of ATR crystals the use of piranha solutions is still required.
[42] Terry, J.; Linford, M. R.; Wigren, C.; Cao, R. Y.; Pianetta, P.; Chidsey, C. E. D. *Appl. Phys. Lett.* **1997**, *71*, 1056-1058.
[43] Wojtyk, J. T. C.; Tomietto, M.; Boukherroub, R.; Wayner, D. D. M. *J. Am. Chem. Soc.* **2001**, *123*, 1535-1536.
[44] Barnes, W. L.; Dereux, A.; Ebbesen, T. W. *Nature* **2003**, *424*, 824-830.
[45] On the basis of scanning tuneling microscopy (STM) experiments and investigations of the reaction behavior of 1-alkenes with silicon wafers with varying types and levels of doping a new reaction mechanism was proposed in a later stage of the research (Chapter 3).
[46] Bansal, A.; Li, X. L.; Yi, S. I.; Weinberg, W. H.; Lewis, N. S. *J. Phys. Chem. B* **2001**, *105*, 10266-10277.
[47] Zhang, J. F.; Cui, C. Q.; Lim, T. B.; Kang, E. T.; Neoh, K. G.; Lim, S. L.; Tan, K. L. *Chem. Mater.* **1999**, *11*, 1061-1068.
[48] Bergerson, W. F.; Mulder, J. A.; Hsung, R. P.; Zhu, X. Y. *J. Am. Chem. Soc.* **1999**, *121*, 454-455.
[49] Kim, N. Y.; Laibinis, P. E. *J. Am. Chem. Soc.* **1998**, *120*, 4516-4517.
[50] Lee, E. J.; Bitner, T. W.; Ha, J. S.; Shane, M. J.; Sailor, M. J. *J. Am. Chem. Soc.* **1996**, *118*, 5375-5382.
[51] Hong, L.; Sugimura, H.; Furukawa, T.; Takai, O. *Langmuir* **2003**, *19*, 1966-1969.
[52] Linford, M. R.; Chidsey, C. E. D. *Langmuir* **2002**, *18*, 6217-6221.
[53] Wei, F.; Zhao, X. S. *Thin Solid Films* **2002**, *408*, 286-290.
[54] Boukherroub, R.; Wayner, D. D. M. *J. Am. Chem. Soc.* **1999**, *121*, 11513-11515.

Chapter 3

Visible Light Attachment of Monolayers on Hydrogen-Terminated Si(100) and Si(111): Effect of Wavelength and Doping*

Abstract – The very mild method for the attachment of high-quality organic monolayers on crystalline silicon surfaces using visible light as introduced in Chapter 2 was further developed and explored. By using visible light sources, from 447 to 658 nm, a variety of 1-alkenes and 1-alkynes were attached to hydrogen-terminated Si(100) and Si(111) surfaces at room temperature. The presence and the quality of the monolayers were evaluated by static water contact angles, X-ray photoelectron spectroscopy, and IR spectroscopy. Monolayers prepared by thermal, UV light, or visible light initiation were compared. Additionally, the ability of infrared reflection-absorption spectroscopy to study organic monolayers on silicon was explored. A reaction mechanism is discussed on the basis of investigations of the reaction behavior of 1-alkenes with silicon wafers with varying types and levels of doping. Finally, a series of mixed monolayers derived from the mixed solutions of a 1-alkene and an ω-fluoro-1-alkene were investigated to reveal that the composition of the mixed monolayers was directly proportional to the molar ratio of the two compounds in the solutions.

* A slightly modified version of this chapter has been published:
Sun, Q.-Y.; de Smet, L. C. P. M.; van Lagen, B.; Giesbers, M.; Thüne, P. C.; van Engelenburg, J.; de Wolf, F. A.; Zuilhof, H.; Sudhölter, E. J. R. *J. Am. Chem. Soc.* **2005,** *127*, 2514-2523.

3.1 Introduction

In Chapter 2 we introduced an easy and mild route to modify planar Si surfaces via the use of visible light (447 nm). Angle-resolved X-ray photoelectron spectroscopy (ARXPS), infrared spectroscopy, and contact angle measurements were used to show the formation of densely packed monolayers. However, no systematic study has as yet been reported on the influence of the nature and degree of doping, the variation of the irradiation wavelength, and the type of silicon surface [Si(100) vs Si(111)]. In addition, no detailed surface studies by scanning force techniques and X-ray reflectivity measurements have yet been made, nor a fully unambiguous comparison between the thermal and this new photochemical method regarding the obtainable density of the resulting monolayers. Finally, no systematic evaluation has yet been undertaken on the applicability of IRRAS (infrared reflection-absorption spectroscopy) measurements in the analysis of organic monolayers. Such an evaluation would be highly useful, given the ease of use of this technique in the analysis of organic monolayers, as recently shown by us in a study of organic monolayers covalently attached to silicon nitride surfaces.[1] In this chapter we aim to address these issues and in combination with our earlier work, try to develop an overall picture of the scope and mechanism of this mild attachment reaction.

3.2 Experimental

3.2.1 General Information

PE 40/60, MeOH, EtOH, and CH_2Cl_2 were distilled prior to use. Distilled CH_2Cl_2 – used as a solvent in chemical reactions – and acetonitrile were distilled over CaH_2 prior to use. Mesitylene (Fluka, 99%) was distilled and stored on $CaCl_2$. The dried mesitylene was filtered to remove traces of $CaCl_2$. 1-Decene (Fluka, 97%), 1-hexadecene (Sigma, ~99%), and 10-undecenoic acid (Acros, 99%) were distilled at least twice at reduced pressure. Triethylamine (TEA; Acros, 99%) was dried over KOH. 1-Docosene (TCI America, 99+%), 10-undecen-1-ol (Aldrich, 98%), acetone (Acros, 99+%), methanesulfonyl chloride (Janssen Chimica, 99%), KF (Jansen Chimica, p.a.), and 18-crown-6 (Acros, 99%) were used as received. HF (Fluka, 50% p.a.-plus) was diluted with demineralized H_2O. 10-Undecenoic acid methyl ester (**3.1**) was prepared and purified as described earlier.[2] The synthesis of 10-undecenoic acid, 2,2,2-trifluoroethanol ester (**3.2**) was prepared as described in §2.2.2. All reactions were performed under a nitrogen atmosphere. The synthesis of the 1-alkynes

is described elsewhere.[3] Straight-chain alkanes for the IRRAS calibration were obtained from Aldrich (99+% purity).

Single-polished Si(100): n-type, 500-550 μm thick, resistivity 1-2 Ωcm (Seltec Silicon, Mitsubishi Silicon America); p-type, 375 μm thick, resistivity 1-2 Ωcm (Bayer Solar Freiberg, Germany); n-type, 500-550 μm thick, resistivity 0.008-0.02 Ωcm; p-type, 500-550 μm thick, 0.01-0.02 Ωcm (Addison Engineering, San Jose). Single-polished Si(111): n-type, 475-550 μm thick, resistivity 1-5 Ωcm (Addison Engineering, CA); p-type, 500-550 μm thick, resistivity 0.009-0.012 Ωcm (Addison Engineering). In this chapter silicon with resistivities of 1-5 and 0.008-0.02 Ωcm is referred to as lowly doped and highly doped, respectively. Lowly doped n-type Si(100) was used throughout this chapter, unless specifically noted otherwise.

3.2.2 Purification and Analysis of Synthesized Compounds

Thin-layer chromatography (TLC) was performed on Merck silica gel 60F254 plastic sheets, and detection was realized by charring with an aqueous solution of $KMnO_4$. Column chromatography was conducted by elution of a column of Merck Kieselgel silica (230-400 mesh) using eluents as specified below. NMR spectra were recorded on a Bruker AC-E 400 spectrometer in $CDCl_3$ (dried over Al_2O_3) at room temperature. Gas chromatography (GC) measurements were performed on a Hewlett-Packard 5890 series II chromatograph that was equipped with a DB-17 column and an FID detector. GC samples were dissolved in ethyl acetate or diethyl ether.

3.2.3 Synthesis of 11-Fluoro-1-Undecene

10-Undecen-1-ol (8.501 g, 49.92 mmol) was dissolved in 65 mL of dry CH_2Cl_2, and 10.4 mL (7.59 g, 75 mmol) of triethylamine was added. The stirred solution was cooled to -10 °C, and 8.6 g (75 mmol) of mesyl chloride in 20 mL of dry CH_2Cl_2 was added dropwise at such a rate that the temperature of the solution was not higher than 0 °C. Thirty minutes after the addition was accomplished, TLC (PE 40/60:CH_2Cl_2 = 1:4) showed that hardly any starting material (R_f = 0.17) was left, and a product with R_f = ~0.38 was formed. The solution was stored at -35 °C until further workup. The yellow suspension was washed with 200 mL of 0.5 M HCl and the product extracted with CH_2Cl_2 (5 × 75 mL). The combined organic layers were washed with saturated $NaHCO_3$ (3×) and dried over Na_2SO_4. After filtration the solvent was removed under a reduced pressure, yielding 12.786 g of crude product. TLC and ^{1}H NMR showed that 10-undecenyl mesylate was pure enough for further use.

KF (5.8 g, 100 mmol) and 18-crown-6 (26.4 g, 100 mmol) were dissolved in acetonitrile (50 mL). The solution was heated to 60 °C, and to the resulting white suspension was added 12.394 g (49.9 mmol) of 10-undecenyl mesylate dissolved in 50 mL of acetonitrile over a period of 45 min. Subsequently, the solution was refluxed overnight. The course of the reaction was followed by TLC and ^{1}H NMR via the workup of small analytical samples. After 20 h, ^{1}H NMR showed that about 60% of the 10-undecenyl mesylate was still present, and therefore, 1 equivalent of KF and 18-crown-6 were added to the reaction mixture. After another 20 h, TLC and ^{1}H NMR showed that most of the starting material had disappeared. The solvent was removed under a reduced pressure. PE 40/60 (200 mL) and water (100 mL) were added to the mixture. The organic layer was separated, and the water layer was washed twice with PE 40/60 (100 mL). The combined organic layers were washed with brine (300 mL) and dried over Na_2SO_4. After filtration, evaporation yielded 7.228 g of crude product. Column chromatography (PE 40/60 as eluent) yielded 4.173 g (24 mmol, 48%) of 11-fluoro-1-undecene.

TLC R_f (PE 40/60:CH_2Cl_2 = 1:4) = 0.81 and R_f (PE 40/60) = 0.44; GC R_t (115 °C) = 6.8 min; **^{1}H NMR** δ 5.88-5.78 (m, 1H), 5.04-4.94 (m, 2H), 4.51 and 4.39 (dt, 2H, *J* 47.2 Hz, *J* ~6.2 Hz), 2.10-2.05 (q, 2H, *J* ~6.8 Hz), 1.77-1.65 (m, 2H), and 1.42-1.37 (m) and 1.33 (br s, 12H); **^{13}C NMR** δ 139.45, 114.48, 85.22, and 83.59 (*J* 163.5 Hz), 34.21, 30.93, and 30.74 (*J* 19.3 Hz), and 29.88, 29.80, 29.64, 29.51, 28.33, 25.59, and 25.54 (*J* 5.4 Hz); **MS** *m*/*z* 172.1622 (calcd for $C_{11}H_{21}F$, 172.1627).

3.2.4 Sample Cleaning and Etching

Si samples were first wiped with a tissue that was saturated with chemically pure acetone. After that, the samples were sonicated for at least 10 min in acetone. Then the samples were placed in an oxygen plasma cleaner (Harrick PDC-32G) for 10 min. Subsequently, the Si(100) samples were etched in 2.5% aqueous HF for 2 min, while Si(111) samples were etched in an argon-saturated 40% aqueous NH_4F solution for 15 min under an argon atmosphere. To recycle the relatively expensive attenuated total reflection (ATR) crystals, they were cleaned by oxidative removal of a previously formed monolayer in "piranha solution" (H_2SO_4:35% H_2O_2 = 2:1 (v/v)) at ~85 °C for 1 h (*caution: piranha solutions should be handled with great care*),[3] and subsequently etched with HF as described above.

3.2.5 Monolayer Preparation

3.2.5.1 Photochemical Method

A solution (1.5-3 mL, 0.1-0.5 M) of (a) 1-alkene(s) or 1-alkyne in mesitylene was flushed with argon for at least 30 min before the freshly etched hydrogen-terminated Si sample was added. After that, the solution was flushed for another 30 min. Then, the argon inlet was moved to a position just above the solution to change from a bubbling solution to a decent gas flow. After that, the lamp – in all cases fixed at a distance of 0.5 cm from the reaction vessel – was turned on. For the modification of ATR crystals two lamps were used. The setup was covered with aluminum foil. Depending on the wavelength, different vessels with a rectangular bottom part – as depicted in Figure 2.1 – were used (quartz vessel for 254 nm and conventional glassware for all other wavelengths). After illumination for the desired time, the sample was removed from the solution, and the surface was excessively rinsed with PE 40/60, EtOH, and CH_2Cl_2, respectively. The following models of double-bore lamps were obtained from Jelight Co. Inc. (Irvine, CA): 82-3309-2 (254 nm), 84-2051-2 (371 ± 19 nm = width at half of the maximum intensity), 84-247-2 (447 ± 32 nm), 84-213-2 (504 ± 30 nm), and 84-236-1 (658 ± 14 nm).

3.2.5.2 Thermal Method

A solution (8.5 mL, 0.2 M) of 1-alkene(s) in mesitylene was placed in a small three-necked flask fitted with a nitrogen inlet, a reflux condenser with a $CaCl_2$ tube, and a stopper. The solution was refluxed for at least 45 min under a flow of nitrogen. Subsequently, a cleaned and freshly etched sample was added to the refluxing solution, while a slow nitrogen flow was maintained. After 2 h the modified sample was removed from the solution and excessively rinsed with PE 40/60, EtOH, and CH_2Cl_2, respectively.

3.2.6 Monolayer Characterization

(a) *Contact Angle Measurements*. In all cases where modified samples were analyzed by different techniques a small piece (~5 mm × 10 mm) was cut from the sample directly after cleaning. Static water contact angles were obtained using an Erma G-1 contact angle meter (volume of the drop of ultrapure water, 3.5 μL). Contact angles of two or three drops were measured. The error of the contact angles is ±1°.

(b) *IRRAS*. FT infrared reflection-absorption spectra were recorded on a Bruker Tensor 27 instrument equipped with a variable-angle reflection Auto Seagull accessory. A Harrick

grid polarizer was installed in front of the detector for measuring spectra with p-polarized (parallel) radiation with respect to the plane of incidence at the sample surface. Single-channel transmittance spectra (4096 scans) were collected using a spectral resolution of 4 cm^{-1}. All (data derived from) spectra shown in this chapter are a result of spectral subtraction of modified samples with a cleaned native oxide-covered silicon sample without any further data manipulation.

(c) *XPS*. XPS measurements were performed on a VG Ionex system equipped with a Clam II analyzer and a standard AlKα X-ray source. Spectra were taken in normal emission at 10^{-9} mbar within 10 min. All C_{1s} peaks corresponding to hydrocarbons were calibrated to a binding energy of 285.0 eV to correct for the energy shift caused by charging.

(d) *X-ray Reflectivity*. X-ray reflectivity measurements were performed on a Panalytical X'Pert Pro diffractometer using CuKα radiation (tube settings 40 kV and 40 mA). The data were collected using a fixed divergence slit of 1/32° and a parallel plate collimator on the diffracted beam side. The layer thickness is calculated from the interference fringes. The error in the measurement is depicted as the standard deviation of five measurements on the same sample.

(e) *Atomic Force Microscopy (AFM)*. Surface topography was imaged using a Nanoscope III atomic force microscope (AFM Digital Instruments, Santa Barbara, CA). The contact mode (CM-AFM) with silicon nitride cantilevers (Digital Instruments) with a spring constant of about 0.58 N/m was used.

3.3 Results and Discussion

3.3.1 Formation of Organic Monolayers on Si(100) and Si(111) using 447 nm Light

Table 3.1 lists the static water contact angles of the Si(100) and Si(111) surfaces modified by a variety of 1-alkenes and 1-alkynes and two esterified-1-alkenes (compounds **3.1** and **3.2**) using 447 nm light (15 h). In Chapter 2 it was shown that the monolayer formation of 1-hexadecene on Si(100)–H was complete after 10 h. The contact angles of the nonfunctionalized monolayers indicate a high hydrophobicity, and the values are comparable with those of high-quality monolayers prepared under thermal conditions.[3] The contact angles of monolayers of compounds **3.1** and **3.2** are lower due to the presence of the polar functionality, and in both cases comparable to those of monolayers prepared via thermal methods. Finally, the differences between the contact angles of monolayers of compounds **3.1** and **3.2** on Si(100) and Si(111) are small, which indicates that after monolayer formation the top of the organic monolayer does not obviously "display" the character of the silicon

substrate anymore. These initial characterizations drove us to more detailed investigations using, X-ray reflectivity and AFM.

Table 3.1 Static water contact angles (deg) of monolayers on silicon surfaces prepared by 447 nm irradiation and thermal methods.[a]

Reactants	447 nm Si(100)	447 nm Si(111)	Thermal Si(100)
$CH{\equiv}C–C_{10}H_{21}$	108	109	108[b]
$CH{\equiv}C–C_{12}H_{25}$	110	110	110[b]
$CH{\equiv}C–C_{14}H_{29}$	110	110	110[b]
$CH_2{=}CH–C_{10}H_{21}$	109	109	108[c]
$CH_2{=}CH–C_{12}H_{25}$	108	110	108[c]
$CH_2{=}CH–C_{14}H_{29}$	109	110	109[c]
$CH_2{=}CH–C_8H_{16}COOCH_3$ (**3.1**)	78	75	77[c]
$CH_2{=}CH–C_8H_{16}COOCH_2CF_3$ (**3.2**)	85	86	88[d]

[a] Conditions: irradiation method, 15 h, room temperature; thermal method, heating in a neat reactant[2] or refluxing for 2 h in a 0.2 M solution in mesitylene.[3] All experiments were performed at least twice, experimental error ±1°; [b] From reference 3; [c] From reference 2; [d] Newly obtained using conditions as described in reference 3.

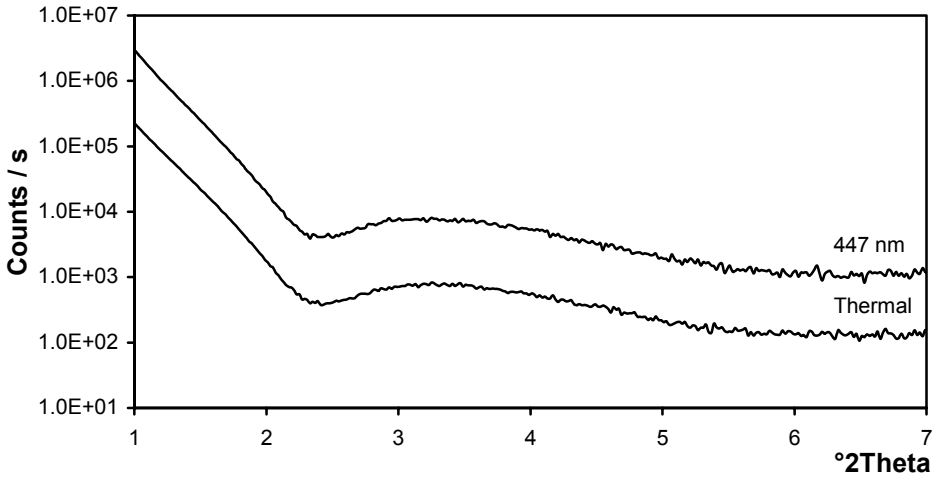

Figure 3.1 X-ray reflectivity profiles for *n*-docosyl monolayers on lowly doped n-Si(100) prepared via the thermal and visible light (447 nm, 15 h) methods. For clarity the intensities of the visible light data have been multiplied by a factor of 10.

X-ray reflectivity measurements were performed to compare *n*-docosyl (*n*-$C_{22}H_{45}$) monolayers on Si(100) prepared via either visible light or thermal attachment methods. 1-Docosene was chosen as the alkene, since this yielded a monolayer with sufficient thickness to obtain quantitatively reliable X-ray reflectivity data. Figure 3.1 shows the X-ray reflectivity profiles for two monolayers obtained by 447 nm irradiation or thermal treatment, respectively. Just like the static water contact angles of these layers (~107°), the X-ray reflectivity profiles are almost identical. The monolayer thickness obtained from the X-ray data is 26 ± 1 Å for both monolayers. Using the calculated length of an all-*trans*-docosyl tail (27.9 Å),[4] the tilt angle with respect to the normal of the surface can be calculated. This results in a tilt angle of 15-26°, of which the top limit is close to the tilt angles of thinner alkyl monolayers.[3]

Monolayers of 1-hexadecene on Si(100) and Si(111) – prepared via the thermal and visible-light methods (447 nm) – were evaluated using CM-AFM. In Figure 3.2 the corresponding section analyses are presented for the photochemically prepared samples. CM-AFM shows that after wet etching and monolayer formation flat surfaces can be maintained, and no significant differences were observed between thermally and photochemically prepared samples. In addition, the modified Si(111) surface (Figure 3.2, right) remains a bit more smooth than the Si(100) surface (Figure 3.2, left). The observed flatness is of the same order of magnitude as reported recently by Cattaruzza et al. for the thermal functionalization of H-terminated Si(100) with 6-heptynoic acid methyl ester.[5] In addition, Wayner and co-workers used AFM to study decyl-modified Si(111) surfaces prepared via different techniques, and reported atomically flat terraces.[6]

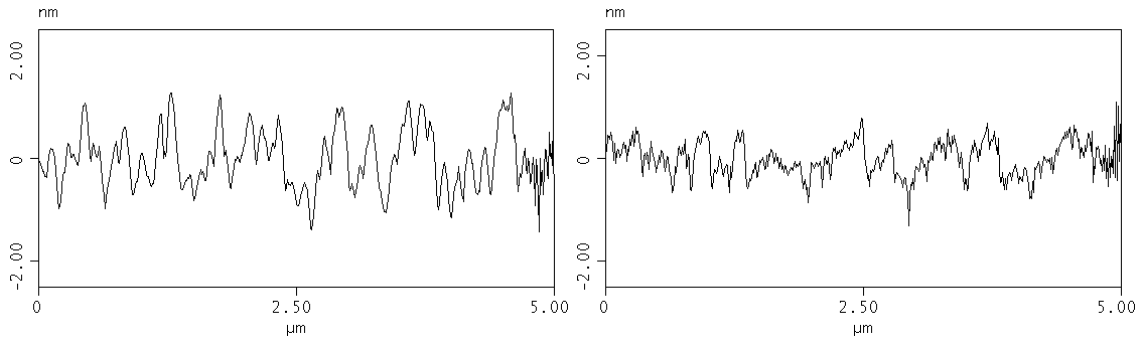

Figure 3.2 Section analysis obtained via contact mode AFM of photochemically prepared *n*-hexadecyl-modified Si(100) (left) and Si(111) (right) wafers [447 nm, 15 and 5 h, respectively].

3.3.2 Effect of Irradiation Wavelength

The possibility to achieve monolayer attachment even under milder conditions was tested via the study of the photochemical reaction over a wide range of wavelengths (254-658 nm, Table 3.2) using phosphorescent lamps with various emission maxima (see §3.2.5.1), and via the use of a wide-spectrum fluorescent lamp in combination with the appropriate wavelength filters. The maximum contact angles of an *n*-hexadecyl monolayer that can be achieved using light of 371 nm to up to at least 658 nm on both H-terminated Si(100) and Si(111) are comparable with that of high-quality monolayers prepared by UV light (254 nm) or thermal initiation reaction, ~108-110°. This indicates the possibility to obtain densely packed monolayers under a wide range of mild conditions and the resulting compatibility with biomaterials, one example of which can be found in the direct attachment of labile sialic acid derivatives that have limited stability at high temperature (see Chapter 4).

Table 3.2 Static water contact angles (deg) of 1-hexadecene-derived monolayers on lowly doped n-Si(100) (15 h of irradiation) and lowly doped n-Si(111) (5 h of irradiation) prepared by different wavelengths.

λ (nm)	n-Si(100)	n-Si(111)
254	109	110
371	109	110
447	109	109
504	108	110
658	108	110

The easiest way to obtain fully covered modified Si wafers is to use cheap wide-spectrum phosphorescent "high-efficiency" lamps, possibly in combination with appropriate wavelength filters. Broad-spectrum (15 W, 400-730 nm) lamps, in combination with light filters that remove all light below 500, 550, or 600 nm, yielded *n*-hexadecyl monolayers with a contact angle of ≥108° upon irradiation for 14 h. The quality of the monolayer seems to be dependent more on the humidity of the surroundings and the completeness of oxygen removal than on the precise light source used.

Upon irradiation with UV light (254 nm) the color of a 1-alkene in mesitylene solution becomes yellow, indicating the photochemical formation of side products.[7] The use of visible light of 371-658 nm did not result in a color change. Gas chromatography experiments indeed showed the formation of additional products after irradiation with UV light, while the

composition of the solution did not change detectably upon irradiation with 447 nm light. The (likely almost) unchanged nature of alkene/mesitylene solutions after 371-658 nm irradiation allows the use of recycled alkene/mesitylene mixtures after minimal purification efforts (washing the complete solution through a small silica plug to remove trace amounts of any polymers), which is specifically advantageous in light of the synthetic efforts that are sometimes required to obtain functionalized alkenes.

One of the most versatile functional groups to have available on the surface would be the carboxylic acid moiety. In the thermal reaction this can only be obtained via the use of, e.g., esters,[2,8-11] as the direct attachment of compounds with free hydroxyl moieties yields undesirable reactivity of those functional groups, leading to Si–O(CO)R bond formation. Hydrolysis of the ester, e.g., by treatment with potassium *tert*-butoxide in DMSO, then yields carboxylic acid-modified monolayers with contact angles of ~52°.[8] However, recently, Liu et al. showed that this deprotection method diminishes the amount of attached alkyl tails in the monolayer.[10] Interestingly, Wayner and co-workers recently reported ATR spectra of monolayers of undecenylic acid on hydrogen-terminated Si(111), which were prepared by direct irradiation ($\lambda \approx 300$ nm) of a solution of 1-undecenylic acid, but no contact angle data were given.[11]

To further investigate this, we studied the direct attachment of 10-undecenoic acid on hydrogen-terminated Si(100) by UV (254 nm) and visible (447 and 658 nm) light. The contact angles of the resulting layers prepared by visible light were 66-68° in all three cases, while in the case of the thermal reaction a contact angle of 79° was observed. The result of 66-68° in combination with ATR-IR data that display a strong C=O signal implies the presence of a significant amount of free carboxylic acid groups in the monolayer, but also suggests that no densely packed monolayer of acid-terminated alkyl chains is formed, as significantly lower contact angles are to be expected in that case (e.g., reported contact angles of acid-terminated monolayers on gold are in the range of 0 to ~15°).[12,13] The thermally obtained value of 79° is indicative of a mixture of Si–C-bound, acid-terminated alkyl chains and Si–O-bound undecenoyl chains. The presence of the latter linkage is shown upon treatment with dilute HF solutions: short treatment of the photochemically prepared monolayers does not affect their contact angles, while the contact angle of the thermally obtained monolayers decreases to 73°, caused by the replacement of highly apolar Si–O undecenoyl chains by Si–H sites. In addition, it can be concluded that the photochemical method works as well for all three wavelengths (254, 447, and 658 nm) that were used.

3.3.3 Infrared Reflection-Absorption Spectroscopy

Detailed information about the structure of organic monolayers can frequently be obtained by infrared spectroscopy. Features derived from C–H stretching vibrations or functional groups such as esters or amides can reveal the presence[1,2,10,14-17] as well as conversion[1,2,10,16] of attached molecules. Furthermore, the precise positions of the antisymmetric and symmetric C–H stretching vibration bands in an IR spectrum of a monolayer may provide information about the quality of the monolayers, since they can be compared with those of C–H bands of isotropic and crystalline materials.[15] Due to the low absorbance of an organic monolayer and the concomitantly low signal-to-noise ratio, one usually has to rely on ATR spectroscopy, a method in which the signal-to-noise ratio is enhanced by multiple internal reflections of the IR beam in a modified double-polished ATR crystal. Alternatively, infrared spectra can also be obtained by external reflection techniques such as IRRAS.[18] IRRA spectra can be obtained using a commercially available variable-angle reflection accessory in combination with a standard IR spectrophotometer. This technique would potentially be advantageous as it allows easy measurements of vibrational features and subsequent other characterizations (X-ray reflectivity, XPS, water contact angles) all on the same sample, which is harder to do using ATR crystals (both technically and pricewise).

Figure 3.3 gives a typical example of the C–H stretching region of an *n*-hexadecyl monolayer on hydrogen-terminated Si(100) obtained by IRRAS. As can be seen from the spectrum in Figure 3.3, IRRAS clearly shows the presence of a covalently attached organic monolayer. Table 3.3 summarizes the IRRAS results of *n*-hexadecyl monolayers on Si(100) and Si(111). For one wavelength (447 nm, 15 h) the study was extended by the preparation of monolayers with different types of 1-alkenes/1-alkynes on Si(100) and Si(111). The results of that variation are presented in Table 3.4.

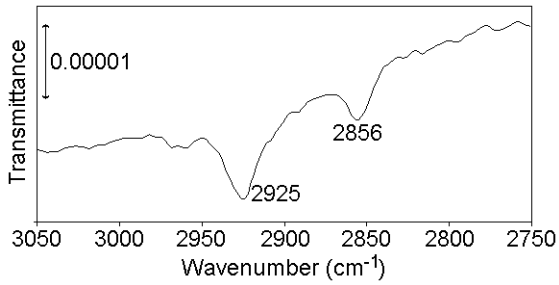

Figure 3.3 C–H stretching vibration region of the IRRA spectrum of a photochemically (447 nm) obtained *n*-hexadecyl monolayer on hydrogen-terminated Si(100) (IR reflection angle 68°, p-polarized light).

Table 3.3 IRRAS data of the antisymmetric and symmetric C–H stretching vibrations of n-hexadecyl monolayers on hydrogen-terminated Si(100) and Si(111) surfaces obtained by different attachment methods.[a]

Method	Si(100)		Si(111)	
	ν_a(C–H)	ν_s(C–H)	ν_a(C–H)	ν_s(C–H)
Thermal	2923	2854	2923	2854
254	2926	2856	2925	2856
371	2925	2853	2925	2856
447	2925	2856	2924	2855
504	2924	2855	2924	2854
658	2926	2855	2924	2856

[a] IRRAS data: p-polarized light, IR reflection angle 68°, in inverse centimeters. Irradiation time: 254 nm, 3 h; 371, 447, 504, and 658 nm, 15 h.

Table 3.4 IRRAS data of the anti-symmetric and symmetric C–H stretching vibrations of organic monolayers on hydrogen-terminated Si(100) and Si(111) surfaces obtained for different 1-alkenes and 1-alkynes upon irradiation with 447 nm light for 15 h.[a]

Reactants	Si(100)		Si(111)	
	ν_a(C–H)	ν_s(C–H)	ν_a(C–H)	ν_s(C–H)
$CH{\equiv}C–C_{10}H_{21}$	2927	2854	2925	2854
$CH{\equiv}C–C_{12}H_{25}$	2925	2854	2922	2852
$CH{\equiv}C–C_{14}H_{29}$	2925	2855	2922	2852
$CH_2{=}CH–C_{10}H_{21}$	2926	2855	2924	2857
$CH_2{=}CH–C_{12}H_{25}$	2925	2855	2925	2856
$CH_2{=}CH–C_{14}H_{29}$	2925	2856	2924	2855
$CH_2{=}CH–C_8H_{16}COOCH_3$ (**3.1**)	2930	2855	2925	2856
$CH_2{=}CH–C_8H_{16}COOCH_2CF_3$ (**3.2**)	2931	2855	2925	2857

[a] IRRAS data: p-polarized light, IR reflection angle 68°, in inverse centimeters.

On average, IRRAS on the monolayers yields peak positions corresponding to antisymmetric and symmetric C–H stretching vibrations at 2925 and 2856 cm^{-1}, respectively (Tables 3.3 and 3.4). When compared with ATR data obtained on such monolayers, it is evident that these IRRAS values are all higher. The obtained values were slightly different for different types of monolayers, but – as expected on the basis of IRRAS theory[18] – also

depended on IRRAS parameters, such as the incidence angle. In addition, the C–H stretching vibrations of samples that were prepared by our standard thermal procedure[19] were observed in IRRAS at consistently higher wavenumbers than in ATR (Table 3.3, 2923 and 2854 cm^{-1} versus 2921 and 2852 cm^{-1}, respectively).[2] Therefore, a detailed investigation was desirable to obtain a clear picture of the potential of IRRAS in the study of such monolayers.

First, it was investigated whether IRRAS could also provide information about the degree of disorder (liquidlike or solidlike) in such thin layers, via measurement of thin layers of a homologous series of liquid and solid alkanes (*n*-$C_{12}H_{26}$ to *n*-$C_{24}H_{50}$) deposited on Si wafers with their native oxide layer still present. All spectra were obtained at an incidence angle of 68° with p-polarized light, since it was found for an *n*-hexadecyl monolayer on Si(100) that angles in the range of ~60° to ~70° gave the best signal-to-noise ratio. Figure 3.4 shows the results for the antisymmetric and symmetric stretching vibrations for the different chain lengths.

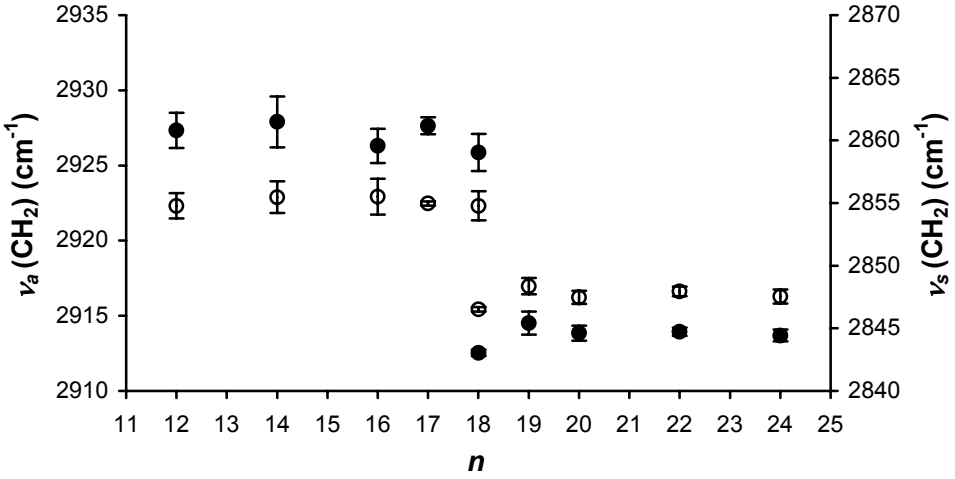

Figure 3.4 IRRAS band maxima for the antisymmetric (solid symbols) and symmetric (open symbols) C–H stretching vibrations of deposited alkane layers on Si(100) as a function of the chain length *n* of alkanes (C_nH_{2n+2}) (IRRAS data: p-polarized light, IR reflection angle 68°, in inverse centimeters).

It can be seen that the measured wavenumbers for the antisymmetric (~2928 cm^{-1}) and symmetric (~2856 cm^{-1}) C–H stretching vibrations of the liquid alkanes (n < 18) are comparable with the values found with conventional IR.[20] In contrast, the IRRAS values for the antisymmetric and symmetric C–H stretching vibration bands of the solid alkanes (n > 17) are found to be lower than the conventional IR values: 2914 cm^{-1} (vs 2920 cm^{-1}) and 2848 cm^{-1} (vs 2850 cm^{-1}), respectively. The results show that for the conditions used (68°,

p-polarized light) application of IRRAS yields in principle a larger difference between crystalline/nonisotropic media and isotropic media than conventional infrared measurements: 14 cm^{-1} (vs 8 cm^{-1}) for the antisymmetric C–H stretching vibration and 8 cm^{-1} (vs 6 cm^{-1}) for the symmetric C–H stretching vibration. The situation is best seen at the data points obtained for *n*-$C_{18}H_{38}$ (mp = 29-30 °C). At temperatures <15 °C solidlike data points are obtained, while at temperatures >35 °C the peaks belonging to a liquid state are observed. In fact, during the melting of solid octadecane two sharp peaks for both the symmetric and antisymmetric C–H stretching vibrations are observed, indicating the simultaneous presence of two distinct phases, i.e., degrees of organization. As IRRAS only uses external reflections, in contrast to ATR that relies on internal reflections, IRRAS is more broadly applicable, e.g., to IR-absorbing substrates (e.g., Si_3N_x).[1] In combination with the rather straightforward and fast implementation of the measurements, and the fact that it allows multiple techniques on the same surface, IRRAS is a potentially useful and informative infrared technique.

Analysis of the IRRAS data in Tables 3.3 and 3.4 shows that both the thermally and photochemically prepared covalently attached monolayers on silicon seem to fall in the regime of disordered materials. This is in contrast with ATR data on the same samples, which seem to indicate a substantial degree of anisotropy, i.e., some degree of ordering, perhaps stemming from the CH_2 moieties bound most closely to the surface. A more detailed analysis of this difference would be desirable, given the ease of use of IRRAS, but is outside the scope of the present study. At the moment it suffices to say that IRRAS is a viable technique to display the presence or absence of functional groups on the surface, and that the relation between ATR-obtained values for the C–H stretching vibrations in organic monolayers on silicon and the ordering of such monolayers deserves more detailed attention.

The usefulness of IRRAS can, e.g., be shown with IRRAS measurements of monolayers of compounds **3.1** and **3.2** (two bottom entries in Table 3.4). Not only can the antisymmetric and symmetric C–H stretching vibrations be observed, but also a clear C=O stretching vibration indicative of an ester can be observed (Figure 3.5). Hydrolysis of such esters can easily be followed by IRRAS as shown by our recent work on silicon nitride.[1] All in all, we believe IRRAS measurements to be a novel and convenient tool for the study of covalently attached organic monolayers.

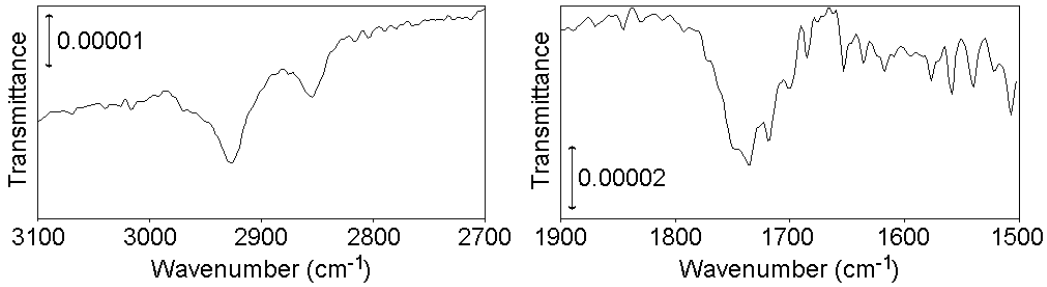

Figure 3.5 C–H (left) and C=O (right) stretching vibration regions of the IRRA spectrum of an n-type Si(100) modified with compound **3.1** using irradiation with 447 nm light (IR reflection angle 68°, p-polarized light).

3.3.4 Effect of the Type of Silicon: Doping Type, Doping Concentration, and Orientation

Hamers and co-workers studied the photoattachment of alkenes on partly I-terminated Si(111) and Si(100),[21] and reported significant effects of the doping of the Si wafers. Following this approach, we selected four different types of Si(100) wafers, lowly and highly doped n-type and lowly and highly doped p-type Si(100), and two types of Si(111), to perform a more systematic study. The surfaces were etched and modified with 1-hexadecene using 447 nm light. The contact angles of the resulting monolayers are plotted as a function of the irradiation time (Figure 3.6a). For any given irradiation time, the contact angles of monolayers on n-type Si(100) are higher as compared to those of monolayers on p-type Si(100). Since the preparation conditions (including light intensity) were constant, it can be concluded that the efficiency of the photochemical monolayer formation on n-type Si(100) is higher than on p-type Si(100). From Figure 3.6a it can also be seen that covalent attachment follows the rate order: highly doped n ≥ lowly doped n > lowly doped p > highly doped p.

Figure 3.6b presents the time-dependent contact angles of 1-hexadecene-derived monolayers on lowly doped n-type and highly doped p-type Si(111). According to the contact angle data, monolayer formation on Si(111) is complete after about 5 h, while it takes – using the same light intensity – about 10 h on Si(100). Despite the significant difference for the initially measured water contact angles for n- and p-type Si(111), the time at which the plateau value is reached depends only slightly on the doping type (4 vs 5 h for the n- and p-types, respectively), and the final contact angle (~109°) is identical in both cases.

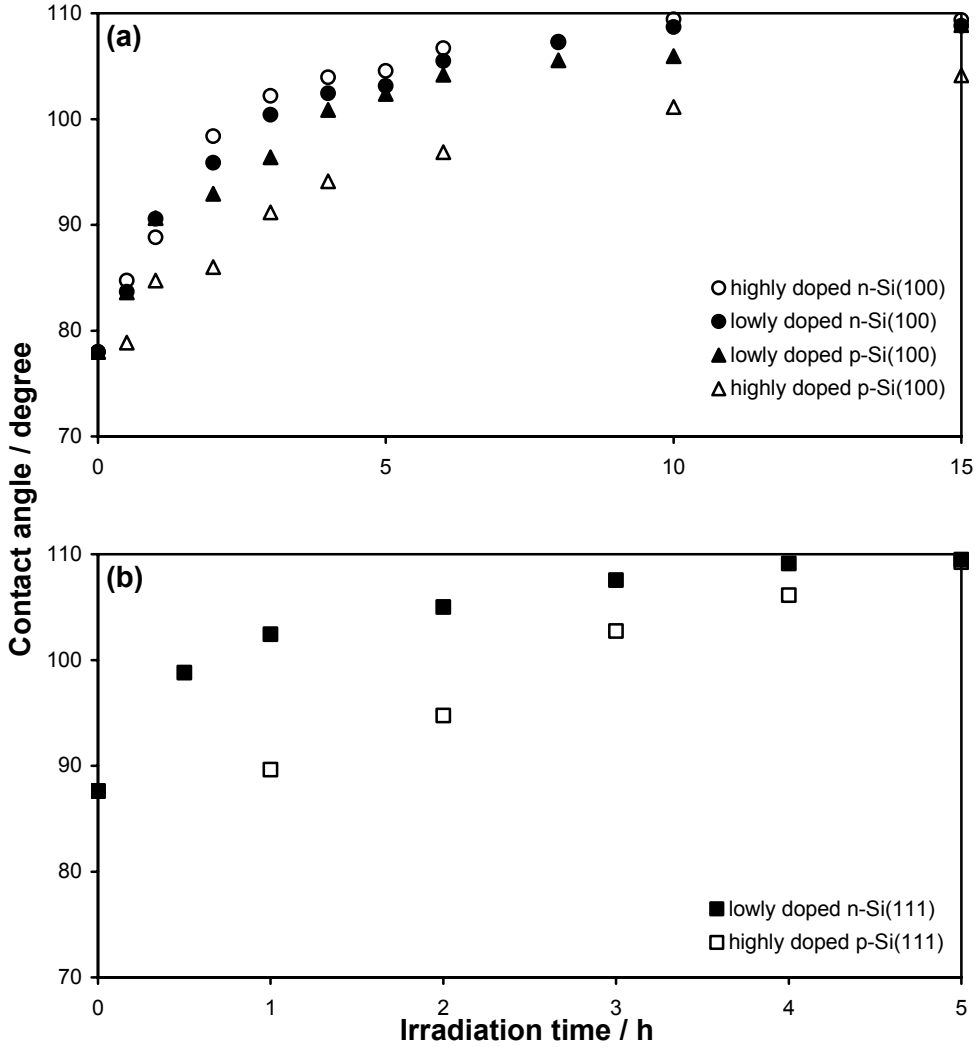

Figure 3.6 Water contact angles of *n*-hexadecyl monolayers as a function of irradiation time for different types of (a) Si(100) and (b) Si(111).

The differences between the reaction efficiency of lowly doped n-type silicon and heavily doped p-type Si(100) were also studied for 254, 371, 504, and 658 nm light (Figure 3.7). For all presented wavelengths, hydrogen-terminated n-type silicon surfaces are more reactive toward unsaturated hydrocarbons than p-type silicon surfaces. Note that different lamps with different intensities were used in this experiment. As a result comparison of efficiencies is only allowed for the different types of silicon that were modified with the same wavelength. The different reaction times required to obtain the plateau contact angles for the different wavelengths are in fact the result of differences in light intensity. However, it is evident that, using 254, 504, and 658 nm light, the high contact angles obtained at n-type Si(100) (~109°) could not be obtained at p-type Si(100). For practical purposes the use of n-type Si(100) or n-type Si(111) is therefore strongly advocated.

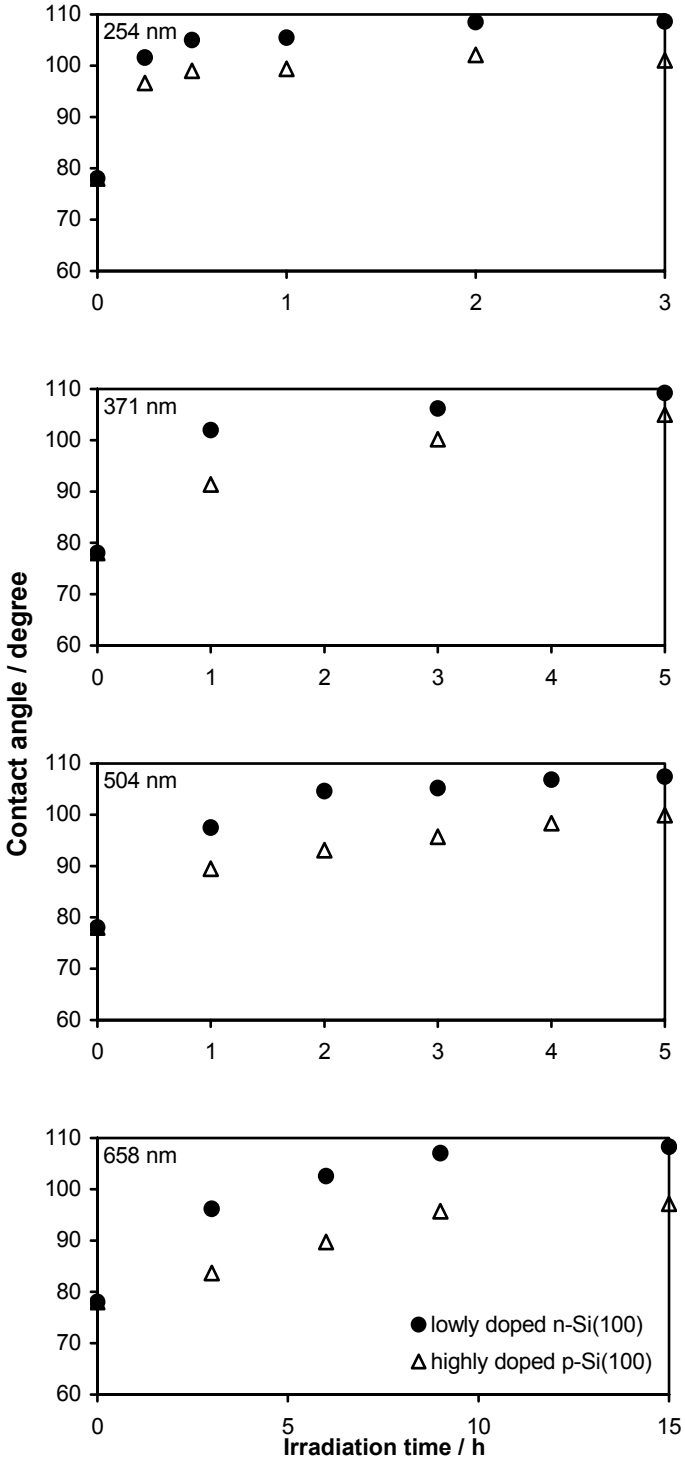

Figure 3.7 Contact angles of *n*-hexadecyl monolayers as a function of irradiation time for lowly doped n-type Si(100) and highly doped p-type Si(100) using 254, 371, 504, and 658 nm light, respectively.

The reactivity of H-terminated silicon toward 1-alkenes in the absence of both heat and light was also studied. When a freshly etched hydrogen-terminated Si(100) sample in an argon-saturated 1-hexadecene/mesitylene solution was kept in the dark for 15 h at room

temperature, the contact angle of the sample did not change (~78°). Since an increase of the contact angle would indicate monolayer formation and a decrease would imply oxidation, it can be concluded that the hydrogen-terminated surface was stable during this experiment. IRRAS showed low amounts of C–H stretching vibrations. Most likely there is some attachment due to surface defects/dangling bonds. However, to obtain a hydrophobic monolayer, light or heat is required.

While the present work clearly displays the scope of the visible light attachment, the mechanism of this reaction is much less clear. In Chapter 2 we hypothesized that an electron/hole pair dissociation mechanism (Scheme 2.3) would be feasible. However, two arguments cause us to refine our hypothesis. First, using scanning tunneling microscopy (STM) on partially formed monolayers of 1-decene on hydrogen-terminated Si(111), we showed, in collaboration with Eves and Lopinski, that the reaction likely proceeds via a radical chain mechanism.[22] This suggests that after some initiation process reactive sites/dangling bonds are formed at the surface that can initiate a chain reaction. Second, and more complex, is the role of supposed band bending in these materials,[21,23] since the surface is in contact with a nonconducting solution. Therefore, it is presently difficult to ascertain the degree of band bending that does actually occur in these wafers in contact with a mesitylene solution, while additionally other factors – e.g., faster oxidation of p-type hydrogen-terminated silicon than n-type hydrogen-terminated silicon – might also play a role. This complication also arises for the case of UV light initiation, as the top left graph in Figure 3.7 shows a dopant dependence for that wavelength as well, which cannot be fit into the mechanism (Scheme 2.3) proposed for that reaction[24] without involving a silicon substrate-dependent parameter.

The discussion of the mechanism of the visible light-induced reaction therefore needs to be limited to a rather broad delineation. The cleavage of a Si–H bond requires light of <350 nm, whereas <540 nm is needed for the cleavage of a Si–Si bond. Since attachment and the formation of hydrophobic monolayers can be established with visible light of wavelengths even larger than 650 nm, an initiation step involving a (homolytic) cleavage of the Si–H or Si–Si bonds is not possible. Therefore, a different initiation is required. In addition, the mechanism presented in Scheme 2.3 cannot explain the observation of island formation in the attachment of 1-decene to hydrogen-terminated Si(111) as shown by STM.[22]

We therefore tentatively propose a new mechanism in Scheme 3.1. Due to the formation of delocalized radical cations at the silicon surface (electrons temporarily being moved to the bulk) upon excitation thereof, this surface is susceptible to nucleophilic attack. Such a

reaction may result in a Si–Si bond cleavage in a concerted manner, as in Si–Si-containing radical cations the Si–Si bond is not very strong, while the resulting Si-centered cation at the surface is highly stabilized by the neighboring Si atoms. As a result we obtain the structure at the bottom left in Scheme 3.1, with a β-CH radical site. This radical can pick up a H atom, and leave a Si radical at the surface that is available for the attachment of a second alkene. A chain mechanism can also rationalize the differences in efficiency between Si(100) and Si(111). Since the Si(111) is more flat as compared to Si(100) (see, e.g., Figure 3.2), the chain formation on the latter surface will be hampered due to larger steps between the terraces. As a result the monolayer formation on Si(111) is more efficient.

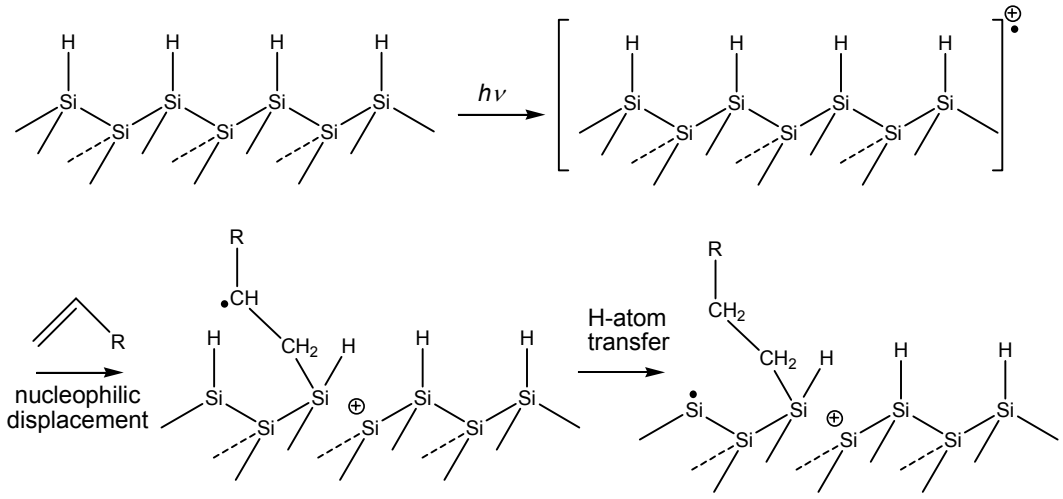

Scheme 3.1 Proposed mechanism for the initiation of the light-induced reaction.

3.3.5 Mixed Monolayers

An important issue in the preparation of well-defined surfaces with highly functionalized materials, e.g., for application in sensor technology, is the control over the amount and depth distribution of sensing functionalities in mixed monolayers. In Chapter 2, we revealed the relation between the ratio of two esterified 1-alkenes in solution and their relative amounts in the resulting mixed monolayer as prepared with the visible light method. XPS showed a linear relation between the amount of fluorine in the monolayer and the mole fraction of the fluorine-containing ester in the solution used in the preparation of the monolayer (Figure 2.7), but we could – in hindsight – not fully exclude trace amounts of carbonyl group-related photochemistry. To allow a completely unambiguous study of mixed monolayers obtained via both thermal attachment and visible light attachment, we aimed to keep the system as stable and as simple as possible by choosing 1-decene and 11-fluoro-1-undecene as a binary system. The latter compound was synthesized in two steps from the commercially

available alcohol derivative. For each of the six different ratios that was used a solution of the two 1-alkenes in mesitylene was divided over the photochemical and thermal setups, to ensure the comparability of the two methods. After the modification of hydrogen-terminated Si(100), the resulting monolayers were studied with water contact angles (Figure 3.8) and XPS (Figure 3.9).

The water contact angles of the mixed monolayers were plotted against the mole fraction of 11-fluoro-1-undecene in the mesitylene solution (Figure 3.8, top). The contact angles of monolayers prepared with 100% 1-decene (mole fraction of F-compound, 0) are the same for both preparation techniques. However, for every mole fraction >0 the contact angle of a thermally prepared monolayer is slightly higher than that of the corresponding photochemically prepared monolayer.

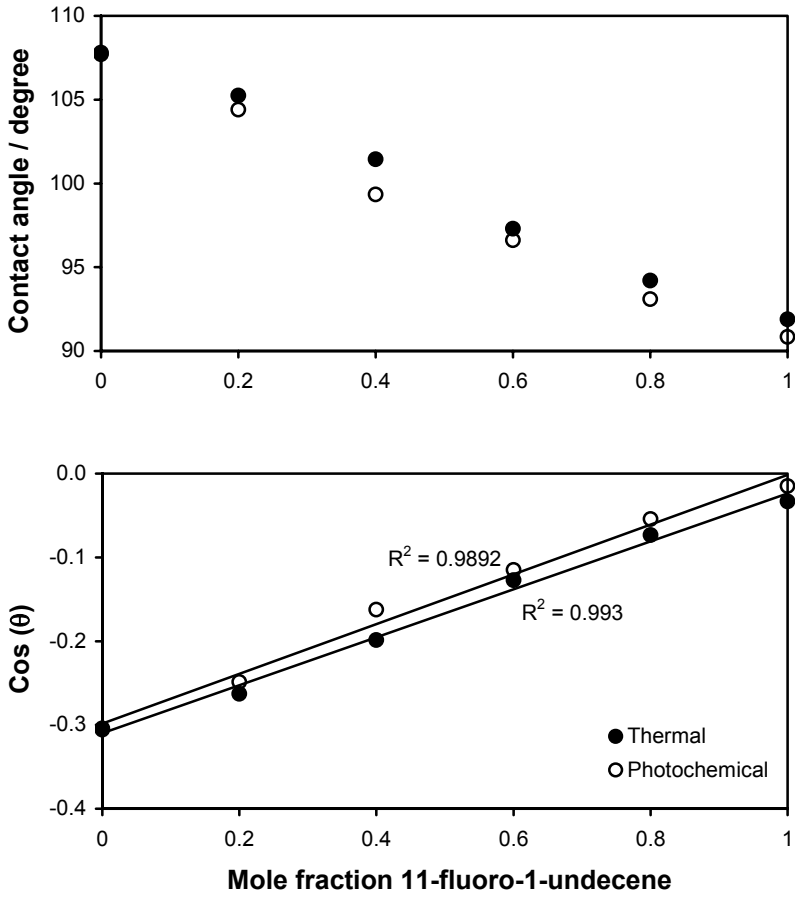

Figure 3.8 Water contact angle (top) and cosine of the water contact angle (bottom, linear least-squares fit) of mixed monolayers derived from 11-fluoro-1-undecene and 1-decene as a function of the mole fraction of 11-fluoro-1-undecene in the mesitylene solution used for the thermal (solid symbols) and visible light (open symbols) modification of H-terminated Si(100).

According to Cassie,[25] the contact angle θ of a drop of water on a heterogeneous surface made up of patches of two different types of polarities is related to the contact angle θ_i of each of the patches via the following equation:

$$\cos\theta = f_1 \cos\theta_1 + f_2 \cos\theta_2 \qquad [3.1]$$

The cosine of the water contact angles of the mixed monolayers was plotted against the mole fraction (Figure 3.8, bottom). The linear trend lines have high R^2 values, indicating that Cassie's relation is applicable to this binary system. Two other binary systems on silicon[10,16] that were studied with Cassie's relation showed a lower correlation between solution composition and wetting behavior than the present data. Most likely this is related to the nature of the functional groups, which differ relatively little regarding shape, size, and polarity in the present case, and thus provides a more ideal application for the Cassie relation.

Figure 3.9 presents the results of XPS measurements (F_{1s}/Si_{2p} ratio) of the mixed monolayer, and clearly shows a linear relation between the amount of F on the surface and in solution for both the photochemical and thermal methods. The presence of a small amount of F for the 1-decene monolayer (0% 11-fluoro-1-undecene in solution) is the result of the etching procedure.

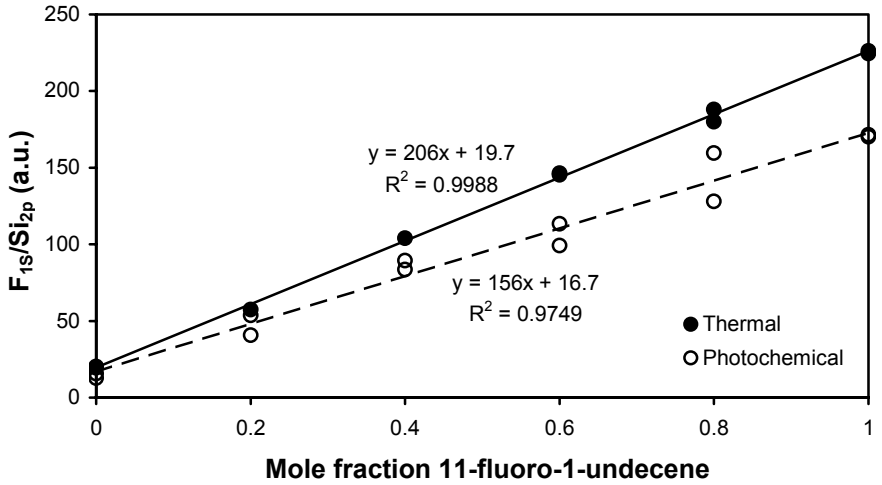

Figure 3.9 XPS F_{1s}/Si_{2p} ratio of mixed monolayers of 11-fluoro-1-undecene and 1-decene as a function of the percentage of 11-fluoro-1-undecene in the mesitylene solution used for the thermal (solid symbols) and visible light (open symbols) modification of H-terminated Si(100).

The data show that the distribution of two molecules on the surface can be controlled via their ratio in the solution that is used for the preparation. However, the slope of the given trend lines is different for the two preparation techniques, and the visible light method results according to these XPS data in a grafting density that is about 25% lower than obtained via the thermal method. It is currently unclear to which degree this is a general feature of the photochemical method, or whether this is typical for the systems in the present study, given the observation (Figure 3.8) that for this system the contact angles of the photochemically prepared samples are systematically somewhat lower than for the thermally prepared samples, which is not the case for other systems in the present study (e.g., Table 3.1). Photoreactivity of specifically the 11-fluoro-1-undecene can be excluded as its cause, not only because 11-fluoro-1-undecene does not display any significant light absorption at 447 nm, but also because gas chromatography analysis of samples before and after irradiation does not display any photoproducts, and yields a constant amount of 11-fluoro-1-undecene (in comparison to an internal standard). More detailed studies are therefore required to clarify this observation.

Very recently, Liu et al. also used two techniques – IR and water contact angle measurement – to study mixed ω-carboxyalkyl/alkyl monolayers on Si(111).[10] The absorbance ratio $\nu(C=O)/\nu_{antisymm}(CH_2)$ showed a nearly linear relation with the mole fraction of the ester, while the correlation between surface and solution composition based on contact angles was clearly different. By stating that the Cassie relation is debatable, particularly when the surface contains two totally dispersed species, the authors believe that the spectroscopic data provide more reliable composition information than the wetting studies. Our data display a good applicability of Cassie's law, but we agree that quantitative information is better obtained from other sources, such as XPS in the present study.

3.4 Conclusions

Well-defined and highly stable organic monolayers on silicon surfaces can easily be prepared by irradiating a hydrogen-terminated silicon wafer with visible light at room temperature in the presence of a 1-alkene or 1-alkyne. Using a combination of water contact angles, X-ray reflectivity, X-ray photoelectron spectroscopy, atomic force microscopy, and infrared reflection-absorption spectroscopy, it was shown that high-quality monolayers can be formed in this manner. The reaction is rather flexible with regard to the wavelength of irradiation (371 to larger than 650 nm) and light source, and thus can avoid any light absorption by the agent that needs to be attached. These extremely mild conditions are

compatible with a very large variety of biologically active moieties that can be covalently linked to the reactive alkene or alkyne functionality. This method thus allows the development of patterned, (bio)active monolayers, via the combination of (bio)organic chemistry, surface science, and (nano)lithographic techniques.

Finally, a mechanism for this reaction was tentatively proposed, and the use of IRRAS for the study of organic monolayers was evaluated and proposed as an easy alternative for attenuated total reflectance IR spectroscopy.

Acknowledgment

Dr. Greg Lopinski and dr. Dan Wayner (NRC, Ottawa, Canada) and dr. Alex Sieval (Nano-C, Groningen, The Netherlands) are thanked for stimulating discussions.

References and Notes

[1] Arafat, A.; Schröen, K.; de Smet, L. C. P. M.; Zuilhof, H.; Sudhölter, E. J. R. *J. Am. Chem. Soc.* **2004**, *126*, 8600-8601.

[2] Sieval, A. B.; Demirel, A. L.; Nissink, J. W. M.; Linford, M. R.; van der Maas, J. H.; de Jeu, W. H.; Zuilhof, H.; Sudhölter, E. J. R. *Langmuir* **1998**, *14*, 1759-1768.

[3] Sieval, A. B.; Opitz, R.; Maas, H. P. A.; Schoeman, M. G.; Meijer, G.; Vergeldt, F. J.; Zuilhof, H.; Sudhölter, E. J. R. *Langmuir* **2000**, *16*, 10359-10368.

[4] This value was obtained via a semi-empiric calculation (MOPAC, PM3, closed shell restricted) in Chem3D Pro.

[5] Cattaruzza, F.; Cricenti, A.; Flamini, A.; Girasole, M.; Longo, G.; Mezzi, A.; Prosperi, T. *J. Mater. Chem.* **2004**, *14*, 1461-1468.

[6] Boukherroub, R.; Morin, S.; Bensebaa, F.; Wayner, D. D. M. *Langmuir* **1999**, *15*, 3831-3835.

[7] Cornelisse, J. *Chem. Rev.* **1993**, *93*, 615-669.

[8] Strother, T.; Hamers, R. J.; Smith, L. M. *Nucleic Acid Res.* **2000**, *28*, 3535-3541.

[9] Lin, Z.; Strother, T.; Cai, W.; Cao, X.; Smith, L. M.; Hamers, R. J. *Langmuir* **2002**, *18*, 788-796.

[10] Liu, Y.-J.; Navasero, N. M.; Yu, H.-Z. *Langmuir* **2004**, *20*, 4039-4050.

[11] Boukherroub, R.; Wayner, D. D. M.; Wojtyk, J. T. C. *US Patent 6677163* (January 13, 2004).

[12] Jennings, G. K.; Laibinis, P. E. *J. Am. Chem. Soc.* **1997**, *119*, 5208-5214.

[13] Laibinis, P. E.; Whitesides, G. M. *J. Am. Chem. Soc.* **1992**, *114*, 1990-1995.

[14] Linford, M. R.; Chidsey, C. E. D. *J. Am. Chem. Soc.* **1993**, *115*, 12631-12632.

[15] Linford, M. R.; Fenter, P. E.; Eisenberger, P. M.; Chidsey, C. E. D. *J. Am. Chem. Soc.* **1995**, *117*, 3145-3155.

[16] Sieval, A. B.; Linke, R.; Heij, G.; Meijer, G.; Zuilhof, H.; Sudhölter, E. J. R. *Langmuir* **2001**, *17*, 7554-7559.

[17] Boukherroub, R.; Wayner, D. D. M. *J. Am. Chem. Soc.* **1999**, *121*, 11513-11515.

[18] Brunner, H.; Mayer, U.; Hoffmann, H. *Appl. Spectrosc.* **1997**, *51*, 209-217.

[19] Sieval, A. B.; Vleeming, V.; Zuilhof, H.; Sudhölter, E. J. R. *Langmuir* **1999**, *15*, 8288-8291.

[20] Snyder, R. G.; Strauss, H. L.; Ellger, C. A. *J. Phys. Chem.* **1982**, *86*, 5145-5150.

[21] Cai, W.; Lin, Z.; Strother, T.; Smith, L. M.; Hamers, R. J. *J. Phys. Chem. B* **2002**, *106*, 2656-2664.

[22] Eves, B. J.; Sun, Q.-Y.; Lopinski, G. P.; Zuilhof, H. *J. Am. Chem. Soc.* **2004**, *126*, 14318-14319.

[23] Sun, Q.-Y.; de Smet, L. C. P. M.; van Lagen, B.; Wright, A.; Zuilhof, H.; Sudhölter, E. J. R. *Angew. Chem. Int. Edit.* **2004**, *43*, 1352-1355.

[24] Cicero, R. L.; Linford, M. R.; Chidsey, C. E. D. *Langmuir* **2000**, *16*, 5688-5695.

[25] Cassie, A. B. D. *Discuss. Faraday Soc* **1948**, *3*, 11-16.

Chapter 4

Covalently Attached Carbohydrates on Silicon Surfaces*

Abstract – This chapter describes the synthesis of different alkenylated monosaccharide derivatives and the preparation and characterization of monolayers on silicon containing these compounds. The derivatives were alkenylated at the C-1 position, while the remaining hydroxyl groups were protected. Mixed monolayers containing these carbohydrate derivatives on hydrogen-terminated were analyzed by attenuated total reflection infrared spectroscopy (ATR-IR) and (angle-resolved) X-ray photoelectron spectroscopy (ARXPS).

* This chapter is based on:

- de Smet, L. C. P. M.; Stork, G. A.; Hurenkamp, G. H. F.; Sun, Q.-Y.; Topal, H.; Vronen, P. J. E.; Sieval, A. B.; Wright, A.; Visser, G. M.; Zuilhof, H.; Sudhölter, E. J. R. *J. Am. Chem. Soc.* **2003**, *125*, 13916-13917.
- de Smet, L. C. P. M.; Pukin, A. V.; Stork, G. A.; de Vos, C. H. R.; Visser, G. M.; Zuilhof, H.; Sudhölter, E. J. R. *Carbohydr. Res.* **2004**, *339*, 2599-2605.

4.1 Introduction

Only very recently the construction of carbohydrate arrays on glass has been reported.[1,2] This allows for optical or spectroscopic detection of specific carbohydrate-protein interactions. Given the essential role of carbohydrates in many biological processes, the development of new carbohydrate sensing elements will likely provide a tremendous stimulus to this field. The application of modified silicon in this area can open up a whole new field of research, as the semi-conducting nature of the substrate provides a unique feature in silicon-based biosensing.[3-5] This latter property allows for detection of selective recognition of, e.g., antibodies to oligosaccharide receptors via changes in capacitance. An example of this principle can be found in a recent study in which real time capacitance measurements were performed to monitor DNA hybridization on oligodeoxynucleotide-modified silicon.[6]

Apart from our work, there is on other example of attached monosaccharides on crystalline silicon. The work of Shirahata et al.[7] describes the preparation of homogeneous monolayers of allyl α-D-galactopyranoside on the Si(100)–H surface. The authors observed specific adsorption of ricinus communis agglutinin (RCA_{120}) molecules from a contacting solution as well as nonspecific adsorption on the Si–O area.

For the direct preparation of well-defined monolayers of carbohydrate derivatives on silicon surfaces at least two structure properties are required: a) presence of an ω-alkenyl tail in order to perform the hydrosilylation reaction, and b) protection of the hydroxyl groups – of both alcohols and acids – in order to prevent the interfering reaction between these groups and the hydrogen-terminated silicon surface.[8-10]

In §4.3.1 the synthesis of three monosaccharides with those properties is described. In §4.3.2 mixed monolayers containing those monosaccharide derivatives were characterized. In contrast to the work of Shirahata et al.[7] we have chosen carbohydrate derivatives that do not have properties regarding any specific adsorption. In our case, the compounds were used to develop different methods and conditions to produce the first case of well-defined carbohydrate-substituted monolayers. Two methods were used to obtain this aim: a thermal method (refluxing in mesitylene) and an extremely mild photochemical method (irradiation with 447 nm).

4.2 Experimental

4.2.1 General Information

CH_2Cl_2 and CH_3CN were distilled over CaH_2. Distilled MeOH was dried over 3Å molecular sieves. Pyridine was dried over KOH. All solvents for extractions and chromatography were distilled. All reactions were carried out under a nitrogen or argon atmosphere with glassware dried at ≥120 °C. Commercially available reagents were used without purification. Thin layer chromatography (TLC) was performed on E. Merck Silica Gel 60F254 plastic sheets, and detection was realized by either of the following methods: charring with a solution of $KMnO_4$(aq), molybdenum reagents [ammonium molybdate (21 g), ammonium cesium(IV) sulfate (1.8 g), water (469 mL), and H_2SO_4 (31 mL)], 5% (v/v) sulfuric acid in MeOH and subsequent heating or UV detection. Column chromatography was conducted by elution of a column of Merck Kieselgel silica (230-400 Mesh) using eluents as specified below. NMR spectra were recorded on a Bruker AC-E 200 or a Bruker DPX 400 spectrometer in solvents as specified below at room temperature.

Samples of compounds **4.3**, **4.6**, and **4.10** were subjected to accurate Mass Spectroscopy (MS) on a high-resolution quadrupole time-of-flight mass spectrometer (QTOFMS) with lock mass correction.[11] The QTOF mass spectrometer (Ultima, Waters Corporation) was equipped with an electrospray ionization (ESI) source and was calibrated with 0.05% phosphoric acid in 50% acetonitrile. The carbohydrate derivatives were dissolved and diluted in 75% acetonitrile and subsequently injected at 10 µL/min using a syringe pump (Harvard Apparatus PHD2000). The following settings were applied: desolvation temperature of 250 °C with a nitrogen gas flow of 300 L/h, capillary spray at 2.5 kV, source temperature of 120 °C, cone voltage at 35 eV with 50 L/h nitrogen gas flow, collision energy ranging from 3 to 10 eV (depending on compound). Ions in the m/z range 70 to 1500 were detected in centroid mode, using a scan time of 0.9 s and an interscan delay of 0.1 s. In case the mass signal was not detectable or too low for reliable accurate mass measurements, formic acid (0.1%) or ammonium acetate (2 mM) was added to enhance the signal. Leucine enkaphalin in 50% acetonitrile plus 2 mM ammonium acetate was used as a lock mass (recorded every 10 s), injected at a flow rate of 10 µL/min using a separate syringe pump. MassLynx software version 4.0 (Waters) was used to control the MS and to calculate accurate masses.

Hydrogen-terminated silicon surfaces were obtained via etching of single polished, native oxide-covered n-Si(100) wafers in 2.5 % aqueous HF solution for 1-2 min. Monolayer

preparation was performed using the conditions as described in §3.2.5. Photochemical modifications in this chapter were performed using 447 nm light. The total alkene concentration of the samples studied in this chapter was in the range of 0.05 M to 0.1 M.

Infrared spectra (512 scans, 0.25 cm^{-1}) of the monolayers were recorded on a Perkin Elmer 1725X FT-IR spectrometer, equipped with a liquid nitrogen-cooled MCT detector, using a fixed angle multiple reflection attachment (Harrick Scientific). The infrared light was incident on one of the 45° bevels of the ATR crystal. Spectra of the monolayers were recorded with *s*- and *p*-polarized light, which yielded almost identical results. A clean Si ATR crystal was used as a background. All crystals were cleaned in chloroform before mounting. The region spectra shown in Figure 4.1 are the result of spectral subtraction of modified samples with a cleaned native oxide-covered silicon ATR crystal without any further data manipulation.

4.2.2 Synthesis of Carbohydrate Derivatives

10-Undecenyl 2,3,4,6-Tetra-*O*-Acetyl-β-D-Glucopyranoside (4.3)

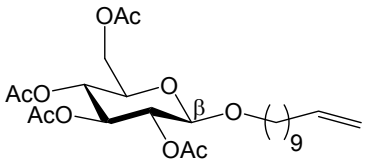

4.3

A solution of penta-*O*-acetyl-β-D-glucopyranose (**4.1**) (6.59 g, 16.9 mmol), 10-undecen-1-ol (**4.2**) (7.5 mL, 37.2 mmol) and 4Å molecular sieves (3.5 g) in CH_2Cl_2 (dry, 30 mL) was stirred at room temperature. Subsequently, $SnCl_4$ (2.0 mL) was added in one portion by syringe. After 6.5h $NaHCO_3$ (2.5 g) and $MgSO_4$ (2.5 g) were added. The solution was filtered over a celite layer and the filtrate was concentrated under reduced pressure. Column chromatography (PE 40/60:EtOAc = 4:1) yielded **4.3** (3.20 g, 38%) as a colorless oil.

TLC R_f (PE 40/60:EtOAc = 1:1) = 0.44; **^{1}H NMR** (200 MHz, $CDCl_3$): δ 5.90-5.69 (m, 1H, C*H*=CH_2), 5.20 (t, 1H, *J* 9.3 Hz, H-3), 5.07 (t, 1H, *J* 9.5 Hz, H-2), 5.05-4.85 (m, 2H, CH=*C*H_2), 4.47 (d, 1H, *J* 7.9 Hz, H-1), 4.30-4.22 (dd, 1H, $J_{6,6'}$ 12.3 Hz, $J_{5,6}$ 4.6 Hz, H-6, 4.15-4.08 (dd, 1H, $J_{6,6'}$ 12.2, $J_{5,6'}$ 2.4 Hz, H-6'), 3.91-3.80 (dt, 1H, ^2J 9.6, ^3J 6.3 Hz, OCH_a), 3.72-3.63 (m, 1H, H-5), 3.38-3.52 (dt, 1H, ^2J 9.6, ^3J 6.7 Hz, OCH_b), 2.07-1.98 (m, 14H, CH_2CH=CH_2 + 4 × OCH_3 at 2.07, 2.03, 2.01, 1.99), 1.70-1.47 (m, 2H, OCH_2CH_2), 1.25 (s, 12H, $(CH_2)_6$); **^{13}C NMR** (50 MHz, $CDCl_3$): δ 170.7, 170.4, 169.4, 169.3 (4 × C=O), 139.2 (*C*H=CH_2), 114.1 (CH=*C*H_2), 100.8 (C-1), 72.9 (C-3), 71.7 (C-5), 71.3 (C-2), 70.3 (OCH_2), 68.5 (C-4), 62.0 (C-6), 33.8 (*C*H_2CH=CH_2), 29.5, 29.4, 29.4, 29.3, 29.1, 28.9 (6 × CH_2), 25.8

(OCH_2CH_2), 20.8 (CH_3), 20.7 (3 × CH_3); **QTOFMS** $[M-H]^-$ 499.2541 (calcd 499.2543; Δ ppm = -0.4); $[M+H]^+$ 501.2711 (calcd 501.2699; Δ ppm = 2.3).

10-Undecenyl β-D-Glucopyranoside (4.4)

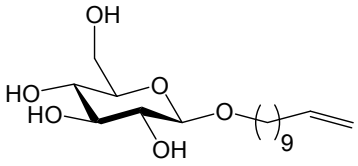

4.4

Compound **4.3** (2.62 g, 5.23 mmol) was dissolved in MeOH (dry, 30 mL). Freshly prepared 1M $NaOCH_3$ (150 μL) was added. The solution was stirred at room temperature and the conversion was followed by TLC (EtOAc). After ~2 h the starting material (R_f ~ 0.5) was converted into a more polar compound (R_f ~ 0.2). The reaction was quenched by adding Dowex-50 [H^+] resin. After standing overnight, the mixture was filtered, and the filtrate was concentrated, yielding **4.4** (1.66 g, 96%) as a colorless viscous oil.

TLC R_f (PE 40/60:EtOAc = 1:1) = ~0; **^{1}H NMR** (200 MHz, CD_3OD): δ 5.90-5.70 (m, 1H, C*H*=CH_2), 5.02-4.88 (m, 2H, CH=*C*H_2), 4.23 (d, 1H, *J* 7.7 Hz, H-1), 3.95-3.83 (m, 2H), 3.69-4.46 (m, 2H), 3.39-3.03 (m, 6H), 2.05-1.97 (q, 2H, *J* ~6.7 Hz, CH_2CH=CH_2), 1.64-1.55 (m, 2H, OCH_2CH_2), 1.31 (s, 12H, $(CH_2)_6$); **^{13}C NMR** (50 MHz, CD_3OD): δ 140.2 (*C*H=CH_2), 114.7 (CH=*C*H_2), 104.2 (C-1), 78.1, 77.9, 75.1, 71.6 (C-3, C-5, C-2, and C-4), 70.9 (OCH_2), 62.7 (C-6), 34.9 (*C*H_2CH=CH_2), 30.6, 30.2, 30.1, 29.0, 27.5, 27.1 (6 × CH_2 and OCH_2CH_2).

10-Undecenyl 6-*O*-Trityl-β-D-Glucopyranoside (4.5)

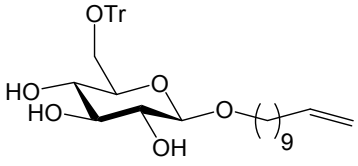

4.5

Compound **4.4** (1.66 g, 5.01 mmol) was dissolved in pyridine (dry, 19 mL). Tritylchloride (1.67 g, 6.00 mmol) and a catalytic amount of DMAP were added. The mixture was stirred at room temperature. The reaction was followed by TLC (PE 40/60:EtOAc = 2:1; R_f product = ~0,8). After 24h the reaction mixture was poured onto ice water (ca. 150 mL). The mixture was extracted with CH_2Cl_2 (2 × 60 mL and 2 × 30 mL, respectively). The combined organic layers were washed with $NaHCO_3$ (3 × 50 mL). The organic layer was dried over $MgSO_4$, filtered, and concentrated. Traces of pyridine were co-evaporated with toluene (3×). Column chromatography (CH_2Cl_2:MeOH = 19:1 with 1 drop of TEA per 100 mL) yielded **4.5** (1.84 g, 64%).

TLC R_f (CH_2Cl_2:MeOH = 19:1) = ~0.3; **^{1}H NMR** (200 MHz, $CDCl_3$): δ 7.47-7.23 (m, 15H, aromatic H), 5.91-5.70 (m, 1H, C*H*=CH_2), 5.02-4.90 (m, 2H, CH=*C*H_2), 4.26 (d, 1H, *J* 7.5 Hz, H-1), 3.55-3.39 (m, 7H), 3.27 (bs, 1H), 3.10 (bs, 1H), 2.76 (bs, 1H), 2.07-1.97 (q, 2H, *J* ~6.8 Hz, CH_2CH=CH_2), 1.72-1.57 (m, 2H, OCH_2CH_2), 1.27 (s, 12H, $(CH_2)_6$); **^{13}C NMR** (50 MHz,

$CDCl_3$): δ 143.5 (C-6–OC*C*), 139.2 (*C*H=CH_2), 128.6, 127.9, 127.1 (aromatic C), 114.1 (CH=*C*H_2), 102.4 (C-1), 87.1 (C(phenyl)$_3$), 76.2, 73.6, 73.6, 72.2 (C-2, C-3, C-4, and C-5), 70.1 (OCH_2), 64.4 (C-6), 33.8 (*C*H_2CH=CH_2), 29.6, 29.5, 29.4, 29.1, 28.9 (CH_2), 26.0 (OCH_2*C*H_2).

10-Undecenyl 2,3,4-*O*-(3-Trifluoromethylbenzoyl)-6-O-Trityl-β-D-Glucopyrano-side (4.6)

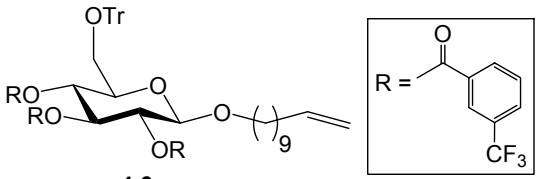

4.6

Compound **4.5** (0.91 g, 1.58 mmol) was dissolved in pyridine (dry, ~10 mL). The solution was stirred at 0 °C and 3-(trifluoro-methyl)benzoyl-chloride (1.46 mL, 9.66 mmol) and a catalytic amount of DMAP were added. The course of the reaction was followed by TLC. After 44h the mixture was poured into ice water (~135 mL). The mixture was separated and the aqueous layer was extracted with CH_2Cl_2 (50, 25, and 25 mL, respectively). The combined organic layers were washed successively with saturated $NaHCO_3$ (50 mL) solution and twice with water (50 and 35 mL, respectively). The organic layer was dried over $MgSO_4$. The solution was concentrated under reduced pressure and traces of pyridine were removed by co-evaporation with small volumes of toluene (4×). Column chromatography (CH_2Cl_2:PE 40/60 = 1:1) yielded **4.6** (1.33 g, 77%).

TLC R_f (PE 40/60:CH_2Cl_2 = 1:1) = 0.41; R_f (PE 40/60:EtOAc = 1:1) = 0.25; **^{1}H NMR** (200 MHz, $CDCl_3$): δ 8.15-6.98 (m, 27H, aromatic H), 5.9-5.5 (m, 1H, C*H*=CH_2), 5.79-5.59 (m, 4H), 4.95-4.74 (m, 3H), 4.76 (d, 1H, ^3J 7.8 Hz, H-1), 3.96-3.92 (dt, 1H, ^2J 9.7, ^3J 6.3 Hz, OCH_a), 3.83-3.78 (m, 1H, H-5), 3.58-3.53 (dt, 1H, ^2J 9.7, ^3J 6.7 Hz, OCH_b), 3.38-3.32 (dd, 1H, $J_{6,6'}$ 10.5, $J_{5,6}$ 2.2 Hz, H-6), 3.19-3.11 (dd, 1H, $J_{6,6'}$ 10.6, $J_{5,6'}$ 4.6 Hz, H-6'), 1.98-1.87 (q, 2H, J ~7.0 Hz, C*H*$_2$CH=CH_2), 1.23-1.13 (m, 12H, $(CH_2)_6$); **^{13}C NMR** (50 MHz, $CDCl_3$): δ 164.8, 163.9, 163.5 (3 × C=O), 143.4 (C-6–OC*C*), 139.2 (*C*H=CH_2), 132.9, 132.8, *131.5*, *130.7*, *130.2*, 129.9, *129.6*, 129.0, 128.6, 127.7, 127.0, 126.7 (aromatic C atoms, quaternary C atoms in italics), ~120.8 and ~115.4 (2 × 3 signals from quartet, $J_{C,F}$ 273 Hz, CF_3. N.B. Only two signals of each quartet were observed, since the other two overlap with the signals from the aromatic region; the shift of each quartet is about 3 Hz), 114.1 (CH=*C*H_2), 101.0 (C-1), 86.7 (C(phenyl)$_3$), 74.1, 73.5, 72.7, 69.9 (C-2, C-3, C-4, and C-5), 70.1 (OCH_2), 62.2 (C-6), 33.8 (*C*H_2CH=CH_2), 29.5, 29.4, 29.3, 29.1, 28.9 (6 × CH_2), 26.0 (OCH_2*C*H_2); **QTOFMS** $[M-H]^-$ not found (calcd 1089.3624), $[M-H+HCOOH]^-$ 1135.3696 (calcd 1135.3679; Δ ppm = 1.5); $[M+H]^+$ 1091.3823 (calcd 1091.3780; Δ ppm = 3.7).

Methyl (5-acetamido-4,7,8,9,-tetra-*O*-acetyl-3,5,-dideoxy-D-*glycero*-β-D-*galacto*-nonulopyranosylchloride) onate (4.9)

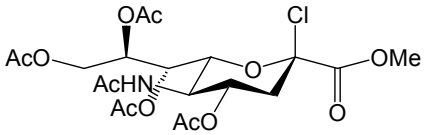

4.9

A suspension of compound **4.7** (1.5 g, 4.85 mmol) in 50 mL of MeOH, containing 1.5 g of Amberlite IR-120 (H^+) was stirred overnight at room temperature. After that, a second portion of 1.5 g of Amberlite IR-120 (H^+) was added. After stirring for another 7 h a clear solution was obtained. The resin was filtered off, and the solution was evaporated giving a dark viscous oil. The latter was dissolved in minimal amount of MeOH, and Et_2O was added to turbidity. Upon standing methyl N-acetyl-α-D-neuraminate (**4.8**) crystallized (1.6 g).

Freshly distilled acetyl chloride (30 mL) was added dropwise to ice-cooled methyl N-acetyl-α-D-neuraminate (**4.8**) (0.8 g, 2.47 mmol) over 15 min. The suspension was allowed to warm to room temperature and was stirred for 48 h. The reaction mixture was evaporated to dryness and co-evaporated a few times with dry toluene at 35 °C. The residue was crystallized from a benzene/hexane/Et_2O mixture to give compound **4.9** (0.83 g, 66%) as a colorless solid. The ^1H NMR and ^{13}C NMR spectra of compounds **4.8** and **4.9** data were in accordance with those in literature.[12]

Methyl (undec-10-enyl 5-acetamido-4,7,8,9,-tetra-*O*-acetyl-3,5,-dideoxy-D-*glycero*-D-*galacto*-nonulopyranosylchloride) onate (4.10)

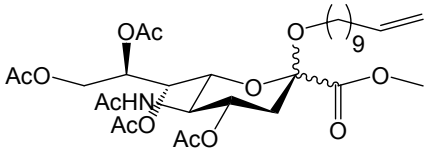

4.10

Compound **4.9** (0.15 g, 0.294 mmol) was dissolved in dry acetonitrile (5 mL) containing 10-undecen-1-ol (**4.2**) (0.1 g, 0.588 mmol) and 4 Å molecular sieves (1 g). The mixture was stirred for 1h at room temperature in the dark, and then silver triflate (0.15 g, 0.588 mmol) was added in one portion. The mixture was stirred at 35-45 °C for 48 h. After cooling to room temperature the solids were filtered off through Celite, and washed thoroughly with acetonitrile. The filtrate was diluted with EtOAc (15 mL), washed successively with 5% $NaHCO_3$, saturated aqueous $Na_2S_2O_3$ and finally with brine. The organic layer was dried over Na_2SO_4, and the solvent removed *in vacuo* at 35 °C. According to NMR the residue was a mixture containing the α:β isomers in a ratio of 3:2. Chromatography (EtOAc:PE 40/60, gradient from 1:1 to 100% EtOAc) of the residue on a column of silica gel afforded (in order of elution) β glycoside **4.10** (0.04 g, 21%), α/β glycoside **4.10** (0.04, 21%), and α glycoside **4.10** (0.07 g, 37%).

α-isomer: **TLC** R_f (EtOAc) = 0.45; **^{1}H NMR** (400 MHz, $CDCl_3$): δ 5.88-5.79 (m, 1H, C*H*=CH_2), 5.41 (ddd, 1H, $J_{7,8}$ 8.2 Hz, $J_{8,9}$ 5.5 Hz, $J_{8,9'}$ 2.7 Hz, H-8), 5.35 (dd, 1H, $J_{7,8}$ 8.2, $J_{6,7}$ 1.9 Hz, H-7), 5.15 (d, 1H, $J_{5,NH}$ 9.6 Hz, NH), 5.03-4.93 (m, 2H, CH=CH_2), 4.86 (ddd, 1H, $J_{3,4}$ 12.3 Hz, $J_{4,5}$ 9.9 Hz, $J_{3',4}$ 4.65 Hz, H-4), 4.33 (dd, 1H, $J_{9,9'}$ 12.4 Hz, $J_{8,9'}$ 2.7 Hz, H-9'), 4.17-4.04 (m, 3H, H-5, H-6, H-9), 3.81 (s, 3H, CH_3O), 3.77 (dt, 1H, ^2J 9.4, ^3J 6.4 Hz, OCH_a), 3.22 (dt, 1H, ^2J 9.4, ^3J 6.6 Hz, OCH_b), 2.60 (dd, 1H, $J_{3,3'}$ 12.8, $J_{3',4}$ 4.7 Hz, H-3'), 2.16-1.90 (m, 18H, H-3, CH_2CH=CH_2, 5 Ac at 2.16, 2.15, 2.06, 2.04, 1.90), 1.54 (m, 2H, OCH_2CH_2), 1.32-1.26 (m, 12H, $(CH_2)_6$); **^{13}C NMR** (100 MHz, $CDCl_3$): δ 171.5, 171.1, 170.60, 170.56, 170.4, 169.0 (6 × C=O), 139.6 (*C*H=CH_2), 114.5 (CH=*C*H_2), 99.1 (C-2), 72.8 (C-6), 69.6 (C-4), 69.1 (C-8), 67.8 (C-7), 65.5 (OCH_2), 62.7 (C-9), 53.0 (OCH_3), 50.1 (C-5), 38.5 (C-3), 34.2 (*C*H_2CH=CH_2), 30.0 (OCH_2CH_2), 29.9, 29.8, 29.7, 29.5, 29.3, 26.3 ($(CH_2)_6$), 23.6, 21.5, 21.30, 21.25, 21.2 (5 × *C*H_3C(O)).

β-isomer: **TLC** R_f (EtOAc) = 0.50; **^{1}H NMR** (400 MHz, $CDCl_3$): δ 5.89-5.79 (m, 1H, C*H*=CH_2), 5.43-5.41 (m, 1H), 5.31-5.19 (m, 3H), 5.04-4.94 (m, 2H, CH=CH_2), 4.81 (dd, 1H, $J_{9,9'}$ 12.4 Hz, $J_{8,9'}$ 2.5 Hz, H-9'), 4.19-4.10 (m, 2H), 3.94-3.89 (m, 1H), 3.82 (s, 3H, CH_3O), 3.47 (dt, 1H, ^2J 9.4 Hz, ^3J 6.4 Hz, OCH_a), 3.33 (dt, 1H, ^2J 9.4 Hz, ^3J 6.7 Hz, OCH_b), 2.48 (dd, 1H, $J_{3,3'}$ 12.9 Hz, $J_{3',4}$ 5.0 Hz, H-3'), 2.17-1.90 (m, 18H, H-3, CH_2CH=CH_2, 5 Ac at 2.17, 2.09, 2.05, 2.04, 1.90), 1.59 (m, 2H, OCH_2CH_2), 1.34-1.28 (m, 12H, $(CH_2)_6$); **^{13}C NMR** (100 MHz, $CDCl_3$): δ 171.1, 170.7, 170.5, 170.20, 170.18, 167.6 (6 × C=O), 139.2 (*C*H=CH_2), 114.1 (CH=*C*H_2), 98.5 (C-2), 72.1 (C-6), 71.7 (C-4), 69.0 (C-8), 68.5 (C-7), 64.2 (OCH_2), 62.4 (C-9), 52.6 (OCH_3), 49.5 (C-5), 37.5 (C-3), 33.8 (*C*H_2CH=CH_2), 29.6 (OCH_2CH_2), 29.50, 29.45, 29.4, 29.1, 28.9, 26.5 ($(CH_2)_6$), 23.6, 21.4, 21.3, 21.2 (5 × *C*H_3C(O)).

α/β mixture: **QTOFMS** $[M-H]^-$ 642.3124 (calcd 642.3126; Δ ppm = -0.3); $[M+H]^+$ 644.3311 (calcd 644.3262; Δ ppm = 4.4).

4.3 Results and Discussion

4.3.1 Synthesis of Alkenylated Carbohydrate Derivatives

Using $SnCl_4$ as a Lewis acid catalyst,[13] 10-undecen-1-ol (**4.2**) was attached to penta-*O*-acetyl-β-D-glucopyranose (**4.1**) resulting in compound **4.3** (Scheme 4.1, step a). After purification via column chromatography compound **4.3** was directly available for the attachment on the hydrogen-terminated surface. It is obvious that all remaining hydroxyl groups need to be protected in order to avoid random binding of the alkenylated carbohydrate derivatives via either the 1-alkene or hydroxyl functionality.[8,14]

Shirahata et al. used allyl α-D-galactopyranoside to modify the Si(100)–H surface.[7] Although free hydroxyl groups will also react with this surface the authors did not discuss the resulting aspecificity of the hydrosylilation. Another relevant difference between allyl α-D-galactopyranoside and the carbohydrate derivatives presented in this chapter is the length of the alkenyl chain. Due to the twisted conformation of the bonds closest to the Si surface (Si–C–C–C), a rapidly deteriorating monolayer quality is observed for alkenes with alkyl chains that are shorter than 12 atoms.[15] For this reason the use of 10-undecen-1-ol (the longest ω-alkene-1-ol commercially available) to alkenylate carbohydrates is advocated, and applied in the present work.

Apart from the direct attachment to the silicon surface (vide infra), compound **4.3** was also applied in the three-step synthesis of compound **4.6** (Scheme 4.1, steps b-d, respectively). In the first step the acetyl groups are removed according to the general deacetylation method developed by Zemplén and Pascu.[16]

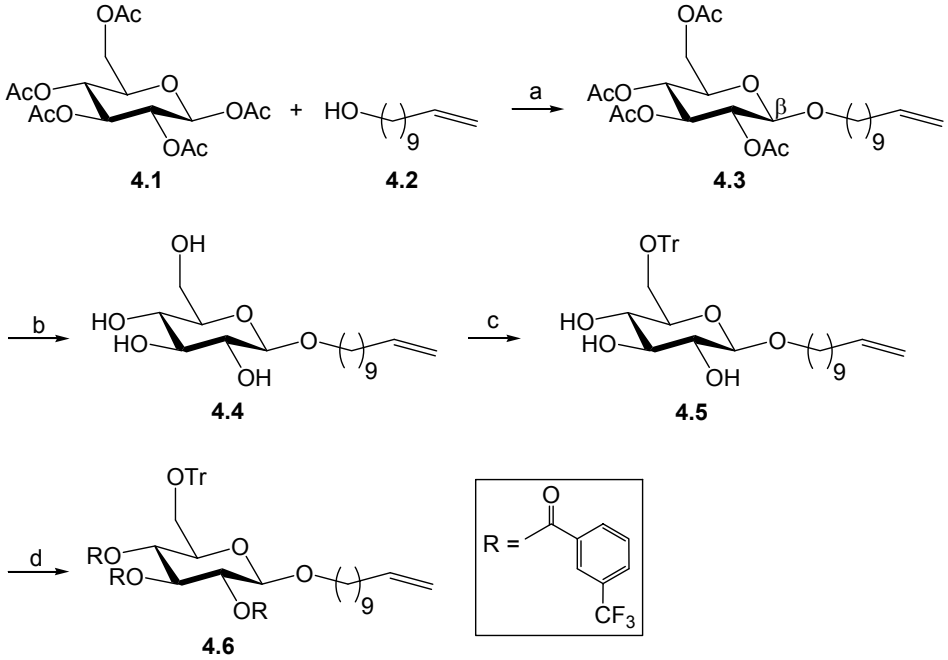

Scheme 4.1 Reagents and conditions: (a) $SnCl_4$ in dry CH_2Cl_2, rt, 38-56%; (b) $NaOCH_3$ in MeOH, rt, 96%; (c) Ph_3CCl, DMAP in pyridine, rt, 64%; (d) 3-(trifluoromethyl)-benzoylchloride, DMAP in pyridine, rt, 77%.

The use of $NaOCH_3$ in MeOH afforded compound **4.4** in an almost quantitive yield. Using trityl chloride,[17] the primary hydroxyl group at C-6 was tritylated yielding compound **4.5**. Subsequently, the remaining three free hydroxyl groups were protected with trifluoromethylbenzoyl groups,[17] giving compound **4.6** in a good yield.

In the synthesis of compound **4.6** the trityl group was introduced in order to have a handle to synthesize oligosaccharides. Detritylation[18] would result in a glucose derivative with only one free hydroxyl group at C-6, which can be linked with a glycosyl donor yielding an oligosaccharide. The trifluoromethylbenzoyl protection group was chosen since the fluorine atom proved to be a good probe for XPS studies of monolayers with compound **4.6**.[19,20]

Apart from the derivatization of penta-*O*-acetyl-β-D-glucopyranose (**4.1**), we also used sialic acid **4.7** as a starting compound. Sialic acids are a crucial component in oligosaccharides that play a role in cell recognition processes.[17c,21,22] Their chemistry frequently requires more subtle procedures for regio- and stereoselective introduction of glycosidic linkages.[17c,21,23-25] Sialic acid-containing carbohydrates are thermally not very stable, but can in combination with our visible-light approach nevertheless be linked smoothly to the Si surface.[19,20]

Protection of the hydroxyl groups that are present in commercially available sialic acid (compound **4.7**) took place in two steps (Scheme 4.2, steps a and b, respectively). Treatment of **4.7** with acidified MeOH gave the methyl glycoside **4.8**.[26] Acetylation of **4.8** with AcCl[26] acetylates all the hydroxyl groups including the one at C-1. At C-1 this is followed by the in situ formation of the α/β chloride at the anomeric centre yielding **4.9**. The glycosylation conditions used in step c of Scheme 4.2 were obtained from the work of Tomoo et al.[27] The alkenylation was promoted with AgOTf and according to NMR the crude product was a mixture containing the α:β isomers of compound **4.10** in a ratio of 3:2. The total yield was 79%.

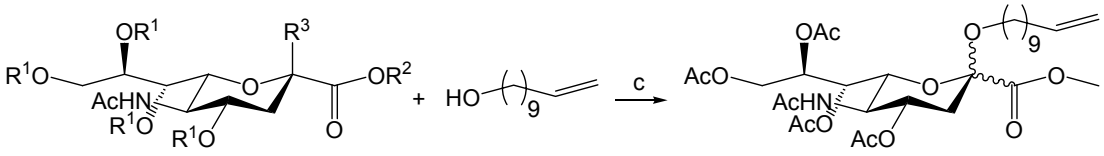

		R^1	R^2	R^3
a	**4.7**	H	H	OH
a	**4.8**	H	Me	OH
b	**4.9**	Ac	Me	Cl

Scheme 4.2 Reagents and conditions: (a) MeOH, (H^+) resin, rt; (b) AcCl, rt, 48h, 66%; (c) dry CH_3CN (dark), rt, 1h; AgOTf, stirred at 35-45 °C for 48 h, 79%.

In conclusion, the synthesis of three different protected alkenylated monosaccharides (compounds **4.3**, **4.6**, and **4.10**) is reported. By making use of a thermal method as well as the visible-light method mixed monolayers containing these compounds were prepared. In §4.3.2 the data on the characterization of the resulting monolayers are presented and discussed.

4.3.2 Characterization of Covalently Attached Carbohydrates on Silicon Surfaces

A mixture of compound **4.3** (0.66%) and 1-decene (99.4%) in refluxing mestiylene (2 h) with a total alkene concentration of 0.1 M was used to modify a Si(100) wafer thermally. Characterization of this surface using attenuated total reflectance IR (ATR-IR) measurements (Figure 4.1) displays the presence of carbonyl groups, which are present in this monolayer, and not in a reference monolayer obtained under identical conditions using only 1-decene. The position of the strong C=O peak of unattached compound **4.3** was found to be ~1757 cm^{-1} (neat between NaCl windows, measured on a recorded on a Bruker Vector 22 FT-IR spectrometer, resolution 2 cm^{-1}). The position of the C=O feature of compound **4.3** in the monolayer is in the region of 1738-1726 cm^{-1}, resulting in a difference of about 20-30 cm^{-1} with respect to the free carbohydrate derivative. Such a large peak shift did not occur in the preparation of ester-functionalized monolayers,[28] and the origin of this shift is not clear. The position of the symmetric C–H stretch vibration at 2925 cm^{-1} shows that this and other sugar-containing monolayers are not well-ordered, which is partly due to the relatively bulky sugar moiety and partly intrinsic to the Si(100)–H surface, as this is not molecularly flat as, e.g., Si(111)–H.[29]

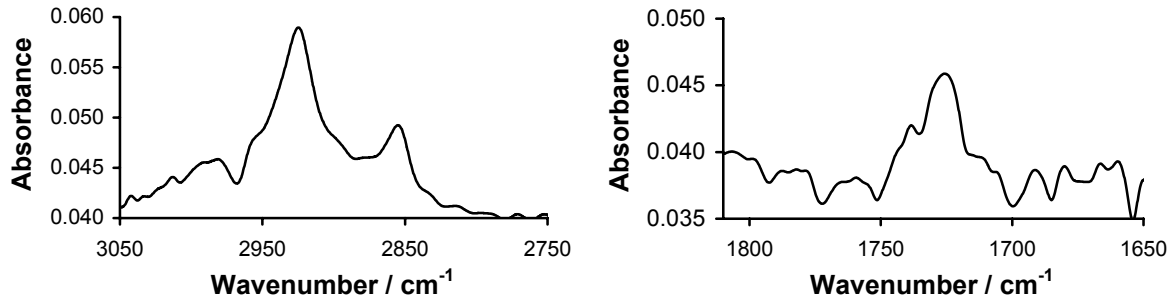

Figure 4.1 ATR-IR region spectra (*p*-polarized) of a covalently attached monolayer on Si(100) obtained by the thermal method, using a mixture of **4.3** (0.66 %) and 1-decene (99.4 %) in refluxing mesitylene.

A mixture of compound **4.6** and 1-dodecene in mesitylene with a total alkene concentration of 0.05 M was used to thermally obtain a modified Si(100) surface. Characterization of this surface using X-ray photoelectron spectroscopy (Figure 4.2, top) shows the attachment of the protected glucose moiety. The inset of Figure 4.2 is a magnification of the area specific for fluorine. Deconvolution of the peak clearly shows the presence of two types of fluorine. Even though the corresponding peaks are not baseline separated, this situation can be analyzed by angle-resolved XPS (ARXPS). From the relative depth profile obtained by ARXPS (Figure 4.2, bottom) and the corresponding binding energies it can be concluded that $F_{1s}A$ is bound to silicon via a Si–F bond that is likely introduced during the etching procedure, while $F_{1s}B$ is bound to carbon. The amount of silicon-bound fluorine is dependent on the etching procedure, and the data in Figure 4.2 thus also show the potential of ARXPS to analyze this even for fluorine-containing monolayers.

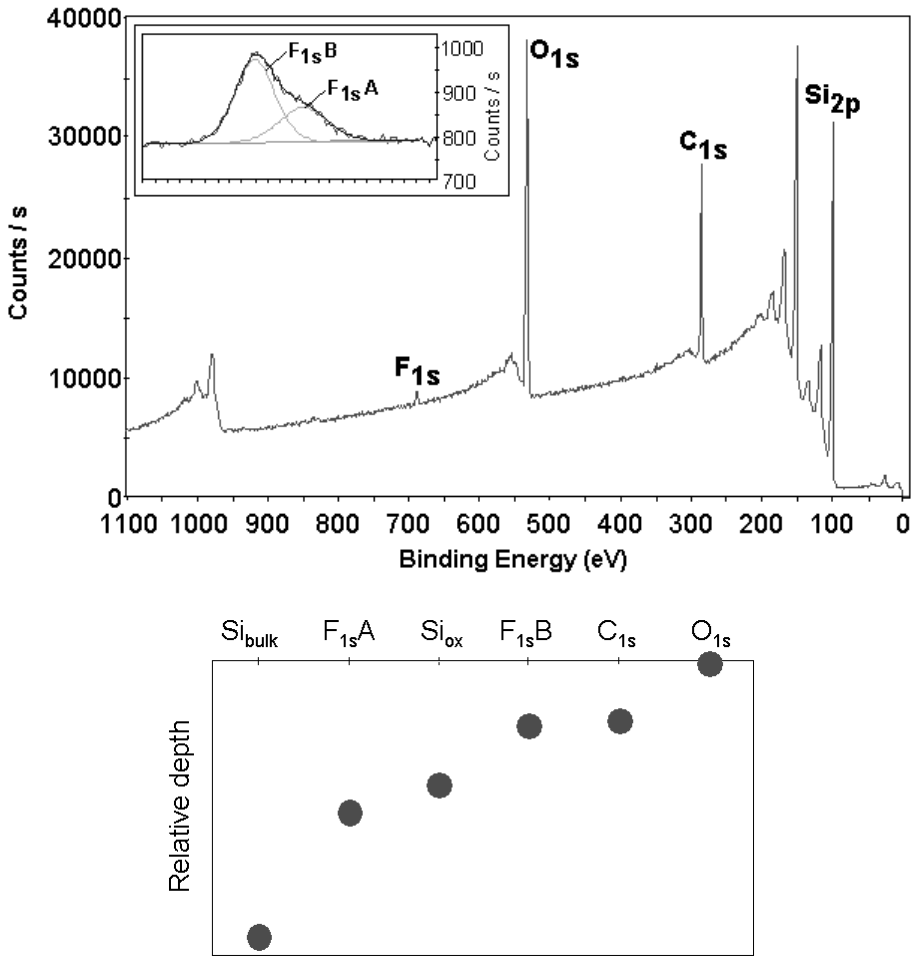

Figure 4.2 XPS spectrum (top) and relative depth profile (bottom) of a thermally attached mixed monolayer on Si(100) obtained from a mixture of compound **4.6** (12%) and 1-dodecene (88%) in mesitylene. The inset shows the presence of two different types of F atoms on the surface.

The value of the visible-light attachment becomes evident for surface modification with sialic acid derivative **4.10**. Sialic acids are a crucial component in oligosaccharides that play a role in cell recognition processes.[17,21,22] Their chemistry frequently requires more subtle procedures for regio- and stereoselective introduction of glycosidic linkages.[17,21,24,25,30] Sialic acid-containing saccharides display a diminished thermal stability, but are transparent for 447 nm light, which allows for the room-temperature attachment of **4.10** to Si(100)–H surfaces. The high sensitivity of XPS allows for the detection of the single N atom in a monolayer obtained from a solution of 25 % of **4.10** and 75 % of 1-dodecene in mesitylene. The XPS data for the N_{1s} region show a clear signal for the monolayer containing **4.10**, which is absent in a reference monolayer of 1-hexadecene (Figure 4.3, top).

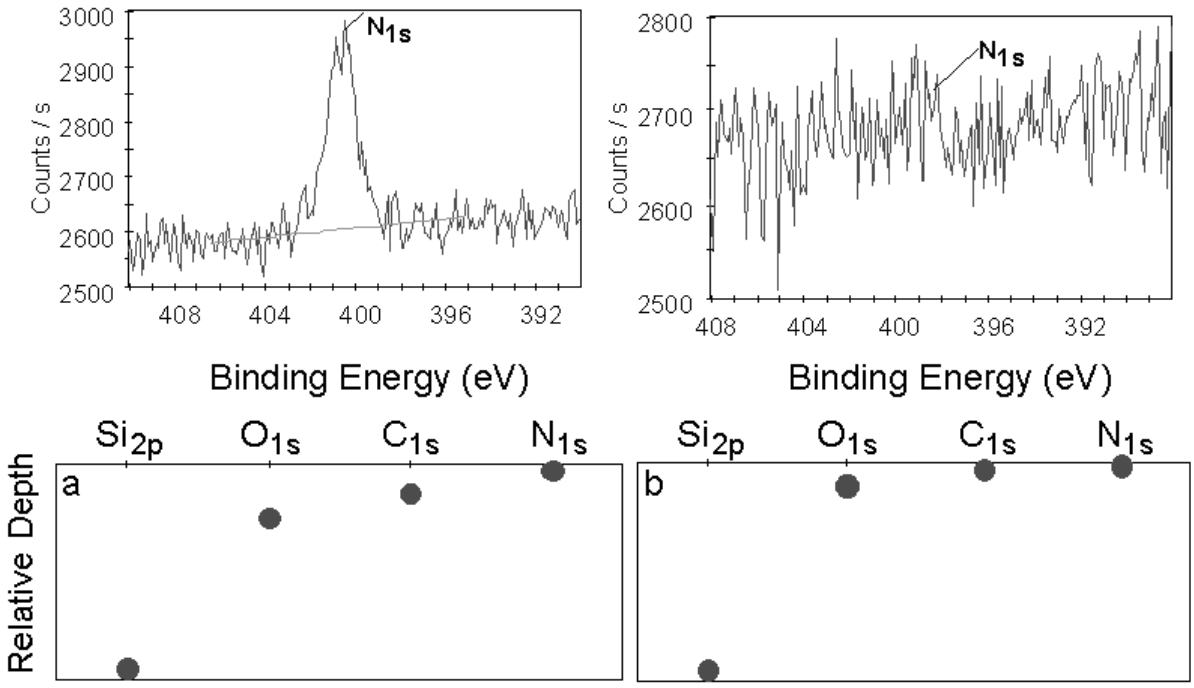

Figure 4.3 (top) XPS spectrum (N_{1s} region) of a covalently attached monolayer containing **4.10** (top left), and a reference spectrum of a monolayer obtained from 1-hexadecene (top right) that shows the absence of this signal in unfunctionalized alkyl monolayers. (bottom) Relative depth profiles of mixed monolayers on Si(100) using different percentages of **4.10** (25%, a and 50%, b) and 1-dodecene as obtained via parallel angle-resolved XPS measurements.

To check whether the disorder in monolayers containing 25% and 50% of compound **4.10** results in burial of the head group in the monolayer, relative depth profiles of monolayers were obtained using ARXPS (Figure 4.3, bottom). This displays nitrogen as – on

average – the highest element in the monolayer. The alkyl chains of **4.10** and 1-dodecene yield a clear C_{1s} signal, which is on average located closer to the Si surface, and in fact somewhat higher than the oxygen signal. This unresolved signal is composed of oxygen atoms that are part of the sugar and of surface-bound oxygen. The latter is nearly absent in unfunctionalized alkyl monolayers,[31] but is usually present in small amounts in functionalized monolayers.[32] At the bottom of the analyzed layer silicon was detected. This profile supports the picture that the sialic acid moiety basically sticks out above the monolayer and is accessible for any bio-active material. In addition, Figure 4.3 (bottom) illustrates that the plots of two different samples are very similar, showing the low sample-to-sample variation.

4.4 Conclusions

The synthesis of three different alkenylated monosaccharides derivatives suitable for the direct attachment to hydrogen-terminated silicon surfaces is described. Mixed monolayers of these compounds with non-functional alkenes were prepared on crystalline Si(100)–H and characterized with different techniques. The development of such new carbohydrate-based sensing elements opens the access to new classes of bio-sensors.

Acknowledgment

The authors thank dr. Klaus Simon (ASML) for various helpful discussions. Furthermore, we thank Jan Blaas and Harry Jonker (Plant Research International) for instrumental assistance.

References and Notes

[1] Wang, D.; Liu, S.; Trummer, B. J.; Deng, C.; Wang, A. *Nat. Biotechnol.* **2002**, *20*, 275-281.
[2] Kiessling, L. L.; Cairo, C. W. *Nat. Biotechnol.* **2002**, *27*, 234-235.
[3] Willner, I.; Katz, E. *Angew. Chem., Int. Ed.* **2000**, *39*, 1180-1218.
[4] Dancil, K.-P. S.; Greiner, D. P.; Sailor, M. J. *J. Am. Chem. Soc.* **1999**, *121*, 7925-7930.
[5] Collins, B. E.; Dancil, K.-P.; Abbi, G.; Sailor, M. J. *Adv. Funct. Mat.* **2002**, *12*, 187-191.
[6] Wei, F.; Sun, B.; Guo, Y.; Zhao, X. S. *Biosens. Bioelectron.* **2003**, *18*, 1157-1163.
[7] Shirahata, N.; Yonezawa, T.; Miura, Y.; Kobayashi, K.; Koumoto, K. *Langmuir* **2003**, *19*, 9107-9109.
[8] Sieval, A. B.; Demirel, A. L.; Nissink, J. W. M.; Linford, M. R.; van der Maas, J. H.; de Jeu, W. H.; Zuilhof, H.; Sudhölter, E. J. R. *Langmuir* **1998**, *14*, 1759-1768.
[9] Küller, A.; Eck, W.; Stadler, V.; Geyer, W.; Gölzhäuser, A. *Appl. Phys. Lett.* **2003**, *82*, 3776-3778.
[10] Zharnikov, M.; Küller, A.; Shaporenko, A.; Schmidt, E.; Eck, W. *Langmuir* **2003**, *19*, 4682-4687.
[11] Wolff, J.-C.; Eckers, C.; Sage, A. B.; Giles, K.; Bateman, R. *Anal. Chem.* **2001**, *73*, 2605-2612.

[12] Ogura, H.; Furuhata, K.; Itoh, M.; Shitori, Y. *Carbohydr. Res.* **1986**, *158*, 37-51.
[13] Fraser-Reid, B.; Udodong, U. E.; Wu, Z.; Ottoson, H.; Merritt, J. R.; Rao, C. S.; Roberts, C.; Madsen, R. *Synlett.* **1992**, 927-942.
[14] Asanuma, H.; Lopinski, G. P.; Yu, H. Z. *Langmuir* **2005**, *21*, 5013-5018.
[15] Sieval, A. B.; van den Hout, B.; Zuilhof, H.; Sudhölter, E. J. R. *Langmuir* **2000**, *16*, 2987-2990.
[16] Zemplén, G.; Pascu, E. *Ber. Dtsch. Chem. Ges.* **1929**, *62*, 1613-1618.
[17] Lindhorst, T. K. *Essentials of Carbohydrate Chemistry and Biochemistry*. Wiley-VCH: Weinheim, 2nd ed.: San Francisco, 2003.
[18] Ding, X.; Wang, W.; Kong, F. *Carbohydr. Res.* **1997**, *303*, 445-448.
[19] de Smet, L. C. P. M.; Stork, G. A.; Hurenkamp, G. H. F.; Sun, Q.-Y.; Topal, H.; Vronen, P. J. E.; Sieval, A. B.; Wright, A.; Visser, G. M.; Zuilhof, H.; Sudhölter, E. J. R. *J. Am. Chem. Soc.* **2003**, *125*, 13916-13917.
[20] Sun, Q.-Y.; de Smet, L. C. P. M.; van Lagen, B.; Wright, A.; Zuilhof, H.; Sudhölter, E. J. R. *Angew. Chem., Int. Edit.* **2004**, *43*, 1352-1355.
[21] Sears, P.; Wong, C.-H. *Angew. Chem. Int. Ed.* **1999**, *38*, 2300-2324.
[22] Stryer, L. *Biochemistry*. W. H. Freeman and Company: San Francisco, 4th ed.: 1995.
[23] Kiefel, M. J.; von Itzstein, M. *Chem. Rev.* **2002**, *102*, 471-490.
[24] Haberman, J. M.; Gin, D. Y. *Org. Lett.* **2001**, *3*, 1665-1668.
[25] Demchenko, A. V.; Boons, G.-J. *Chem. Eur. J.* **1999**, *5*, 1278-1283.
[26] Kuhn, R.; Lutz, P.; MacDonald, D. L. *Chem. Berichte* **1966**, *99*, 611-617.
[27] Tomoo, T.; Kondo, T.; Abe, H.; Tsukamoto, S.; Isobe, M.; Goto, T. *Carbohydr. Res.* **1996**, *284*, 207-222.
[28] Sieval, A. B.; Demirel, A. L.; Nissink, J. W. N.; Linford, M. R.; van der Maas, J. H.; de Jue, W. H.; Zuilhof, H.; Sudhölter, E. J. R. *Langmuir* **1998**, *14*, 1759-1768.
[29] AFM measurements (Digital Instruments Nanoscope IIIa; tapping mode with Si cantilever) show a surface roughness of about 1 nm (~ 7 Si atoms). Zuilhof, H. - unpublished results.
[30] Kiefel, M. J.; von Itzstein, M. *Chem. Rev.* **2002**, *102*, 471-490.
[31] Sieval, A. B.; Linke, R.; Zuilhof, H.; Sudhölter, E. J. R. *Adv. Mat.* **2000**, *12*, 1457-1460.
[32] See also: Zhang, L.; Li, L.; Chen, S.; Jiang, S. *Langmuir* **2002**, *18*, 5448-5456.

Chapter 5

Fibrinogen Adsorption on Hexa(Ethylene Glycol)-Terminated Monolayers on Silicon Surfaces*

Abstract – In this chapter, two hexa(ethylene glycol)-derivatives ($H_2C=CH(CH_2)_8(CO)(OCH_2CH_2)_6OCH_3$ and $H_2C=CH(CH_2)_9(OCH_2CH_2)_6OCH_3$) were attached to crystalline Si(100)–H and Si(111)–H surfaces. The resulting monolayers were characterized with water contact angle studies, X-ray diffraction, infrared reflection absorption spectroscopy (IRRAS) and ellipsometry. The layers were exposed to a buffered fibrinogen solution, showing that the protein adsorption was reduced by 28-37% in comparison to hydrogen-terminated silicon. No significant effects were observed for the different linkage group or crystal facets. In contrast to our results, monolayers of $H_2C=CH(CH_2)_9(OCH_2CH_2)_6OCH_3$) on Si(111)–H described in literature were successful in preventing the adsorption of fibrinogen. Most likely this discrepancy originates from different monolayer packing densities due to different preparation methods.

* de Smet, L. C. P. M.; van Geldrop, J.; Fokkink, R. G.; Jenneskens, L. W.; Zuilhof, H.; Sudhölter, E. J. R.

5.1 Introduction

5.1.1 Bio-resistant Materials

The uncontrolled, non-specific adsorption of proteins and cells on artificial constructs negatively affects a diverse range of phenomena of interest. Examples include biomedical issues like the fouling of implants[1] and contact lenses,[2] and the opsonization[l] of drug delivery vehicles.[3-5] Other examples include the colonization of marine organisms on ship hulls and marine structures, and the fouling of industrially interesting surfaces like filtration membranes and microsieves.[6] Finally, in the biosensor area, suppression of nonspecific interactions is essential for the realization of satisfactory sensitivity and selectivity.[7]

Over the past decades there has been an extensive search for coatings that minimize the adhesion of biomolecules. One of the most attractive ways to achieve bioresistant properties is the preparation of films of poly(ethylene glycol) (PEG/PEO) derivatives.[8,9] Self-assembled monolayers (SAMs) of oligo(ethylene glycol) derivatives attracted a lot of attention since the first report of low bioadhesion by Prime and Whitesides in the early 1990s.[10] Extensive research has been directed to the modification of gold surfaces using thiol-functionalized oligo(ethylene glycol) derivatives.[10-15] Soon after, thiol-functionalized ethylene glycols were studied on silver[16,17] and monolayers of oligo(ethylene glycol)-terminated alkyltrichlorosilanes were prepared on the SiO_2 surface.[18-20]

The current ideas on the mechanism of protein resistance are briefly outlined in §5.1.2. Next, §5.1.3 deals with an overview on the literature on oligo(ethylene glycol) derivatives on H-terminated silicon, a research topic that has commenced recently and is also the topic of this chapter.

5.1.2 Mechanism of Protein Resistance

Andrade and De Gennes theoretically studied the protein resistance character of surfaces grafted with poly(ethylene glycol) using concepts related to colloid stabilization.[21] Steric repulsion, Van der Waals attraction and hydrophobic interaction free energies are considered in their model, which is only applicable for long ethylene glycol derivatives. The model was improved by Szleifer et al. using the single-chain mean-field (SCMF) theory,[22] which also could be used to rationalize the inertness of systems with a high density of short ethylene glycol chains ($n \geq 6$), including SAMs. Although both models provide some insight

[l] Opsonization is the process where particles such as microorganisms become coated with molecules, which allows them to bind to receptors on phagocytes.

regarding the mechanism of protein resistance, they do not provide an explanation of the bio-resistance on the molecular level.[23]

Initially, the mechanism for the bioresistant properties of methoxy oligo(ethylene glycol)-terminated monolayers was rationalized based on the differences observed between gold and silver substrates.[16,24] Tri- and hexa(ethylene glycol)-terminated monolayers on the gold surfaces are completely bio-resistant, while the corresponding monolayers the silver surface only partially hamper protein adsorption. These observations were related to the differences in the packing density of the ethylene glycol chains on silver and gold substrates. It was rationalized that due to the smaller surface sites on silver substrates monolayers were packed more densely as compared to analogous monolayers on gold. Hence, chains attached to silver are arranged in an ordered, all-*trans* configuration while on the gold surface a disordered, helical configuration is present. The latter has a strong dipole field[25] and provides a template for water nucleation, while water is unstable on a surface of planar ethylene glycol chains, as suggested by Monte Carlo simulations.[26,27] These calculations were supported by sum frequency generation measurements that indicated the penetration of water into the ethylene glycol SAMs on gold causing the monolayers to become amorphous.[28,29]

Interestingly, in a later stage hexa(ethylene glycol) monolayers on silver were also shown to display helical chain configurations.[17] Grunze and co-workers related the lateral packing density of the monolayers to the protein resistance. The upper limit of lateral packing density for bioresistant monolayers was found to be ~3.85 molecules/nm^2, which is close to the maximum packing density of a defect-free alkanethiol SAM on gold with 100% coverage (4.67 molecules/nm^2). Oligo(ethylene glycol) monolayers on gold turned out to have lateral packing densities lower than this value, while comparable layers on silver have higher values.

Very recently, simulations of more complete systems consisting of protein and SAMs terminating with different groups – including a hydroxyl-terminated tetra(ethylene glycol) derivative – in the presence of explicit water molecules and ions were performed.[30,31] The studies showed that a tightly bound layer of water to the ethylene glycol chains is mainly responsible for the large repulsion hydration force and that the surface density of the chain correlates with the surface resistance. In another study of the same research group the addition of water to ethanol – the assembly solvent – realized higher packing densities on gold as compared to the use of ethanol only and the more densely packed SAMs indeed

allowed the adsorption of proteins.[32] Again, this supports that the stability of the interfacial water layer dominates the protein adsorption behavior.

5.1.3 Oligo(Ethylene Glycol) Derivatives on H-terminated Silicon

The main drawback of the SAMs summarized in §5.1.1 is their low stability: monolayers of thiols can be easily desorbed from the gold surface,[33-35] and Si–O linked monolayers are prone to hydrolysis.[36] Only very recently the hydrosilylation chemistry of unsaturated compounds with hydrogen-terminated silicon surfaces[37-39] – which yield monolayers linked via a very stable Si–C bond – was combined with the elegant properties of ethylene glycol derivatives. Since 2003, three research groups have reported on the construction of Si–C linked oligo(ethylene glycol) layers on silicon.[40-46]

The initial interest of the research group of Cai was the modification of AFM tips with CH_2=$CH(CH_2)_9(OCH_2CH_2)_3OCH_3$ via the thermal method in mesitylene.[40] It was shown that the modified silicon tips effectively reduced the nonspecific interactions of fibrinogen and bovine serum albumin (BSA). Being surprised that this approach had not been reported yet the authors prepared protein-resistant monolayers on Si(111), and measured their water contact angles and thickness before and after treatment with fibrinogen.[41] In this work it was shown that with respect to the hydrophobic Si(111)–H surface, tri-, hexa-, and nona(ethylene glycol)-terminated monolayers reduced the adsorption of fibrinogen with 30, 95, and 98%, respectively. In order to facilitate the removal of trace amounts of water during the monolayer attachment they developed a practical procedure for the photo-induced surface hydrosilylation, in which only 1 mg of the alkenes without solvent was required. Cai and coworkers also used conductive AFM (c-AFM) lithography to build nanometric protein arrays on protein-resistant monolayers on silicon surfaces.[43] In a later stage, they compared the resistance to protein adsorption as well as the stability of monolayers of hepta(ethylene glycol) derivatives on H-terminated Si(111) and Si(100).[44] The results indicated that the monolayers on the Si(111) surface were more stable under a wide variety of conditions, including biological buffer, acid, and base than on Si(100). The hepta(ethylene glycol)-terminated reduced the adsorption of fibrinogen by 97-98%, which is in line with their initial study on the series containing 3 to 9 ethylene glycol units per attached chain.[41]

The group of Hamers and coworkers prepared mixed monolayers containing both amine and tri(ethylene glycol) functionalities on diamond and silicon surfaces by a UV-light procedure.[42] Fluorescence imaging was used to study the binding of fluorescently tagged avidin, BSA, casein, and fibrinogen to these surfaces and the results were compared with

those of equivalent layers on the gold surface. After protein treatment fluorescence intensities were measured and it was shown that the nonspecific adsorption of all of the studied proteins could be reduced by at least 60% on silicon, by 70% on diamond, and by 90% on gold surfaces. In a subsequent study[47] the protein adsorption was monitored by fluorescence scanning as a function of the length of the ethylene glycol chain and the terminal functional group. It was found that high-quality tri(ethylene glycol) monolayers formed on silicon and diamond surfaces were as effective as tri(ethylene glycol) SAMs on gold at resisting nonspecific avidin adsorption.

Böcking et al. reported two studies on oligo(ethylene glycol) functionalized Si–C linked monolayers on Si(111)–H.[45,46] Thermally prepared monolayers of tri(ethylene glycol) derivatives displayed a reduced protein anti-fouling as compared to equivalent layers on gold.[45] Based on X-ray photoelectron spectroscopy, water contact angles, and X-ray reflectivity they rationalized that this was due to a reduced lateral packing density of the chains. They report a value of 3.0-3.1 molecules nm^{-2} and concluded that the resulting monolayer arrangement allowed a collapse of the monolayer components. Despite the fact that this value is lower than the maximally allowed value of the lateral packing density reported by Herrwerth et al. (~3.85 molecules nm^{-2}) for proper antifouling behavior,[17] the monolayers on silicon were not fully bio-resistant. This suggests, apart from an upper limit, also the presence of a lower limit of the lateral packing density to get proper anti-fouling behavior. In addition, Böcking et al. prepared *t*-butyldimethylsilyl-protected tetra(ethylene oxide) monolayers for further derivatization, and again they observed a smaller than expected layer thickness, indicating that the layer had collapsed, most likely due to a reduced grafting density.[46]

5.1.4 Aim of the Research

The initial project strategy in our laboratory dates from the beginning of the period in which the first papers on the topic of oligo(ethylene)glycols on H-terminated silicon surfaces appeared in the literature. In one project the influence of chirality in the oligo(ethylene glycol) derivatives on the protein resistance behavior was studied.[48] Tetra(ethylene glycol) derivatives were chosen for synthetic reasons, which with hindsight – in line with the work of Cai and coworkers[41] – appeared to be too short. For that reason we used hexa(ethylene)glycol derivatives in this study as monolayers of these molecules on Si(111)–H are known to have bio-resistant properties.[41]

The observed differences in protein resistance between oligo(ethylene)glycol-derived monolayers on gold and silver as described in §5.1.2 shows the importance of the nature of the substrate. Hence we are interested in the influence of the substrate orientation by studying monolayers of oligo(ethylene)glycol derivatives on the Si(100) and Si(111) surface. Via the recent work of Cai and coworkers information on this issue became public during the progress of this study as outlined in §5.1.3.[44]

Finally, the conformation of the oligo(ethylene glycol) tail is a relevant factor in the ability of a monolayer to prevent or reduce the adsorption of proteins. Apart from the nature of the substrate also the design of the oligo(ethylene glycol) tails itself can influence this aspect. Hence, it is interesting to study whether there is a difference between compounds that have a different linker group between the ethylene glycol unit and the alkenyl tail, since this might influence the monolayer arrangement.

In this chapter we aim to address these different issues by the preparation of monolayers of two different alkenylated hexa(ethylene glycol) derivatives (Figure 5.1) on the Si(100) and Si(111) surface. The hexa(ethylene glycol) unit of compound **5.1** is linked to the alkenyl chain via the ester functionality. In compound **5.2** the link has been established via an ether bond. Both compounds were attached to hydrogen-terminated Si(100) and Si(111) surfaces via the visible light method, which has been described in Chapters 2 and 3. The use of the undecenyl tail is advocated due a rapidly deteriorating monolayer quality for shorter alkenes[49] and is also used by the groups of Cai, Hamers and Gooding. In addition, the use of undecenyl derivatives makes it possible to compare the results with comparable monolayers on gold,[11,12,14,16,17] silver[16,17] and silica.[18]

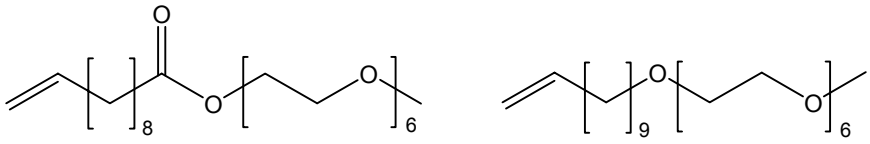

5.1 **5.2**

Figure 5.1 Structures of alkenylated hexa(ethylene glycol) derivatives coupled via an ester (compound **5.1**) and ether (compound **5.2**) group, respectively.

5.2 Experimental Section

5.2.1 General Information

1-Hexadecene (Fluka, ≥99.0%) was distilled twice under reduced pressure. Fibrinogen was obtained from Sigma (Fraction I, type I-S: from bovine plasma).

Single-polished n-Si(100) [500-550 µm thick, resistivity 1.0-2.0 Ωcm, Seltec Silicon, Mitsubishi Silicon America] and n-Si(111) [475-550 µm thick, resistivity 1-5 Ωcm, Addison Engineering, CA] were used for surface modifications.

Preparation of phosphate-buffered saline (hereafter: PBS): 6.177 g of Na_2HPO_4 (Merck, 98%) and 1.014 g NaH_2PO_4 (Merck, pro-analyse) was dissolved in 100 mL of distilled water. 20 mL of this solution and 8.7 g of NaCl (Acros, 99.5%) were made up to 1 L of PBS. This yields a buffer with a pH of 7.4. The (calculated) ion strength of this buffer is 0.21 M.

5.2.2 Organic Synthesis of Alkenylated Hexa(Ethylene Glycol) Derivatives

All reactions were carried out under a dry nitrogen atmosphere. Commercially available reagents were used without purification. Ether was distilled from sodium-benzophenone prior to use. Pyridine was distilled over KOH and stored over 4 Å molecular sieves. Column chromatography was performed using Acros silicagel 0.035-0.070 mm, pore diameter ca. 6 nm. Thin layer chromatography was performed on Merck silicagel 60 F254. Spots were detected by the use of iodine vapor and/or UV light. NMR spectra were recorded on a Bruker AC 300 spectrometer operating at 300.13 MHz for ^{1}H NMR and at 75.47 MHz for ^{13}C NMR. Infrared spectra (neat samples) were recorded on a Perkin Elmer System 2000 equipped with an ATR set-up.

2-(2-(2-(2-(2-(2-methoxyethoxy)ethoxy)ethoxy)ethoxy)ethoxy)ethanol (hereafter: HO–EO_6Me) was synthesized[50] using a strategy according to the highly selective synthesis as published by Keegstra et al.,[51] which makes use of (ethylene glycol) chain prolongation via reactions between trityl-protected and tosyl-activated (ethylene glycol) derivatives.

2-(2-(2-(2-(2-(2-Methoxyethoxy)ethoxy)ethoxy)ethoxy)ethoxy)ethyl Undec-10-enoate (5.1)

17.78 g of HO–EO_6Me (60.0 mmol) and 5.14 g of pyridine (65.0 mmol) were dissolved in 100 mL ether. Via a dropping funnel 12.35 g of 10-undecenoyl chloride (61.0 mmol) in 50 mL ether was added. After stirring overnight the reaction mixture was filtered in order to remove the pyridine salt, and subsequently concentrated under reduced pressure. The oily residue

was taken in *n*-hexane, washed twice with water and dried over $MgSO_4$. Hexane was removed with a rotary evaporator and the residue purified via column chromatography (eluent $CHCl_3$) yielding compound **5.1** as a colorless oil (22.53 g, 48.0 mmol, 81%).

^{1}H NMR ($CDCl_3$) δ 5.87-5.73 (m, 1H), 5.00-4.91 (m, 2H), 4.22 (t, 2H), 3.71-3.65 (m, 20H), 3.55 (t, 2H), 3.38 (s, 3H), 2.32 (t, 2H), 2.03 (q, 2H), 1.62 (t, 2H), 1.29 (m, 10H); **^{13}C NMR** ($CDCl_3$) δ 173.49 (C=O), 138.84 (*C*H=CH_2), 113.93 (CH=*C*H_2), 71.70 (OCH_2), 70.34 (9 × OCH_2), 69.96 (OCH_2), 63.11 (O*C*H_2C=O), 58.74 (OCH_3), 33.93 (*C*H_2C=O), 33.53 (*C*H_2CH=CH_2), 29.02 (CH_2), 28.95 (CH_2), 28.83 (CH_2), 28.80 (CH_2), 28.63 (CH_2), 24.63 (CH_2); **IR** 3073 (w), 2925 (s), 2857 (s), 1735 (s), 1639 (w), 1456 (m), 1350 (m), 1246 (m), 1105 (s), 853 (m); **MS** *m*/*z* 462.3195 (calcd for $C_{24}H_{46}O_8$, 462.3193).

11-(2-(2-(2-(2-(2-(2-Methoxyethoxy)ethoxy)ethoxy)ethoxy)ethoxy)ethoxy)undec-1-ene (5.2)

A solution of HO–EO_6Me (20.00 g, 67.5 mmol) in 5 mL of 50% KOH was heated to 100 °C. 7.00 g of 11-bromo-undecene (30.0 mmol) was added and the mixture was stirred for 24h at 100 °C. After 24 h the reaction mixture was cooled to room temperature, diluted with 10 mL demi-water and washed six times with 20 mL of *n*-hexane. The organic layer was washed once with 10 mL water, dried over $MgSO_4$ and concentrated under reduced pressure yielding a yellow oil. 13.52 g of the crude product was purified by column chromatography (eluent: $CHCl_3$) yielding compound **5.2** as a colorless oil (9.87 g, 22.0 mmol, 73%).

^{1}H NMR ($CDCl_3$) δ 5.87-5.74 (m, 1H), 5.01-4.91 (m, 2H), 3.67-3.65 (m, 20H), 3.56 (m, 4H), 3.44 (t, 2H), 3.38 (s, 3H), 2.04 (q, 2H), 1.57 (m, 2H), 1.28 (m, 12H); **^{13}C NMR** ($CDCl_3$) δ 139.15 (*C*H=CH_2), 114.05 (CH=*C*H_2), 71.82 (OCH_2), 71.38 (OCH_2), 70.46 (10 × OCH_2), 69.92 (OCH_2), 58.87 (OCH_3), 33.66 (*C*H_2CH=CH_2), 29.50 (CH_2), 29.38 (CH_2), 29.30 (2 × CH_2), 28.96 (CH_2), 28.78 (CH_2), 25.93 (CH_2); **IR** 3073 (w), 2924 (s), 2856 (s), 1641 (w), 1457 (m), 1350 (m), 1298 (m), 1249 (m), 1104 (s), 853 (m); **MS** *m*/*z* 448.3403 (calcd for $C_{24}H_{48}O_7$, 448.3400).

5.2.3 Monolayer Preparation using Visible Light

Homogenous monolayers of 1-hexadecene and compounds **5.1** (ester-linked) and **5.2** (ether-linked) were prepared on n-Si(100) and n-Si(111) by using visible light (0.1 M in mesitylene, 447 nm, 15 h). Details about the cleaning of the surfaces and the monolayer preparation can be found in §3.2.4 and §3.2.5.1. For each combination of 1-alkene/type of

silicon three independent samples were prepared and characterized. Modified samples that were not directly used for the adsorption studies were stored under vacuum in a dessicator.

5.2.4 Monolayer Characterization

The monolayers were characterized by the measurement of water contact angles, infrared reflection-absorption spectroscopy (IRRAS), and X-ray reflectivity (§3.2.6).

In addition, ellipsometry was used to measure the thickness of the monolayers before and after the protein adsorption experiment. Ellipsometric measurements were performed with a computer-controlled null ellipsometer (Sentech SE-400) with a He–Ne laser (λ = 632.8 nm) and an incident angle of 70°. The mode 'polarizer + retarder, aperture, strict' was used. The ellipsometric layer thickness was measured using a three-layer model in the ellipsometry software from Sentech. Values of 3.85 and 0.020 were used for the refractive index (n) and the imaginary refractive index (k) of silicon, respectively. In all cases the ellipsometric thickness and the refractive index of the organic layer were measured. Subsequently, the ellipsometric thickness was also measured for a given refractive index for the organic layer (n = 1.45).[41] In both cases the measurements were performed at six different spots in each sample. The reported mean thickness of the layers was calculated by averaging the layer thickness of three separately prepared samples.

Equation 5.1 gives the relation between the refractive indices of the monolayer (n_a) and solvent/air (n_s) via the adsorbed amount Γ [kg m^{-2}], which is the adsorbed mass of material per unit area, the thickness of the monolayer (d_a), and *dn/dc* the refractive index increment:[52]

$$n_a = n_s + \frac{\Gamma}{d_a}\frac{dn}{dc} \qquad [5.1]$$

Note that Γ/d_a is the concentration of the adsorbed material in the adsorbed layer and that the maximum value equals the density of the adsorbate (ρ_a in kg m^{-3}). Equation 5.1 can be written as:

$$\Gamma = \frac{\left(n_a - n_s\right) d_a}{dn/dc} \qquad [5.2]$$

showing that (for n_s = 1),

$$\Gamma \sim \left(n_a - 1\right) d_a \qquad [5.3]$$

In other words, the amount of adsorbed material scales with the measured refractive index minus 1.0 (= the refractive index of air) multiplied by the measured thickness. In this chapter n_a and d_a were measured both, and accordingly both parameters can be used to calculate the relative amount of adsorbed material. Note that Equation 5.3 can also be used to calculate the relative amounts of organic material (attached 1-alkenes) present in a monolayer on the silicon surface. In that case, not the physisorbed protein layer but the chemisorbed monolayer is referred to as the 'adsorbed material'.

5.2.5 Adsorption Studies

Modified silicon samples were cut into two pieces. Each part was placed in a separate vial and covered with 5 ml of water. To each vial 10 ml of solution of a) PBS (pH = 7.4) or b) PBS with fibrinogen (1 mg/ml). As the isoelectric point of fibrinogen is 5.5 the net charge of the protein is negative at pH = 7.4. After 1 h ~12.5 ml of each solution was removed and the resulting solution was diluted with ~20 ml of water. Again most of the solution was removed (keeping the sample wet all the time). This dilution process was repeated 4 times to avoid Langmuir-Blodgett-like protein transfer at the water-air interface upon removal of the sample. Subsequently the sample was taken from the solution and rinsed excessively with water. After drying with a flow of N_2 the samples were subjected to contact angle and ellipsometry measurements. The mean thickness of the modified samples was calculated by averaging the layer thickness of three separately prepared samples. In the case of the H-terminated samples only one sample was studied.

5.3 Results and Discussion

First, the properties of monolayers derived from compounds **5.1** and **5.2** on Si(100)–H and Si(111)–H surfaces are discussed in §5.3.1. The layers were prepared photochemically (447 nm) from alkene solutions in mesitylene, a method of which the development and application possibilities were outlined in Chapters 2 and 3. Subsequently, the effects of the exposure to the buffer solution and buffered protein solution are presented and discussed in §5.3.2.

5.3.1 Monolayer Characterization

Table 5.1 (column A) presents the water contact angles measured on monolayers of 1-hexadecene and compounds **5.1** and **5.2** on Si(100)–H and Si(111)–H surfaces, respectively.

Table 5.1 Static water contact angles (deg) after monolayer preparation (A), exposure to a PBS solution (B) and exposure to a PBS-buffered fibrinogen solution (C).

Compound	Si	A (deg)	B (deg)	C(deg)
H-terminated	(100)	78	-	82 ± 3
1-hexadecene	(100)	104 ± 1	95 ± 4	73 ± 3
5.1 (ester)	(100)	68 ± 2	64 ± 2	72 ± 2
5.2 (ether)	(100)	73 ± 2	64 ± 2	69 ± 2
H-terminated	(111)	87	-	76 ± 1
1-hexadecene	(111)	107 ± 1	100 ± 2	75 ± 2
5.1 (ester)	(111)	67 ± 2	65 ± 1	72 ± 2
5.2 (ether)	(111)	72 ± 2	66 ± 1	70 ± 2

First, we discuss the water contact angle of monolayers from compound **5.2**. The water contact angle of visible light-prepared ether-linked hexa(ethylene glycol)-derived monolayers is 72-73°. Using a different preparation method, Cai and coworkers reported 49° and 46° for the advancing and receding contact angle of monolayers of compound **5.2** on Si(111),[41] indicating a higher wettability as compared the layers prepared in this chapter. There are two reports on thiol-functionalized methyl-terminated hexa(ethylene glycol) derivatives on gold.[12,17] Prime and Whitesides[12] reported advancing contact angles of ~48°, although it is difficult to obtain accurate data from their wettability plots and Herrwerth et al.[17] reported advancing contact angles of 67°. This latter value is very close to the contact angles we found for methyl-terminated hexa(ethylene glycol) monolayers on silicon.

The water contact angles of monolayers of the ester-linked hexa(ethylene glycol) derivative compound **5**.**1** (67-68°) are slightly lower as compared to the ether-linked layers (72-73°). In both cases the water contact angles of the monolayers are higher as compared to the values that were found in another study, in which ester-linked and ether-linked tetra (ethylene glycol) derivatives on the H-terminated Si(100) surfaces were reported to yield water contact angles of 64° and 63°, respectively.[48]

It has to be noted that the contact angles reported in this chapter were measured directly after placing a drop of water onto the modified silicon samples. Soon after, the contact angles decreased due to the adsorption of water by the organic monolayer. This could be one of the reasons why the contact angles reported here are higher as compared to those of the research groups of Cai and Gooding.

The crystal facets do not influence the water contact angle of monolayer: for both the ester and ether the difference between layers on Si(100) and Si(111) is ≤1°. Yam et al. did observe differences in contact angle and monolayer thickness for hepta(ethylene glycol) derivative on Si(100) and Si(111) for irradiation times as short as 30 minutes, but upon increasing the reaction time, comparable properties for the monolayers for both surface orientations were found.[44] Based on previous studies in our laboratory,[53] we adjusted the irradiation times to the specific substrate orientations and used reaction times of at least 5 and 15 h for Si(111) and Si(100), respectively.

In conclusion, the wettability data showed that the hexa(ethylene glycol) layers on silicon prepared in this chapter are more hydrophobic than the layers prepared by Cai and coworkers and than equivalent layers on gold. In addition, the ester-linked monolayers are slightly more hydrophilic as compared to the ether-linked monolayers, which can be attributed to both some more disorder in the monolayer and the higher polarity of the ester moiety.

The modified samples were also studied with IRRA spectroscopy,[54] a viable technique to display the presence or absence of functional groups on the surface.[53,55] We observed a difference in the resolution of the IRRAS data of the modified Si(100) and Si(111) samples. The observed lower resolution of modified Si(111) samples is probably related to the difference in amplitude – and hence sensitivity – that was found for the different surfaces: at a reflection angle of 68° the amplitude of the signal is ~480-600 and 70-75 for lowly doped n-Si(100) and lowly doped n-Si(111), respectively. Earlier it was found that the use of highly doped Si(100) resulted in a signal amplitude of only 20-40.[48] At this stage the origin of the low signal amplitudes in IRRAS of lowly doped n-Si(111) and highly doped n-Si(100) is unclear. Due to the low resolution of the IRRAS data, no useful data for the Si(111) were obtained.

The alkane CH_2-stretching vibrations of the Si(100) samples are given in Table 5.2. The averaged stretching vibrations reflect a liquid-like rather than a solid-like environment, implying disordered monolayer. In a previous study we reported that thermally and photochemically prepared covalently attached non-functionalized monolayers on crystalline silicon surface also fell into the regime of disordered materials.[53] The reported value of 2921 cm^{-1} for a thiol-functionalized hydroxyl-terminated hexa(ethylene glycol) derivative on gold indicated a more ordered packing,[16] but the difference might also be related to the type of spectroscopy that was used.

Table 5.2 C–H stretching vibrations of monolayers of compounds **5.1** and **5.2** on Si(100).

Compound	Si	ν_a (cm^{-1})	ν_s (cm^{-1})
5.1 (ester)	(100)	2927.0 ± 0.5	2858.0 ± 2.8
5.2 (ether)	(100)	2927.1 ± 0.2	2857.7 ± 3.0

Figure 5.2 depicts X-ray reflectivity profiles for monolayers of compounds **5.1** and **5.2** on Si(100) and Si(111) prepared using visible light (447 nm). Only one or two minima were observed before the background was reached because of the thin nature of the layers. This was also observed earlier for other non-functionalized[53,56] and oligo(ethylene glycol) functionalzed[46] thin organic monolayers on silicon. The thickness depicted in Table 5.3 results from a complete fit of the X-ray reflectivity profiles.

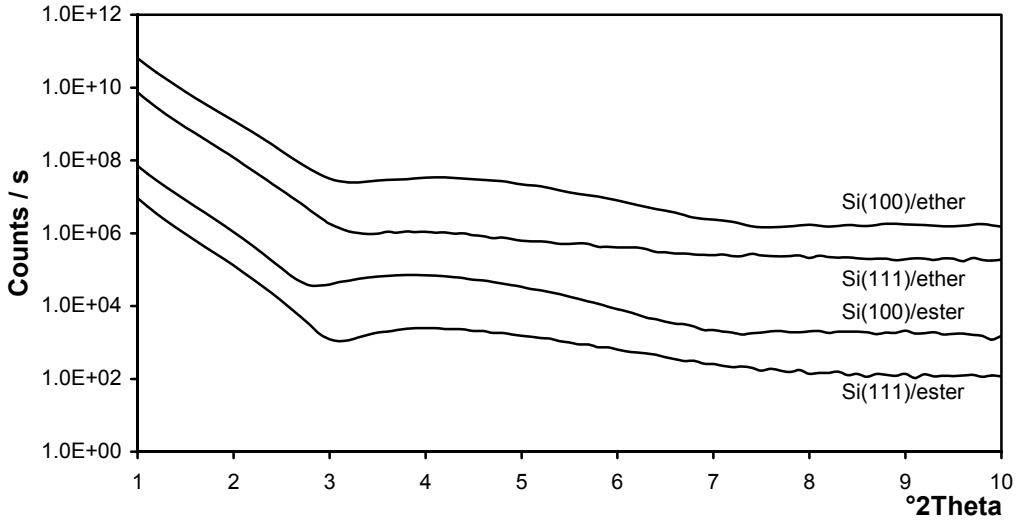

Figure 5.2 X-ray reflectivity profiles for monolayers of compounds **5.1** (ester) and **5.2** (ether) on Si(100) and Si(111) prepared using visible light (447 nm). For clarity the intensities of the plots labeled with Si(100)/ester, Si(111)/ether, and Si(100)/ether are multiplied by 10, 10^3, and 10^4, respectively.

Table 5.3 Monolayer thickness as measured by X-ray reflectivity.

Compound	Si	Thickness (Å)	Error (Å)	Roughness (Å)
5.1 (ester)	(100)	21.0	± 1	2-3
5.2 (ether)	(100)	19.5	± 1	2-3
5.1 (ester)	(111)	19.5	± 1	3.5
5.2 (ether)	(111)	18.0	± 2	4

The values are in the range of 18-21 Å, which is much lower than the calculated length of a hexa(ethylene glycol)molecule in all-*trans* configuration (~38 Å, Figure 5.3).[57] Taking this calculated value into account a monolayer thickness of ~21 Å implies an average tilt angle of the terminal methyl group with the normal of the surface of 57°. A comparable observation has recently been reported by Böcking et al.[46] The thickness of a *t*-butyldimethylsilyl-protected tetra(ethylene oxide) monolayer was found to be only 16-17 Å, about half of the calculated length of the fully stretched molecules. They rationalized that this could be the result of a reduced grafting density, which was supported by the XPS-derived reduced lateral packing density of a tri(ethylene glycol)-terminated monolayer,[45] using a method to quantify surface adsorbate coverages reported by Cicero et al.[58]

The average monolayer thickness of ester-linked hexa(ethylene glycol) monolayers on Si(100) and Si(111) is 1.5 Å higher than that of ether-linked compounds. However, given the experimental uncertainty of X-ray reflectivity (1-2 Å) the difference is not significant.

The layer thickness was also measured with ellipsometry resulting in the ellipsometric thickness. Column A of Table 5.4 presents the ellipsometric monolayer thickness after preparation. Although the average thickness of 1-hexadecene-derived monolayers on the Si(111) surface is slightly higher than on the Si(100) surface (20.3 (± 1.3) vs 18.4 (± 1.1) Å, respectively), the difference is likely not significant due to the experimental error. Both values are close to the values measured with X-ray reflectivity (17.8 Å).[56]

Table 5.4 Ellipsometric monolayer thickness (Å) after monolayer preparation (A), exposure to a PBS solution (B), exposure to a PBS-buffered fibrinogen solution (C) and the difference between C and A (D).

Compound	Si	A (Å)	B (Å)	C (Å)	D (Å)
H-terminated	(100)	-	-	52.0 ± 1.2	52.0 ± 1.2
1-hexadecene	(100)	18.4 ± 1.1	20.9 ± 0.9	62.2 ± 2.6	43.8 ± 2.8
5.1 (ester)	(100)	22.2 ± 1.7	20.6 ± 1.0	57.1 ± 2.6	34.9 ± 3.1
5.2 (ether)	(100)	22.0 ± 1.5	18.9 ± 1.2	56.7 ± 1.4	34.8 ± 2.1
H-terminated	(111)	-	-	48.0 ± 2.1	48.0 ± 2.1
1-hexadecene	(111)	20.3 ± 1.3	21.4 ± 1.7	63.6 ± 1.9	43.3 ± 2.3
5.1 (ester)	(111)	21.4 ± 1.0	20.2 ± 0.6	53.8 ± 1.7	32.4 ± 2.0
5.2 (ether)	(111)	20.2 ± 1.4	18.3 ± 1.5	52.8 ± 2.4	32.5 ± 2.8

The average ellipsometric thicknesses of the hexa(ethylene glycol)-derived monolayers are higher than the thickness as measured by X-ray reflectivity (up to ~2.5 Å). A monolayer of compound **5.2** on Si(111) prepared by Cai and coworkers via a UV method using neat 1-alkene results in an ellipsometric thickness of 27 Å,[59] which indicates a tilt angle with respect to the normal of the surface of 45°. Although the authors write that this angle is comparable with other 1-alkenes on silicon,[60] we believe this value is rather high. Böcking et al., who even measured thinner layers – and hence higher apparent tilt angles – for comparable monolayers rationalized that the monolayers were collapsed due to a lower grafting density.[45,46]

Table 5.5 Calculated values of $(n_a - 1)\, d_a$ [nm] for monolayers on 1-hexadecene and compounds **5.1** and **5.2** on Si(100)–H and Si(111)–H, respectively.

Compound	Si	$(n_a - 1)d_a$ [nm]
1-hexadecene	(100)	8.5 ± 0.5
5.1 (ester)	(100)	9.8 ± 0.4
5.2 (ether)	(100)	9.2 ± 0.7
1-hexadecene	(111)	9.9 ± 0.8
5.1 (ester)	(111)	8.4 ± 0.7
5.2 (ether)	(111)	8.5 ± 0.5

In order to study the amounts of organic materials (reacted 1-alkenes) in monolayers prepared from 1-hexadecene and compounds **5.1** and **5.2** the ellipsometry data of these monolayers was evaluated using Equation 5.3 (Table 5.5). The values for $(n_a - 1)d_a$ in Table 5.5 scale directly with the amounts of attached alkene molecules, and if we assume that *dn/dc* is the same for the three different compounds it is allowed to compare the values of the different compounds. Roughly, the values of $(n_a - 1)d_a$ for the hexadecyl monolayers and monolayers derived from compounds **5.1** and **5.2** are similar. This means that in *terms of mass* the amount of attached alkenes is the same for the three different molecules. Given the difference in molecular weight (1-hexadecene: ~224 g/mol and compounds **5.1** and **5.2**: ~450 g/mol) we conclude that the grafting density – the number of attached molecules per surface area – of compounds **5.1** and **5.2** is ~50% as compared to that of 1-hexadecene.

In the case of all-*trans* configurations the molecular cross-section (A) of an alkyl tail is 0.198 nm^2,[61] whereas lower values have been reported for the oligo(ethylene glycol) chain (0.171-0.184 nm^2).[16,25] In other words, the spatial restriction for the maximal number of

attached molecules of compounds **5.1** and **5.2** is determined by the cross-section of the alkyl chain. In addition, the size of a unit cell on the Si(100)–H and Si(111)–H surface will also affect the number of attached alkenes molecules. Given the relative small size of the units cell (12.77 and 14.75 Å^2 for Si(100) and Si(111), respectively) this aspect will reduce the number of alkenes that will react with the H-terminated surfaces even more. However, since we are interested in the *maximum* lateral packing density, it is sufficient to take only the molecular cross-section of the alkyl tail into account. Since the projected molecular cross-section depends on the tilt angle (α), the maximum lateral packing density (σ in nm^{-2}) can be calculated via Equation 5.4:

$$\sigma = \frac{\cos(\alpha)}{0.198} = \frac{l}{0.198 \times l_0} \qquad [5.4]$$

where *l* (nm) reflects the measured monolayer thickness and l_0 is the molecular length of a hexa(ethylene glycol) derivative in the all-*trans* configuration (3.83 nm for compound **5.2**).[57] The values calculated for σ are presented in Table 5.6. The maximum lateral packing densities of compounds **5.1** and **5.2** are about 52-61% of the value for 1-hexadecene. This is in line with the data obtained via ellipsometry, although this is not surprising since both X-ray reflectivity and ellipsometry measurements yielded comparable values for the monolayer thickness, the parameter that is used for calculating the relative grafting densities and the maximum lateral packing densities.

Table 5.6 The monolayer thickness (*l* in nm, taken from Table 5.3) and the calculated maximum lateral packing density (σ) for monolayers of 1-hexadecene and compounds **5.1** and **5.2** on Si(100)–H and Si(111)–H, respectively.

Compound	Si	*l* (Å)	σ (nm^{-2})
1-hexadecene[a]	(100)	1.78	4.54
5.1 (ester)	(100)	2.10	2.77
5.2 (ether)	(100)	1.95	2.57
5.1 (ester)	(111)	1.95	2.57
5.2 (ether)	(111)	1.80	2.37
5.2 (ether)[b]	(111)	2.7	3.56

[a] Data obtained from X-ray reflectivity measurements on a thermally prepared monolayer reported by Sieval et al.[56]; [b] This calculation is based on the monolayer thickness reported by Yam et al.[41]

In conclusion, the thickness of the hexa(ethylene)glycol monolayers is low with respect to the molecular length, indicating high tilt angles and low grafting densities. The corresponding calculated maximum packing densities are lower than reported by Böcking et al.[45] This indicates – with hindsight – that the monolayers have limited anti-fouling behavior. The maximum lateral packing density calculated for the monolayer derived from compound **5.2** by Yam et al. is higher and indeed shows protein resistance. The bio-resistant properties of the monolayers prepared in this study are discussed in §5.3.2.

In the next section, we address different aspects that might play a role in causing a lower grafting density of oligo(ethylene glycol) derivatives on the silicon surface as compared to similar layers on gold.

First, the nature of the Au–S and Si–C bond is different. The reaction of organic thiols with a gold surface yields close-packed monolayers on the surface. However, the Au–S bond is not thermally stable and the Au–S bond formation is at least partially reversible. As a result the groups slowly drift around on the surface, even at room temperature. In contrast, the Si–C is very stable and consequently attached chains do not wander about on the silicon surface. Consequently, monolayers on silicon do not have self-annealing properties, while monolayers on gold do. Furthermore, the visible light-initiated monolayer formation of 1-alkenes on H-terminated silicon proceeds via a chain reaction that results in island structures.[62,63] Although in this case a reasonably dense layer is formed, the molecules in this layer are not ordered, which can be explained on the basis of the random walk process and the repelling forces between the oligo(ethylene) units of the attached chains.

Secondly, the preparation of monolayers on gold and silicon require solvents with highly different polarities (ethanol vs apolar aromatics, respectively). An alkylated hexa(ethylene glycol) derivative consists of an apolar alkenyl chain and a polar ethylene glycol unit and can therefore be considered as an amphiphile. In fact, this might also explain the observation that thiol and alkenyl hexa(ethylene glycol) derivatives dissolve in ethanol and mesitylene, respectively. However, due to the amphiphilic properties of these compounds the organization in the solutions will be different and this might influence 1) the intramolecular interactions, and hence 2) their conformation and reactivity towards the surface. If this is the case, one might expect a difference between monolayers prepared using thermal and photochemical conditions, since different temperatures are involved.

5.3.2 Bio-resistant Properties

5.3.2.1 Effect of Exposure to Buffer on Wettability and Layer Thickness

After the exposure to a PBS solution without protein (1 h) the contact angles of all the organic monolayers prepared in this chapter decrease with 3-9° (compare column A and B in Table 5.1). These results show that the wetting properties are changed upon the exposure to the buffer. After exposure to the buffer there is no difference anymore in the wetting properties for the ester-linked and ether-linked hexa(ethylene glycol) layer, since they are all in the range of 64-66°. It is likely that the rather polar ethylene glycol chains associate with water molecules, which makes the effective polarity of the monolayer higher. The water contact angles of the monolayers derived from 1-hexadecene also decreased upon the exposure to the buffer solution, indicating that small amounts of water penetrate into the monolayer.

Regarding the ellipsometric thickness there is a difference between the oligo(ethylene glycol) layers and the hydrophobic layers (compare column A and B in Table 5.4). In the case of the 1-hexadecene-derived monolayer the ellipsometric thickness increases with 1-2.5 Å upon exposure to the buffer solution, while those for the hexa(ethylene glycol)-derived monolayers decrease (changes up to ~3 Å).

Unfortunately, the research groups of Cai and Hamers do not report water contact angle data or ellipsometry results on samples that were subjected to protein-free buffer solutions only.

5.3.2.2 Effect of Exposure to Fibrinogen on Wettability and Layer Thickness

The adsorption of fibrinogen on H-terminated Si(100) and Si(111) results in water contact angles of 82 (± 3)° and 76 (± 1)°, respectively. This is comparable with the observations of Yam et al. who report an advancing water contact angle of 80° for a monolayer of fibrinogen on H-terminated silicon.[41]

After exposure to a buffered fibrinogen solution the water contact angles of the hexa(ethylene glycol)-modified samples are all in the range of 69-72°. This is comparable with the values found for on the high-doped n-Si(100) substrates that were modified with layers of tetra(ethylene glycol) derivatives after the exposure to fibrinogen solution.[48] It is difficult to draw conclusions on the bio-resistant properties from the contact angle data only, since the values are not very different form those of monolayers that were freshly prepared

and not exposed to protein solutions. Therefore the measurements on the layer thickness are more informative.

Initially we did not study the fibrinogen adsorption on H-terminated silicon surfaces, since surface oxidation might influence the fibrinogen adsorption. For an HF-cleaned surface, the growth of native oxide in water has two distinct stages, with a very slow growth initially followed by a faster growth.[64] Although the oxide remains relatively thin (~2 Å) for about 3 h before increasing in thickness,[64] the hydrophobicity of the surface will change. Only if the rate of adsorption of fibrinogen onto H-terminated surfaces is much faster than the oxidation rate, the oxidation process will not influence the protein adsorption. However, in order to compare our results with those of Cai and coworkers[41] we used both H-terminated and hexadecyl-modified silicon surfaces as reference models.

The ellipsometric thickness of adsorbed fibrinogen on H-terminated silicon Si(100) and Si(111) was found to be 52.0 (± 1.2) and 48.0 (± 2.1) Å. Yam et al. reported an ellipsometric thickness of 60 Å for adsorbed fibrinogen on Si(111)–H, which was correlated to the size of the protein (~60 × 60 × 450 $Å^3$).[41,44] They concluded that the values indicate the adsorption of a monolayer of fibrinogen. Apart from the values reported by Malmsten and Lassen (~60 × 60 × 450 $Å^3$),[65] two other sets of values for the dimensions of fibrinogen were used in literature for the interpretation of the adsorption of the protein on (modified) surfaces: 50 × 50 × 470 $Å^3$ used by Whitesides and coworkers[14] and 90 x 90 x 450 $Å^3$ used by Brash and coworkers.[66] Using the second mentioned set of dimensions our results imply a monolayer of adsorbed fibrinogen on H-terminated crystalline silicon surfaces.

The relative adsorption of fibrinogen on modified surfaces with respect to H-terminated surfaces can now be obtained in different ways. In Table 5.7 three sets of the relative adsorptions are presented. The data in column A is calculated from the thicknesses that were obtained via the ellipsometry measurements without a fixed refractive index. In the case of column B, the data follows from the calculated values of the relative adsorption via Equation 5.3 (Table 5.5). The data in column C are the result of the ellipsometry measurements with a fixed refractive index for the organic monolayer (n = 1.45), the method that was also used by Cai and coworkers.

It is observed that with respect to etched silicon surfaces, 1-hexadecene-derived monolayers on silicon reduce the adsorption of fibrinogen by 16-23% and 10-13% on the Si(100) and Si(111) surface, respectively. Due to different nature of the etched Si(100) and Si(111) surfaces, we believe it is more informative to compare the bio-resistant properties of oligo(ethylene glycol) derivatives with those of a hydrophobic alkyl-terminated monolayer.

However, as explained earlier in this paragraph, we also added the data on etched surfaces, in order to be able to compare our results with those reported in literature. It is possible that the higher hydrophobicity of hexadecyl monolayers results in a bigger conformational change of the adsorbed protein molecules, a process that has not been discussed in the different studies on oligo(ethylene glycol) derivatives so far. This might explain the lower thickness of the protein layer found on the 1-hexadecene-derived monolayer as compared to etched silicon.

Table 5.7 Three sets of the relative adsorptions (%) with respect to the adsorption on the H-terminated surface calculated from the data of Table 5.4 (A), Table 5.5 (B), and from the ellipsometric thickness measured with fixed *n* (1.45) (C).

Compound	Si	A (%)	B (%)	C (%)
H-terminated	(100)	100	100	100
1-hexadecene	(100)	84	83	77
5.1 (ester)	(100)	67	63	63
5.2 (ether)	(100)	67	63	67
H-terminated	(111)	100	100	100
1-hexadecene	(111)	90	87	87
5.1 (ester)	(111)	68	84	70
5.2 (ether)	(111)	68	80	72

The general trend for all three cases that present the data on the relative adsorptions is that monolayers of hexa(ethylene glycol) derivatives inhibit the adsorption slightly better (28-37%) than hydrogen-terminated silicon. In none of the cases the inhibition results in completely bio-resistant monolayers, which is most likely related to a lower grafting density as outlined in §5.3.1. In addition, analysis method A results in comparable values for the relative adsorption for monolayers of hexa(ethylene glycol) derivatives on Si(100) and Si(111). In the case of method B and C the monolayers on the Si(100) effect slightly lower relative adsorptions as compared to Si(111). No significant differences in bio-repelling behavior were observed between ester- and ether-linked monolayers of hexa(ethylene glycol) derivatives.

5.4 Conclusions

In this chapter we attached two types of hexa(ethylene glycol) derivatives on two types of crystalline silicon surfaces. Although hexa(ethylene glycol) monolayers prepared using 447 nm light prevent the adsorption of fibrinogen to a higher degree than monolayers derived from tetra(ethylene glycol) derivatives, they can not be labeled as bio-resistant, but rather as bio-repelling. No significant differences were found for the use of different linker group or substrate orientation.

These monolayers tolerate more fibrinogen adsorption than comparable monolayers from the Cai research group. Most likely this has to do with the different preparation conditions that have been applied. This idea is supported by a very recent study of Böcking et al.[46] who also observed a relative thin layer for an alkenylated tri(ethylene glycol) derivative on silicon. They rationalized this observation by suggesting that the layer had collapsed, possibly due to a reduced grafting density. Interestingly, they also used a thermal method and diluted the alkenes in an aromatic solvent.

Both the ellipsometric thickness and the refractive index were used to analyze the elliposometry data, which yielded relative amounts of attached chain (grafting densities). The data suggests that the number of attached chains for 1-hexadecene is about twice as high as compared to compounds **5.1** and **5.2**.

To conclude, this chapter demonstrates that the preparation conditions to prepare bio-resistant monolayers on H-terminated silicon with alkenylated oligo(ethylene glycol) derivatives seem to be very critical. Up to now, the results reported by Cai and coworkers are the most promising in terms of bio-resistant monolayers. We believe that monolayers of oligo(ethylene glycol) derivatives on silicon surfaces derived by other methods will be valuable in providing information on the different monolayer morphologies and hence bio-resistant properties that can be obtained. As a result, this will allow one to further improve and design bio-resistant hybrid materials.

Acknowledgment

We thank prof. Willem Norde (Wageningen University and University of Groningen) for stimulating discussions, dr. M. A. Posthumus for mass spectrometry measurements and dr. M. Giesbers for X-ray reflectivity measurements.

References and Notes

[1] Ratner B. D.; Hoffman A. S.; Schoen F. J.; Lemons J. E. (eds) *Biomaterials Science: An Introduction to Materials in Medicine*, New York, Elsevier Academic Press, 2004.

[2] McArthur, S. L.; McLean, K. M.; St John, H. A. W.; Griesser, H. J. *Biomaterials* **2001**, *22*, 3295-3304.
[3] Allen, T. M. *Curr. Opin. Colloid Interface Sci.* **1996**, *1*, 645-651.
[4] Santini, J. T.; Cima, M. J.; Langer, R. *Nature* **1999**, *397*, 335-338.
[5] Lian, T.; Ho, R. J. Y. *J. Pharm. Sci.* **2001**, *90*, 667-680.
[6] Van Rijn, C. J. M. *Nano and Micro Engineered Membrane Technology*, Auqamarijn Research BV, The Netherlands, 2002.
[7] Schneider, B. H.; Dickinson, E. L.; Vach, M. D.; Hoijer, J. V.; Howard, L. V. *Biosens. Bioelectronics* **2000**, *15*, 13-22.
[8] Kingshott, P.; Griesser, H. J. *Curr. Opin. Solid State Mater. Sci.* **1999**, *4*, 403-412.
[9] Vadgama, P. *Annu. Rep. Prog. Chem., Sect. C* **2005**, *101*, 14–52.
[10] Prime, K. L.; Whitesides, G. M. *Science* **1991**, *252*, 1164-1167.
[11] Pale-Grosdemange, C.; Simon, E. S.; Prime, K. L.; Whitesides, G. M. *J. Am. Chem. Soc.* **1991**, *113*, 12-20.
[12] Prime, K. L.; Whitesides, G. M. *J. Am. Chem. Soc.* **1993**, *115*, 10714-10721.
[13] Mrksich, M.; Sigal, G. B.; Whitesides, G. M. *Langmuir* **1995**, *11*, 4383-4385.
[14] Sigal, G. B.; Mrksich, M.; Whitesides, G. M. *J. Am. Chem. Soc.* **1998**, *120*, 3464-3473.
[15] Love, J. C.; Estroff, L. A.; Kriebel, J. K.; Nuzzo, R. G.; Whitesides, G. M. *Chem. Rev.* **2005**, *105*, 1103-1169.
[16] Harder, P.; Grunze, M.; Dahint, R.; Whitesides, G. M.; Laibinis, P. E. *J. Phys. Chem. B* **1998**, *102*, 426-436.
[17] Herrwerth, S.; Eck, W.; Reinhardt, S.; Grunze, M. *J. Am. Chem. Soc.* **2003**, *125*, 9359-9366.
[18] Lee, S. W.; Laibinis, P. E. *Biomaterials* **1998**, *19*, 1669-1675.
[19] Faucheux, N.; Schweiss, R.; Lutzow, K.; Werner, C.; Groth, T. *Biomaterials* **2004**, *25*, 2721-2730.
[20] Sharma, S.; Johnson, R. W.; Desai, T. A. *Langmuir* **2004**, *20*, 348-356.
[21] Jeon, S. I.; Lee, J. H.; Andrade, J. D.; De Gennes, P. G. *J. Colloid Interface Sci.* **1991**, *142*, 149-158.
[22] Szleifer, I. *Curr. Opin. Solid State Mater. Sci.* **1997**, *2*, 337-344.
[23] Ostuni, E.; Chapman, R. G.; Holmlin, R. E.; Takayama, S.; Whitesides, G. M. *Langmuir* **2001**, *17*, 5605-5620.
[24] Wang, R. L. C.; Kreuzer, H. J.; Grunze, M. *J. Phys. Chem. B.* **1997**, *101*, 9767-9773.
[25] Feldman, K.; Hahner, G.; Spencer, N. D.; Harder, P.; Grunze, M. *J. Am. Chem. Soc.* **1999**, *121*, 10134-10141.
[26] Wang, R. L. C.; Kreuzer, H. J.; Grunze, M.; Pertsin, A. J. *Phys. Chem. Chem. Phys.* **2000**, *2*, 1721-1727.
[27] Pertsin, A. J.; Grunze, M. *Langmuir* **2000**, *16*, 8829-8841.
[28] Zolk, M.; Eisert, F.; Pipper, J.; Herrwerth, S.; Eck, W.; Buck, M.; Grunze, M. *Langmuir* **2000**, *16*, 5849-5852.
[29] Wang, R. Y.; Himmelhaus, M.; Fick, J.; Herrwerth, S.; Eck, W.; Grunze, M. *J. Chem. Phys.* **2005**, *122*, 164702.
[30] Zheng, J.; Li, L. Y.; Tsao, H. K.; Sheng, Y. J.; Chen, S. F.; Jiang, S. Y. *Biophys. J.* **2005**, *89*, 158-166.
[31] Zheng, J.; Li, L. Y.; Chen, S. F.; Jiang, S. Y. *Langmuir* **2004**, *20*, 8931-8938.

[32] Li, L. Y.; Chen, S. F.; Zheng, J.; Ratner, B. D.; Jiang, S. Y. *J. Phys. Chem. B* **2005**, *109*, 2934-2941.

[33] Bain, C. D.; Troughton, E. B.; Tao, Y. T.; Evall, J.; Whitesides, G. M.; Nuzzo, R. G. *J. Am. Chem. Soc.* **1989**, *111*, 321-335.

[34] Jennings, G. K.; Laibinis, P. E. *Langmuir* **1996**, *12*, 6173-6175.

[35] Flynn, N. T.; Tran, T. N. T.; Cima, M. J.; Langer, R. *Langmuir* **2003**, *19*, 10909-10915.

[36] Calistri-Yeh, M.; Kramer, E. J.; Sharma, R.; Zhao, W.; Rafailovich, M. H.; Sokolov, J.; Brock, J. D. *Langmuir* **1996**, *12*, 2747-2755.

[37] Wayner, D. D. M.; Wolkow, R. A. *J. Chem. Soc., Perkin Trans. 2* **2002**, 23-34.

[38] Buriak, J. M. *Chem. Rev.* **2002**, *102*, 1271-1308.

[39] Sieval, A. B.; Linke, R.; Zuilhof, H.; Sudhölter, E. J. R. *Adv. Mat.* **2000**, *12*, 1457-1460.

[40] Yam, C. M.; Xiao, Z. D.; Gu, J. H.; Boutet, S.; Cai, C. Z. *J. Am. Chem. Soc.* **2003**, *125*, 7498-7499.

[41] Yam, C. M.; Lopez-Romero, J. M.; Gu, J. H.; Cai, C. Z. *Chem. Commun.* **2004**, 2510-2511.

[42] Lasseter, T. L.; Clare, B. H.; Abbott, N. L.; Hamers, R. J. *J. Am. Chem. Soc.* **2004**, *126*, 10220-10221.

[43] Gu, J. H.; Yam, C. M.; Li, S.; Cai, C. Z. *J. Am. Chem. Soc.* **2004**, *126*, 8098-8099.

[44] Yam, C. M.; Gu, J. H.; Li, S.; Cai, C. Z. *J. Colloid Interface Sci.* **2005**, *285*, 711-718.

[45] Böcking, T.; Gal, M.; Gaus, K.; Gooding, J. J. *Aust. J. Chem.* **2005**, *58*, 660-663.

[46] Böcking, T.; Kilian, K. A.; Hanley, T.; Ilyas, S.; Gaus, K.; Gal, M.; Gooding, J. J. *Langmuir* **2005**, *21*, 10522-10529.

[47] Clare, T. L.; Clare, B. H.; Nichols, B. M.; Abbott, N. L.; Hamers, R. J. *Langmuir* **2005**, *21*, 6344-6355.

[48] van Geldrop, J.; de Smet, L. C. P. M.; Zuilhof, H.; Sudhölter, E. J. R.; Jenneskens, L. W. - manuscript in preparation.

[49] Sieval, A. B.; van den Hout, B.; Zuilhof, H.; Sudhölter, E. J. R. *Langmuir* **2000**, *16*, 2987-2990.

[50] van Geldrop, J.; Scheres, L. M. W.; Jenneskens, L. W. - manuscript in preparation.

[51] Keegstra, E. M. D.; Zwikker, J. W.; Roest, M. R.; Jenneskens, L. W. *J. Org. Chem* **1992**, *57*, 6678-6680.

[52] De Feijter, J. A.; Benjamins, J.; Veer, F. A. *Biopolymers* **1978**, *17*, 1759-1772.

[53] Sun, Q.-Y.; de Smet, L. C. P. M.; van Lagen, B.; Giesbers, M.; Thüne, P. C.; van Engelenburg, J.; de Wolf, F. A.; Zuilhof, H.; Sudhölter, E. J. R. *J. Am. Chem. Soc.* **2005**, *127*, 2514-2523.

[54] Brunner, H.; Mayer, U.; Hoffmann, H. *Appl. Spectrosc.* **1997**, *51*, 209-217.

[55] Arafat, A.; Schroën, K.; de Smet, L. C. P. M.; Sudhölter, E. J. R.; Zuilhof, H. *J. Am. Chem. Soc.* **2004**, *126*, 8600-8601.

[56] Sieval, A. B.; Demirel, A. L.; Nissink, J. W. M.; Linford, M. R.; van der Maas, J. H.; de Jeu, W. H.; Zuilhof, H.; Sudhölter, E. J. R. *Langmuir* **1998**, *14*, 1759-1768.

[57] This value was obtained via a semi-empiric calculation (MOPAC, PM3, closed shell restricted) in Chem3D Pro.

[58] Cicero, R. L.; Linford, M. R.; Chidsey, C. E. D. *Langmuir* **2000**, *16*, 5688-5695.

[59] Yam, C. M.; Lopez-Romero, J. M.; Gu, J.; Cai, C. *Chem. Comm.* **2004**, 2510-2511.

[60] Linford, M. R.; Fenter, P. E.; Eisenberger, P. M.; Chidsey, C. E. D. *J. Am. Chem. Soc.* **1995**, *117*, 3145-3155.

[61] Kjaer, K.; Alsnielsen, J.; Helm, C. A.; Tippman-Krayer, P.; Möhwald, H. *J. Phys. Chem.* **1989**, *93*, 3200-3206.

[62] de Smet, L. C. P. M.; Pukin, A. V.; Sun, Q.-Y.; Eves, B. J.; Lopinski, G. P.; Visser, G. M.; Zuilhof, H.; Sudhölter, E. J. R. *Appl. Surf. Sci.* **2005**, *252*, 24-30.

[63] Eves, B. J.; Sun, Q.-Y.; Lopinski, G. P.; Zuilhof, H. *J. Am. Chem. Soc.* **2004**, *126*, 14318-14319.

[64] Zhang, X. G. *Electrochemistry of Silicon and its Oxide*, Kluwer Academic Publishers: New York, 2001, pp 67-70.

[65] Malmsten, M.; Lassen, B. in: Horbett, T. A.; Brash, J. L.; *Proteins at Interfaces II, Fundamentals and Applications*, American Chemical Society: Washington, DC, 1995; Vol. 602, pp 228-238.

[66] Unsworth, L. D.; Sheardown, H.; Brash, J. L. *Langmuir* **2005**, *21*, 1036-1041.

Chapter 6

Electrical Properties of Organic Monolayers on Crystalline Silicon Surfaces*

Abstract – This chapter describes the characterization of oxide-free Hg/alkyl monolayer/silicon junctions using data derived from current density-voltage (*J*-*V*) and capacitance-voltage (*C*-*V*) measurements. Thermally prepared monolayers of 1-alkenes on n-type and p-type Si(100) were used to study Si|C_nH_{2n+1}|Hg structures (n = 10, 12, 16, and 22). Relevant parameters describing the electrical behavior of these Schottky diodes were derived, such as the diode ideality factor (n), the effective barrier height ($q\phi_{eff}$), the series resistance (R_s), the flatband voltage (V_{fb}), the barrier height ($q\phi_B$), the monolayer dielectric constant (ε_r), the tunneling attenuation factor (β), and the fixed charge density (N_f). The *J*-*V* behavior of the structures could be precisely tuned via the monolayer thickness. Lower diode ideality factors were found for n-type Si as compared to p-type Si. With the exception of decyl monolayers on p-Si similar flatband voltages were found for all silicon–monolayer interfaces. Very low values of N_f were found, given the preparation conditions. Furthermore, the values for $q\phi_{eff}$ and R_s of organic monolayers were higher than those of SiO_2 layers of similar thickness. If 1-alkynes are used instead of 1-alkenes, the resistances were even higher. The electrical parameters indicate a lower degree of silicon surface oxidation for the 1-alkyne-derived monolayer, which was also confirmed by XPS measurements. The ease of fabrication combined with the outstanding electrical properties shows the potential of these Si–C linked monolayers in producing hybrid molecular-silicon devices.

---

* Parts of this chapter have been published or pertain to manuscripts in preparation:

- Faber, E. J.; de Smet, L. C. P. M.; Olthuis, W.; Zuilhof, H.; Sudhölter, E. J. R.; Bergveld, P.; van den Berg, A. *ChemPhysChem* **2005**, *6*, 2153-2166.
- Faber, E. J.; de Smet, L. C. P. M.; Thüne, P. C.; Olthuis, W.; Zuilhof, H.; Sudhölter, E. J. R.; Bergveld, P.; van den Berg, A. - manuscript in preparation.

6.1 General Introduction

Over the last decennia the continuing miniaturization in microelectronics stimulated the research of improved insulating materials as well as of well-defined control of silicon–insulator junctions. One of the candidates to replace silicon dioxide as an insulating material is a covalently attached organic monolayer on the crystalline silicon surface. Organic monolayers can be formed easily via the reaction of 1-alkenes or 1-alkynes with H-terminated silicon surfaces.

Following the pioneering work of Linford et al.[1,2] a thermal method has been further developed[3,4] by the Sudhölter/Zuilhof group for the preparation of high-quality[5] monolayers of 1-alkenes or 1-alkynes[6] on H-terminated silicon surfaces. The procedure involves the use of diluted 1-alkenes or 1-alkyne solutions in aromatic solvents, preferably mesitylene. In addition, molecular modeling studies yielded detailed structural information about the resulting monolayers.[7,8] Furthermore, it was shown that the presence of a monolayer on silicon reduces the number of dangling bonds (surface silicon atoms carrying an unpaired electron) and therefore reduces the surface recombination velocity of electrons and holes formed during band gap excitation of the substrate.[9]

Currently, one of our foci is on the implementation of organic monolayers in electrical circuits and sensor technology. In order to be able to modify H-terminated silicon surfaces directly with (bio-)functional alkenes or alkynes a very mild preparation method using visible light has been developed, as described in Chapters 2 and 3. The importance of the visible-light attachment becomes evident for surface modification with, e.g., labile sugar derivatives, as shown in Chapters 4. In addition, monolayers of oligo(ethylene glycol) derivatives were prepared and their ability to inhibit protein adsorption was studied (Chapter 5).

As all previous issues are related to the development of silicon-based sensors, we report in this chapter on the electrical properties of these monolayers. The research has been conducted in close cooperation with the Lab-on-a-Chip group at the University of Twente. This has resulted in interesting data.[10-12] In this chapter a condensed overview is given of the obtained electrical properties of organic monolayers on crystalline silicon surfaces.

First, a brief outline is given of the types of measurements that are performed to study the semiconductor–insulator interface as well as the electrical insulator properties (§6.2). The focus is on the extraction of relevant parameters from current density-voltage (*J*-*V*) and capacitance–voltage (*C*-*V*) measurements. Second, different types of interface states that can be present in and near the Si/SiO_2 interface are outlined. Subsequently, the electrical properties of metal–insulator–silicon (MIS) diodes derived from different 1-alkenes as

insulator ($Si–C_nH_{2n+1}$ with n = 10, 12, 16, and 22) are presented and discussed in §6.3. Based on the results described in §6.3 the electrical properties of monolayers in MIS diodes were further improved (§6.4).

6.2 Theoretical Background

6.2.1 Energy Band Diagrams of a Metal–Semiconductor Junction

Energy band diagrams are very useful in illustrating which processes take place if an intimate contact is made between a metal and a semiconductor. Here we focus on the energy band diagrams of a metal and n-type silicon before (Figure 6.1a) and after contact (Figure 6.1b). The energy band diagram of n-type silicon has already been discussed in Chapter 1. When the metal (with work function Φ_M) and the semiconductor (with work function Φ_S) are connected, electrons flow from the semiconductor to the metal until the Fermi levels (which are the electrochemical potentials of the electron) are equalized. Here $\Phi_M > \Phi_S$, which is also the case for a contact that consists of Hg and n-type silicon. At equilibrium, the Fermi levels of the metal and semiconductor have become equal and a built-in potential ($q\phi_i$, the amount of band bending at zero bias) has been developed as a result of a depletion of electrons in the space-charge layer (of width W_S). In addition, it becomes clear from Figure 6.1 that the energy barrier for an electron going from the semiconductor to the metal equals $\Phi_M - \Phi_S$, while the energy barrier ($q\phi_B$, the barrier height) for an electron going from the metal to the semiconductor equals $\Phi_M - A_S$, where A_S is the electron affinity of the semiconductor.

If an external potential is applied over the junction, the equilibrium conditions as depicted in Figure 6.1b will be disturbed. Upon applying a positive bias (V_F) to the metal the Fermi level of the metal will decrease (Figure 6.2a). This is called a forward bias, since the internal potential of the junction is now partly compensated by the applied external bias potential, resulting in a smaller $q\phi_i$. Accordingly, additional electrons flow from the semiconductor to the metal, until a new equilibrium is obtained.

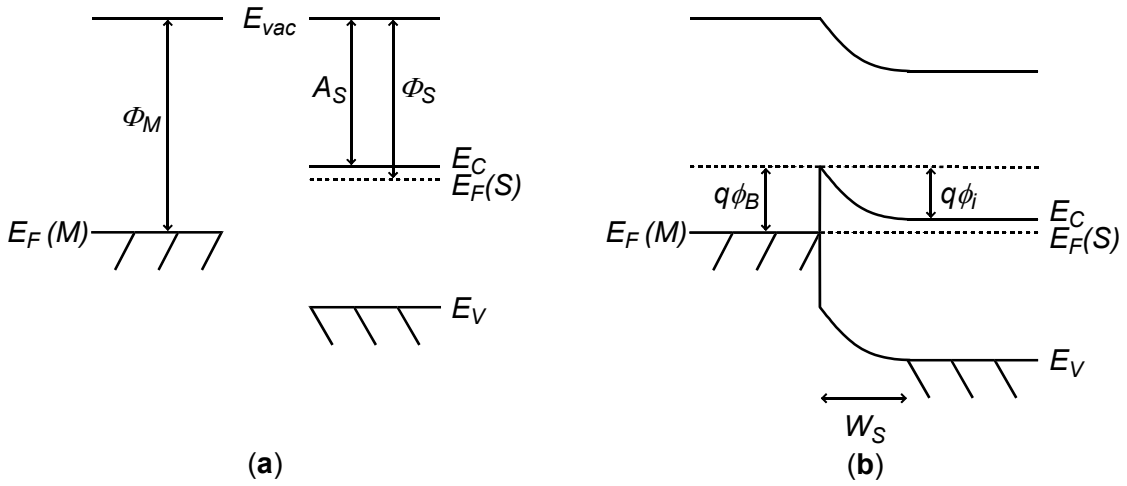

Figure 6.1 Energy band diagrams of a metal and an n-type semiconductor in thermal equilibrium before (a) and after contact (b). E_{vac}, E_V, E_F, and E_C are the energy levels of the vacuum, valence band, Fermi level, and conduction band, respectively. Φ_M and Φ_S are the work functions of the metal and semiconductor; A_S is the electron affinity of the semiconductor, $q\phi_B$ the barrier height and $q\phi_i$ the built-in potential. W_S is the width of the space-charge region.

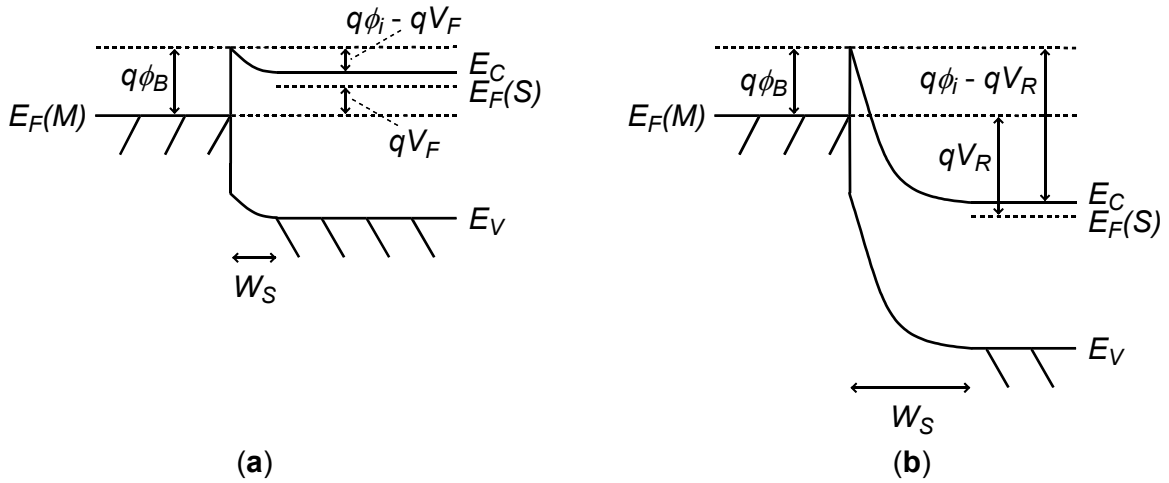

Figure 6.2 Simplified[13] energy band diagrams of a contact that consists of a metal and an n-type semiconductor under (a) forward and (b) reverse bias (V_F and V_R, respectively) conditions. The explanation of the remaining symbols is given in the caption of Figure 6.1. The applied bias affects the energy level E_F of the metal, and consequently the amount of band bending ($q\phi_i$) and the width of the space-charge region (W_S).

When a negative bias (V_R) is applied to the metal, the Fermi energy level of the metal is increased (Figure 6.2b). This is now called reverse bias, resulting in a higher built-in junction potential ($q\phi_i$ is increased by $-qV_R$). As a result the flow of electrons from semiconductor to metal is limited. In Figure 6.3 the charge distributions are given.

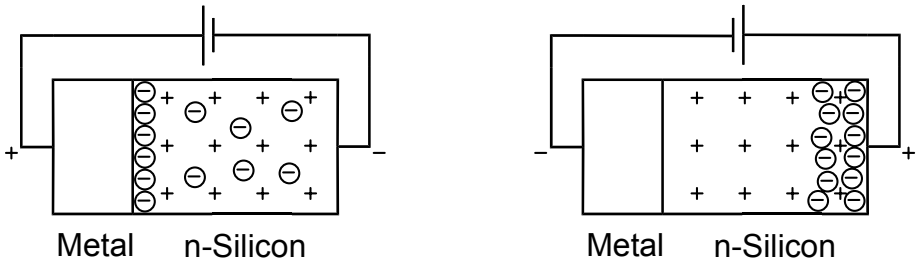

Figure 6.3 Charge distributions that occur in an n-type doped silicon semiconductor in contact with a metal at non-Ohmic behavior (that means that no charge carriers can cross the metal/silicon interface) under forward bias resulting in accumulation (left) and reverse bias resulting in depletion (right). The ionized dopant atoms are positively charged and have fixed positions (+) and electrons are the majority carriers (Θ) that can move.

To summarize, for a junction consisting of a metal and an n-type semiconductor, where electrons in the conduction band are the majority carriers, a large current exists under forward bias (positive bias applied to the metal results in the accumulation of electrons near the interface), while almost no current exists under reverse bias (negative bias applied to the metal results in the depletion of electrons). In the case of p-type silicon, the accumulation of the majority carriers (holes in the valence band) can be established by applying a forward bias (negative bias applied to the metal), while a reverse bias (positive bias applied to the metal) results in the depletion of holes. In other words, in the ideal case (no leakage currents) junctions that consist of a metal and an n-type or p-type semiconductor do hardly display any current flow under reverse bias conditions, while they display increasing electron flow upon increasing the forward bias.

6.2.2 Current-Voltage Behavior

The current through a metal–metal contact scales linearly with the applied voltage according the Ohm's law. The constant of this proportionality is called the resistance (*R* [Ohm]) and equals the potential difference (*V* [V]) over the current (*I* [A]). However, in the case of a metal–semiconductor junction, the behavior is different (Schottky contacts). The corresponding characteristic *J*-*V* and *ln(J)*-*V* plots for an ideal Schottky contact are depicted in Figure 6.4. The current density (*J*)[14] over the Schottky contact scales logarithmically with the applied voltage, as described by the Schottky diode[15] equation:

$$J = J_0 e^{\left(qV/nkT\right)}\left(1 - e^{-qV/kT}\right) = A^* T^2 e^{\left(-q\phi_B/kT\right)} e^{\left(qV/nkT\right)}\left(1 - e^{-qV/kT}\right) \qquad [6.1]$$

where J_0 [A cm^{-2}] is the leakage current, V [V] the applied voltage and n the diode ideality factor[16] ($n \geq 1$). J_0 is the maximum current density under reverse bias conditions.

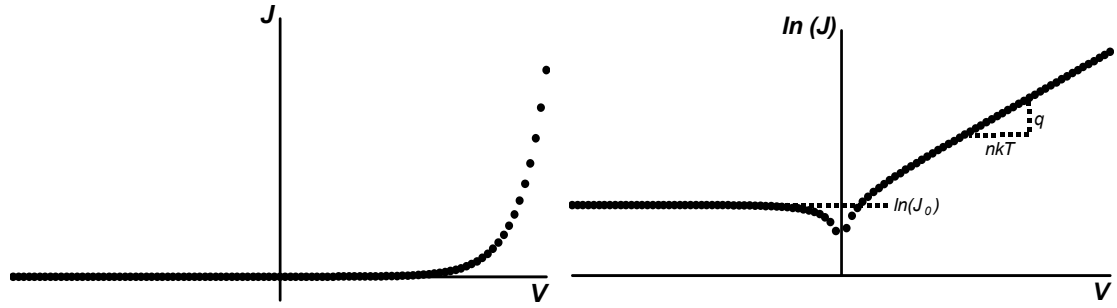

Figure 6.4 Theoretical *J-V* plot and *ln(J)-V* plot of an ideal (diode ideality factor n = 1) Schottky contact that consists of a metal and an n-type semiconductor. For V < 0 (reverse bias, V_R) there is a depletion of electrons and consequently *ln(J)* becomes constant, yielding J_0. For V > 0 (forward bias, V_F) there is an accumulation of electrons and J scales logarithmically with V. The diode ideality factor n can be obtained via the slope of the plot and from J_0 the value of ϕ_{eff} is obtained via Equation 6.1.

The leakage current (J_0) depends on the Richardson's constant (A^* = 110 and 32 AK^{-2}cm^{-2} for n-type and p-type silicon, respectively), the absolute temperature (T [K]), the thermal voltage (kT/q = 25.7 mV at 298 K) and the barrier height ($q\phi_B$ [eV]). If a thin insulator is present between the semiconductor and metal, an extra barrier term is introduced via Equation 6.2. The contribution of the insulator to the barrier height depends on the tunneling constant or attenuation factor (β) and on the thickness of the insulator (l). Selzer et al.[17] and Liu and Yu[18-20] expressed the effective barrier height ($q\phi_{eff}$) by the following equation:

$$q\phi_{eff} = q\phi_B + kT\beta l \qquad [6.2]$$

Equation 6.1 is only valid if the series resistance of the device is very low or zero. However, for higher forward bias voltages (a more positive bias to the metal in contact with n-type silicon), the series resistance R_s [Ωcm^2] becomes higher and Equation 6.1 can be rewritten:

$$J = A^* T^2 e^{\left(-q\phi_{eff}/kT\right)} e^{\left(q(V-JR_s)/nkT\right)} \qquad [6.3]$$

The plot of *d*(V)-*d(ln(J))* gives a straight line with a slope of R_S, as can be deduced from Equation 6.3.[10]

6.2.3 Capacitance-Voltage Behavior

A second type of characterization that can be performed on MIS structures involves the measurement of the capacitance of the monolayer as function of the applied potentials. The capacitance is defined as the total electrical charge through a system divided by the potential. Via *C*-*V* measurements one can derive the flatband voltage (V_{fb} = ϕ_i in Figure 6.1b). The flatband voltage is the electrode potential at which the semiconductor has no excess charge and the bands are not bent. Note that V_{fb} is not influenced by the presence of a very thin insulator, but only by the properties of the silicon–insulator interface. Since *C*-*V* plots are often distorted, it is difficult to obtain V_{fb} analytically. Via the Mott-Schottky technique, in which only the depletion regime of the semiconductor is considered (reverse bias) *C*-*V* data can be analyzed via Equation 6.4 to obtain V_{fb}:

$$\frac{1}{C_{sc}^2} = \frac{2\left(V_{fb} - V_{bias}\right)}{q\varepsilon_0\varepsilon_r N_D A^2} = Z\left(V_{fb} - V_{bias}\right) \qquad [6.4]$$

where C_{sc} [F] is the measured depletion capacitance, ε_0 [F cm^{-1}] is the permittivity of silicon, N_D [cm^{-3}] is the doping concentration, and *A* the area [cm^2] (*Z* is a constant and equals $2/q\varepsilon_0\varepsilon_r N_D A^2$). Using this equation, the linear part of a C^{-2}-V_{bias} plot yields the doping concentration (N_D) via the slope and V_{fb} via the voltage-axis intercept (Figure 6.5).

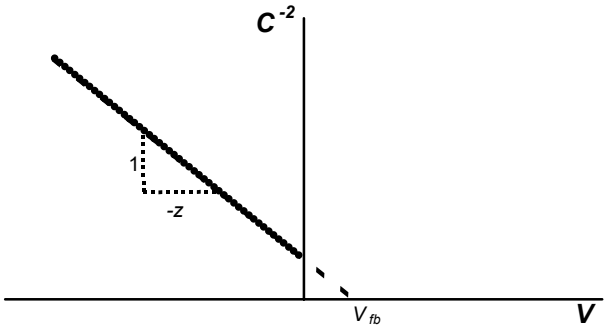

Figure 6.5 Theoretical C^{-2}-*V* plot of an ideal Schottky contact that consists of an n-type semiconductor with an insulator. Note that in the Mott-Schottky theory only the depletion regime of the semiconductor is considered (negative bias on the metal for an n-type semiconductor). V_{fb} follows from the intercept with the bias axis and N_D can be obtained via the slope of the plot ($Z = 2/q\varepsilon_0\varepsilon_r N_D A^2$).

Under conditions of electron accumulation at the silicon semiconductor interface (forward bias for n-type or reverse bias for p-type silicon) the measured capacitance is equal to the insulator capacitance. In that case the thickness or dielectric constant of the insulator can be calculated via:

$$C = \frac{\varepsilon_0 \varepsilon_r A}{l} \qquad [6.5]$$

where ε_0 [F cm^{-1}] is the permittivity of vacuum, ε_r is the dielectric constant of the insulating layer, A [cm^2] is the surface area, and l [cm] is the insulator thickness. However, in the case of thin insulators the capacitance often does not become constant and the extra series capacitance of the accumulation layer, although very large, has to be incorporated:

$$\frac{1}{C} = \frac{1}{C_{ins}} + \frac{1}{C_s} \approx \frac{1}{C_{ins}} - \frac{2kT}{qC_{ins}} \frac{1}{\left(V_{bias} - V_{fb}\right)} \qquad [6.6]$$

where C_{ins} and C_s are the insulator and accumulation capacitance, respectively; V_{bias} and V_{fb} are the applied voltage and the flatband voltage, respectively. Plotting C^{-1} versus $(V_{bias}\text{-}V_{fb})^{-1}$ gives a straight line from which C_{ins} can be derived as the C^{-1} axis intercept.

In addition, the total number of fixed charges (partly oxidized silicon atoms and dangling bonds, see §6.2.5)[21] can be calculated via the insulator capacitance (C_{ins}), the flatband voltage (V_{fb}) and the theoretical flatband voltage[22] ϕ_{MSi} via Equation 6.7:

$$N_f = \frac{C_{ins}\left(\phi_{MSi} - V_{fb}\right)}{qA} \qquad [6.7]$$

6.2.4 Extraction of Parameters from *J-V* and *C-V* Measurements

This paragraph summarizes the extraction routes of several parameters from *J-V* and *C-V* measurements, using the equations given in the previous paragraphs.

From the low forward bias regime of the *ln(J)-V* plot the ideality factor (n) and effective barrier height ($q\phi_{eff}$) can be obtained (Equation 6.1). From Mott-Schottky (*C-V*) measurements the barrier height ϕ_B is obtained via V_{fb} – which equals voltage-axis intercept of the C^{-2}-V_{bias} plot – and subsequently the attenuation factor β can be derived via Equation 6.2. From the higher forward bias regime the insulation properties (R_s) of the monolayer can be derived via Equation 6.3.

Apart from ϕ_B, Mott-Schottky analysis of the *C*-*V* data yields the doping concentration (N_D) via the slope of the C^{-2}-V_{bias} plot (Equation 6.4). The obtained information can be used to verify the procedure since the doping is known from the wafer specifications. Via Equation 6.6 and subsequently Equation 6.5 the dielectric constant (ε_r) of the alkyl monolayer can be obtained. Finally, the amount of fixed charges (N_f) present at the interface can be calculated via Equation 6.7.

6.2.5 Interface States and Fixed Charges

The presence of interfacial imperfections in the semiconductor-insulator system facilitates the recombination of separated holes and electrons, obtained by optical band gap excitation. In order to get a clear picture on the possible types of charges and states that can be present near the interface of silicon and the organic monolayer, we give a brief overview of the variety of charges and states that can be associated with the thoroughly studied Si/SiO_2 system.[21,23]

Important sources for the recombination of separated electron/hole pairs involve crystal lattice defects and the presence of impurities. Unsaturated bound silicon atoms – dangling bonds – cause energy states in the band gap region of silicon. They form pathways via which electrons and holes can recombine easily, especially when these energy states are located near the middle of the band gap (midgap levels). The distribution of these energy states is generally presented via the interface trap density, which is a function of the trap energy in relation to the valence band energy. Another example of traps originate from the disruption of the periodicity of the silicon lattice near the surface by stretched Si–Si bonds (Figure 6.6).[21,24]

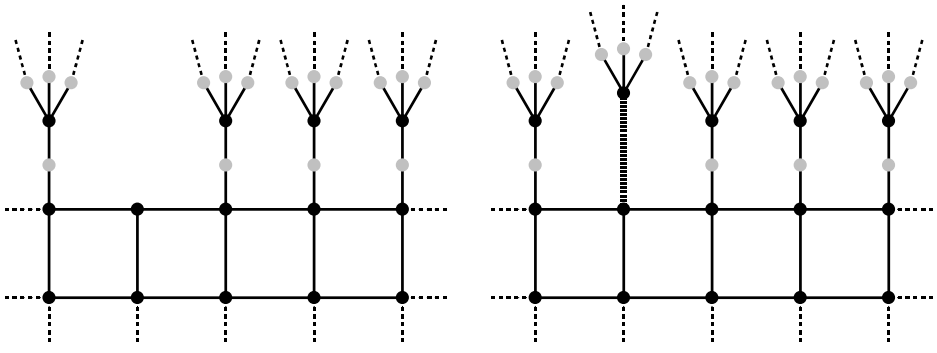

Figure 6.6 Two possible interfacial defects in the model of Sakurai and Sugano[24]: (left) silicon dangling bond ($Si_3{\equiv}Si^{\bullet}$ dangling bond) and (right) stretched Si-Si weak bond with O-vacancy at the interface. The black and gray dots denote Si and O, respectively.

6.3 Molecular Tuning of Metal–Insulator–Silicon (MIS) Diodes

6.3.1 Introduction

Via the construction of metal–insulator–semiconductor (MIS) devices one can obtain information about the electrical properties of the insulator. Several methods are available to make a metal contact to a monolayer, like, e.g., the traditional method of metal deposition or the use of a mercury 'soft' metal contact. The use of the latter method overcomes problems that are often accompanied with the traditional metal deposition technique, like changing the surface properties or damaging the monolayer, although a recent study of Cahen and coworkers shows the construction of non-destructive reproducible electrical contacts via indirect electron beam evaporation of Pd.[25] For fundamental studies the use of mercury is more convenient as it is a simple, fast, and very reproducible way of contacting a monolayer.

The research groups of Vuillaume[26-29] and Cahen[17,30-32] built MIS devices to study the properties of monolayers of alkoxy silanes on SiO_2. Although it was shown that the insulation properties of SiO_2 improved upon the attachment of these monolayers, the construction of the device makes it impossible to investigate the influence of the alkyl monolayer itself.

Kar et al. were the first who prepared oxide-free metal–alkyl monolayer–silicon junctions.[33] After the monolayer preparation, the junction was completed by the evaporation of aluminum.[34] Electrical studies showed remarkably low interface trap densities for monolayers of 1-octadecene on p-type silicon. Soon after, Liu and Yu reported comprehensive studies in this area on monolayers using a mercury 'soft' metal contact. Their work covers the characterization of n-Si|C_nH_{2n+1}|Hg MIS structures (n = 6, 8, 10, and 12),[18] and compared the n-Si|$C_{12}H_{25}$|Hg MIS structure with n-Si|SiO_2|Hg,[19] p-Si|$C_{12}H_{25}$|Hg MIS structures with p-Si|SiO_2|Hg, and p-Si|SiO_2|$SiO_3C_{12}H_{25}$|Hg with p-Si–H|Hg.[20] Recently, Miramond and Vuillaume, studied the influence of substrate doping on the quality of Si|$C_{18}H_{37}$|Al MIS structures.[35] It was found that organic monolayers bound to highly doped n-type wafers resulted in a lower electrical performance as compared to similar monolayers on highly and lowly doped p-type and lowly doped n-type silicon. The monolayers on highly doped n-type silicon were of lower quality and it was suggested that due to the doping, the Si-based radicals become more nucleophilic. Consequently, the rate of addition to 1-octadecene decreased, resulting in a larger incorporation of impurities and hence in more disordered monolayers.

In §6.3 the focus is on oxide-free metal/alkyl monolayer/silicon junctions derived from longer 1-alkenes as compared to Liu and Yu using a mercury 'soft' metal contact. Thermally

prepared monolayers on n-type and p-type Si(100) were used to study Si|C_nH_{2n+1}|Hg structures (n = 10, 12, 16, and 22). Figure 6.7 gives a schematic representation of the Si–alkyl monolayer–Hg structure. More details about the set-up, the sample preparations and measurements conditions can be found in literature.[10]

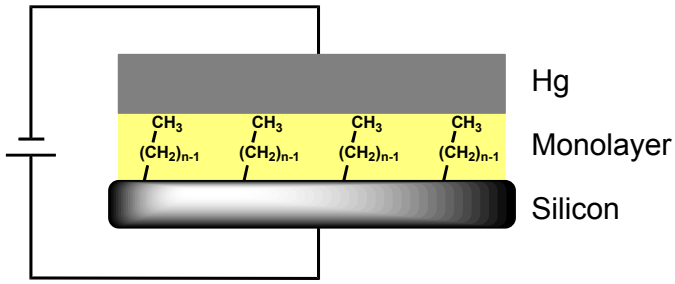

Figure 6.7 Schematic representation of a Si–alkyl monolayer–Hg structure (not to scale). In this study both n-type and p-type Si(100) was used in combination with four different alkyl chain lengths (n = 10, 12, 16, and 22). In this chapter we use the symbol $C_{10\text{-}22}$ to specify the monolayers and $nC_{10\text{-}22}$ and $pC_{10\text{-}22}$ to specify modified n-type and p-type silicon samples, respectively.

6.3.2 Results and Discussion

The *log(J)-V*, *C-V*, and C^{-2}-*V* plots are presented and briefly described in §6.3.2.1. Afterwards we focus on the parameters (*n*, ϕ_{eff}, R_S, ε_r, N_t, and β) derived from these data.

6.3.2.1 Plots Derived from *J-V* and *C-V* Measurements

Figure 6.8 gives the *log(J)-V* plots of H-terminated, oxide- and alkyl-covered p-type and n-type silicon substrates. First we note that the difference in *J-V* behavior between the Hg|p-type Si (good Schottky behavior) and Hg|n-type Si (poor Schottky contact or even an Ohmic behavior) contact is due to intrinsic differences in the barrier heights.[36]

The presence of SiO_2 on p-type silicon results in a more constant value for J_0 in the reverse bias regime as compared to H-terminated p-type silicon. This behavior has been reported before.[37] In the case of n-type silicon, the presence of a SiO_2 layer changes the behavior from Ohmic to Schottky contacts, which is also consistent with data reported in literature.[18,37,38]

All *J-V* curves of p-type silicon modified with 1-alkenes have the same Schottky diode characteristic shape. The magnitude of the current density can be precisely tuned by varying the length of the 1-alkenes, as was also observed by others.[18,20,29] Although the 1-hexadecene-derived layer is thinner as compared to the SiO_2 layer (1.78 ± 0.02 nm versus 1.99 ± 0.06 nm), the organic monolayer displays higher insulating properties.

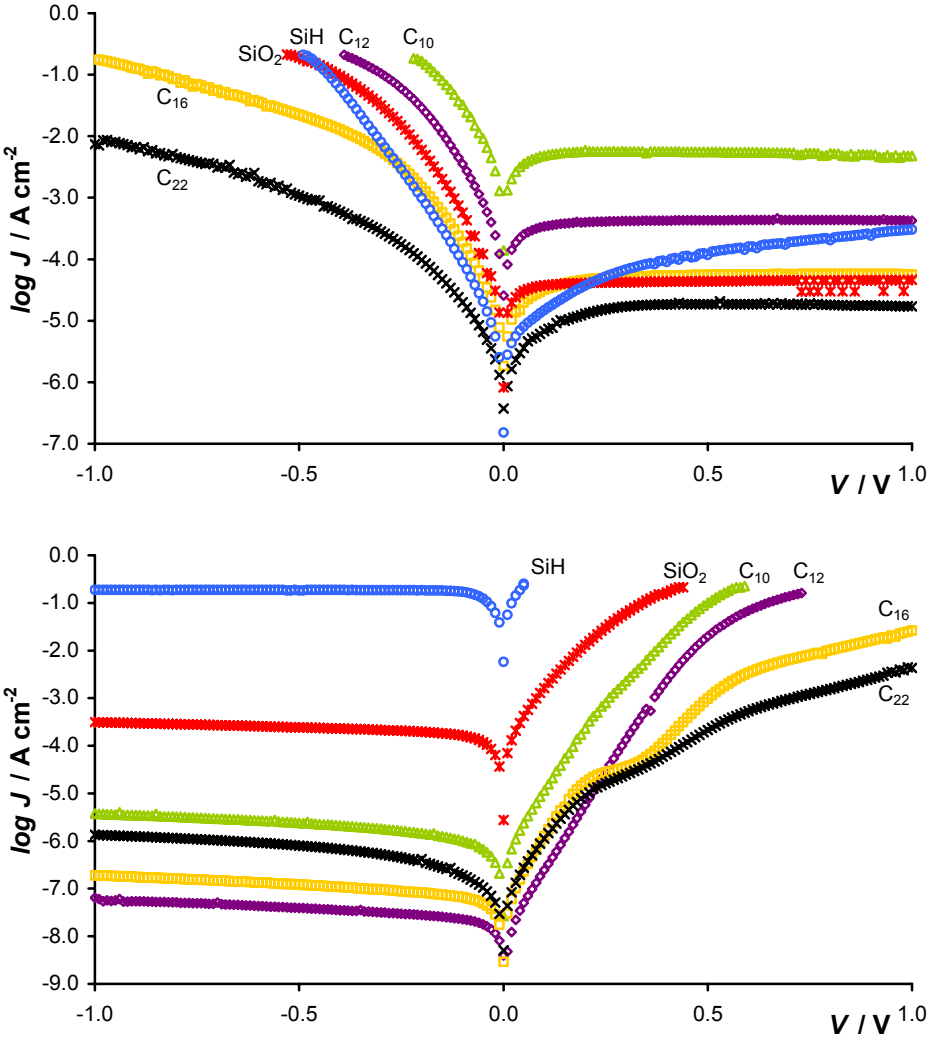

Figure 6.8 Current density versus bias voltage data for different insulators on (top) p-type silicon ($V < 0$: accumulation of holes and $V > 0$: depletion of holes), and (bottom) n-type silicon ($V < 0$: depletion of electrons and $V > 0$: accumulation of electrons).

The modification of n-type silicon with 1-alkenes displays a different *J-V* behavior than p-type silicon. As can be seen from the lower leakage currents in the depletion regime, the organic monolayers clearly display better insulating properties than n-type Si–H or SiO_2. Where the *J-V* curves of the C_{10} and C_{12} monolayers have their usual shape, the curves of C_{16} and C_{22} show a different behavior in the accumulation regime. A comprehensive discussion on this observation has been reported in our full paper.[10] Briefly, the observed difference could be the result of either mercury leakage through the C_{16} and C_{22} monolayers or possible differences in the structural layer properties that influence the transport mechanism.[39]

Figure 6.9 presents the *C*-*V* plots of the different MIS structures studied in this chapter. The *C*-*V* plots for all H-terminated samples and samples with C_{10}, C_{12}, and SiO_2 insulators on both types of silicon are typical for metal–semiconductor junctions where the capacitance in accumulation increases sharply with the applied voltage.[40] The additional peak of the pSi–C_{10} curve at -0.2 V might be related to a larger amount of interface charges. The *C*-*V* curves for samples with C_{16} and C_{22} insulators on both types of silicon show a plateau in the accumulation regime around |1 V| and increase strongly for higher voltages. The presence of a plateau indicates the formation of a real capacitance.

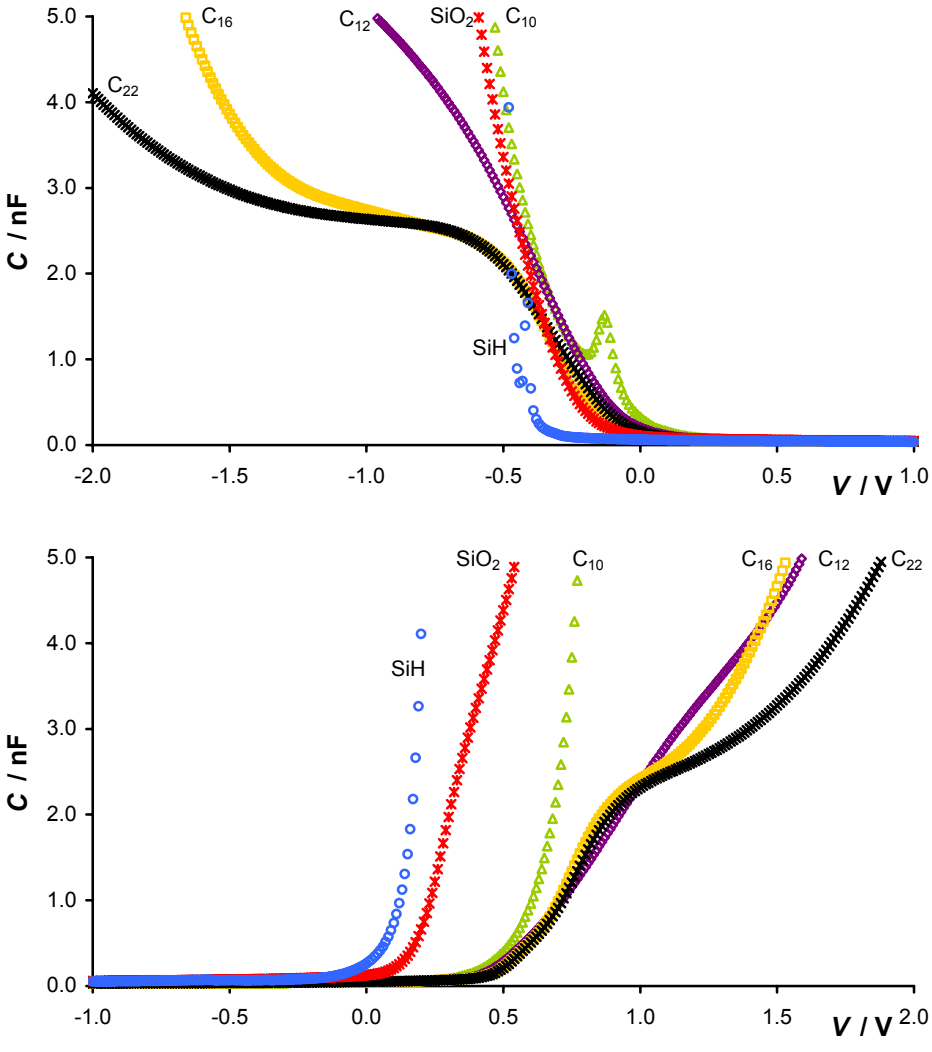

Figure 6.9 Capacitance-voltage plots for different insulators on (top) p-type silicon ($V < 0$: accumulation of holes and $V > 0$: depletion of holes), and (bottom) n-type silicon ($V < 0$: depletion of electrons and $V > 0$: accumulation of electrons).

Figure 6.10 shows the *C-V* data for the different insulators on n-type silicon in the Mott-Schottky form. The plots of the modified p-type silicon surfaces are linear in the region of 0.2 to 1.0 V (data not shown).

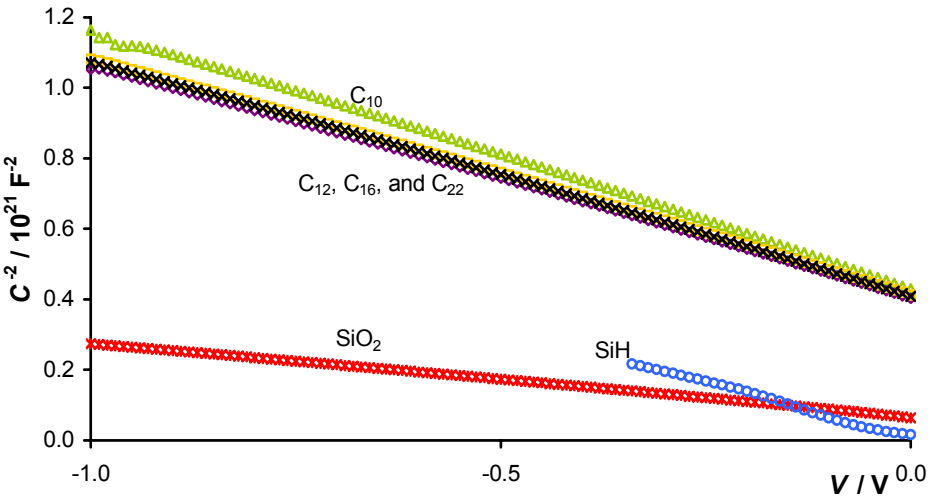

Figure 6.10 Mott-Schottky (C^{-2} versus V) plots for insulators on n-type silicon.

6.3.2.2 Barrier Height and Series Resistance

Table 6.1 shows the ideality factor, the barrier height and the series resistance of p-Si|C_nH_{2n+1}|Hg and n-Si|C_nH_{2n+1}|Hg structures as derived from the current density-voltage measurements. First we discuss the ideality factors, which were obtained from the low forward bias regime as depicted in Figure 6.4. The observed difference in the ideality factor for H-terminated p-type and n-type silicon is related to the intrinsic difference in barrier heights.[36] In case of the modified surfaces, the ideality factor increases with increasing monolayer thickness, with the exception of the pC_{10} sample. In addition, the modification of n-type silicon results in more ideal diode behavior as compared to p-type silicon.

The effective barrier height ($q\phi_{eff}$) increases with increasing monolayer thickness on p-type silicon, which is in line with Equation 6.2. In other words, the barrier for electrons from the metal to the semiconductor increases upon using longer 1-alkenes. In the case of n-type silicon the data on the barriers heights shows a different trend. While the values for $q\phi_{eff}$ increase from SiH, C_{10} to C_{12}, they decrease upon further increase of monolayer thickness. This could be the result of either mercury leakage through the monolayer or possible differences in the structural layer properties that influence the mechanism of transport.[39] At this stage the origin of the deviating behavior of the nC_{16} and nC_{22} samples is unclear.

Further, it can be concluded that the series resistance of monolayers on p-type silicon is strongly affected by the monolayer thickness. Upon increasing the monolayer thickness, the resistance increases nearly exponentially, showing that the insulating properties can precisely tuned via the use of 1-alkenes of different molecular length.

Table 6.1 The ideality factor (n), effective barrier height ($q\phi_{eff}$), and the series resistance (R_s) for different combinations of p-type and n-type Si(100) and monolayers.

	n	$q\phi_{eff}$ [eV]	R_S [Ωcm^2]
pSiH	1.49 ± 0.05	0.695 ± 0.002	- [a]
pC_{10}	1.78 ± 0.05	0.528 ± 0.002	0.49 ± 0.04
pC_{12}	1.57 ± 0.01	0.593 ± 0.001	0.99 ± 0.03
pC_{16}	1.69 ± 0.02	0.663 ± 0.001	4.14 ± 0.05
pC_{22}	2.16 ± 0.07	0.709 ± 0.002	22.84 ± 0.05
$pSiO_2$	1.43 ± 0.04	0.649 ± 0.007	1.31 ± 0.05
nSiH	3.40 ± 0.30	0.461 ± 0.003	0.225 ± 0.05 [b]
nC_{10}	1.22 ± 0.07	0.806 ± 0.005	1.18 ± 0.03
nC_{12}	1.34 ± 0.04	0.880 ± 0.003	1.39 ± 0.03
nC_{16}	1.34 ± 0.02	0.837 ± 0.001	- [c]
nC_{22}	1.63 ± 0.03	0.827 ± 0.002	- [c]
$nSiO_2$	1.67 ± 0.07	0.644 ± 0.003	1.03 ± 0.04

[a] The resistance could not be calculated, as the *J-V* plot does not bend away sufficiently in the forward bias regime (Figure 6.8, top). [b] R_S has been calculated via the Ohm's law in the region of 0-0.06 V. [c]) R_S could not be obtained due to the observation of distorted *J-V* plots in the higher forward bias regime.

As the *J-V* plots of the nC_{16} and nC_{22} samples were somewhat distorted (Figure 6.8, bottom) in the higher forward bias regime no values for R_s could be obtained. The values of nC_{10} and nC_{12} are slightly higher as the series resistance of the corresponding layers on p-type silicon, which might be related to the observed differences in the fixed charges *(vide infra*). In particular, the extraction of $q\phi_{eff}$ from the *J-V* measurements is known to be sensitive towards interface defects.[18-20,40]

Replacement of the SiO_2 layer by an organic monolayer of an equivalent thickness results in a higher effective barrier height and resistance as shown in Table 6.1. In addition

the leakage currents through organic monolayers are about 10 times as low as compared to SiO_2 of the same thickness.[10]

To conclude, the excellent insulating properties of Si–C linked organic monolayers on crystalline silicon surfaces clearly make them attractive for alternative gate insulators.

6.3.2.3 Dielectric Properties

Given the absence of a plateau in the accumulation regime of C_{10} and C_{12} layers on both p-type and n-type silicon (Figure 6.9) the insulating properties seem to be insufficient to result in a capacitor behavior. However, the *C*-*V* curves of the C_{16} and C_{22} layers do show a plateau in the accumulation regime implying the formation of an insulator capacitance. The values of the capacitance could be obtained via Equation 6.6 (Table 6.2). Subsequently, Equation 6.5 yielded the dielectric constant (k or ε_r), also known as the relative permittivity ($\varepsilon_r = \varepsilon / \varepsilon_0$), which is a measure of the ability of a material to be polarized by an electric field.

Table 6.2 Capacitance (C) and dielectric constant (ε_r) for C_{16} and C_{22} monolayers on p-type (left) and n-type (right) Si(100).

Insulator	C (nF)	ε_r
pC_{16}	3.2 ± 0.2	1.7 ± 0.1
pC_{22}	2.8 ± 0.2	2.2 ± 0.2

Insulator	C (nF)	ε_r
nC_{16}	3.6 ± 0.2	1.9 ± 0.1
nC_{22}	3.5 ± 0.1	2.8 ± 0.1

In literature, different values for the dielectric constants of alkyl monolayers are reported. Values of 2 and 2.7 ± 0.3 were found for alkyl monolayers of thiol derivatives on the gold surface[41,42] and a value of 2.13 has been reported for an octadecyl monolayer on hydrogen-terminated silicon.[33] These values, as well as most of the values reported in Table 6.2, are lower than the average value found by Yu et al. (3.3 ± 0.6).[43] It is expected that the presence of some oxide will increase the effective dielectric constant, since ε_r = 3.9 for SiO_2. This would imply that C_{22} samples contain a little bit more oxide as compared to the others, which is in line with static water contact angles data (100-102° for C_{22} and 108-109° for C_{16}). In addition, the low water contact angles, 90.6 ± 3.0° up to 101 ± 7.5° and the corresponding high dielectric constants found by Yu et al. are in line with these observations.[43]

6.3.2.4 Insulator Charges

Using the insulator capacitance C_{ins} in combination with Equation 6.7 the amount of fixed charges was calculated (Table 6.3). State-of-the-art MOS structures show values for N_f of

the order of 10^9-10^{11} cm^{-2} for Si(100).[44] The samples as presented in Table 6.3 have remarkably low amounts of fixed charge, especially if one takes into account that the monolayers were fabricated using wet-bench chemistry at low temperatures as compared to MOS structure fabrication conditions. Via the cross section of an attached alkyl chain (19.8 $Å^2$ / cos(26°) = 22.0 $Å^2$)[45] the number of attached chains per fixed charged was calculated (Table 6.3), showing only one fixed charge for per ~750 and ~170 attached alkenes, on p-type and n-type silicon, respectively.

The number of fixed charges of modified n-type silicon surfaces is about 4.5 times is high as compared to p-type silicon. Kar et al. who studied the density of interface charged traps found a comparable qualitative behavior for both types of silicon.[33] They attributed the difference to the influence of the Fermi level on the ability to form a Si–C bond. In the case of n-type silicon the surface silicon radical is likely to be saturated with electrons from the conduction band. The resulting stabilized sites are less susceptible for the reaction with electron-rich alkenes, as compared to the unsaturated sites on p-type silicon. In §6.4 the interesting results on the low number of fixed charges are further studied for monolayers prepared with 1-alkenes and 1-alkynes, respectively.

Table 6.3 Total number of fixed charges per cm^2 and charge per attached chain (with a cross section of 22.0 $Å^2$) calculated for C_{16} and C_{22} monolayers on p-type and n-type silicon surfaces.

Insulator	N_f [cm^{-2}]	Attached chains / charge
pC_{16}	$(5.8 \pm 1.0)\cdot10^{11}$	784
pC_{22}	$(6.2 \pm 2.0)\cdot10^{11}$	733
nC_{16}	$(2.7 \pm 0.2)\cdot10^{12}$	168
nC_{22}	$(2.7 \pm 0.1)\cdot10^{12}$	168

6.3.2.5 Tunneling Constants

By the evaluation of the tunneling constant one can obtain information about the contributions of hole and electron tunneling to the overall transport mechanism. Theoretical values mentioned for hole and electron tunneling through alkyl layers are 0.4-0.8 $Å^{-1}$ and 0.8-1.0 $Å^{-1}$, respectively.[17] Here, the tunneling constants were calculated from the difference in the barrier height and effective barrier heights, using Equation 6.2 (Table 6.4).

Apart from pC_{10} the results of the modified p-type silicon samples indicate a larger dependency for holes as compared to electrons. This has also been found in literature, where hole tunneling is thought to be more efficient than electron tunneling.[17,39] In contrast,

the tunneling parameters of nC_{10} and nC_{12} are high, which indicates a less efficient tunneling process. To the best of our knowledge, such high values have not been reported yet in literature.

Table 6.4 Tunneling constants for monolayers on p-type (left) and n-type (right) silicon.

Insulator	β [Å^{-1}]	Insulator	β [Å^{-1}]
pC_{10}	1.00 ± 0.05	nC_{10}	1.18 ± 0.04
pC_{12}	0.43 ± 0.09	nC_{12}	1.30 ± 0.06
pC_{16}	0.46 ± 0.04	nC_{16}	0.87 ± 0.02
pC_{22}	0.46 ± 0.06	nC_{22}	0.58 ± 0.02

6.3.3 Conclusions

Covalently attached alkyl monolayers on silicon surfaces offer hybrid materials with, from an electronic point of view, promising insulating and passivating properties. The monolayer resistance could be precisely tuned via the alkyl chain length and the numbers of fixed charges were, given the monolayer preparation conditions, relatively low. The *J*-*V* data on the nC_{16} and nC_{22} sample was different in the higher forward bias regime, either due to mercury leakage through the monolayer or possible differences in the structural layer properties that influence the mechanism of transport. Given the numerous possibilities for the chemical modification in combination with their excellent electrical properties as compared to SiO_2, Si–C linked organic monolayers on crystalline silicon surfaces are a very attractive candidate for future gate insulators.

6.4 Improved Electrical Monolayer Properties: 1-Alkenes versus 1-Alkynes

6.4.1 Introduction

In §6.3 it was presented that metal–insulator–semiconductor (MIS) structures of 1-alkene-derived monolayers (Si–C_nH_{2n+1} with n = 10, 12, 16, and 22) showed – in terms of insulating properties and amount of fixed charges – outstanding silicon–interface properties and that the electrical behavior could be precisely tuned via the chain length. However, while the insulating properties of such alkyl monolayers were clearly better than those of a thermal silicon oxide layer of comparable thickness, it would be of significant interest to further increase these. Therefore, in this paragraph the comparison of the electrical properties of monolayers derived from 1-alkenes and 1-alkynes is presented.

The use of 1-alkynes might be favored, since previous work in our labs[6] and those of others[46] has shown that alkynes form two Si–C bonds per reacting molecule on porous silicon and Si(100). Up to the year of 2000, the alkyne C≡C bond has been found to react either once[2,47-51] or twice,[46] depending on the experimental conditions. The use of catalysts or white light-supported reaction results in alkenyl attachment, while the thermal reaction of 1-octadecyne with porous silicon without any catalyst has been reported to yield two Si–C bonds per molecule. The thermal reaction of 1-alkynes with the Si(100)–H was studied by Sieval et al.[6] The results from IR spectroscopy and X-ray reflectivity measurements indicated bis-silylation, which was supported by quantum mechanical calculations. Afterwards, theoretical calculations of Yuan et al. supported the formation of only one Si–C bond upon the reaction between 1-alkynes and the Si(111)–H surface.[52] The authors report that the results of their calculations are in line with the IR data on the UV-promoted reaction of 1-octyne on Si(111)–H.[47] In addition, they write that only one Si–C bond is formed in the case of thermal conditions, referring to the work of Linford et al.[2] However, this is not correct, since the cited study reports only two reactions involving a 1-alkyne, which are both peroxide-catalyzed. To the best of our knowledge no studies have been reported regarding the number of Si–C bonds that have been formed upon the *thermal* reaction of 1-alkynes with Si(111)–H.

Characteristic of 1-alkene or 1-alkyne-derived monolayers on the H-terminated silicon surface is that the molecular cross-section of the attached alkyl chain prevents reaction of all individual Si–H bonds, i.e., upon formation of a densely packed monolayer on Si(111) about 50-55% of the Si–H sites has reacted,[7,8] while on Si(100) this is about 30-35%. The remaining surface Si–H bonds can in principle react with oxygen, yielding a structure such as depicted in Scheme 6.1 top right, in which both the formation of silanol groups and backside incorporation of oxygen atoms are illustrated. XPS analysis of such monolayers has shown that the amount of oxygen being incorporated after formation of densely packed monolayers is very small even after storage for months under ambient conditions,[5] but never completely absent. This is of specific importance for the electrical properties of such surfaces, which are determined to a large degree by surface defects such as caused by (partial) oxidation.

In the case of Si(100)–H, formation of a densely packed 1-alkyne-derived monolayer yields a smaller number of unreacted Si–H sites than formation of a 1-alkene-derived monolayer (Scheme 6.1). Therefore we hypothesized that attachment of 1-alkynes will lead to a decrease in the number of surface defects that might result in fixed charges, and thus to

a concomitant increase in insulating properties. The present paragraph presents such data by the study of the metal–insulator–semiconductor (MIS) structures using a mercury probe as described §6.2 and §6.3.[10] These are complemented by X-ray photoelectron spectroscopy (XPS) measurements to correlate the amount of oxygen present with the electrical properties.

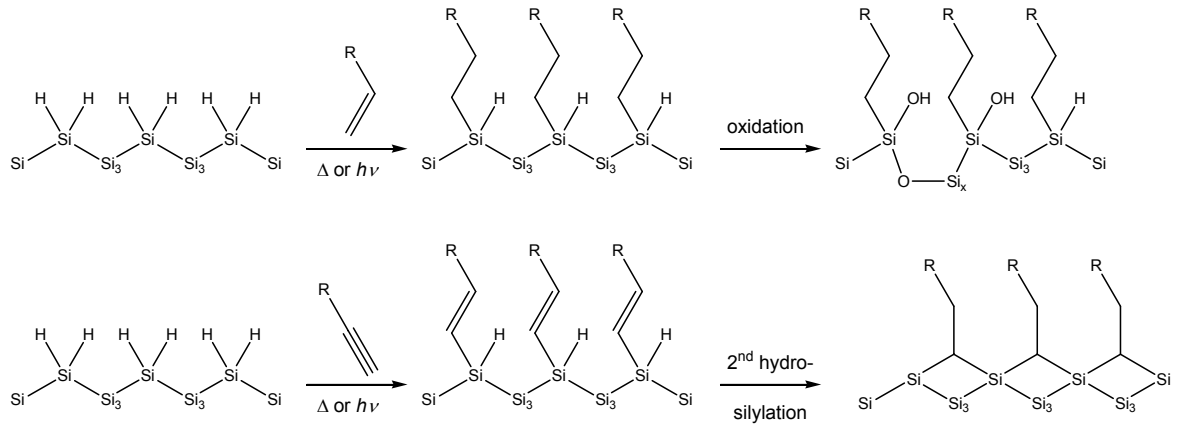

Scheme 6.1 Attachment and partial oxidation of monolayers derived from 1-alkenes (top) and 1-alkynes (bottom) on crystalline Si(100) surfaces.

Apart from the introduction of oxygen via a process as depicted in Scheme 6.1, one can also hypothesize the reaction of remaining dangling bonds oxygen. Examples of possible structures are given in Scheme 6.2. Again, in terms of fixed charges a difference between the use of 1-alkenes and 1-alkynes might be expected. Given the low amounts of Si–O as measured via XPS on modified silicon samples, even up to 3 months after preparation,[5] we believe this pathway has a minor contribution.

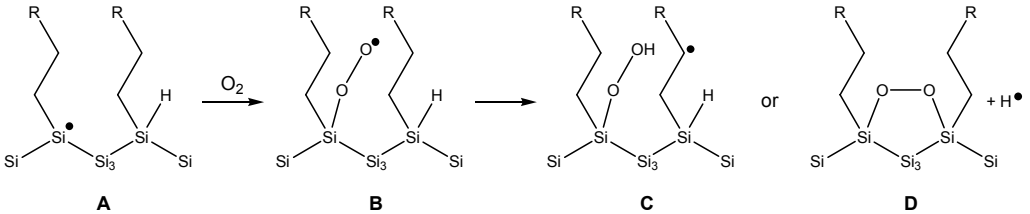

Scheme 6.2 Schematic representation of the remaining dangling bonds on a 1-alkene-modified Si(100) surface (A), which can be oxidized (B), and perhaps abstract a hydrogen radical from a nearby alkyl chain (C) or silicon atom (D).

6.4.2 Experimental Section

1-Octadecene (Fluka, ≥95%) was distilled twice under reduced pressure. The synthesis and purification of 1-octadecyne from 1-octadecene is described in literature.[6]

Two different types of single-polished silicon 4-inch wafers were used (n-Si(100): 1-10 Ωcm and n-Si(111): 1-5 Ωcm). The wafers for samples used in the Hg-probe characterization were provided with a metallic back contact as described in literature.[10] The samples for the XPS measurements were taken from the same type of wafers (without back contact).

Octadecyl monolayers derived from 1-octadecene and 1-octadecyne were prepared via the thermal method (§3.2.5.2). The 1-alkene or 1-alkyne solution in mesitylene was 0.2 M.

The electrical characterization of the samples was performed as described earlier,[10] according to a sequence of *J-V* and *C-V* measurements.[11]

The XPS measurements were performed on a VG Ionex system equipped with a Clam II analyzer and a standard AlKα X-ray source. Spectra were taken in normal emission at 10^{-9} mbar within 10 minutes. All C_{1s} peaks corresponding to hydrocarbons were calibrated to a binding energy of 285.0 eV to correct for the energy shift caused by charging. The data in the Si_{2p} region was fitted using the three different contributions: Si_{2p3}, Si_{2p1}, and Si_{2p}(Ox), at 99.33, 99.93, and 102.47 eV, respectively. For each combination of reagent/substrate facets two independent samples were prepared and studied with XPS.

6.4.3 Results and Discussion

6.4.3.1 Plots Derived from *J-V* and *C-V* Measurements

Figure 6.11 (top) presents the *log(J)-V* and Mott-Schottky plots of Si(100) and Si(111) substrates that are H-terminated or modified with 1-octadecyne or 1-octadecene. A distinct feature in the *J-V* plots of Figure 6.11 is that sample modified with 1-octadecyne yields a leakage current that is at least twice as low as compared to the one of 1-octadecene-derived monolayers. Furthermore, the deviation of the *J-V* behavior in the forward bias regime was also observed for monolayers of 1-hexadecene and 1-docosene on n-type Si(100), as described in §6.3. From the plots the effective barrier height and monolayer resistance were obtained, as reported and discussed in §6.4.3.2.

The Mott-Schottky plots are presented in Figure 6.11 (bottom) and were all found to be linear in the regime of -0.1 V to 0 V. Extrapolation of the plots yields V_{fb} and the thus obtained values are presented and discussed in §6.4.3.3.

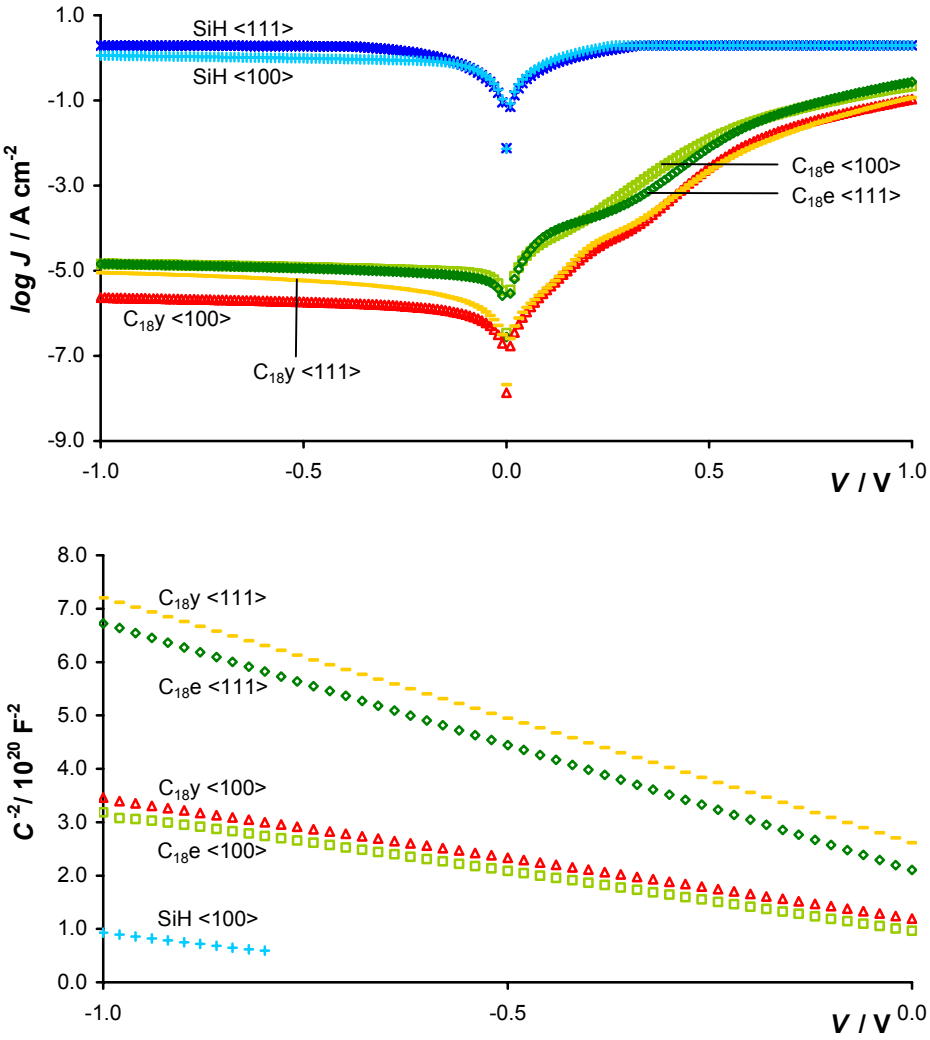

Figure 6.11 The *log(J)-V* plots (top) and Mott-Schottky plots (bottom) of Si(100) and Si(111) substrates that are H-terminated or modified with 1-octadecyne (C_{18}y) or 1-octadecene (C_{18}e). The current density values of the Si–H samples clip at 1.95 A/cm^2 due to the current compliance of the *I-V* meter. No capacitance data for the n-Si(111)–H could be obtained due to their Ohmic character. The nSi(100)–H surface showed only capacitive behavior in the regime of -1.0 to -0.8 V.

6.4.3.2 Barrier Height and Series Resistance

Table 6.5 presents the effective barrier heights and the series resistance for different MIS structures. The effective barrier height increases clearly upon the modification of H-terminated surfaces. In addition, it can be seen that the use of 1-octadecyne yields effective barrier heights that are ~0.08 eV higher than those of 1-octadecene-derived monolayers, indicating that the former results in structure with better interface properties (i.e., less defects). Note that C_{18} monolayers derived from 1-octadecene and 1-octadecyne

have the same thickness. As a result, any difference can be attributed to the different reactive group (alkene vs alkyne).

Based on theoretical calculations one can expect a difference between the number of Si–C bonds upon the reaction of 1-alkynes with the hydrogen-terminated surfaces of Si(100)[6] and Si(111),[52] respectively. However, the $q\phi_{eff}$ values for each type of reagent (alkene/alkyne) are comparable, irrespective the substrate orientation, indicating that the amounts of undesired charges (remaining amounts of Si–H sites, dangling bonds, oxidized silicon) is comparable.

Table 6.5 The effective barrier height and the series resistance for etched and modified n-Si(100) and n-Si(111) surfaces.

Compound	Silicon	$q\phi_{eff}$ [eV]	R_S [Ωcm^2]
H-terminated	n-Si(100)	0.419 $\pm$ 0.001	0.134 $\pm$ 0.003 [a]
H-terminated	n-Si(111)	0.424 $\pm$ 0.001	0.163 $\pm$ 0.004 [a]
1-octadecene	n-Si(100)	0.678 $\pm$ 0.001	2.15 $\pm$ 0.04
1-octadecene	n-Si(111)	0.684 $\pm$ 0.002	2.19 $\pm$ 0.03
1-octadecyne	n-Si(100)	0.763 $\pm$ 0.004	3.36 $\pm$ 0.03
1-octadecyne	n-Si(111)	0.761 $\pm$ 0.006	3.24 $\pm$ 0.03

[a] R_S has been calculated for the SiH samples by the Ohm's law in the region of 0-0.2 V.

Values for R_S were obtained in the regime of high forward bias voltages (0.7-0.8 V) via Equation 6.3. Due to the Ohmic behavior of the Si–H/Hg structures, the total resistance of the H-terminated Si(100) samples could not be obtained via Equation 6.3. Nevertheless, R_s could be estimated via Ohm's law. The low values for R_s of the H-terminated surfaces indicate that the resistance at the back electrode contact with the silicon bulk has only a small contribution to the total device series resistance. The presence of an octadecyl monolayer results in higher series resistances.

A monolayer of 1-octadecene on n-type Si(100) resulted in a resistance of 2.15 Ωcm^2, which is in line with the values found for monolayer of 1-decene and 1-dodecene on the same substrate as given in Table 6.1 (1.18 and 1.39 Ωcm^2, respectively).

The use of 1-octadecyne yields a significantly higher series resistance as compared to 1-octadecene. Again no significant differences between Si(100) and Si(111) were observed, which is in contrast with SiO_2 layers on Si(100) and Si(111).[53]

To conclude this paragraph, the improved electrical properties of 1-alkynes over 1-alkenes on the Si(100)–H surface can be associated with the number of Si–C bonds that are formed, resulting in lower amounts of remaining Si–H. This is in agreement with our expectation as outlined in §6.4.1. The situation for Si(111) is more complex, since 1-octadecyne results in a higher resistance on both surfaces as compared to 1-octadecene. After all, if indeed only one Si–C bond is formed for the reaction of 1-octadecyne with Si(111)–H,[52] no differences in the series resistance with 1-octadecene-derived monolayer are expected. The results might indicate that monolayers derived from 1-alkenes are better packed than monolayers derived from 1-alkenes. The origin of the observed differences in barrier height and resistance of monolayers prepared via 1-alkenes and 1-alkynes will be further discussed in the next paragraphs.

6.4.3.3 Flatband Potential and Insulator Charges

Initially, our aim was to obtain the number of insulator charges via the approach as described in §6.2.3, in which the insulator capacitance (C_{ins}) is used to calculate the amount of fixed charges with Equation 6.7. However, no plateau values in the *C*-*V* plots were observed for the C_{18} layers on n-type and p-type Si(100) and Si(111) and hence no insulator capacitances could be obtained via the method used in §6.3. Alternatively, the data on V_{fb} can be used to study the silicon–monolayer interfaces (Table 6.6).

Table 6.6 The flatband voltage (V_{fb}) and the theoretical flatband potential[22] (ϕ_{MSi}) of the six different structures used in this study.

Compound	Silicon	V_{fb} [V]	ϕ_{MSi} [V]
H-terminated	n-Si(100)	-0.46 ± 0.07 [a]	0.20
H-terminated	n-Si(111)	- [b]	0.18
1-octadecene	n-Si(100)	0.45 ± 0.01	0.20
1-octadecene	n-Si(111)	0.46 ± 0.01	0.18
1-octadecyne	n-Si(100)	0.54 ± 0.01	0.19
1-octadecyne	n-Si(111)	0.58 ± 0.01	0.18

[a] The Mott-Schottky analysis for n-Si(100)–H could only be performed for the data from -1.0 to -0.8 V and hence the possibilities to fit the data were limited. This could explain the deviating value of V_{fb}. A negative value for V_{fb} indicates the presence of large amounts of positive charges; [b] The Mott-Schottky analysis for n-Si(111)–H could not be carried out since no depletion layer was formed on this sample due to its Ohmic behavior.

The silicon surfaces modified with 1-octadecyne show values for V_{fb} that are more positive as compared to those of 1-octadecene. In all cases the theoretical flatband potential[22] ϕ_{MSi} (0.18-0.20 V) is lower, indicating the presence of negative charges as was also found for the surfaces modified with C_{10}, C_{12}, C_{16}, and C_{22} 1-alkenes.[10] Oxide formation on silicon surfaces is generally accompanied with the introduction of positive charges,[53] resulting in more negative values for V_{fb}. Given the observed difference in V_{fb} this implies that the 1-octadecene-derived monolayers on n-type silicon contain more oxygen as compared to the 1-octadecyne-derived monolayers. This result is in line with the results obtained via the *J-V* measurements, which show higher values for the effective barrier height and series resistance for alkynes than for alkenes, as discussed in §6.4.3.2.

Very recently Kar et al. published a method to analyze the capacitance in a different way.[54] In their theory it is reasoned that a plot of $(C^{-1} \times d(C)/d(V))^{0.5}$ versus C (where C is corrected for the series resistance) under conditions of charge accumulation gives a straight line of which the intercept with the C-axis yields the capacitance of the isolator. They successfully applied this theory in the analysis of the *C-V* data of several high-K dielectrics. The theory of Kar et al. was used to analyze the *C-V* data of the silicon samples modified with 1-octadecene and 1-octadecyne and indeed a linear trend was observed in the capacitance range of 3.0-4.0 nF (plots are not shown). The thus obtained values for C_{ins} as well as the dielectric constants, calculated via Equation 6.5 with l = 19.5 Å as measured by Sieval et al. for monolayers derived from 1-octadecene[3] are presented in Table 6.7.

Table 6.7 Capacitance (obtained via the method of Kar et al.),[54] dielectric constant (calculated via Equation 6.5 with l = 19.5 Å)[3], and number of fixed charges of the silicon samples modified with 1-octadecyne and 1-octadecene.

Compound	Silicon	C_{ins}[a] [nF]	ε_r [-]	N_f [cm^{-2}]
1-octadecyne	n-Si(100)	5.2 ± 0.5	3.0 ± 0.1	(3.0 ± 0.1)·10^{12}
1-octadecene	n-Si(100)	6.7 ± 0.5	3.9 ± 0.3	(2.8 ± 0.1)·10^{12}
1-octadecyne	n-Si(111)	4.8 ± 0.5	2.8 ± 0.1	(3.2 ± 0.1)·10^{12}
1-octadecene	n-Si(111)	6.3 ± 0.5	3.7 ± 0.1	(2.9 ± 0.1)·10^{12}

[a] As the contact areas were different for the samples studied in §6.3 and §6.4 (3.7 ·10^{-3} and 5.2 10^{-3} cm^2, respectively), the capacitances in this column were obtained by dividing the measured values by a factor of (5.2 / 3.7 =) 1.405, allowing direct comparison of the values for the capacitance in Tables 6.2 and 6.7.

The capacitance of the 1-alkene-derived monolayers (and consequently the dielectric constant, via Equation 6.5) is higher than the values obtained for the 1-alkyne-derived monolayers. Apart from R_S, $q\phi_{eff}$, and V_{fb} also the values of C_{ins} and ε_r indicate larger amounts of oxide in the monolayers derived from 1-alkenes as compared to 1-alkynes. In addition, the numbers of fixed charges have been calculated via Equation 6.7 and the values for the insulator capacitance (Table 6.7). Although the thus obtained numbers of fixed charges are low and of the same order of magnitude as those found for layers of 1-hexadecene and 1-docosene on n-type Si(100), the data are somewhat puzzling. The numbers of fixed charges of the 1-alkyne-derived monolayers are slightly higher than those of the 1-alkene-derived monolayers, irrespective of the surface facets. Before discussing this remarkable observation, which seems to be not consistent with the remaining electrical data, we first present the re-analyzed the *C-V* data on the C_{16} and C_{22} samples using the method of Kar et al. (Table 6.8).[54] In order to facilitate the comparison, the data obtained via the plateau values in the C-V plots – as presented and discussed in §6.3 – have been added to Table 6.8 as well.

Table 6.8 Capacitance, dielectric constant, number of fixed charges calculated using the method of Kar et al.[54] for monolayers derived from 1-hexadecene and 1-docosene on n-type and p-type Si(100) surface (top). The data as obtained via the *C-V* plateau values (§6.3) has been added in order to compare both methods (bottom).

		C_{ins} via method Kar et al.		
Compound	Silicon	C_{ins} [nF]	ε_r [-]	N_f [cm^{-2}]
1-hexadecene	n-Si(100)	3.3 ± 0.2	1.6 ± 0.1	$(2.5 \pm 0.2)\cdot10^{12}$
1-docosene	n-Si(100)	3.0 ± 0.1	2.4 ± 0.1	$(2.3 \pm 0.1)\cdot10^{12}$
1-hexadecene	p-Si(100)	3.1 ± 0.1	1.6 ± 0.1	$(5.7 \pm 1.0)\cdot10^{11}$
1-docosene	p-Si(100)	2.7 ± 0.2	2.4 ± 0.1	$(5.9\cdot\pm 2.0)\cdot10^{11}$

		C_{ins} via *C-V* plateau values (§6.3)		
Compound	Silicon	C_{ins} [nF]	ε_r [-]	N_f [cm^{-2}]
1-hexadecene	n-Si(100)	3.6 ± 0.2	1.9 ± 0.1	$(2.7 \pm 0.2)\cdot10^{12}$
1-docosene	n-Si(100)	3.5 ± 0.1	2.8 ± 0.1	$(2.7 \pm 0.1)\cdot10^{12}$
1-hexadecene	p-Si(100)	3.2 ± 0.2	1.7 ± 0.1	$(5.8 \pm 1.0)\cdot10^{11}$
1-docosene	p-Si(100)	2.8 ± 0.2	2.2 ± 0.2	$(6.2 \pm 2.0)\cdot10^{11}$

Although there are some small differences (3-16%) between the C_{ins} data analyzed via method of Kar et al. and the method via the *C-V* plateaus the data on ε_r and N_f is very comparable, in particular for the p-type silicon substrates. Both methods give the same trend and hence the method of Kar et al., which has only very recently become available to us, does not force us to change the conclusions drawn in §6.3.

The data in Tables 6.7 and 6.8 show for the samples modified with 1-octadecene and 1-octadecyne higher values for the capacitance (and hence the dielectric constant) as compared to the data on monolayers prepared from 1-hexadecene and 1-docosene. This indicates that the samples studied in §6.4 contain more oxide as compared to the samples studied in §6.3. Nevertheless, the data presented in Table 6.7 points to a difference between monolayers derived from 1-alkenes and 1-alkynes.

The presence of more oxide makes it difficult to draw conclusions from the observed trend in the numbers of fixed charges for monolayers prepared from 1-alkenes en 1-alkynes. More oxidation will result in more defects and this might result in the charge compensation. This issue and the effect of aging on the electrical characteristics of modified silicon samples are more extensively discussed elsewhere.[55]

6.4.3.4 X-ray Photoelectron Spectroscopy

In order to measure the degree of oxidation, modified silicon samples were subjected to X-ray photoelectron spectroscopy (XPS). The Si_{2p} regions of monolayers of 1-octadecyne on n-S(100) and n-Si(111) surfaces are given in Figure 6.12. From the Si_{2p} region of the resulting XPS data the surface area of the Si_{2p}(ox) and Si_{2p}(non-ox) contributions were obtained. Table 6.9 presents the complete set of data on the XPS measurements.

For both types of silicon, the degree of oxidation – calculated via $Si_{2p}(Ox)/(Si_{2p1} + Si_{2p3})$ – of 1-octadecene-derived structures is higher as compared to those of 1-octadecyne-derived structures. This would be in line with the involvement of a significant contribution of bis-silylation in the case of 1-alkynes, with a concomitant reduction of the surface oxidation. In addition, the XPS data is in line with the data of V_{fb}, $q\phi_{eff}$, and ε_r.

Despite the higher amount of Si–H bonds that is present on the Si(100) surface, the degree of oxidation of the modified Si(111) surface is higher as compared to the Si(100) surface, as follows from Table 6.9. It is known that substrate conditions play an important role in the growth of native oxide on the silicon surface and it has been reported that the oxide growth rate on Si(111) is higher than on Si(100), both for native oxide as well as for

thermal oxide.[23,56] Also the type of doping and its concentration affect the oxide growth, but in this study these two parameters are similar for Si(100) and Si(111).

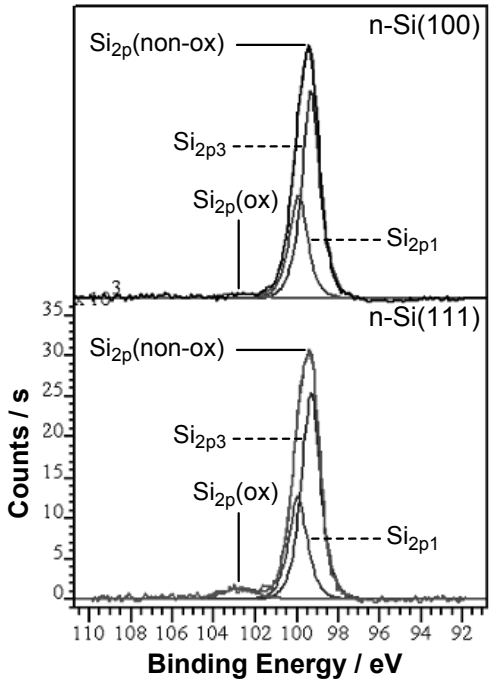

Figure 6.12 Si_{2p} regions of 1-octadecyne-derived monolayers on n-Si(100) (top) and n-Si(111) (bottom). The data is indicated by labels via solid lines, while the fit curves of the Si_{2p3} and Si_{2p1} peaks are indicated by labels via dashed lines. The scaling on the y-axis of the top figure is the same is of the bottom figure.

Table 6.9 Averaged values for $Si_{2p}(Ox)/(Si_{2p1} + Si_{2p3})$, which reflect the degree of oxidation on n-(Si(100) and n-Si(111) samples modified with 1-octadecene and 1-octadecyne.

Compound	Silicon	$Si_{2p}(Ox)/(Si_{2p1} + Si_{2p3})$
1-octadecyne	n-Si(100)	0.030 (±0.003)
1-octadecene	n-Si(100)	0.049 (±0.002)
1-octadecyne	n-Si(111)	0.060 (±0.005)
1-octadecene	n-Si(111)	0.093 (±0.002)

6.4.4 Conclusions

High-quality organic monolayers were prepared by the thermal reaction of 1-alkenes and 1-alkynes with the H-terminated silicon surface. The attachment of the monolayer inhibits surface oxidation and the monolayers are very stable, as they are linked via a covalent Si–C bond. In addition, they allow the integration of sensing functionalities, which makes them

highly interesting for the further development of silicon-based sensor technology. Therefore extensive electrical measurements have been performed to characterize these monolayers in this respect.

Via multiple *J-V* and *C-V* measurements $q\phi_{eff}$, R_S, and V_{fb} have been derived to obtain information on the electrical properties of the monolayer and the silicon-monolayer interface. It was found that 1-alkynes have superior insulating properties as compared to 1-alkenes. The resistance of the former type of layers was higher and additionally, the values for V_{fb} indicated lower degrees of oxidation. This was indeed confirmed by XPS measurements. Concerning the electrical data there was no significant influence of substrate orientation. However, XPS showed that the monolayers on the Si(111) surface contained more oxygen as compared to Si(100). In addition, a method recently published by Kar et al. was used to evaluate the *C-V* data on the silicon substrates modified with 1-octadecene and 1-octadecyne. This analysis revealed that the C_{18}-covered silicon samples seem to contain more oxide as compared to the C_{10}, C_{12}, C_{16}, and C_{22}-modified samples studied in §6.3, as indicated by the higher values for the dielectric constant. This might be due to aging of the C_{18}-samples. Nevertheless, the data presented in paragraph points to an interesting difference between the electrical properties of monolayers derived from 1-alkenes and 1-alkynes. The ease of fabrication and the outstanding electrical properties show the potential of, in particular, 1-alkyne-derived monolayers in the fabrication of creating hybrid molecular-silicon devices.

References and Notes

[1] Linford, M. R.; Chidsey, C. E. D. *J. Am. Chem. Soc.* **1993**, *115*, 12631-12632.

[2] Linford, M. R.; Fenter, P.; Eisenberger, P. M.; Chidsey, C. E. D. *J. Am. Chem. Soc.* **1995**, *117*, 3145-3155.

[3] Sieval, A. B.; Demirel, A. L.; Nissink, J. W. M.; Linford, M. R.; van der Maas, J. H.; de Jeu, W. H.; Zuilhof, H.; Sudhölter, E. J. R. *Langmuir* **1998**, *14*, 1759-1768.

[4] Sieval, A. B.; Vleeming, V.; Zuilhof, H.; Sudhölter, E. J. R. *Langmuir* **1999**, *15*, 8288-8291.

[5] Sieval, A. B.; Linke, R.; Zuilhof, H.; Sudhölter, E. J. R. *Adv. Mat.* **2000**, *12*, 1457-1460.

[6] Sieval, A. B.; Opitz, R.; Maas, H. P. A.; Schoeman, M. G.; Meijer, G.; Vergeldt, F. J.; Zuilhof, H.; Sudhölter, E. J. R. *Langmuir* **2000**, *16*, 10359-10368.

[7] Sieval, A. B.; van den Hout, B.; Zuilhof, H.; Sudhölter, E. J. R. *Langmuir* **2000**, *16*, 2987-2990.

[8] Sieval, A. B.; van den Hout, B.; Zuilhof, H.; Sudhölter, E. J. R. *Langmuir* **2001**, *17*, 2172-2181.

[9] Sieval, A. B.; Huisman, C. L.; Schonecker, A.; Schuurmans, F. M.; van der Heide, A. S. H.; Goossens, A.; Sinke, W. C.; Zuilhof, H.; Sudhölter, E. J. R. *J. Phys. Chem. B* **2003**, *107*, 6846-6852.

[10] Faber, E. J.; de Smet, L. C. P. M.; Olthuis, W.; Zuilhof, H.; Sudhölter, E. J. R.; Bergveld, P.; van den Berg, A. *ChemPhysChem* **2005**, *6*, 2153-2166.

[11] Faber, E. J.; de Smet, L. C. P. M.; Thüne, P. C.; Olthuis, W.; Zuilhof, H.; Sudhölter, E. J. R.; Bergveld, P.; van den Berg, A. - manuscript in preparation.

[12] Faber, E. J.; de Smet, L. C. P. M.; Groeneveld, W.; Sparreboom, W.; Olthuis, W.; Zuilhof, H.; Sudhölter, E. J. R.; Bergveld, P.; van den Berg, A. - manuscript in preparation.

[13] Upon biasing, the thermal equilibrium situation in a metal-semiconductor contact (as present in Figure 6.1b) is no longer maintained and therefore the corresponding energy diagrams get rather complex, especially in the space-charge region. Here, the aim is to show that positive and negative biases have an opposite effect on the band bending ($q\phi_i$ and W_S), respectively.

[14] The current density J is defined by the electric current per unit area: $J = I / A$ (A cm^{-2}).

[15] A conventional diode consists of two regions of semiconductor each having a different type of dopant, resulting in a p-n junction diode. In theory, a diode allows an electric current flow in only one direction. In this chapter we focus on a variation of a diode, the metal-semiconductor junction of which the electrical behavior can be described using the Schottky diode theory. As a result, we do not discuss the operation of a diode itself. The Light-Emitting Diode (LED) is probably the most well-known type of diode as it emits light and is used in many applications.

[16] The diode ideality factor n is a measure how closely an I-V characteristic matches the ideal characteristic.

[17] Selzer, Y.; Salomon, A.; Cahen, D. *J. Phys. Chem. B.* **2002**, *106*, 10432-10439.

[18] Liu, Y. J.; Yu, H. Z. *ChemPhysChem* **2002**, *3*, 799-802.

[19] Liu, Y. J.; Yu, H. Z. *ChemPhysChem* **2003**, *4*, 335-342.

[20] Liu, Y. J.; Yu, H. Z. *J. Phys. Chem. B.* **2003**, *107*, 7803-7811.

[21] Nicollian, E. H.; Brews, J. R. *MOS Physics and Technology*, Wiley: New York, 1982, pp822-826.

[22] The theoretical flatband voltage can be calculated via the work functions of the metal and the silicon. More information can be found in reference [10].

[23] Zhang, X. G. *Electrochemistry of Silicon and its Oxide*, New York: Kluwer Academic/Plenum Publishers, 2001.

[24] Sakurai, T.; Sugano, T. *J. Appl. Phys.* **1981**, *52*, 2889-2896.

[25] Haick, H.; Ambrico, M.; Ghabboun, J.; Ligonzo, T.; Cahen, D. *Phys. Chem. Chem. Phys.* **2004**, *6*, 4538-4541.

[26] Fontaine, P.; Goguenheim, D.; Deresmes, D.; Vuillaume, D.; Garet, M.; Rondelez, F. *Appl. Phys. Lett.* **1993**, *62*, 2256-2258.

[27] Boulas, C.; Davidovits, J. V.; Rondelez, F.; Vuillaume, D. *Phys. Rev. Lett.* **1996**, *76*, 4797-4800.

[28] Vuillaume, D.; Boulas, C.; Collet, J.; Davidovits, J. V.; Rondelez, F. *Appl. Phys. Lett.* **1996**, *69*, 1646-1648.

[29] Collet, J.; Lenfant, S.; Vuillaume, D.; Bouloussa, O.; Rondelez, F.; Gay, J. M.; Kham, K.; Chevrot, C. *Appl. Phys. Lett.* **2000**, *76*, 1339-1341.

[30] Cohen, R.; Zenou, N.; Cahen, D.; Yitzchaik, S. *Chem. Phys. Lett.* **1997**, *279*, 270-274.

[31] Chai, L.; Cahen, D. *Mat. Sci. Eng. C-Bio. S.* **2002**, *19*, 339-343.

[32] Selzer, Y.; Salomon, A.; Cahen, D. *J. Am. Chem. Soc.* **2002**, *124*, 2886-2887.

[33] Kar, S.; Miramond, C.; Vuillaume, D. *Appl. Phys. Lett.* **2001**, *78*, 1288-1290.

[34] Unfortunately, the conditions for the evaporation process are not specified. No changes in the surface properties or damage due to the evaporation of the aluminum method have been reported. In addition, no yield of the contact has been reported.

[35] Miramond, C.; Vuillaume, D. *J. Appl. Phys.* **2004**, *96*, 1529-1536.

[36] The ideal barrier height for n-type silicon equals $q\phi_{B(n)} = q\phi_M - qA_S$ (= 0.44 eV) and for p-type silicon: $q\phi_{B(p)} = E_g + qA_S - q\phi_M$ (= 0.67 eV). See also reference [10].

[37] Severin, P. J.; Poodt, G. J. *J. Electrochem. Soc.* **1972**, *119*, 1384-1389.

[38] Donald, D. K. *J. Appl. Phys.* **1963**, *34*, 1758-1762.

[39] Salomon, A.; Cahen, D.; Lindsay, S.; Tomfohr, J.; Engelkes, V. B.; Frisbie, C. D. *Adv. Mat.* **2003**, *15*, 1881-1890.

[40] Schroder, K. *Semiconductor Material and Device Characterization*, 2nd edition, Wiley: New York, 1998.

[41] Slowinski, K.; Chamberlain, R. V.; Miller, C. J.; Majda, M. *J. Am. Chem. Soc.* **1997**, *119*, 11910-11919.

[42] Rampi, M. A.; Schueller, O. J. A.; Whitesides, G. M. *Appl. Phys. Lett.* **1998**, *72*, 1781-1783.

[43] Yu, H. Z.; Morin, S.; Wayner, D. D. M.; Allongue, P.; de Villeneuve, C. H. *J. Phys. Chem. B* **2000**, *104*, 11157-11161.

[44] Plummer, J. D.; Deal, M. D.; Griffin, P.B. *Silicon VLSI Technology, Fundamentals, Practice and Modeling*, Prentice Hall, New Jersey, 2000, p294.

[45] Kjaer, K.; Alsnielsen, J.; Helm, C. A.; Tippman-Krayer, P.; Möhwald, H. *J. Phys. Chem.* **1989**, *93*, 3200-3206.

[46] Bateman, J. E.; Eagling, R. D.; Worrall, D. R.; Horrocks, B. R.; Houlton, A. *Angew. Chem. Int. Ed.* **1998**, *37*, 2683-2685.

[47] Cicero, R. L.; Linford, M. R.; Chidsey, C. E. D. *Langmuir* **2000**, *16*, 5688-5695.

[48] Buriak, J. M.; Allen, M. J. *J. Am. Chem. Soc.* **1998**, *120*, 1339-1340.

[49] Holland, J. M.; Stewart, M. P.; Allen, M. J.; Buriak, J. M. *J. Solid State Chem.* **1999**, *147*, 251-258.

[50] Buriak, J. M.; Stewart, M. P.; Geders, T. W.; Allen, M. J.; Choi, H. C.; Smith, J.; Raftery, D.; Canham, L. T. *J. Am. Chem. Soc.* **1999**, *121*, 11491-11502.

[51] Stewart, M. P.; Buriak, J. M. *Angew. Chem. Int. Ed.* **1998**, *37*, 3257-3260.

[52] Yuan, S. I.; Cai, Z. T.; Jiang, Y. S. *New J. Chem.* **2003**, *27*, 626-633.

[53] Sze, S. M. *Semiconductor Devices: Physics and Technology*, Wiley: New York, 1985, pp197-200.

[54] Kar, S.; Rawat, S.; Rakheja, S.; Reddy, D. *IEEE Electron Device Lett.* **2005**, *52*, 1187-1193.

[55] Faber, E J., PhD Thesis, University of Twente, The Netherlands, Chapter 2 - in preparation.

[56] Raider, S. I.; Flitsch, R.; Palmer, M. J. *J. Electrochem. Soc.* **1975**, *122*, 413-418.

Chapter 7

Mechanism of the Hydrosilylation Reaction of Alkenes at Porous Silicon: Experimental and Computational Deuterium Labeling Studies*

Abstract – The mechanism of the formation of Si–C bonded monolayers on silicon by reaction of 1-alkenes with hydrogen-terminated porous silicon surfaces has been studied by both experimental and computational means. We propose that monolayer formation occurs via the same radical chain process as at single-crystal surfaces. Highly deuterated porous silicon and FTIR spectroscopy were used to provide evidence for this mechanism by identifying the IR bands associated with the C–D bond formed in the proposed propagation step. A broad band around 2100 cm^{-1} was observed upon alkylating deuterated surfaces. By the support of ab initio and density functional theory calculations on small molecule models these broad 2100 cm^{-1} features are assigned to C–D bands arising from the involvement of surface D atoms in the hydrosilylation reactions, while the line broadening can be explained partly by interaction with neighboring surface atoms/groups.

* This chapter has been published:
de Smet, L. C. P. M.; Zuilhof, H.; Sudhölter, E. J. R.; Lie, L. H.; Houlton, A.; Horrocks, B. R. *J. Phys. Chem. B* **2005**, *109*, 12020-12031.

7.1 Introduction

A variety of methods for the formation of robust, Si–C bonded monolayers at hydrogen-terminated silicon surfaces have been reported.[1-23] The reaction of 1-alkenes with the hydrogen-terminated silicon surface is a flexible reaction, since monolayers can be formed by photochemical[9,10,19,21-23] or thermal[1,5,24,25] means or by employing catalysts ($EtAlCl_2$ or H_2PtCl_6) on porous silicon and single-crystal surfaces.[3,12,26] The surface modification has also been explored for 1-alkynes.[27,28] In many cases little or no oxidation of the silicon sample occurs in parallel with the monolayer formation.[29] Si–C bonded organic monolayers formed from the reaction of 1-alkenes or 1-alkynes with hydrogen-terminated surfaces have attracted considerable interest due to their stability and structural order.[1,3,28,30-32] These monolayers have been used as a platform for several immobilization chemistries, e.g., DNA,[33-35] polymer grafting,[36] further organic reactions,[7,32] or solid-phase oligosynthesis.[37-39] They have also been used to cap silicon nanoparticles.[39,40]

The structure of monolayers formed on silicon by hydrosilylation of 1-alkenes and 1-alkynes has been studied by polarized FTIR and contact angle experiments, X-ray analysis,[1,17,27] impedance spectroscopy,[41-43] and a variety of theoretical techniques including molecular mechanics,[44] molecular dynamics,[45] and density functional computations.[44,46-51] The monolayers show a substantial degree of ordering, and an approximately all-*trans* conformation of the alkyl chains with a well-defined tilt angle between the surface normal and the alkyl chains of ca. 30° is observed.[1,32,44] Polarized visible-IR sum frequency spectra provide evidence that the monolayer forms epitaxially on Si(111) substrates with some solidlike order but significant numbers of gauche defects.[52-54] The presence of CH_2 features in these sum frequency spectra was consistent with the computational studies,[44,45] which suggest the torsional angles at the base of the alkyl chain deviate from the values for the ideal all-*trans* conformation–a "twisted stem" model.[52] Since the Si–C and Si–Si bonds are covalent and rather inert, the ordering cannot be explained as the result of an annealing process like that which is believed to operate in thiol-based self-assembled monolayers (SAMs) on gold surfaces.[55] The mechanism of the monolayer-forming reaction of 1-alkenes with hydrogen-terminated silicon is therefore critical to the understanding of the physicochemical properties of the monolayers. Linford et al.[1] suggested a radical chain mechanism in which a silyl radical attacks the 1-alkene to form the Si–C bond, and a radical center on the β-carbon atom is formed. This kinetic chain propagates by abstraction of an H atom from the nearest-neighbor Si atom by the carbon-centered radical (Scheme 7.1).

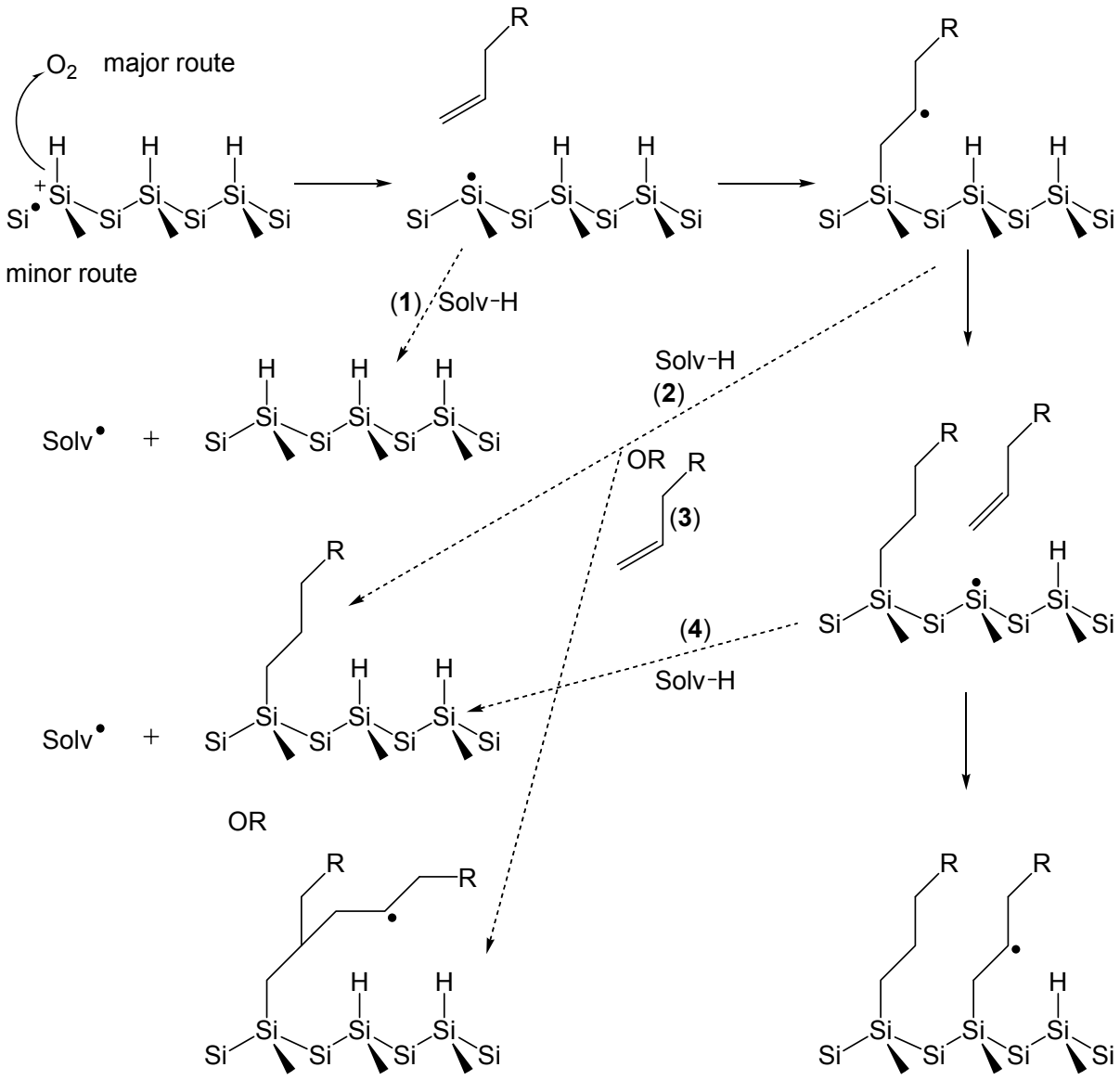

Scheme 7.1. Proposed reaction scheme for the formation of alkyl monolayers on H-terminated silicon by a thermal hydrosilylation reaction. The scheme commences in the top left corner of the diagram with a radical initiation step, which is either abstraction of a hydrogen atom, e.g., by trace oxygen, or another reaction involving the majority carriers (holes) followed by loss of a proton. The extent to which each process actually occurs is discussed in the text; the major pathway is indicated by the solid arrows showing the propagation of the radical chain and the formation of the monolayer. The dashed arrows indicate the various plausible side reactions we consider and are numbered 1-4.

According to such a mechanism the monolayer grows by addition of 1-alkenes to the end of a kinetic chain, which walks across the surface, rather than stepwise at random individual Si sites. Some direct evidence for this mechanism has been provided for Si(100)–H surfaces in ultrahigh vacuum on which monolayers formed from styrene were observed to propagate

along rows of Si atoms starting from individual dangling bonds.[56] More recently, the reaction of styrene with the Si(111)–H face has been studied and islands containing on the order of 20 phenyl rings were formed at the sites of single dangling bonds,[50,57] while also the visible light-induced wet-chemical attachment reaction of 1-decene[21,22] proceeds via the formation of islands.[58] Several open questions remain, since it is not clear in general what conditions are required for this to happen. For example, propene molecules did not show the behavior displayed by styrene.[56] There is also a question as to whether the growing chain generates a structure determined by a self-avoiding random walk[9] or, as may occur in the case of styrene/Si(111)–H, some attractive interaction between the molecules leads to the formation of islands.[57,59] Further, there is comparatively little information on whether the same mechanism operates in the hydrosilylation of porous silicon, where direct observation by scanning tunneling microscopy (STM) is unlikely to be possible.

Some attempts to test the mechanism by deuterium labeling experiments and FTIR have also been made.[60,61] The essence of these experiments is to follow the fate of the H (or D) atoms on the surface as the reaction proceeds, since the radical chain mechanism (Scheme 7.1) predicts that the surface H atoms become incorporated into the monolayer at the β-carbons of the alkyl chains. Using styrene-d_8, Stewart and Buriak reported the observation of C–H stretches in transmission FTIR upon reaction with hydrogen-terminated porous silicon samples.[60] Since a different behavior of propene compared to styrene has been observed on single-crystal Si(100)–H by ultrahigh-vacuum STM,[56] the reaction of straight-chain 1-alkenes on porous silicon is of interest because such molecules are very frequently employed for surface modifications. We have previously studied the reaction of undec-1-ene from dilute (0.1 M) toluene solution on deuterated, abraded silicon crystals by transmission FTIR and found no evidence for incorporation of deuterium as would be indicated by the radical chain mechanism.[61] Wolkow and Wayner have suggested that this result can also be interpreted as a primary kinetic isotope effect on the abstraction of D atoms and that the C–D signals may be too weak to detect.[20] In previous work we were not able to study porous silicon, since the observation of C–D bonds was complicated by the overlap of residual Si–H bands with the C–D stretches. However, in this report, we have prepared and characterized highly deuterated porous silicon surfaces, which have a higher surface area than abraded silicon and allow us to analyze the intensity of the features in the 2100 cm^{-1} region. Using such highly deuterated surfaces, we are able to demonstrate the presence of C–D stretching bands in the monolayer, which supports the proposed radical chain mechanism on porous silicon under thermal reflux of undec-1-ene from both toluene and benzene solutions. The

evidence for the presence of C–D bonds comes from the enhancement in the intensity in the 2100 cm^{-1} region and a theoretical analysis of the factors determining the intensity and broadening of the peaks observed in this region. We also compare the results from the room-temperature Lewis acid ($EtAlCl_2$) catalyzed reactions of undec-1-ene, which would be expected to occur via a mechanism similar to that of hydrosilylation in molecular chemistry.[62]

7.2 Experimental Section

7.2.1 Materials

All common reagents were obtained from Sigma-Aldrich at 99% purity. Benzene, predried over sodium wires, was dried in a potassium-coated Schlenk flask or over molecular sieve beads (type 3 Å from Sigma-Aldrich). Toluene was freshly distilled (over Na) before use. Benzene-d_6 (99.96 at. % D, Sigma-Aldrich) and EtOD (C_2H_5OD, 99 at. % D, GOSS Scientific Instrument, Ltd., Essex, U.K.) were dried over molecular sieves before use. D_2O (99.9 at. % D, Cambridge Isotope Laboratories, Andover, MA), 48% (w/w) HF in H_2O (Fluka), toluene-d_8 (99.94 at. % D, Cambridge Isotope), $EtAlCl_2$ (1.0 M in hexanes, Sigma-Aldrich), and styrene (99+%, Sigma-Aldrich) were all used as received.

In a sealed plastic system, 40% (w/w) DF in D_2O (Fluorochem Ltd., Derbyshire, U.K.; custom preparation with no atom percent D specified by manufacturer) was stored under a blanket of dry nitrogen (from boil-off of the local liquid N_2 storage facility). Samples were transferred by syringe and used immediately for preparation of deuterated porous silicon.

7.2.2 Porous Silicon

Silicon wafers (<100> oriented; boron-doped, p-type, 10 Ωcm resistivity, Compart Technology, Cambridge, U.K.) were degreased in acetone before production of a clean oxide layer by immersion in freshly prepared "piranha" solution (1:1 (v/v) concentrated H_2SO_4 and 30% H_2O_2) for 10 min. Hydrogen-terminated porous silicon (PS–H) was formed by galvanostatic anodization of a cleaned, freshly oxidized, boron-doped p-Si(100) wafer. The oxide was removed from one side by abrasion, and a thin In/Ga film or Al foil was applied to ensure good contact with the electrode. The sample was placed in a Teflon cell, and a hydride layer was formed by subsequent addition of 48% (w/w) aqueous HF (5 min). Subsequently, the HF solution was replaced by the electrolyte, which was a 1:1 (v/v) solution of 48% aqueous HF and ethanol and etched galvanostatically. Current densities of either 12.7 or 38.1 mA cm^{-2} were applied for 6.5 min. These etching conditions were chosen to

produce highly uniform PS layers, which are stable under the reaction conditions used for the hydrosilylation, and to minimize cracking of the porous layer, rather than to optimize the luminescence properties. The porous silicon was then rinsed in deionized water (Millipore, 18 ΩM cm), immersed in 48% aqueous HF, rinsed in deionized water, dried in a stream of dry nitrogen, immersed in hexane for a few min, dried again in a stream of nitrogen, and finally stored under vacuum. Any residual water in the pores was removed by heating to ca. 100 °C for at least 3 h on a standard vacuum line using only grease-free joints, e.g., Young's taps.

To produce deuterium-terminated porous silicon (PS–D), a clean one-side abraded Si(100) sample was placed in a Teflon cell and a deuterium layer was formed by a subsequent addition of 40% DF in D_2O. After a few minutes, an equivalent amount of C_2H_5OD was added, and subsequently, a current density of either 12.7 or 38.1 mA cm^{-2} was applied. After 6.5 min, the sample was rinsed with D_2O, dried in a stream of nitrogen, and finally heated to ca. 100 °C for at least 3 h on a grease-free vacuum line to remove trace water. Generally we employed a current density of 12.7 mA cm^{-2} to produce hydrogen-terminated porous silicon (PS–H) and 38.1 mA cm^{-2} for deuterium-terminated material (PS–D) for experiments in which we were interested in studying the effect of hydrosilylation on the infrared spectra. This is because, as discussed below, these current densities produce similar intensities of the Si–H_x and Si–D_x stretching features in the FTIR spectra. A larger current density is required to produce the same intensity of the PS–D band because the oscillator strength of the Si–D vibration is lower (*vide infra*). A few experiments (Figure 7.1), in which we were studying the spectroscopy of PS–H and PS–D rather than the effect of hydrosilylation, were carried out with 12.7 mA cm^{-2}/(6.5 min) for PS–D for comparison of the H/D site densities. We also prepared some PS–H samples using HF(aq) diluted to 40% for comparison with the DF, which was only available at 40% (w/w).

An IR spectrum of each porous silicon sample was recorded before further use. If contamination was present as indicated by low-intensity C–H vibration modes in the 2900-3000 cm^{-1} region, it was easily removed by rinsing the sample in hexane and/or CH_2Cl_2. If the IR spectrum indicated substantial amounts of oxidation, the sample was reetched by immersing it in a 1:1 (v/v) solution of 48% aqueous HF and EtOH (or 40% DF in D_2O and EtOD) for a few minutes.

7.2.3 Formation of Monolayers

To avoid possible contamination of the samples by adventitious hydrocarbons, all reactions were performed under strict Schlenk line conditions, using entirely grease-free joints (Young's taps), and the vacuum line was isolated from the rotary pump by a liquid nitrogen-cooled trap. A wide variety of solvents have been used for the formation of 1-alkene monolayers on H-terminated Si(100) surfaces[8] and porous silicon.[26] Sieval et al. showed that well-ordered monolayers on H-terminated single-crystal Si(100) can be formed in toluene, xylene, cumene, tert-butylbenzene, and mesitylene.[8] The latter was identified as the solvent of choice, since the quality of the monolayer was high at significantly lower 1-alkene concentrations (down to 2.5% (v/v)). Since toluene, which is cheaper than mesitylene and available at high isotopic purity, was found to give high-quality monolayers from 10% (v/v) solutions,[8] we chose toluene as the solvent for most of the hydrosilylation reactions.

To perform a thermally induced reaction, a porous silicon sample was added to a 10% (v/v) solution of alkene and organic solvent (toluene or benzene), and subsequently the solution was heated at reflux for ~18 h. After the reaction, samples were rinsed with toluene followed by dichloromethane (2×) and dried in a stream of nitrogen. In the case of benzene, samples were rinsed with dichloromethane (2×) only. Some reactions were also carried out using neat 1-alkenes; these reactions were carried out at the same temperature as the toluene reflux (ca. 110 °C). Previous workers have obtained monolayers at porous silicon by thermal hydrosilation using, e.g., neat reagent and slightly lower temperatures that show very little oxidation.[25]

To investigate the role of trace oxygen and light in the initiation step some reactions were carried out in the dark and with freeze-pump-thaw degassed solutions. Traces of oxygen and possible peroxides in the undec-1-ene/toluene reaction mixture were removed in a two-step process: the reaction mixture was poured over a neutral alumina column (BDH, Poole, U.K.; neutral Brockmann grade I) and collected in a Schlenk flask. This Schlenk flask was subjected to three freeze-pump-thaw cycles (using a liquid N_2 Dewar flask) on a grease-free vacuum line. Finally, the porous Si chip was inserted under a flow of N_2, and the hydrosilylation reaction was performed under reflux as above.

Lewis acid-catalyzed hydrosilylation reactions were performed in a horizontally oriented Schlenk flask. A few drops of $EtAlCl_2$ (1.0 M in hexanes), and subsequently a few drops of the neat alkene concerned, were carefully added onto a freshly prepared porous silicon sample using a syringe inserted into the flask. After 18 h, the excess of unreacted alkene and $EtAlCl_2$ was removed by rinsing with ethanol, deionized water and dichloromethane (2×).

7.2.4 Infrared Spectroscopy

Spectra (unpolarized) were obtained using an ATI Mattson Genesis Series FTIR spectrometer fitted with a deuterated triglycine sulfate (DTGS) detector in the normal transmission alignment. Spectra of both alkylated and unmodified porous silicon were referenced against an unetched piece of Si(100) wafer and have been baseline-corrected. The resolution is 4 cm^{-1} and 32 scans have been co-added and averaged. The integrated peak intensity, denoted as *A*, was calculated by using the integration option of the instrument-supplied software, WinFIRST.[63] A few spectra were recorded at higher resolution (0.25 cm^{-1}, Figure 7.2) using a Bio-Rad Excalibur spectrometer with an MCT detector and also baselined with the instrument-supplied (Merlin) software.

To compare different samples, the integrated absorbances were normalized with respect to the integrated absorbance of the $Si–H_x$ vibrations at 2100 cm^{-1} before the alkylation reaction ($A(Si–H_x)_0$), and are denoted as A_n. This enables us to compare integrated absorbances between samples since $A(Si–H_x)_0$ is proportional to the number of sites available for reaction. In the case of the C–H vibrations at 2925 cm^{-1}, the normalized integrated peak intensity $A_n(C–H)$,

$$A_n(C-H) = \frac{A(C-H)}{A(Si-H_x)_0} \qquad [7.1]$$

yields the degree of alkylation (Equation 7.1). The subscript ‘0’ in this equation and throughout the text indicates a quantity relating to the sample before reaction with alkene.

7.2.5 NMR Spectroscopy

Deuterated solvents were assessed for isotopic purity by ^1H NMR using a 500 MHz spectrometer (JEOL, Lambda 500). Benzene-d_6 and toluene-d_8 contained traces of C_6D_5H and $C_6D_5CD_2H$.

7.2.6 Computational Methods

Assignment of the IR spectra was aided by density functional and ab initio calculations on small molecule models of silicon surface. It has previously been observed that small silicon clusters provide reasonable models of the localized vibrational modes.[64-66] Calculations were performed without symmetry assumptions using either the Titan program package[67] or GAMESS/ PC-GAMESS.[68,69] Geometries and harmonic frequencies were

evaluated using density functional theory (DFT) calculations at the B3LYP/6-31G(d) or HF/6-31G(d) levels. The default grids of both DFT programs were used and no significant differences in optimized geometries were found. Titan does not allow one to obtain the intensities of vibrational modes at DFT level when the problem is solved by the (default) analytic method of frequency calculation. As a result, the calculations were performed using a numerical method by applying the option 'NMDER=2'.

To mimic the solid surface while minimizing the computational cost, the hydrogen atoms on the model cluster that do not correspond to those on the actual surface ('X') were replaced by tritium atoms or pseudo-hydrogen atoms of mass equivalent to Si (denoted as Q, available only in GAMESS). Depending on which aspect of the system was of interest, different model Si clusters were used. Small clusters of the form $SiX_3SiH_2SiX_3$ and $SiX_3SiD_2SiX_3$ [61] were adequate to compute the ratio of integrated absorbances of Si–H/D stretches on porous silicon. In these calculations, the pseudo-hydrogen atom mass was set equal to that of silicon to avoid intensity effects from an unphysical coupling of the Si–D and Si–T modes. To compute the normalized intensity of the C–D stretch in an undecyl chain with a deuterium atom at the β-carbon on a silicon surface, the Si atom of the C–Si bond was connected to just three SiX_3 groups. This model is referred to as $Si_4X_9C_{11}H_{22}D$. In cases where information regarding the modes of both the surface and alkyl chain was required, i.e., to probe the interactions between Si–H and C–H stretching modes, another model was used; the length of the alkyl tail was reduced from 11 to 4 atoms for reasons of computational cost, while the silicon-cluster was enlarged to 13 atoms. The surface was <111> orientated, for simplicity and computational considerations, resulting in 7 surface Si–H bonds and 15 tritium atoms ($Si_{13}T_{15}H_7$). The alkyl tail, if present, was attached to the central silicon atom, leaving 6 unreacted surface Si–H sites. In this case, X = T is sufficient because Si–H and Si–T modes do not couple strongly.[65,66]

7.3 Results and Discussion

To test the radical chain mechanism for the formation of Si–C bonded monolayers on hydrogen-terminated porous silicon FTIR spectroscopy was used to detect incorporation of deuterium originating from the surface termination into the monolayer. First, we discuss the preparation of the deuterated surfaces and then investigate the possibility of H/D exchange between the surface and the solvent, in the absence of alkene, but under the conditions of the reaction (refluxing toluene or benzene). Next, we investigate whether deuterium can be transferred from the solvent to the monolayer during the alkylation reaction. Finally, we test

directly whether the transfer of deuterium atoms from the surface to the monolayer occurs for both thermal and Lewis acid-catalyzed reactions and compare the intensity of the C–D vibrational spectroscopic features with ab initio and density functional theory (DFT) calculations on small-molecule models of the porous silicon surface.

7.3.1 Comparison of Deuterium-Terminated (PS–D) versus Hydrogen-Terminated (PS–H) Porous Silicon

The IR spectrum of hydrogen-terminated porous silicon (PS–H) shows bands at 2087, 2112, and 2138 cm^{-1}, which are attributed to Si–H, $Si–H_2$, and $Si–H_3$ stretching modes, respectively (Figure 7.1, spectrum A).[61,70] Other well-resolved features of the absorption spectrum include the $Si–H_2$ scissors mode (910 cm^{-1}) and $Si–H_2$ bending and Si–H wagging modes (665 and 627 cm^{-1}, respectively). The experimental integrated absorbance of the $Si–H_x$ stretching modes of a porous silicon sample prepared at 12.7 mA cm^{-2} for 6.5 min lies in the range 4-7 cm^{-1}. The IR spectrum of a deuterium-terminated porous silicon (PS–D) sample (Figure 7.1, spectrum B) shows two sets of three peaks, one at 1518, 1529, 1554 cm^{-1}, which corresponds to the Si–D, $Si–D_2$, and $Si–D_3$ stretching modes,[65,66] and another, less intense set around 2100 cm^{-1} is due to minority $Si–H_x$ species as described above. The low-intensity peak at ~1100 cm^{-1} is due to small amounts of silicon oxide. Si–HD and Si–H wagging modes are resolved as well.[61] The use of DF in D_2O and EtOD and 38.1 mA cm^{-2} for 6.5 min in the porous silicon preparation resulted in integrated absorbances between 1-2 and 4-7 cm^{-1} for $Si–H_x$ and $Si–D_x$, respectively. For the majority of the experiments described below we employed a current density of 38.1 mA cm^{-2} to prepare PS–D in order to maximize the intensity of the Si–D features. The only exceptions were the experiments of Figure 7.1 in which we compared the density of D and H sites on PS using the same current density of 12.7 mA cm^{-2} for both PS–H and PS–D. The spectra of the PS–D surfaces produced in this study are similar to those published in a previous report[71,72] except in one aspect; these authors reported that the structures of the absorption bands of the Si–H and Si–D stretching modes are similar. However, we observed a difference in the intensity ratio of the different stretching modes for the PS–H and PS–D surfaces. In the case of PS–H surfaces, the order of peak intensities observed is $Si–H_2$ > Si–H > $Si–H_3$, while on our deuterated surfaces we find $Si–D_2$ > Si–D > $Si–D_3$ and Si–H > $Si–H_2$ > $Si–H_3$. Approximate values for the ratios of these intensities are required to calculate the total relative abundance of Si–H and Si–D species as described below.

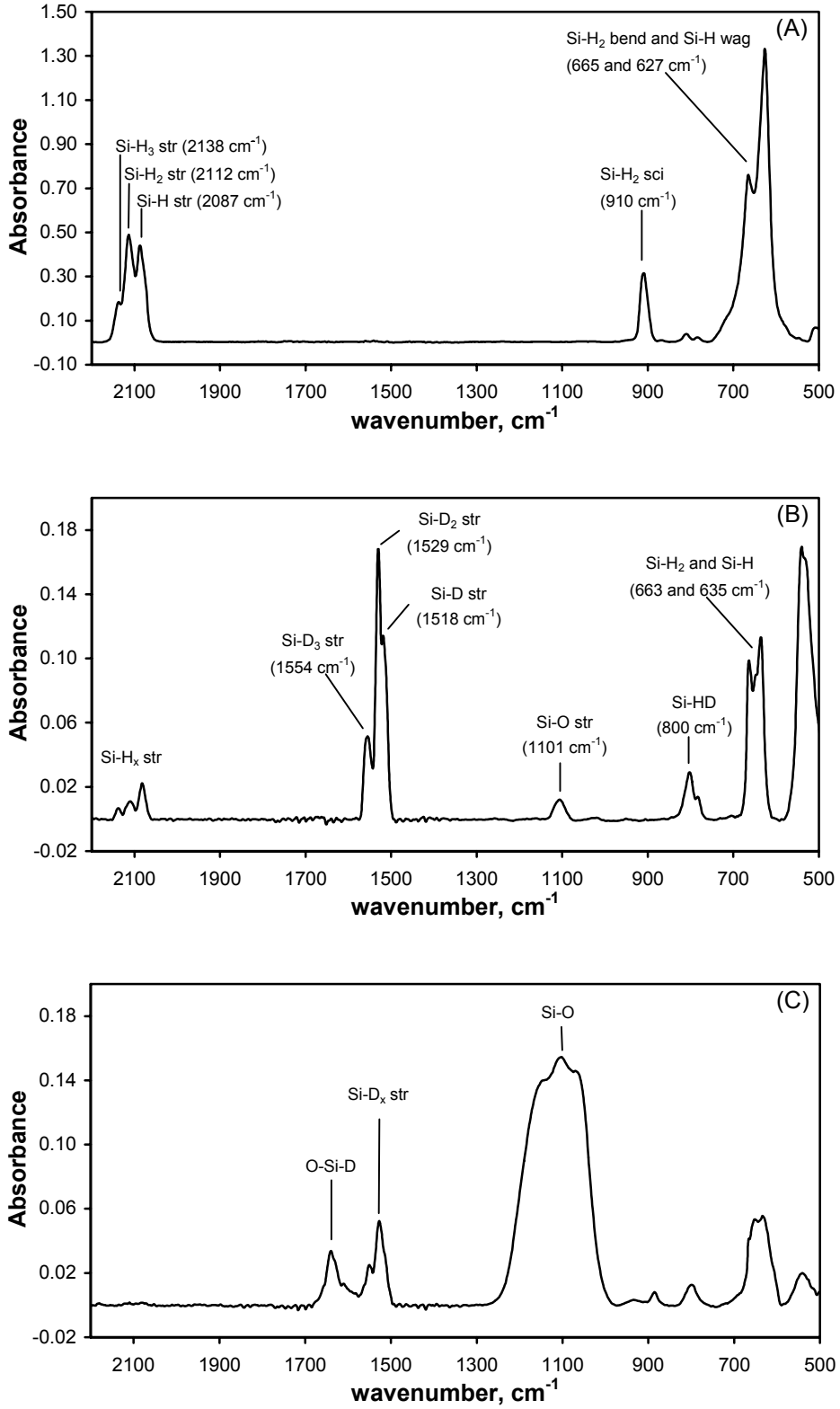

Figure 7.1 Baseline-corrected FTIR spectra of hydrogen- and deuterium-terminated porous silicon. Freshly prepared PS–H (A) and PS–D (B) samples and (C) an oxidized PS–D surface. In all spectra the background was a piece of unetched single-crystal wafer. The resolution is 4 cm^{-1}, and 32 scans have been co-added and averaged.

Given the low density of Si–H on the PS–D surface, it is likely that the relative abundance of Si–H can be explained as a statistical effect. Since $Si–H_3$ is still observed despite the H/D ratio being ca. 1:10 (*vide infra*), the distribution is not purely statistical and the origin of the relatively high intensity of $Si–H_3$ is not clear to us, but may be an isotope effect dependent on the details of the reaction of protons from HF with the surface during the etching process. Since the HF and DF solutions were provided at concentrations of 48 and 40%, respectively, by the manufacturer, we made a comparison of FTIR spectra of PS–H samples grown from 40 and 48% HF. These showed no difference in the shape of the $Si–H_x$ band and only a 6% drop in intensity on diluting the HF solution to the same concentration (40%) as the DF solution.

To calculate the ratio of H:D atoms using the measured intensities, the relation between the oscillator strength and the reduced mass of both systems is needed. Using various H-terminated Si clusters as models (more details of this calculation can be found in §7.3.9), the ratio of the integrated absorbance of all the Si–H/Si–D stretches was found to be 1.89 at the B3LYP/6-31G(p)-level. This number was obtained using a ratio of 3:3:1 for the relative abundances of the SiH, SiH_2, and SiH_3 bands in the $Si–H_x$ stretching region based on the assignment of these bands in the experimental PS–H spectra by previous workers[65,66] and the observed intensity pattern. It is worth noting that this ratio is only weakly dependent on the relative abundances, and therefore the precise assignment of the individual $Si–H_x$ modes is not critical for the analysis in this report. Using this theoretical ratio of oscillator strengths, it was found that for a current density of 12.7 mA cm^{-2} (6.5 min) the use of deuterated media results in $N(D)/N(H) = 1.30$, where N is the number of atoms on the PS–H and PS–D surfaces prepared from 40% HF and 40% DF, respectively. The effect of increasing the HF concentration to 48% was ca. 6%. Matsumoto et al. reported a smaller excess of D sites; their observed ratio is $N(D)/N(H) = 1.06$,[70] under broadly similar etching conditions on 3-5 Ωcm resistivity p-Si. The reason is not clear, but presumably relates to an isotope effect on one or more steps in the etching process.

Approximately 92% of the Si–H/Si–D sites on PS–D were D-terminated, as determined from the integrated absorbances of the $Si–H_x$ vs $Si–D_x$ moieties. This observation can be rationalized on the basis that the isotopic purity of the DF/D_2O was less than 100% and the anodization was performed in an open cell. Further, kinetic isotope effects leading to preferential reaction of surface sites with protons from HF are possible.

Finally, it is worth noting that the hydrogen atoms present in $Si–H_x$ moieties on a PS–D surface are chemically available as shown by oxidation of a PS–D sample by immersion for

5 h in D_2O/EtOD (Figure 7.1, spectrum C). The combination of ethanol/water is known to result in oxidation of porous silicon; the role of the ethanol is to wet the hydrophobic pores.[73] The high-intensity peak at ~1100 cm^{-1} is attributed to oxide, while the peak at ~1640 cm^{-1} corresponds to O–Si–D stretching modes. The region around 2100 cm^{-1}, corresponding to $Si–H_x$ stretching vibrations, is peak-free, although absorptions between 600 and 700 cm^{-1} suggest that the oxidized sample retains a small number of H-terminated sites.

7.3.2 Isotopic H/D Exchange Experiments in Toluene and Benzene

Because the solvent is a potential source for hydrogen atoms (Scheme 7.1), we investigated whether H or D atoms can be transferred between the solvent and the surface under typical hydrosilylation conditions, i.e., refluxing benzene or toluene in the absence of 1-alkenes. If this is the case, then this would have to be taken into account in using deuterium labeling to follow the fate of the surface H/D atoms during hydrosilylation of an alkene.

PS–H samples were refluxed for 18 h in either benzene-d_6 or toluene-d_8. No $Si–D_x$ stretching vibrations (expected between ~1530 and ~1560 cm^{-1})[70] were found in the FTIR spectrum of a PS–H sample after the reflux (data not shown), indicating that no D atoms from the solvent are abstracted by surface-bound silyl radicals. PS–D samples were also refluxed in nondeuterated solvents to determine whether D atoms from the silicon surface can be incorporated into the solvent molecules. For both toluene and benzene, the integrated absorbances of the $Si–H_x$ and $Si–D_x$ stretching vibrations were unchanged after reflux. In addition, the total number of sites, either hydrogen- or deuterium-terminated, was unaffected by the process of refluxing. This is consistent with the mechanism in Scheme 7.1 in the sense that if it were necessary to have a separate initiation event for each alkyl species which bonds to the surface, one might expect that under reflux there would be detectable H/D exchange between the surface and solvent even in the absence of alkene.

7.3.3 Thermal Reaction of 1-Alkenes with PS–H in Toluene and Benzene

If the hydrosilylation of 1-alkenes on the silicon surface does involve the abstraction of hydrogen atoms from the solvent (Scheme 7.1, arrows 1, 2, and 4), it is likely that benzene, which lacks easily abstracted hydrogen atoms, would be a much poorer choice of solvent than toluene, which ranks among the best solvents for this reaction.[8] To test this idea, the monolayer formation reaction was performed both in benzene and toluene with dilute solutions of undec-1-ene. The characteristic absorptions in the 2900 cm^{-1} region due to C–H

vibration modes (~2958, ~2925, and ~2855 cm^{-1}) and those around 2100 cm^{-1} due to the $Si–H_x$ stretching vibrations were observed as previously reported.[4,24] The peak at 1100 cm^{-1} is attributed to Si–O, while the peak at ~1470 cm^{-1} corresponds to the CH_2 scissors vibrations. The integrated intensities of the alkyl bands are collected in Table 7.1.

To compare degrees of alkylation, the integrated absorbances, normalized with respect to the integrated peak intensity of the $Si–H_x$ vibrations before the modification, were determined according to Equation 7.1. Intensities of the $Si–H_x$ vibrations after reflux were also normalized in an analogous manner. In all cases there is a loss of $Si–H_x$ intensity upon reaction ($A_n(Si–H_x)$ ~ 0.8), but a more precise quantification is difficult, due to some overlap of the $Si–H_x$ and O–Si–H bands.

The overall efficiency of monolayer formation in both benzene and toluene can be deduced from the total integrated absorbance of the C–H stretching modes of the methylene and methyl moieties of the undecenyl chain. This value, A_n(C–H), is presented in Table 7.1. Taking account of sample-to-sample variations that are intrinsic to the use of PS, the amount of covalently bound alkyl chains is independent of the solvent (benzene vs toluene), isotopic substitution in the solvent (nondeuterated vs perdeuterated solvents), and reaction pressure/temperature (open and sealed reaction vessels of benzene). In summary, variation of the reaction medium in a variety of ways, including the absence or presence of easily abstracted hydrogen atoms, does not affect the extent of monolayer formation by hydrosilylation on porous silicon to a significant degree.

Table 7.1 Thermal alkylation of PS–H with undec-1-ene. Normalized integrated absorbances, A_n(C–H), of the C–H stretching modes of alkylated PS–H samples prepared by heating 1-alkenes in different solvents (O indicates an open system, i.e., heated to normal boiling point; S, a sealed system).

Solvent	System	A_n(C–H)
benzene	O, reflux at 79 °C	2.43 ± 0.10
benzene	S, ca. 110 °C	2.99 ± 0.45
benzene-d_6	S, ca. 110 °C	2.23 ± 0.52
toluene	O, reflux at 110 °C	2.44 ± 0.10
toluene-d_8	O, reflux at 110 °C	2.46 ± 0.52

7.3.4 Thermal Reaction of 1-Alkenes with PS–H in Deuterated Solvents

In this type of experiment we looked for C–D stretching vibrations in the IR spectra after hydrosilylation as an indication of a possible role of solvent molecules as a source of hydrogen atoms for the carbon radical (Scheme 7.1, arrow 2). The wavenumber of the symmetric stretching vibration in CD_4 is 2109 cm^{-1},[74] which is, unfortunately, in the region of the Si–H_x stretching vibrations. However, a difference might be expected in the shape or the intensity of peaks in the 2100 cm^{-1} region in comparison with nondeuterated solvents. Since we have shown (*vide supra*) that hydrogen atoms are not transferred between the surface and the solvent, abstraction of hydrogen/deuterium atoms by the carbon radical (Scheme 7.1, arrow 2) from the solvent would show up as increased normalized intensity, $A_n(2100)$.

The normalized intensities in the 2100 cm^{-1} region after hydrosilylation were $A_n(2100)$ = 0.77 ± 0.12 in deuterated solvents (toluene-d_8 and benzene-d_6 data combined) and 0.79 ± 0.07 in nondeuterated solvents. The intensity in this region was therefore identical, and any contribution of C–D stretching modes must be less than the uncertainty. The observed scatter was largely associated with variations in the amount of oxidation occurring. No other differences in the FTIR spectra between deuterated and nondeuterated solvents were observed. In all cases the characteristic Si–H_x triplet changes into a single broad peak at ~2095 cm^{-1} upon alkylation (Figure 7.2). A small increase in intensity on the low wavenumber side of the peak, previously assigned to Si atoms bonded to both C and H, is also observed.[18,24]

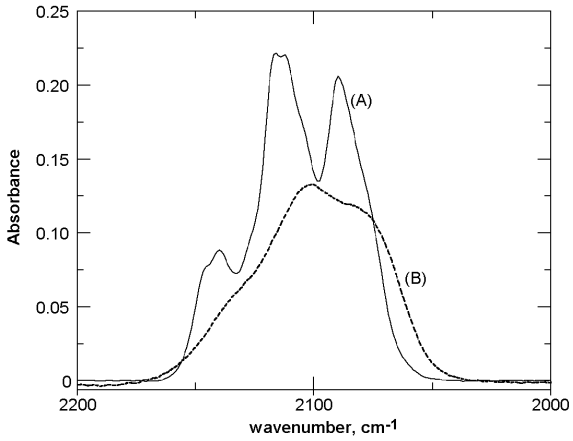

Figure 7.2 High-resolution (0.25 cm^{-1}) FTIR spectra of the Si–H_x stretching bands on PS–H before (A) and after (B) thermal alkylation with 10% (v/v) undec-1-ene in toluene. In both spectra the background was a piece of unetched single-crystal wafer. The resolution is 0.25 cm^{-1}, and 40 scans have been co-added and averaged.

7.3.5 Thermal Reaction of 1-Alkenes with PS–D

The abstraction of hydrogen atoms from the PS surface in the thermally induced alkylation can be studied using PS–D samples and analyzing the region around 2100 cm^{-1} in the IR spectrum for possible C–D stretching modes. This can be done in a quantitative way, as the intensity of the potentially troublesome $Si–H_x$ bands on the PS–D surfaces prepared in this report is relatively small. A typical spectrum of an undec-1-ene-derived monolayer on PS–D is given in Figure 7.3.

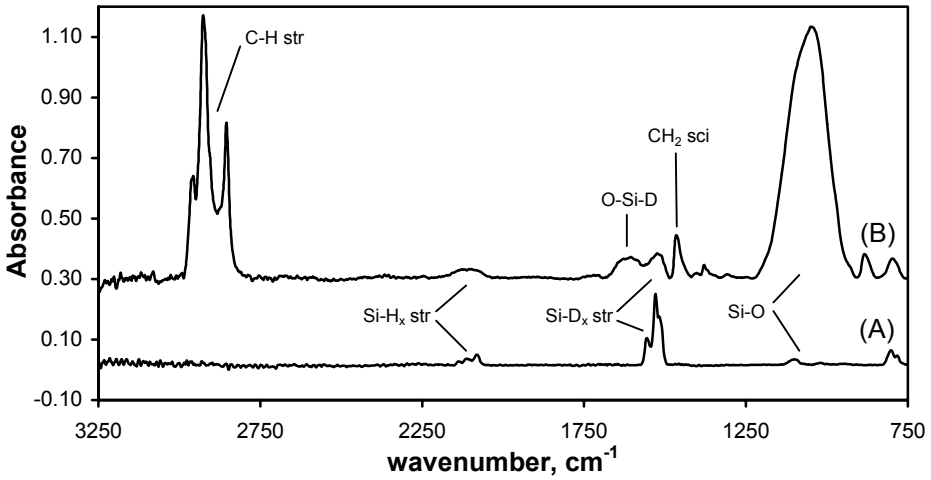

Figure 7.3 Baseline-corrected FTIR spectra of a PS–D sample before (bottom, A) and after (top, B) hydrosilylation in 10% (v/v) undec-1-ene in toluene. The top spectrum is offset by 0.3 absorbance units. In both spectra the background was a piece of unetched single-crystal wafer. The resolution is 4 cm^{-1}, and 32 scans have been co-added and averaged.

Upon reaction, C–H stretching vibrations around 2900 cm^{-1} and CH_2 scissor vibrations at ~1470 cm^{-1} appear, in addition to oxide-related features at ~1100 and 1580-1690 cm^{-1}. The normalized integrated absorbance (A_n) is defined as:

$$A_n(C-H) = \frac{A(C-H)}{A(Si-H_x)_0 + gA(Si-D_x)_0} \qquad [7.2]$$

A_n measures the degree of alkylation via the C–H stretching features after alkylation (A(C–H)) and the absorption bands from the etched surface before alkylation ($A(Si–H_x)_0$, $A(Si–D_x)_0$). The subscript ‘0‘ indicates a quantity relating to the sample before reaction. The numerical factor g = 1.89 takes account of the isotope effect on the integrated absorbance

and is obtained from computations on small-molecule models below (see Table 7.5). The data for the degree of alkylation according to Equation 7.2 is presented in Table 7.2. In addition, the integrated peak intensity in the 2100 cm^{-1} region after modification, $A_n(2100)$ relative to this total number of sites, is presented, which enables quantification of the number of C–D bonds formed by the radical chain mechanism (Scheme 7.1).

Table 7.2 Thermal alkylation of PS–D with undec-1-ene, incorporation of D atoms into C–D bonds from the PS–D surface as measured by the normalized integrated absorption, $A_n(2100)$, and the degree of alkylation, $A_n(C–H)$. $A_n(2100)$ denotes the features around 2100 cm^{-1} which, in principle, may be due to both $Si–H_x$ and C–D stretching modes. A_n values were computed using Equation 7.2 to account for the difference in intensities of Si–H and Si–D modes.

Solvent	$A_n(2100)$	$A_n(C–H)$
toluene	1.54 ± 0.21	2.96 ± 0.20
benzene	1.67 ± 0.39	3.37 ± 0.42
neat	1.53 ± 0.25	3.36 ± 1.17

For both solvents, an increase in intensity around 2100 cm^{-1} is observed upon alkylation, which is denoted by $A_n(2100) > 1.00$. Hydrosilylation was also performed in neat undec-1-ene as well, and the data show that the degree of alkylation is comparable with the experiments in 10% (v/v) alkene solutions. These data imply that, apart from the $Si–H_x$ modes observed at ~2083, ~2112, and ~2138 cm^{-1}, additional C–D bonds are being formed and observed (and part of the SiH_x lost), which can only be the case if deuterium atoms are abstracted from the PS–D surface and incorporated into the alkyl chain.

The broadness of the peak around 2100 cm^{-1} may be explained by the possibility that reaction with the surface can lead to heterogeneous broadening of $Si–H_x$ and C–D modes. Boukherroub and co-workers suggested this possibility in order to rationalize the apparent disappearance of the Si(111)–H stretch without the appearance of new absorptions upon reaction with aldehydes.[75] Such broadening is also observed in other modifications, e.g., in the electrochemical modification of Si(111)–H by aryldiazonium ion.[11] In addition, simple physisorption of a hydrocarbon on the Si(111)–H surface results in an increase in the peak width of the Si–H monohydride stretch.[75]

Given the fact that a porous silicon surface contains mono-, di-, and trihydride groups, it is not surprising that the Si–H peaks are broad. In the case of alkylated PS, there is the additional possibility that the C–D bond interacts with $Si–H_x$ bonds on the surfaces, resulting

not only in peak broadening and overlap but also in a transfer of intensity. Figure 7.2 shows the Si–H_x stretching band of PS–H at higher resolution before and after alkylation by 10% (v/v) undec-1-ene in toluene. Aside from the reduction in the total integrated intensity, two effects of alkylation are apparent: the three peaks merge into a single broad band, and there is a net increase in intensity on the low-wavenumber side of the band, which has previously been assigned to the influence of Si–C bonds on the Si–H frequency.[24,61] The influence of oxidation also has to be taken into consideration as it can be seen in Figure 7.3 that the largest increase in the 2100 cm^{-1} region upon alkylation of PS–D is found for the higher wavenumbers, adjacent to the region in which O–Si–H modes can be expected. As a result, part of the intensity might be the result of the presence of an O–Si–H mode. However, this cannot explain an increase in Si–H intensity overall since oxidation is known to result in a net loss of Si–H intensity. Additionally, the oscillator strength of the O–Si–H modes is not much higher than that of the Si–H_x modes.[3,26,61,73]

In an attempt to remove trace Si–H_x, which is one of the possible two contributions to the bands in the 2100 cm^{-1} region, alkylated PS samples were lightly oxidized by immersing the sample into a 25% (v/v) EtOD in D_2O solution.[73] These conditions did not result in a significant change in shape and intensity of the broad peak at ~2100 cm^{-1}, which is at least consistent with an assignment of the 2100 cm^{-1} feature to C–D species. However, since the alkyl monolayer will protect the sample against oxidation somewhat,[3,26] it is not safe to conclude from this observation alone that there is no Si–H_x attribution to the 2100 cm^{-1} peak. Attempts to preoxidize samples of PS–D to remove the trace Si–H were not useful due to the reduced amount of Si–D remaining for hydrosilylation and the possible contamination of the PS with the water/ethanol mixture, leading to extensive oxidation. We did observe, however, that the addition of 5% (v/v) D_2O to the toluene/undec-1-ene mixture used for thermal hydrosilylation did not affect the degree of alkylation significantly.

7.3.6 Thermal Reaction of Styrene with PS–D

It has previously been reported in a molecularly resolved STM study[56] that styrene favors the chain mechanism compared to a straight chain alkene, i.e., propene in the original work. This was rationalized on the basis of the stability of the carbon radical intermediate on the surface.

Thermal hydrosilylation of styrene was performed as for undec-1-ene. However, styrene is very susceptible to polymerization, and even in the dilute (10% (v/v)) styrene solutions used, some polymerization took place. After 18 h reaction time, the viscosity of the solution

was increased; however, the polymerized material was soluble and easily removed by washing. For both toluene and benzene the integrated peak intensity at 2100 cm^{-1} increases upon reaction (A_n(2100) > 1; see Table 7.3), although this increase seems slightly higher in the experiments with toluene. In this respect, the results of styrene and undec-1-ene are comparable; the integrated peak intensity in the 2100 cm^{-1} region increases upon reaction in both cases, which is an indication for the formation of C–D bonds.

Table 7.3 Thermal alkylation of PS–D with styrene. Integrated absorbances (A, cm^{-1}) of several modes before and after the thermal reaction of styrene with PS–D and the degree of alkylation, A_n(C–H). A_n(2100) refers to the features around 2100 cm^{-1}, which in principle may be due to both Si–H_x and C–D stretching modes. A_n values were computed using Equation 7.2 to account for the difference in intensities of Si–H and Si–D modes.

Concentration and solvent	A(Si–H_x)	A(2100)	A(C–H)	A_n(2100)	A_n(C–H)
neat styrene	1.58 ± 0.02	1.45 ± 0.71	10.4 ± 4.8	0.93 ± 0.47	0.89 ± 0.42
10% in toluene	1.93 ± 0.35	4.16 ± 0.55	5.44 ± 1.6	1.93 ± 0.16	0.40 ± 0.13
10% in benzene	1.78 ± 0.14	2.96 ± 0.32	6.76 ± 3.5	1.66 ± 0.12	0.44 ± 0.23

There is a noticeable difference between styrene and undec-1-ene with regard to the peak shape of the absorptions at 2100 cm^{-1}. For undec-1-ene and other 1-alkenes, the peaks due to residual Si–H_x broaden, sometimes to the extent that they cannot be resolved, and a single band is observed. For styrene, the peak did not broaden as dramatically; after the reaction, three peaks could still be distinguished at ~2082, ~2103, and ~2134 cm^{-1} at approximately the same wavenumbers as before the reaction (spectrum B2 in Figure 7.4). Although it appears that the vibrational energies do not change upon the addition of styrene, the peaks are not as well resolved, which may be due to small amounts of C–D absorptions. The difference in the shape of the 2100 cm^{-1} region absorption peak between styrene and undec-1-ene can be rationalized on the basis that the degree of reaction is smaller; cf., A_n(C–H) data in Tables 7.2 and 7.3. The smaller degree of reaction with styrene is likely to result from its tendency to polymerize under the reaction conditions employed here.

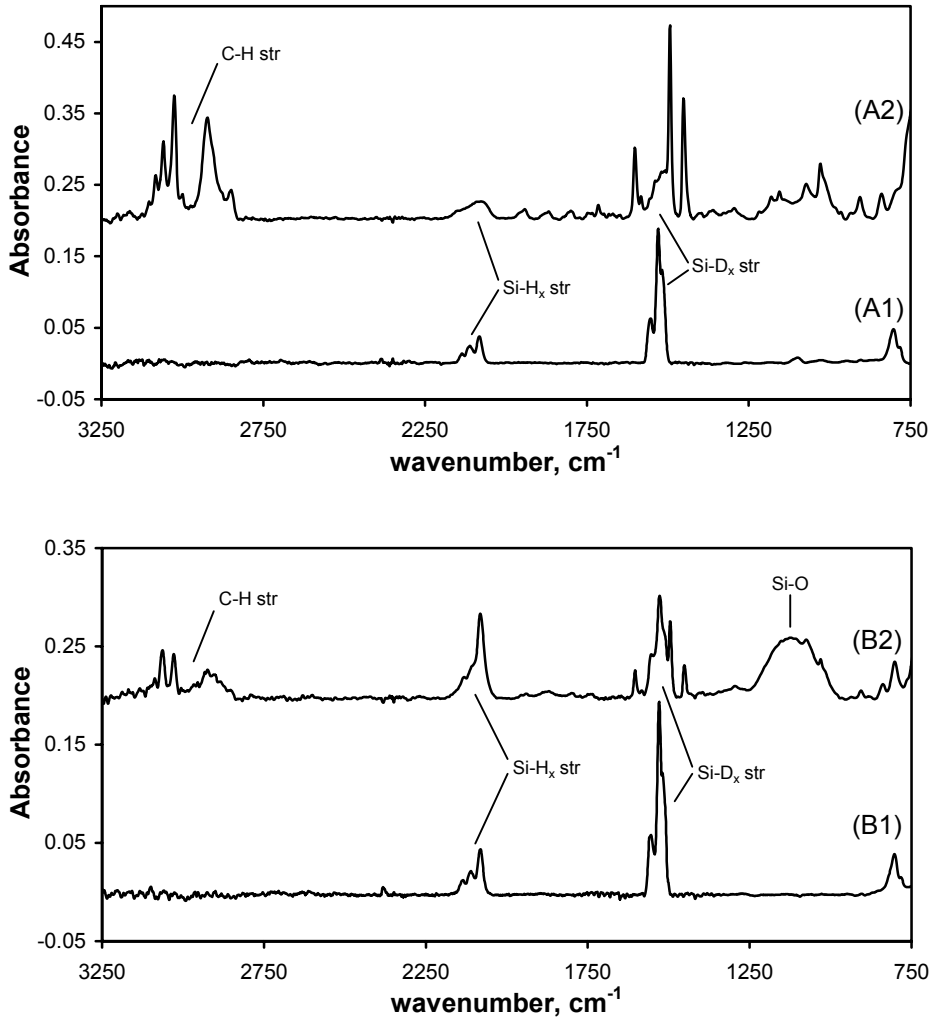

Figure 7.4 Baseline-corrected FTIR spectra of a styrene monolayer on a PS–D surface and corresponding PS–D surfaces before reaction (A1 and B1) and after reaction using neat (A2) and 10% (v/v) styrene in toluene (B2). In each panel the top spectrum is offset by 0.2 absorbance units for clarity. In all spectra the background was a piece of unetched single-crystal wafer. The resolution is 4 cm^{-1}, and 32 scans have been co-added and averaged.

7.3.7 Source of Radicals in Thermal Hydrosilylation of PS–H and PS–D

So far we have discussed the fate of H/D atoms and the propagation of the chain, but not the source of the radicals, i.e., the initiation step. There are several possibilities: (1) photochemical initiation, (2) reaction of trace oxygen with the H-termination, and (3) thermal processes involving the breaking of Si–Si or Si–H bonds by reactions of holes or electrons. Certainly, photochemical initiation has been reported for the derivatization of single crystal[9,22,23] and porous silicon by 1-alkenes.[19] However, the source of the radicals in the thermal hydrosilylation reaction employed in this and other reports[8,24] is not clear. To test the

various possibilities, we have determined the extent of alkylation of porous silicon by 10% (v/v) undec-1-ene in toluene under conditions where stray light, water and/or oxygen, and peroxides were carefully excluded by freeze-pump-thaw degassing of the reaction mixture after passing down a column of neutral alumina. We find essentially no difference in the extent of alkylation with careful exclusion of trace water or stray light by enclosing the Schlenk flask in black paper. However, when the reaction is carried out with rigorous degassing by the freeze-pump-thaw method on the vacuum line and the 1-alkene/toluene is passed through neutral alumina to remove peroxides,[76,77] we find that the extent of alkylation drops from 2.51 ± 0.25 (Table 7.1) to 0.41 ± 0.10 in the absence of oxygen. Further, about 90% of the intensity of the Si–H stretch remains and the peaks are well resolved and not broadened as observed at higher levels of alkylation. We therefore conclude that the major initiation step in the thermal hydrosilylation reaction is a process involving abstraction of hydrogen atoms from the surface by trace oxygen. The promotion of molecular hydrosilylation reactions by oxygen is known,[78] and it appears reasonable to conclude that a similar process occurs on the hydrogen-terminated silicon surface.

7.3.8 Lewis Acid-Catalyzed Reaction of Undec-1-ene with PS–D

Buriak and co-workers have reported a mild and quite general approach for covalent modification of the surface of porous silicon through $EtAlCl_2$-catalyzed hydrosilylation of readily available 1-alkynes and 1-alkenes.[26,76,77,79] Asao et al. proposed a mechanism for the molecular version of this type of reaction, in which the H atom shifts from the Si to the C atom of a Lewis acid-alkene intermediate.[62] This should also lead to incorporation of D atoms at the β-carbon on PS–D surfaces. In comparison with the thermal alkylation in toluene, the degree of oxidation is very low in the case of the reaction with the Lewis acid ($EtAlCl_2$). In this reaction we can therefore expect a negligible contribution of O–Si–H modes to the broad peak at 2100 cm^{-1}.

Figure 7.5 depicts an FTIR spectrum of an undec-1-ene monolayer on a PS–D surface prepared with $EtAlCl_2$ as catalyst. Only a small absorption around 1100 cm^{-1}, specific for oxide formation, is observed, indicating that the use of Lewis acid indeed results in a very low degree of oxidation. There are several factors which favor this: (1) the reaction is carried out at ambient temperature, (2) no solvent is required which reduces the likelihood of introducing trace water and oxygen, and (3) the $EtAlCl_2$ reacts rapidly with trace water to form insoluble aluminum species.

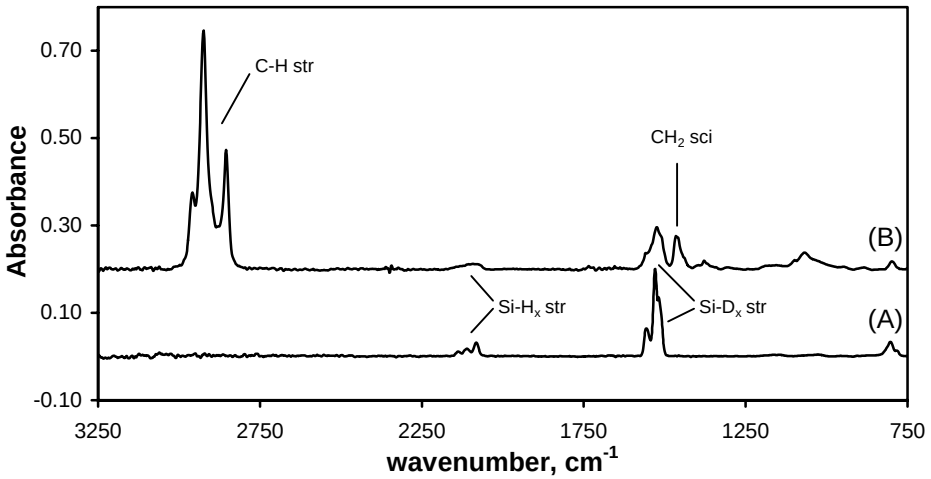

Figure 7.5 Baseline-corrected FTIR spectrum of an undec-1-ene monolayer on a PS–D surface prepared with Lewis acid (B) and the spectrum before reaction (A). The top spectrum is offset by 0.2 absorbance units. In both spectra the background was a piece of unetched single-crystal wafer. The resolution is 4 cm^{-1}, and 32 scans have been co-added and averaged.

Table 7.4 $EtAlCl_2$-catalyzed alkylation of PS–D with undec-1-ene; experimental peak intensities (*A*, cm^{-1}) of several modes after preparation of PS–D and after $EtAlCl_2$-catalyzed reaction of undec-1-ene and the degree of alkylation, A_n(C–H) according to Equation 7.2.

	After etching		After alkylation		
Solvent	$A(Si–H_x)_0$	$A(Si–D_x)$	A(2100)	A(C–H)	A_n(C–H)
neat undec-1-ene	1.47 ± 0.25	6.87 ± 0.73	1.54 ± 0.42	26.2 ± 3.8	2.00 ± 0.46

Table 7.4 shows the relevant data of the Lewis acid-catalyzed addition of undec-1-ene. The mean degree of alkylation of the three fresh samples is 2.00 ± 0.46. This is slightly lower than the average values for the thermal reaction of PS–D samples (see Table 7.2) in toluene (2.96 ± 0.20) and benzene (3.37 ± 0.42). The observation of a lower coverage in case of the use of Lewis acids is in line with the results of Boukherroub et al.[79] The trends in the changes around 2100 cm^{-1} for the thermally induced and Lewis acid-catalyzed addition of undec-1-ene are the same: in both methods an increased integrated peak intensity in the 2100 cm^{-1} region is observed upon hydrosilylation. Although there is some scatter between samples in the values of $A(Si–H_x)_0$ and A(2100), in each case A(2100) > $A(Si–H_x)_0$. The main differences are a lower degree of alkylation in the Lewis acid-catalyzed reaction but also a much lower extent of oxidation. These observations are again consistent with an assignment

of the 2100 cm^{-1} feature to C–D stretching modes and support the proposed reaction mechanisms.[1,57]

7.3.9 Ab Initio and Density Functional Theory (DFT) Calculations

Since the vibrational frequencies of the Si–H_x, O–Si–H, and C–D bands are quite close, any of these modes might contribute to the observed broad feature at 2100 cm^{-1}. In addition, using the ratio of the integrated absorbances of Si–D and Si–H stretches to determine the composition of the surface with respect to D and H atoms requires knowledge of the ratio of the corresponding oscillator strengths (*g* in Equation 7.2). Computed vibrational frequencies and intensities of models of deuterated surfaces as well as the interaction between the alkyl chains of a monolayer and the remaining Si–H_x bonds were therefore helpful in interpreting the experimental results above. All the computed harmonic vibrational frequencies were scaled with the factors determined by Scott and Radom.[80]

7.3.9.1 Ratio between A_n(Si–H) and A_n(Si–D)

Due to the mass difference, the integrated absorbance of an Si–H stretching mode differs from that of an Si–D mode. In general, the absorbance integrated over a frequency interval should be inversely proportional to the reduced mass, μ, since the factor of $\mu^{-1/2}$ appears twice in the expression for the integrated absorbance: once in the frequency and once via the transition dipole. A calculation of the reduced mass requires a determination of the normal modes. Since the small models $X_3Si–SiH_3$, $(X_3Si)_2–SiH_2–SiX_3$, and $(X_3Si)_3–SiH$ have previously been found to be adequate for computing isotope effects on the frequency,[61] the calculations were performed on these molecules at the B3LYP/6-31G(d) level. The results are collected in Table 7.5.

The X atoms are hydrogen atoms whose only purpose is to satisfy the valence of Si atoms in the cluster, but are not otherwise of interest and are assigned a mass equal to that of silicon (Q) to avoid coupling with the Si–H_x or Si–D_x modes of interest.[61,64-66] It is worth noting that although use of X = tritium (T) is sufficient for many purposes,[65,66] it results in some coupling with Si–D modes and therefore cannot be used in calculations aiming to determine the relative integrated intensity of Si–H_x and Si–D_x modes.

Table 7.5 Ratio of vibrational wavenumbers and intensities of the Si–H and Si–D stretching modes of various small-molecule models of hydrogen-terminated silicon (and their deuterated equivalents), calculated at the B3LYP/6-31G(d) Level. Q denotes a pseudo-hydrogen atom with atomic mass equivalent to Si. When these contributions are weighted 1:3:3 for $Si–H_3$, $Si–H_2$, and Si–H, a mean value of the ratio of integrated intensities for $g = A(Si–H)/A(Si–D) = 1.89$ is obtained (Equation 7.2). All calculations using GAMESS.[68,69]

Molecule	ν(Si–H)/ν(Si–D)	A(Si–H)/A(Si–D)
$(Q_3Si)_3SiH$	1.391	1.950
$(Q_3Si)_2SiH_2$	1.384, 1.397	1.889, 1.840
$(Q_3Si)SiH_3$	1.384, 1.384, 1.405	1.788, 1.788, 1.747

Table 7.5 contains the ratios of vibrational wavenumbers and intensities for $X_3Si–SiH_3$, $(X_3Si)_2–SiH_2–SiX_3$, and $(X_3Si)_3–SiH$. The ratio of intensities is close to 2. This is expected on general grounds since the reduced mass of the Si–H stretching modes should be dominated by the mass of the H atom. The value of g = 1.89 that was employed in Equation 7.2 throughout the text was obtained by averaging over the results for SiH_3, SiH_2, and Si–H with weighting 1:3:3 reflecting the experimental spectra. However, the value was not very sensitive to this ratio (± 0.02).

7.3.9.2 Ratio between A_n(C–H) and A_n(C–D) and Estimation of A(2100)

To get more insight into the origin of the broad peak in the 2100 cm^{-1} region, the ratio of the intensities of the C–H and C–D stretching vibration was calculated. Together with the experimental integrated absorbance of the C–H vibration, this theoretical ratio can be used to estimate the contribution of the C–D stretching vibration to the total integrated absorbance in the 2100 cm^{-1} region. Table 7.6 gives some details and relevant output data of calculations on the $Si(SiX_3)_3C_{11}H_{22}D$ model at two different levels.

Table 7.6 Specification of the calculation method, scaled vibrational energies (ν, cm^{-1}) and computed intensities (A, km mol^{-1}) of the C–H and C–D modes of the $Si(SiX_3)_3C_{11}H_{22}D$ model.

X	Level	ν(C–H)	ν(C–D)	A(C–H)	A(C–D)	A(C–H) /A(C–D)
T	B3LYP[a]	2988.11-2892.14	2153.23	767.56	14.43	53.2
T	HF[a]	2911.27-2834.21	2101.60	852.99	14.89	57.3
Q	HF[b]	2911.27-2834.21	2101.59	852.44	14.80	57.6

[a] Calculations using Titan.[67]; [b] Calculations using GAMESS.[68,69]

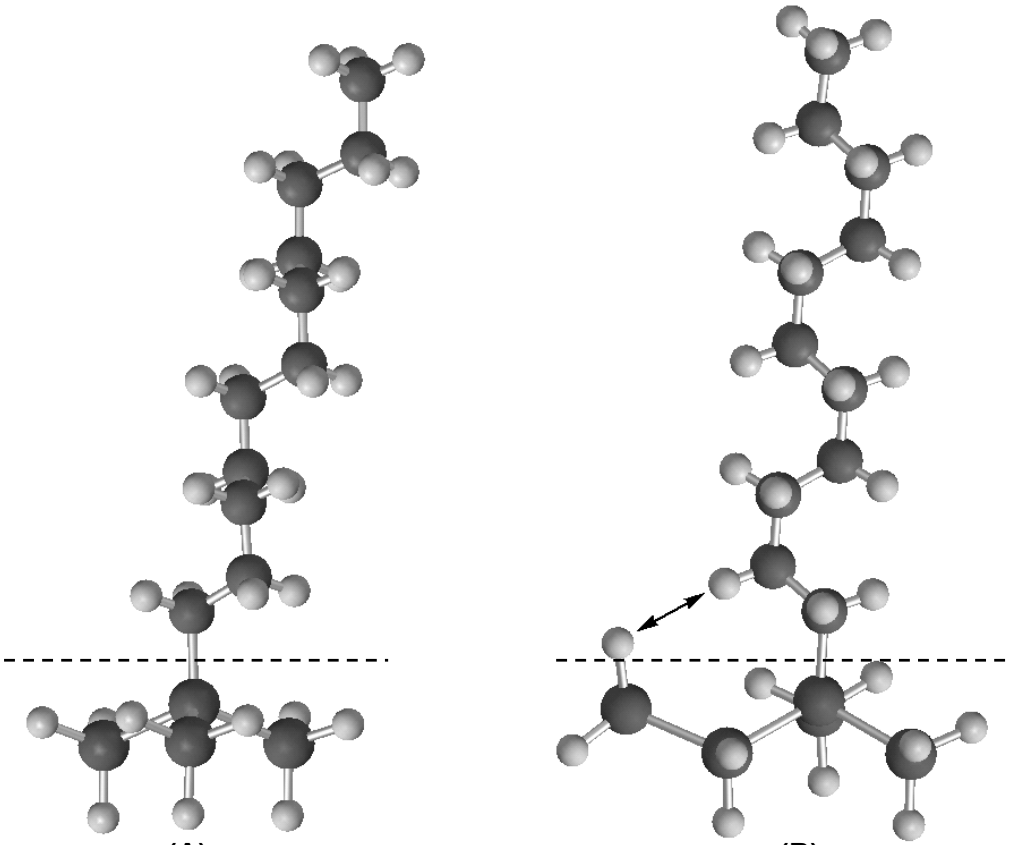

Figure 7.6 Optimized structures of (A) $Si_4X_9C_{11}H_{22}D$ and (B) $Si_5X_{10}HC_{11}H_{22}D$ at the B3LYP/6-31G(d) level. (A) All denoted X are pseudo-hydrogen atoms terminating the silicon valences, but not representing atoms on the actual surface and are assigned masses equivalent to T. (B) The arrow indicates an interaction between the C–D and Si–H stretching vibrations discussed in the text. All other H atoms bonded to Si are pseudoatoms (X), which satisfy the valence of the Si atoms but are assigned higher masses in order to remove artifacts due to coupling with Si–H bonds of interest. In both figures the Si atoms and the pseudoatoms are located below the dashed lines.

The calculated vibrational energy of the C–D bond at the B3LYP/6-31G(d) level is 2153.23 cm^{-1}, close to the (Si–H) region calculated at the same level (Table 7.5). Figure 7.6A shows the optimized structure of this model at the B3LYP/6-31G(d) level.

Using the HF/6-31G(d) model, the scaled vibrational wavenumber of the C–D band is quite close to the literature value of this mode in CD_4 (2109 cm^{-1}).[74] The ratio of the intensities of the C–H and C–D bands computed by DFT and HF methods differs by about 10%. The effect of replacing the T atoms by Si atoms is smaller than this uncertainty, as can be seen from the data in the last two rows of Table 7.6. This justifies the use of T atoms in some cases where the particular software package does not allow assignment of an arbitrary mass.

Table 7.7 Thermal alkylation of PS–D with undec-1-ene; integrated absorbances (cm^{-1}) in the 2100 cm^{-1} region upon thermal reaction of undec-1-ene with PS–D. The calculated value for the integrated absorbance at 2100 cm^{-1} is determined from Equation 7.3 and the experimental integrated absorbance *A*(C–H).

Concn and solvent	Expt *A*(C–H)	Expt *A*(2100)	Calcd *A*(2100)
neat undec-1-ene	41.8 ± 4.0	1.85 ± 0.06	1.77 ± 0.05
10% in toluene	42.0 ± 11.1	2.42 ± 0.19	2.05 ± 0.13
10% in benzene	42.4 ± 2.4	2.22 ± 0.13	1.90 ± 0.23

Table 7.7 compares the observed and calculated values of integrated absorbance in the 2100 cm^{-1} region after thermal hydrosilylation of undec-1-ene on PS–D. The values in the last column of this table were calculated as the sum of contributions from *A*(C–D) and *A*(Si–H_x), rewritten in terms of experimentally accessible quantities, as

$$A(2100) = A(C-H)f + 0.8A(Si-H_x)_0 \qquad [7.3]$$

Equation 7.3 uses a value for A_n(Si–H_x), taken from several experiments on alkylation of PS–H samples, of 0.8. The corresponding value on PS–D samples is not known but is expected to be similar. For the calculation of *A*(2100) the experimental value for *A*(C–H) and the calculated ratio *f* = *A*(C–D)/*A*(C–H) = 1/53.2 are used. From Table 7.7 it can be seen that the major part of the change in intensity in the 2100 cm^{-1} region can be accounted for satisfactorily by the formation of a C–D bond via the radical chain mechanism of Chidsey and co-workers (illustrated in Scheme 7.1).[1] The difference may be the result of several factors; no account is made for the effect of small amounts of oxidation, and there is the possibility of an interaction between C–D and Si–H/D_x stretching vibrations leading to intensity changes. The latter possibility is neglected in the calculations based on the $Si(SiX_3)_3C_{11}H_{22}D$ model.

7.3.9.3 Interaction between C–D and Si–H

A possible explanation for the observed broadening of the peak in the 2100 cm^{-1} region upon alkylation is an interaction between the C–D and Si–H_x stretching vibrations due to the close proximity of the hydrogens on the β-carbon to neighboring Si–H sites. Such an interaction may affect the frequency of the normal mode and also lead to intensity borrowing, which would affect the value of *A*(2100)/*A*(Si–H_x)$_0$. To study this possibility, a calculation

(B3LYP/6-31G(d) level) was performed on the $Si(SiX_3)_3C_{11}H_{22}D$ model (Figure 7.6A) in which one X pseudoatom was replaced by an $SiHX_2$ group to make $Si_5X_{10}HC_{11}H_{22}D$ (Figure 7.6B). As expected, the C–D and Si–H_x bonds give rise to two normal modes at 2151.1 and 2158.8 cm^{-1}, with intensities of 98.3 and 30.3 km mol^{-1}, respectively. These correspond to in-phase and antiphase stretching vibrations of the Si–H and C–D bonds indicated by an arrow in Figure 7.6B. For $Si(SiX_3)_3C_{11}H_{22}D$ (model A) where there is no possibility of such an interaction; the intensity of the C–D stretching vibration was only 14.43 km mol^{-1} (see Table 7.6). Calculations on the $Si_{13}X_{15}H_aD_b$ model indicate the contribution of a single Si–H bond, is between 74.3 and 67.9 km mol^{-1}. From these calculations it can be concluded that there is a significant interaction between the C–D and neighboring Si–H bond, resulting in increased intensities in the modes around 2100 cm^{-1} than in cases where these atoms do not have the possibility to interact.

To better represent the surface, calculations on a larger silicon cluster were performed (Figure 7.7). Parts A and B of Tables 7.8 give the wavenumber and integrated absorbances of the surface (Table 7.8A) and the alkyl chain (Table 7.8B) of calculations on the $Si_{13}X_{15}H_aD_bC_4H_cD_d$ model at the B3LYP/6-31G(d) level.

Table 7.8A Range of scaled vibrational energies (ν, cm^{-1}) and summed intensities (A, km mol^{-1}) of the Si–H and Si–D mode of the $Si_{13}X_{15}H_aD_bC_4H_cD_d$ model calculated using Titan[67] at the B3LYP/6-31G(d) level.

a	b	c	d	ν(Si–H)	ν(Si–D)	A(Si–H)	A(Si–D)
6	0	9	0	2141.8-2120.9		493.2	
6	0	8	1	2138.4-2110.2		503.4	
0	6	8	1		1539.0-1526.4		281.0

Table 7.8B Range of scaled vibrational energies (ν, cm^{-1}) and summed intensities (A, km mol^{-1}) of the C–H and C–D mode of the $Si_{13}X_{15}H_aD_bC_4H_cD_d$ model calculated using Titan[67] at the B3LYP/6-31G(d) level.

a	b	c	d	ν(C–H)	ν(C–D)	A(C–H)	A(C–D)
6	0	9	0	2992.0-2902.5		207.9	
6	0	8	1	2994.7-2901.3	2150.3	190.4	16.49
0	6	8	1	2991.9-2902.4	2152.1	191.1	8.78

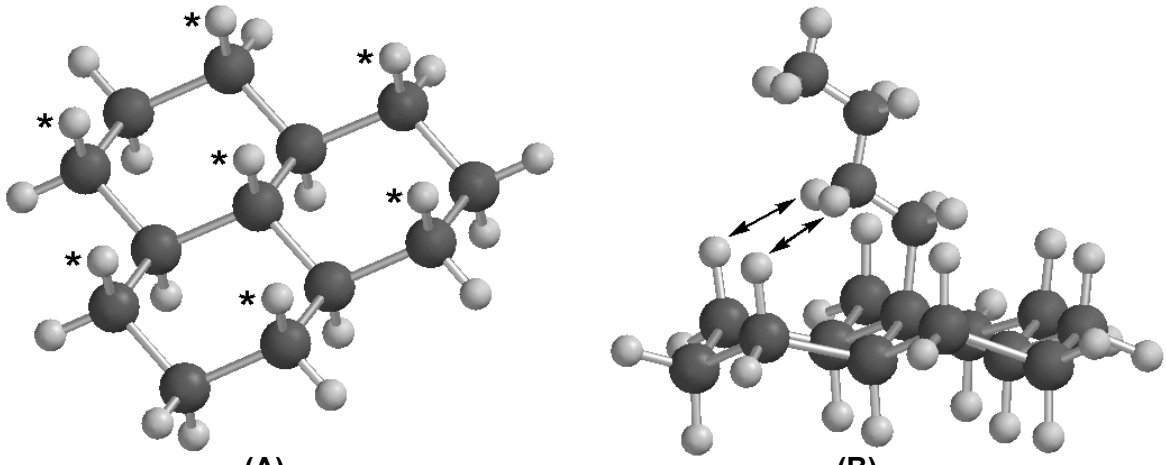

Figure 7.7 Optimized structures of (A) $Si_{13}X_{15}H_aD_b$ and (B) $Si_{13}X_{15}H_aD_bC_4H_cD_d$ at the B3LYP/6-31G(d) level. (A) The asterisks denote the hydrogen atoms (H_aD_b) of interest; the rest are pseudo-hydrogen atoms (X) which satisfy the valences of the Si cluster but are assigned masses equivalent to T to avoid artifacts due to coupling with Si–H modes of interest. (B) The arrow indicates an interaction between the C–D (at the β-carbon) and Si–H stretching vibrations discussed in the text.

Figure 7.7B depicts the optimized structure of $Si_{13}X_{15}H_6C_4H_9$ at this level. The presence of a H-terminated surface shifts the vibrational energy of the C–D bond only 1-2 cm^{-1} as follows from comparison of the data in Tables 7.6 and 7.8b. Its intensity, however, is influenced to a larger extent by the presence of Si–H bonds. The calculation on the $Si(SiX_3)_3C_{11}H_{22}D$ model, an alkyl chain bonded on an Si–H free silicon cluster, gave an intensity of 14.43 km mol^{-1} for the vibrational intensity of the C–D bond, using the B3LYP functional and 6-31G(d) basis set. For the (shorter) alkyl tail on the Si_{13} cluster, the intensity of this mode is ca. 14% higher (16.49 km mol^{-1}; see Table 7.8b). It was observed that the C–D bond has strong interactions with the H atoms indicated by arrows in Figure 7.7B, which is the result of the staggered conformation seen looking down the C–Si bond with respect to the position of the H atoms on the β-carbons and the Si–Si bonds on the surface. Substitution of the 6 H atoms on the alkylated surface by D atoms gives an intensity of 8.78 km mol^{-1} for *A*(C–D). The latter result is expected, since the frequencies of the C–D and Si–D are well separated.

To summarize, the calculations on model clusters indicate that there is a significant interaction between H/D atoms on the β-carbons and the surface termination. This interaction is most significant for C–D and Si–H stretching modes whose frequencies are very similar. This type of interaction can contribute to the broadness of the residual $Si–H_x$ stretching band observed on alkylated porous silicon.

7.4 Conclusions

Combined experimental data on the thermal hydrosilylation of deuterated porous silicon with 1-alkenes and theoretical investigations of alkylated silicon clusters support a radical chain mechanism[1,26,76,77] for the formation of covalent alkyl monolayers on porous silicon. In addition, the results of reactions carried out with strict control over the conditions (atmosphere, light, water) point to initiation of this reaction by trace amounts of oxygen. The Lewis acid-catalyzed hydrosilylation reaction of porous silicon was also studied, and the expected incorporation of hydrogen atoms from the surface in the alkyl chain was observed. Finally, the frequently observed broadening of $Si–H_x$ vibrations left after the (partial) coverage of PS by hydrosilylation of alkenes is shown to have a contribution from the interaction between the $Si–H_x$ groups and the second CH_2 moiety in the monolayer.

Acknowledgment

We thank dr. Dawei Guo (Wageningen University) for computational assistance. EPSRC for funding under Grants GR/M69104 and AF/990206 (B.R.H./A.H.) and The Research Council of Norway (L.H.L.). L.C.P.M.dS. thanks Wageningen University ("Stichting Wagenings Universiteits Fonds"), the Royal Institution of Engineers (Netherlands KIVI), and the Fundatie van de Vrijvrouwe van Renswoude for financial support.

References and Notes

[1] Linford, M. R.; Fenter, P.; Eisenberger, P. M.; Chidsey, C. E. D. *J. Am. Chem. Soc.* **1995**, *117*, 3145-3155.
[2] Linford, M. R.; Chidsey, C. E. D. *J. Am. Chem. Soc.* **1993**, *115*, 12631-12632.
[3] Buriak, J. M. *Chem. Commun.* **1999**, 1051-1060.
[4] Buriak, J. M. *Chem. Rev.* **2002**, *102*, 1271-1308.
[5] Sung, M. M.; Kluth, G. J.; Yauw, O. W.; Maboudian, R. *Langmuir* **1997**, *13*, 6164-6168.
[6] Hovis, J. S.; Hamers, R. J. *J. Phys. Chem. B* **1997**, *101*, 9581-9585.
[7] Boukherroub, R.; Wayner, D. D. M. *J. Am. Chem. Soc.* **1999**, *121*, 11513-11515.
[8] Sieval, A. B.; Vleeming, V.; Zuilhof, H.; Sudhölter, E. J. R. *Langmuir* **1999**, *15*, 8288-8291.
[9] Cicero, R. L.; Linford, M. R.; Chidsey, C. E. D. *Langmuir* **2000**, *16*, 5688-5695.
[10] Effenberger, F.; Gotz, G.; Bidlingmaier, B.; Wezstein, M. *Angew. Chem. Int. Ed.* **1998**, *37*, 2462-2464.
[11] de Villeneuve, C. H.; Pinson, J.; Bernard, M. C.; Allongue, P. *J. Phys. Chem. B.* **1997**, *101*, 2415-2420.
[12] Zazzera, L. A.; Evans, J. F.; Deruelle, M.; Tirrell, M.; Kessel, C. R.; McKeown, P. *J. Electrochem. Soc.* **1997**, *144*, 2184-2189.
[13] Bansal, A.; Li, X. L.; Lauermann, I.; Lewis, N. S.; Yi, S. I.; Weinberg, W. H. *J. Am. Chem. Soc.* **1996**, *118*, 7225-7226.

[14] Ozanam, F.; Vieillard, C.; Warntjes, M.; Dubois, T.; Pauly, M.; Chazalviel, J.-N. *Can. J. Chem. Eng.* **1998**, *76*, 1020-1026.
[15] Dubois, T.; Ozanam, F.; Chazalviel, J.-N. *Proc. Electrochem. Soc.* **1997**, *97-7*, 296-310.
[16] Gurtner, C.; Wun, A. W.; Sailor, M. *Angew. Chem. Int. Ed.* **1999**, *38*, 1966-1968.
[17] Fidelis, A.; Ozanam, F.; Chazalviel, J.-N. *Surf. Sci.* **2000**, *444*, L7-L10.
[18] Lie, L. H.; Patole, S. N.; Hart, E. R.; Houlton, A.; Horrocks, B. R. *J. Phys. Chem. B.* **2002**, *106*, 113-120.
[19] Stewart, M. P.; Buriak, J. M. *J. Am. Chem. Soc.* **2001**, *123*, 7821-7830.
[20] Wayner, D. D. M.; Wolkow, R. A. *J. Chem. Soc., Perkin Trans. 2* **2002**, 23-34.
[21] de Smet, L. C. P. M.; Stork, G. A.; Hurenkamp, G. H. F.; Sun, Q.-Y.; Topal, H.; Vronen, P. J. E.; Sieval, A. B.; Wright, A.; Visser, G. M.; Zuilhof, H.; Sudhölter, E. J. R. *J. Am. Chem. Soc.* **2003**, *125*, 13916-13917.
[22] Sun, Q.-Y.; de Smet, L. C. P. M.; van Lagen, B.; Wright, A.; Zuilhof, H.; Sudhölter, E. J. R. *Angew. Chem. Int. Ed.* **2004**, *43*, 1352-1355.
[23] Sun, Q.-Y.; de Smet, L. C. P. M.; van Lagen, B.; Giesbers, M.; Thüne, P. C.; van Engelenburg, J.; de Wolf, F. A.; Zuilhof, H.; Sudhölter, E. J. R. *J. Am. Chem. Soc.* **2005**, *127*, 2514-2523.
[24] Bateman, J. E.; Eagling, R. D.; Worrall, D. R.; Horrocks, B. R.; Houlton, A. *Angew. Chem. Int. Ed.* **1998**, *37*, 2683-2685.
[25] Boukherroub, R.; Wojtyk, J. T. C.; Wayner, D. D. M.; Lockwood, D. J. *J. Electrochem. Soc.* **2002**, *149*, H59-H63.
[26] Buriak, J. M.; Allen, M. J. *J. Am. Chem. Soc.* **1998**, *120*, 1339-1340.
[27] Stewart, M. P.; Robins, E. G.; Geders, T. W.; Allen, M. J.; Choi, H. C.; Buriak, J. M. *Physica Status Solidi A* **2000**, *182*, 109-115.
[28] Sieval, A. B.; Opitz, R.; Maas, H. P. A.; Schoeman, M. G.; Meijer, G.; Vergeldt, F. J.; Zuilhof, H.; Sudhölter, E. J. R. *Langmuir* **2000**, *16*, 10359-10368.
[29] Sieval, A. B.; Linke, R.; Zuilhof, H.; Sudhölter, E. J. R. *Adv. Mat.* **2000**, *12*, 1457-1460.
[30] Sailor, M. J.; Lee, E. J. *Adv. Mat.* **1997**, *9*, 783-793.
[31] Sailor, M. J.; Heinrich, J. L.; Lauerhaas, J. M. *Stud. Surf. Sci. Catal.* **1997**, *103*, 209-235.
[32] Sieval, A. B.; Demirel, A. L.; Nissink, J. W. M.; Linford, M. R.; van der Maas, J. H.; de Jeu, W. H.; Zuilhof, H.; Sudhölter, E. J. R. *Langmuir* **1998**, *14*, 1759-1768.
[33] Strother, T.; Hamers, R. J.; Smith, L. M. *Nucl. Acids Res.* **2000**, *28*, 3535-3541.
[34] Lin, Z.; Strother, T.; Cai, W.; Cao, X. P.; Smith, L. M.; Hamers, R. J. *Langmuir* **2002**, *18*, 788-796.
[35] Strother, T.; Cai, W.; Zhao, X. S.; Hamers, R. J.; Smith, L. M. *J. Am. Chem. Soc.* **2000**, *122*, 1205-1209.
[36] Juang, A.; Scherman, O. A.; Grubbs, R. H.; Lewis, N. S. *Langmuir* **2001**, *17*, 1321-1323.
[37] Pike, A. R.; Lie, L. H.; Eagling, R. A.; Ryder, L. C.; Patole, S. N.; Connolly, B. A.; Horrocks, B. R.; Houlton, A. *Angew. Chem. Int. Ed.* **2002**, *41*, 615-617.
[38] Patole, S. N.; Pike, A. R.; Connolly, B. A.; Horrocks, B. R.; Houlton, A. *Langmuir* **2003**, *19*, 5457-5463.
[39] Lie, L. H.; Patole, S. N.; Pike, A. R.; Ryder, L. C.; Connolly, B. A.; Ward, A. D.; Tuite, E. M.; Houlton, A.; Horrocks, B. R. *Faraday Discuss.* **2004**, *125*, 235-249.
[40] Wang, L.; Reipa, V.; Blasic, J. *Bioconjugate Chem.* **2004**, *15*, 409-412.

[41] Allongue, P.; de Villeneuve, C. H.; Pinson, J. *Electrochim. Acta* **2000**, *45*, 3241-3248.
[42] Allongue, P.; de Villeneuve, C. H.; Pinson, J.; Ozanam, F.; Chazalviel, J.-N.; Wallart, X. *Electrochim. Acta* **1998**, *43*, 2791-2798.
[43] Yu, H. Z.; Morin, S.; Wayner, D. D. M.; Allongue, P.; de Villeneuve, C. H. *J. Phys. Chem. B* **2000**, *104*, 11157-11161.
[44] Sieval, A. B.; van den Hout, B.; Zuilhof, H.; Sudhölter, E. J. R. *Langmuir* **2000**, *16*, 2987-2990.
[45] Zhang, L. Z.; Wesley, K.; Jiang, S. Y. *Langmuir* **2001**, *17*, 6275-6281.
[46] Sieval, A. B.; van den Hout, B.; Zuilhof, H.; Sudhölter, E. J. R. *Langmuir* **2001**, *17*, 2172-2181.
[47] Lua, Y. Y.; Niederhauser, T. L.; Matheson, R.; Bristol, C.; Mowat, I. A.; Asplund, M. C.; Linford, M. R. *Langmuir* **2002**, *18*, 4840-4846.
[48] Reboredo, F. A.; Schwegler, E.; Galli, G. *J. Am. Chem. Soc.* **2003**, *125*, 15243-15249.
[49] Kang, J. K.; Musgrave, C. B. *J. Chem. Phys.* **2002**, *116*, 9907-9913.
[50] Kruse, P.; Johnson, E. R.; DiLabio, G. A.; Wolkow, R. A. *Nano Lett.* **2002**, *2*, 807-810.
[51] Pei, Y.; Ma, J.; Jiang, Y. S. *Langmuir* **2003**, *19*, 7652-7661.
[52] Ishibashi, T.; Ara, M.; Tada, H.; Onishi, H. *Chem. Phys. Lett.* **2003**, *367*, 376-381.
[53] Quayum, M. E.; Kondo, T.; Nihonyanagi, S.; Miyamoto, D.; Uosaki, K. *Chem. Lett.* **2002**, 208-209.
[54] Nihonyanagi, S.; Miyamoto, D.; Idojiri, S.; Uosaki, K. *J. Am. Chem. Soc.* **2004**, *126*, 7034-7040.
[55] Nealey, P. F.; Black, A. J.; Wilbur, J. L.; Whitesides, G. in *Molecular Electronics*; Jortner, J., Ratner, M. A., Eds.; Blackwell Science Ltd.; Oxford, U.K., 1997; Ch. 11, pp 343-368.
[56] Lopinski, G. P.; Wayner, D. D. M.; Wolkow, R. A. *Nature* **2000**, *406*, 48-51.
[57] Cicero, R. L.; Chidsey, C. E. D.; Lopinski, G. P.; Wayner, D. D. M.; Wolkow, R. A. *Langmuir* **2002**, *18*, 305-307.
[58] Eves, B. J.; Sun, Q.-Y.; Lopinski, G. P.; Zuilhof, H. *J. Am. Chem. Soc.* **2004**, *126*, 14318-14319.
[59] Cho, J. H.; Oh, D. H.; Kleinman, L. *Phys. Rev. B* **2002**, *65*, 081310.
[60] Stewart, M. P.; Buriak, J. M. *Angew. Chem. Int. Ed.* **1998**, *37*, 3257-3260.
[61] Bateman, J. E.; Eagling, R. D.; Horrocks, B. R.; Houlton, A. *J. Phys. Chem. B.* **2000**, *104*, 5557-5565.
[62] Asao, N.; Sudo, T.; Yamamoto, Y. *J. Org. Chem* **1996**, *61*, 7654-7655.
[63] *WinFIRST*, v2.10; Analytical Technology Inc.: Madison, WI, 1994.
[64] Burrows, V. A.; Chabal, Y. J.; Higashi, G. S.; Raghavachari, K.; Christman, S. B. *Appl. Phys. Lett.* **1988**, *53*, 998-1000.
[65] Ogata, Y.; Niki, H.; Sakka, T.; Iwasaki, M. *J. Electrochem. Soc.* **1995**, *142*, 1595-1601.
[66] Ogata, Y.; Niki, H.; Sakka, T.; Iwasaki, M. *J. Electrochem. Soc.* **1995**, *142*, 195-201.
[67] Wave function Inc., Irvine, CA, www.wavefun.com; Schrodinger, Inc., Portland, OR, www.schrodinger.com.
[68] GAMMES: Schmidt, M. W.; Baldridge, K. K.; Boatz, J. A.; Elbert, S. T.; Gordon, M. S.; Jensen, J. H.; Koseki, S.; Matsunaga, N.; Nguyen, K. A.; Su, S. J.; Windus, T. L.; Dupuis, M.; Montgomery, J. A. *J. Comput. Chem.* **1993**, *14*, 1347-1363.
[69] Granosvksy, A. A. http://classic.chem.msu.su/gran/gamess/index.html.
[70] Matsumoto, T.; Belogorokhov, A. I.; Belogorokhova, L. I.; Masumoto, Y.; Zhukov, E. A. *Nanotech.* **2000**, *11*, 340-347.

[71] Matsumoto, T.; Masumoto, Y.; Nakashima, S.; Mimura, H.; Koshida, N. *Appl. Surf. Sci.* **1997**, *113-114*, 140-144.

[72] Matsumoto, T.; Masumoto, Y.; Nakashima, S.; Koshida, N. *Thin Solid Films* **1997**, *297*, 31-34.

[73] Bateman, J. E.; Eagling, R. D.; Horrocks, B. R.; Houlton, A.; Worrall, D. R. *Chem. Commun.* **1997**, 2275-2276.

[74] *CRC Handbook of Chemistry and Physics*, 75th ed.; Lide, D. R., Ed.; CRC Press: Boca Raton, FL, 1994.

[75] Boukherroub, R.; Morin, S.; Sharpe, P.; Wayner, D. D. M.; Allongue, P. *Langmuir* **2000**, *16*, 7429-7434.

[76] Buriak, J. M.; Stewart, M. P.; Geders, T. W.; Allen, M. J.; Choi, H. C.; Smith, J.; Raftery, D.; Canham, L. T. *J. Am. Chem. Soc.* **1999**, *121*, 11491-11502.

[77] Holland, J. M.; Stewart, M. P.; Allen, M. J.; Buriak, J. M. *J. Solid State Chem.* **1999**, *147*, 251-258.

[78] Cotton, F. A.; Wilkinson, G. *Advanced Inorganic Chemistry*, 5th Ed.; Wiley: New York, 1988; pp 1255-1256.

[79] Boukherroub, R.; Morin, S.; Bensebaa, F.; Wayner, D. D. M. *Langmuir* **1999**, *15*, 3831-3835.

[80] Scott, A. P.; Radom, L. *J. Phys. Chem.* **1996**, *100*, 16502-16513.

Appendix

Field Effect Transistors*

Abstract – The development of field effect transistor (FET) based sensors for the detection of ionic species in solution is described. This development started about 35 years ago with the invention of the ion-sensitive field effect transistor (ISFET) for the detection of solution pH. Later chemically sensitive field effect transistors (CHEMFETs) have been developed for the detection of many different cations and anions. The first CHEMFETs were based on ion-selective membranes deposited physically on the gate oxide of an ISFET. More durable CHEMFETs were made by linking all membrane components covalently. Finally, the appendix describes the possibilities of a new generation of sensors, based on hybrid organic semiconductor field effect transistors (HOSFETs) in which the monolayers reported in this thesis play a crucial role.

* A comprehensive version of this appendix has been published:
Sudhölter, E. J. R.; de Smet, L. C. P. M.; Zuilhof, H., Proceedings of the 5th European Conference on Precision Agriculture held in Uppsala, Sweden, 9-12 June 2005. Edited by Stafford, J. V., Wageningen Academic Publishers, 17-24.

1 Introduction

A field-effect transistor (FET) is a device in which an electrical field controls the shape and hence the conductivity of a channel in a semiconductor material. The most widely applied field effect transistor is the so-called metal oxide semiconductor field effect transistor (MOSFET). In such a transistor an oxide insulator is sandwiched between the metal gate and the semiconductor. This transistor can be found in almost every micro-electronic device today, where it operates as a binary switch.

It was Piet Bergveld in 1970, who got the idea to remove the metal layer from a MOSFET and to expose the underlying silicon dioxide insulator directly to a sample solution.[1] With this ion-sensitive field effect transistor (ISFET) he was able to detect changes in the pH of the solution. Later it was recognized that a reference electrode is necessary for the proper functioning of an ISFET as a pH sensor. Many publications have appeared on ISFETs and related devices like the EnzymeFETs and ImmunoFETS. Recently, two nicely written papers have appeared, one from Bergveld[2] and the other from Janata,[3] giving their personal views after 30 years of research on FET-based sensors. In these papers it is remarked that commercialization of these ISFETs and CHEMFETs (Chemically sensitive FETs) is unfortunately not very successful. Probably the encountered problems regarding biocompatibility, which is very important for the anticipated biomedical applications, has contributed to stop further industrial developments.[2] However, successful commercialization of ISFETs is foreseen in those application areas, where the vulnerability of using glass electrodes is a serious problem.

2 Ion-Sensitive Field Effect Transistor

An ISFET is a solid-state sensor able to detect protons (pH) in a potentiometric way. A schematic representation of the set-up of a pH measurement using an ISFET is shown in Figure 1. The sensor area exposed to the sample solution is the gate oxide. Usually, thermally grown silicon dioxide of about 100 nm thickness is used. The gate oxide covers the channel of the p-doped silicon semiconductor, which is located between the n-doped source and drain regions. More information on n-type and p-type silicon can be found in Chapter 1. By making a structure in silicon of subsequently n-doped/p-doped/n-doped (i.e., source/channel/drain), a so-called diode is obtained. The source and bulk are shortcut with the ground. If the source and drain are connected to an external voltage source (V_{ds}), no current will flow (I_d = 0), since the junction between p-doped silicon and n-doped silicon acts as an electron barrier.

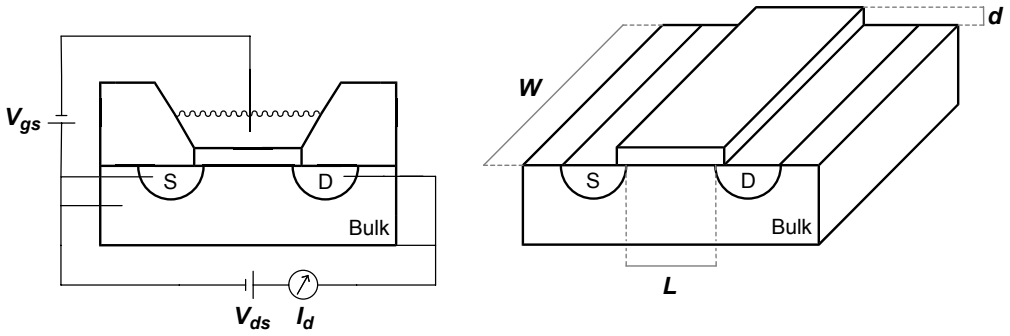

Figure 1. (left) Schematic cross-section of an ISFET and (right) a perspective view illustrating the different dimensions. S = source, D = drain, V_{gs} = bias potential, V_{ds} = drain-source potential, I_d = drain-source current, W = width of the gate, L = length of the gate, and d = insulator thickness.

The holes cannot move into the region where electrons are the charge-transporting species. However, this barrier is sensitive to a voltage V_{gs} applied on the reference electrode with respect to the bulk of the p-doped silicon material. If a positive voltage is applied to the reference electrode a process starts by which the channel (the region between source and drain just below the silicon dioxide insulator) becomes depleted in positive charge carriers (holes). At a certain voltage, the so-called threshold voltage (V_t), charge inversion in the channel occurs. The holes are repelled from the junction and the electrons are attracted to the junction. Under these conditions, the channel behaves like n-doped silicon, the conductivity barrier is absent, and an electron current from source to drain starts to flow. Field-effect based sensors generally operate under these conditions. Further increase of V_{gs} results in an additional increase of I_d. From this picture it is easily recognized that MOSFETs act as a binary switch and/or as an electronic amplifier. If V_{gs} is below V_t no current flows and the switch is 'off'. If V_{gs} is above V_t a current will flow and the switch is 'on'. Since the source-drain current I_d is the result of the changing gate-source voltage, and the current flowing through the insulator will be very low, it is seen that the ratio of these two currents is the mentioned amplification. Typical gate areas are 15 × 500 μm^2 (length × width; length is the distance between source and drain, Figure 1).

Current I_d can be modulated by chemical interactions at the silicon dioxide interface with the solution. In most experimental set-ups not the change of source-drain current I_d is measured as a function of changing sample composition, but V_{gs} is adapted in such a way that the source-drain current I_d is kept constant at a fixed V_{ds}. The change of V_{gs} is then registered. This change of V_{gs} compensates the potential difference at the insulator interface with the sample solution, which is a direct consequence of the chemical interactions at the interface.

ISFETs have shown many benefits, like for instance their small dimensions (individual chips are typically 3 × 4.5 mm), their fast response time on changes in the sample solution, their robustness due to the all-solid state set-up, their high signal-to-noise ratio, and the low output impedance due to the in situ impedance transformation, which makes the electrical output signal less sensitive for external disturbances. In addition, the ISFETs have the possibilities for subsequent integration with other electronic functions. And last but not least, ISFETs can be stored under dry conditions.

The best experimental results for pH sensing have been obtained using silicon(oxy)nitride as the insulator gate material. This material shows a perfect passivation of the semiconductor and has a stable and reproducible pH response.

3 Chemically Sensitive Field Effect Transistor

Field effect transistors sensitive for other ionic species than protons have been made via the deposition of ion-selective membranes on top of the gate oxide. The presence of ionophores in the membrane results in ion selectivity. Generally such membranes are made from plasticized poly(vinylchloride) (PVC), often with the addition of lipophilic ions, having a charge opposite to the charge of the ion to be detected. In essence such membranes are ion-exchanging. If the lipophilic ion is an anion, for instance tetraphenylborate, the membrane exchanges cations.

The membranes can be seen as a buffer for the cation that is selectively exchanged. The electro-chemical equilibrium that exists between the cations in solution near the membrane interface and the cations in the bulk solution determines the surface potential at the membrane solution interface. This membrane surface potential modulates the source-drain current I_d of the semiconductor in a way similar to the pH sensitive ISFETs. Many different ionophores have been investigated successfully and are described in literature. Therefore, a wide variety of CHEMFETs for the detection of cations and anions does exist.[4]

In order to increase the mechanical stability of the deposited ion-selective membranes a lot of research has been performed on the covalent binding of the membrane and its components.[5] To prevent dissolution of the plasticizer to the aqueous phase, intrinsically ‘plastic’ poly(siloxanes) have been used. Durable membranes for the selective detection of potassium (K^+)[6], sodium (Na^+),[7] and lead (Pb^{2+})[8] ions have been made. These ion-selective membranes are not coupled directly to the gate oxide, but are coupled to an intermediate poly(hydroxyethylmethacrylate) hydro-gel layer (polyHEMA) covering the gate. This hydro-gel layer contains a buffer and a certain concentration of the ion to be detected.[9,10] Such a

hydro-gel layer contributes to a much better electrical tuning of the CHEMFETs, as it prevents an undesired potentiometric response due to carbon dioxide (CO_2) diffusing through the membrane. In addition, it fixes the interfacial potentials between membrane and hydro-gel and between hydro-gel and semiconductor in a controllable way.[9,10] The necessity of using an intermediate hydro-gel layer for the fixation of electronic junctions was disputed later.[11]

In contrast to the ISFETs, most membrane-modified CHEMFETs are less robust. Mechanical force can disrupt the membrane and also differences in the osmolality between the sample solution and hydro-gel layer, may cause drift and mechanical disruption of the membrane. Therefore, CHEMFETs have to be used preferably not in direct contact with the sample solution, but in a more controlled way. A possible way is to incorporate CHEMFETs in a flow injection system.[12] The composition of the background solution flowing along the CHEMFETs can be controlled with respect to osmolality and ionic composition. By injection of small volumes of sample solution in the flow, only a plug of sample solution comes during a short time interval in contact with the membrane surface. At that moment the unknown sample solution is measured. After that contact the original solution composition is restored. Possible surface contamination is flushed away easily.

4 Hybrid Organic Semiconductor Field Effect Transistor[13]

In a HOSFET[13] both the metal and insulating oxide layer have been replaced by a functionalized organic monolayer that is covalenty attached via a stable Si–C bond. The organic hydrocarbon tail acts as the insulator, replacing the oxide, and the terminated functional group introduces the sensitivity and selectivity. Different functional groups can be chosen. For instance, carboxylic groups (–COOH)[14-21] or amino groups ($–NH_2$)[22] will introduce pH sensitivity, quaternary ammonium groups ($–NR_4^+$)[23] will introduce anion sensitivity. Also more complex (bio)receptor molecules can be bound covalently to the terminal end of the monolayer. As an example are given crown ethers[24] and calixarenes to introduce cation selectivity, but also monolayers that contain carbohydrates can be prepared (Chapter 4). So far, our research has focused primarily on the coupling of the monolayers to the silicon surface and the properties of the monolayer. A detailed electrical characterization of the attached non-functionalized monolayers is given in Chapter 6. Our initial results on electrochemical characterization of fuctionalized organic monolayer will be published elsewhere.[25] Briefly, preliminary Mott Schottky measurements on mixed monolayers derived from an alkenylated 15-crown-5 derivative (10-25%) and a non-functionalized alkene

(90-75%) showed indeed response for K^+ and Na^+ ions, whereas homogenous monolayers of the non-functionalized alkene did not. The crown ether-containing monolayers were tested in the range of cation concentrations of 10 μM to 95 mM. A response in V_{fb} was recorded in the higher concentration region of 10 to 95 mM, indicating a rather low affinity of the crown ether for the cations. As no differences in the response were observed for the 10 and 25%-functionalized monolayers, the degree of attachment of the alkenylated 15-crown-5 derivative might be limited, due to the size of the bulky crown ether. More experiments are in progress in order to develop sensing organic monolayers covalently attached on silicon. After this development has been optimized on silicon wafers the monolayers can be integrated in FET structures, resulting in the fabrication of HOSFETs.

5 Applications of Field Effect Transistors

For monitoring pH values the ISFETs having a silicon(oxy)nitride gate show a sensitive, stable and reproducible response. Especially under harsh conditions, these sensors perform better than the conventional glass electrodes. These ISFETs are not only applied for the monitoring of pH in meat and milk, but are also useful for pH monitoring in soil, manure, horticulture and of drainage water.

Monitoring of different nutrients (e.g., K^+, Ca^{2+}, NO_3^-) is possible by a range of existing CHEMFETs.[26] These sensors are however vulnerable to mechanical damage, due to the presence of the ion-selective membrane. Use of these CHEMFETs in a flow system under well-controlled conditions is therefore strongly recommended. These CHEMFETs have been applied for the monitoring of nitrate and ammonium in soil samples. Often, the soil samples are first filtered and extracted with water, and subsequently the extract is analyzed using a CHEMFET.

The HOSFETs are expected to become promising candidates for near future monitoring of nutrients and different biomolecules. Besides the mentioned benefits of ISFETs in comparison with conventional ion-selective electrodes (ISEs), HOSFETs have some additional benefits. Due to the absence of an inorganic insulating layer, drift as a result of ion migration in the insulator is also absent. In some way HOSFETs resemble ISFETs, because the different (bio)chemical receptors in HOSFETs are located at the surface of the insulating organic monolayer, like the pH sensitive silanol groups are located at the surface of the inorganic insulator. However, in the case of the HOSFET no junction between the ion-selective membrane and insulator is present. In addition, in contrast to membrane-based CHEMFETs, HOSFET can be stored under dry condition. Chemically and biochemically-

sensitive layers can be introduced in a rather simple way, via direct (Chapters 2 to 4) or indirect methods. Using photo patterning, in principle arrays of many different receptor molecules can be made on a single chip. Such a multi-array sensor can be integrated with micro-channel devices for sample pretreatments (filtering, pre concentration) and in situ calibration and also integrated with other electronic functionalities.

References and Notes

[1] Bergveld, P. *IEEE Trans. Biomed. Eng.* **1970**, *BME-17*, 70.

[2] Bergveld, P. *Sens. Actuators* **2003**, *88*, 1-20.

[3] Janata, J. *Electroanalysis* **2004**, *16*, 1831-1835.

[4] Wróblewski, W.; Mirzynska, B.; Brzózka, Z. *Chem. Anal. (Warsaw)* **1996**, *41*, 697-706.

[5] Lugtenberg, R. J. W.; Egberink, R. J. M.; van den Berg, A.; Engbersen, J. F. J.; Reinhoudt, D. N. *J. Electroanal. Chem.* **1998**, *452*, 69-86.

[6] van der Wal, P. *The Development of a Durable Pottasium Sensor Based on FET-Technology*, PhD Thesis, University of Twente, 1991.

[7] Brunnink, J. A. J. *Sodium-selective CHEMFETs*, PhD Thesis, University of Twente, 1993.

[8] Cobben, P. L. H. M. *Sensors for Heavy Metal Ions based on ISFETs*, PhD Thesis, University of Twente, 1992.

[9] Sudhölter, E. J. R.; van der Wal, P. D.; Skowronskaptasinska, M.; van den Berg, A.; Bergveld, P.; Reinhoudt, D. N. *Anal. Chim. Acta* **1990**, *230*, 59-65.

[10] van der Wal, P. D.; Skowronskaptasinska, M.; van den Berg, A.; Bergveld, P.; Sudhölter, E. J. R.; Reinhoudt, D. N. *Anal. Chim. Acta* **1990**, *231*, 41-52.

[11] Janata, J.; Josowicz, M. *Accounts Chem. Res.* **1998**, *31*, 241-248.

[12] van der Wal, P. D.; Sudhölter, E. J. R.; Reinhoudt, D. N. *Anal. Chim. Acta* **1991**, *245*, 159-166.

[13] Sudhölter, E. J. R.; Zuilhof, H.; Sieval, A. B.; de Smet, L. C. P. M.; Visser, G. M.; Bergveld, P.; Olthuis, W.; Faber, E. J. patent *WO 03098204 (A1)*, **2003**.

[14] Sieval, A. B.; Demirel, A. L.; Nissink, J. W. N.; Linford, M. R.; van der Maas, J. H.; de Jue, W. H.; Zuilhof, H.; Sudhölter, E. J. R. *Langmuir* **1998**, *14*, 1759-1768.

[15] Strother, T.; Cai, W.; Zhao, X. S.; Hamers, R. J.; Smith, L. M. *J. Am. Chem. Soc.* **2000**, *122*, 1205-1209.

[16] Cricenti, A.; Longo, G.; Luce, M.; Generosi, R.; Perfetti, P.; Vobornik, D.; Margaritondo, G.; Thielen, P.; Sanghera, J. S.; Aggarwal, I. D.; Miller, J. K.; Tolk, N. H.; Piston, D. W.; Cattaruzza, F.; Flamini, A.; Prosperi, T.; Mezzi, A. *Surf. Sci.* **2003**, *544*, 51-57.

[17] Li, Y.; Tero, R.; Nagasawa, T.; Nagata, T.; Urisu, T. *Appl. Surf. Sci.* **2004**, *238*, 238-241.

[18] Liu, Y. J.; Navasero, N. M.; Yu, H. Z. *Langmuir* **2004**, *20*, 4039-4050.

[19] Yin, H. B.; Brown, T.; Greef, R.; Wilkinson, J. S.; Melvin, T. *Microelectron. Eng.* **2004**, *73-74*, 830-836.

[20] Asanuma, H.; Lopinski, G. P.; Yu, H. Z. *Langmuir* **2005**, *21*, 5013-5018.

[21] Perring, M.; Dutta, S.; Arafat, S.; Mitchell, M.; Kenis, P. J. A.; Bowden, N. B. *Langmuir* **2005**, *21*, 10537-10544.

[22] Sieval, A. B.; Linke, R.; Heij, G.; Meijer, G.; Zuilhof, H.; Sudhölter, E. J. R. *Langmuir* **2001**, *17*, 7554-7559.

[23] Boiadjiev, V. I.; Brown, G. M.; Pinnaduwage, L. A.; Goretzki, G.; Bonnesen, P. V.; Thundat, T. *Langmuir* **2005**, *21*, 1139-1142.

[24] de Smet, L. C. P. M.; Zuilhof, H; Sudhölter, E. J. R. - unpublished results.

[25] Faber, E. J., PhD Thesis, University of Twente - in preparation.

[26] Artigas, J.; Beltran, A.; Jimenez, C.; Baldi, A.; Mas, R.; Dominguez, C.; Alonso, J. *Comput. Electron. Agr.* **2001**, *31*, 281-293.

Summary

&

‘Samenvatting voor Niet-Chemici’

Summary

In the field of covalently bound organic monolayers on oxide-free silicon (Si) surfaces, a variety of preparative hydrosilylation methods had been developed between 1993 and 2000. These studies allowed initial characterizations of such monolayers, but the conditions that were required to prepare these monolayers (using either high temperatures or UV light) were too harsh to allow direct attachment of (bio-)functional molecules. Therefore we set out to improve this, and this thesis contains the progressive results on the following three topics: extremely mild attachment conditions that are compatible with a very wide variety of biomolecules, highly detailed characterizations of the resulting monolayers and the way they are formed, and finally their integration into electrical devices that are to be used in sensors.

After a general introduction in Chapter 1, Chapter 2 describes the development of an extremely mild and practical method using visible light (447 nm) to attach organic monolayers on flat hydrogen-terminated Si(100) surfaces. High water contact angles were obtained for non-functionalized alkyl monolayers indicating a high monolayer quality. With high-resolution angle-resolved XPS (ARXPS) for the first time depth profiles of the elements in an organic monolayer (~2 nm thickness) were obtained. As nearly all biomolecules do not absorb any of the long-wavelength light that is used to photo-excite the Si, this attachment method is suitable for the direct preparation of (bio)-active monolayers.

In Chapter 3 this very mild visible light method for the attachment of high-quality organic monolayers on crystalline Si surfaces is further developed and explored, with four crucial observations: a) By using visible light sources, from 447 to 658 nm, a variety of 1-alkenes and 1-alkynes can be attached to hydrogen-terminated Si(100) and Si(111) surfaces. Study of such layers by a range of techniques (static water contact angles, XPS, X-ray reflectivity and IR spectroscopy) supports the qualification of ‘high-quality’ monolayers. b) Our novel use of infrared reflection-absorption spectroscopy (IRRAS) makes this a highly useful technique to display the presence or absence of functional groups on the Si surface. c) For a mixed monolayer of 1-decene and an ω-fluoro-1-alkene the composition of the monolayer is directly proportional to the molar ratio of the two compounds in the solutions. d) Finally, dopants display a remarkable and unexpected effect of dopants: with more electron carriers (n-type doping) in the silicon, this surface reaction speeds up. A mechanism was developed that can explain this and other phenomena in this reaction.

Chapters 4 and 5 describe the formation of highly functionalized monolayers. Chapter 4 describes how monosaccharides, including labile sialic acid derivatives, can be incorporated

into the monolayer using the extremely mild attachment chemistry of Chapters 2 and 3. Interestingly, a combination of ATR-IR and ARXPS does not only show the presence of the carbohydrate moieties, but also reveals that the functionalities are on top of the monolayers, and thus available for biomolecular interactions! Chapter 5 reports on oligo(ethylene glycol)-containing monolayers. These were reported by others to be highly efficient in resisting protein adsorption on a variety of inorganic substrates. However, after synthesis and extensive protein adsorption studies onto this surface, it is shown that the bio-resistance is more directly linked to the density of the monolayer than initially hypothesized by others, as – depending on this density – high or low protein resistance was observed. This observation is especially relevant given the high importance of control over the protein adsorption onto such surfaces for bio-sensing applications, and points at the need for much more research in this direction.

In Chapter 6 Hg/alkyl monolayer/silicon junctions are characterized by current density-voltage (*J*-*V*) and capacitance-voltage (*C*-*V*) measurements, yielding a series of relevant parameters describing the electrical behavior of these Schottky diodes. It is shown that the *J*-*V* behavior of the hybrid structures can be precisely tuned via the monolayer thickness. Using thermal preparation conditions very low values for the fixed charge density (N_f) were found. Furthermore, the values for the effective barrier height ($q\phi_{eff}$) and the series resistance (R_s) of organic monolayers are higher than those of SiO_2 layers of similar thickness. By using 1-alkynes instead of 1-alkenes even higher resistances can be obtained. The electrical parameters indicate a lower degree of silicon surface oxidation for the 1-alkyne-derived monolayer, which was also confirmed by XPS measurements.

In Chapter 7 we report on the mechanism of the monolayer formation of 1-alkenes on hydrogen-terminated porous silicon surfaces. It is proposed that monolayer formation occurs via the same radical chain process as at single-crystal surfaces. A broad band around 2100 cm^{-1} was observed in the infrared spectra upon alkylation of deuterated silicon surfaces. By the support of ab initio and density functional theory calculations on small molecule models these broad 2100 cm^{-1} features are assigned to C-D bands arising from the involvement of surface D atoms in the hydrosilylation reactions, while the line broadening can be explained partly by interaction with neighboring surface atoms/groups.

Finally, the appendix describes the development of ion-sensitive and chemically sensitive field effect transistors (ISFETS and CHEMFETs), as well as the possibilities of a new generation of sensors, based on hybrid organic semiconductor field effect transistors (HOSFETs) in which the monolayers reported in this thesis play a crucial role.

Samenvatting voor Niet-Chemici

De titel van dit proefschrift luidt ”Covalent Gebonden Organische Monolagen op Siliciumoppervlakken: Zichtbaar Licht, Karakterisering en Elektrische Eigenschappen”. In deze samenvatting wordt kort uitgelegd wat dit betekent.

Het in dit proefschrift beschreven onderzoek omvat werk aan monolagen. Dit zijn zeer dunne lagen van slechts één molecuul dik, grofweg een duizendste van een duizendste van een millimeter. De materialen waarvan de monolagen zijn gemaakt, heten organisch omdat ze het element koolstof bevatten. Monolagen zijn niet met het blote oog zichtbaar. In dit onderzoek zijn dan ook verschillende, soms zeer geavanceerde technieken gebruikt om de monolagen te bestuderen (karakteriseren). Hierbij is informatie verkregen over bijvoorbeeld de samenstelling, dikte en opbouw van de monolagen.

Organische monolagen kunnen op verschillende soorten materiaal worden aangebracht. Zoals blijkt uit de titel van dit proefschrift is er gewerkt aan oppervlakken van silicium. Silicium is het basismateriaal voor elektronische componenten als transistoren en computer-chips. In deze toepassingen zit op het silicium een dun laagje oxide (gebonden zuurstof) en om verschillende redenen is er een grote vraag naar alternatieven voor dit oxide.

Een siliciumoppervlak kan chemisch worden ontdaan van zijn oxidelaag waarbij een laag aan waterstofatomen gevormd wordt. Zo’n oppervlak kan daarna reageren met organische materialen, waarbij een heel goed vastzittende (covalent gebonden) monolaag wordt gevormd. Er is een grote interesse in deze chemie. Dit komt onder andere omdat zo’n monolaag de mogelijkheid biedt bepaalde materialen (receptoren) aan te brengen die specifiek kunnen binden met geladen deeltjes of moleculen (moleculaire herkenning), waarmee de basis van een sensor gevormd is. Een voorbeeld van dit principe is een monolaag met receptoren die binden met afweerstoffen (antilichamen).

Na een korte inleiding in Hoofdstuk 1 wordt in de Hoofdstukken 2 en 3 de ontwikkeling van een nieuwe, heel milde methode beschreven om organische monolagen op silicium vast

Figuur 1 De vorm van een druppel water op een siliciumoppervlak wordt sterk bepaald door de eigenschappen van dat oppervlak, zoals deze figuur laat zien: silicium voorzien van een oxidelaag (links), een laag waterstofatomen (midden) en een organische monolaag (rechts).

te zetten. Bij deze methode wordt gebruik gemaakt van zichtbaar licht (bijvoorbeeld een gloeilamp). Er is gewerkt met verschillende kleuren van licht (o.a. blauw en rood), ieder met een verschillende energie-inhoud. Veel natuurlijke stoffen veranderen niet door blootstelling aan zichtbaar licht, waarmee deze nieuwe methode de mogelijkheid biedt om biologische materialen direct in één chemische stap vast te zetten. Verder beschrijft èn verklaart het hoofdstuk een heel onverwacht effect, van zowel het type als de hoeveelheid element dat is toegevoegd aan zuiver silicium, op de snelheid waarmee een monolaag wordt gevormd.

In Hoofdstuk 4 staan suikermoleculen centraal. Deze zijn interessant, omdat ze onder andere een rol spelen bij herkenningsprocessen in het afweersysteem. In dit hoofdstuk is aangetoond dat suikerbevattende moleculen op een siliciumoppervlak kunnen worden vastgezet op zo'n manier dat het aangebrachte suikermolecuul net, maar tevens duidelijk boven de monolaag uitsteekt, als een zonnebloem in een korenveld. Hiermee is het oppervlak geschikt gemaakt voor de wisselwerking met bijvoorbeeld antilichamen in oplossing: het uitstekende suikermolecuul kan vanuit die positie eventueel aanwezige stoffen vastgrijpen, wat van belang is voor de ontwikkeling van (diagnostische) sensoren.

In Hoofdstuk 5 staat het voorkómen van aspecifieke, ongewenste interacties centraal. Biomaterialen, zoals algen of eiwitten, hebben de neiging om zich te hechten aan een oppervlak. Dit leidt in de praktijk vaak tot problemen, bijvoorbeeld de aanhechting van algen op scheepswanden en de vervuiling van contactlenzen door lichaamseigen stoffen. Een specifiek aangebrachte monolaag op silicium kan deze aanhechting echter sterk verminderen. Hoofdstuk 5 gaat over de bereiding van dergelijke lagen en het 'vastplakken' van fibrinogeen, een eiwit dat een belangrijke rol speelt bij het stollingsproces van bloed.

In Hoofdstuk 6 worden de elektrische eigenschappen van organische monolagen beschreven. Er is aangetoond dat de elektrische weerstand van een monolaag toeneemt naarmate deze laag dikker wordt. De elektrische eigenschappen van de organische monolagen blijken in een aantal opzichten gunstiger te zijn dan die van siliciumoxide en dit biedt dus een goed uitgangspunt voor verder onderzoek.

In Hoofdstuk 7 zijn zeer poreuze oppervlakken bestudeerd, waarvoor gebruik werd gemaakt van deuterium, een zwaardere vorm van waterstof, die chemisch dezelfde eigenschappen heeft. Door nauwkeurig te kijken naar het effect van dit grotere gewicht is informatie verkregen over het mechanisme van de monolaagbereiding op poreus silicium.

Met de combinatie van deze studies is een grote sprong voorwaarts gemaakt binnen het onderzoek aan gemodificeerde oppervlakken. Hierdoor zijn tal van toepassingen – m.n. richting elektronische apparatuur en (medische) diagnostiek – significant dichterbij gekomen.

Curriculum Vitae

Louis de Smet was born in Oostburg, the Netherlands, on April 6, 1977. After finishing high school (HAVO and VWO) at Scholengemeenschap ’t Zwin in Oostburg, he started his undergraduate studies in Molecular Sciences at Wageningen University in 1996. Within the specialization physical chemistry he spent one year in the Laboratory of Organic Chemistry and Laboratory of Physical Chemistry and Colloid Science. Subsequently he moved to the University of Newcastle upon Tyne (UK) for a six-month stay in the group of dr. Ben Horrocks, working on the chemical modification of porous silicon. He graduated from Wageningen University in 2001 (cum laude). In the same year he started as a Ph.D. student at the Laboratory of Organic Chemistry of Wageningen University under supervision of prof. Ernst Sudhölter and dr. Han Zuilhof. The results of this work are described in this thesis.

List of Publications

Faber, E. J.; de Smet , L. C. P. M.; Olthuis, W.; Zuilhof, H.; Sudhölter, E. J. R.; Bergveld, P.; van den Berg, A., Si–C Linked Organic Monolayers on Crystalline Silicon Surfaces as Alternative Gate-Insulators, *ChemPhysChem* **2005**, *6*, 2153-2166.

de Smet , L. C. P. M.; Pukin, A. V.; Sun, Q.-Y.; Eves, B. J.; Lopinski, G. P.; Visser, G. M.; Zuilhof, H.; Sudhölter, E. J. R., Visible-Light Attachment of Si-C Linked Functionalized Organic Monolayers on Silicon Surfaces, *Appl. Surf. Sci.* **2005**, *252*, 24-30.

de Smet, L. C. P. M.; Zuilhof, H.; Sudhölter, E. J. R.; Lie, L. H.; Houlton, A.; Horrocks, B. R., The Mechanism of the Hydrosilylation Reaction of Alkenes at Porous Silicon: Experimental and Computational Deuterium Labeling Studies, *J. Phys. Chem. B* **2005**, *109*, 12020-12030.

Sun, Q.-Y.; de Smet, L. C. P. M.; van Lagen, B.; Giesbers, M.; Thüne, P. C.; van Engelenburg, J.; de Wolf, F. A.; Zuilhof, H.; Sudhölter, E. J. R., Covalently Attached Monolayers on Crystalline Hydrogen-Terminated Silicon: Extremely Mild Attachment by Visible Light, *J. Am. Chem. Soc.* **2005**, *127*, 2514-2523.

de Smet, L. C. P. M.; Pukin, A. V.; Stork, G. A.; de Vos, C. H. R.; Visser, G. M.; Zuilhof, H.; Sudhölter, E. J. R., Syntheses of Alkenylated Carbohydrate Derivatives Toward the Preparation of Monolayers on Silicon Surfaces, *Carbohydr. Res.* **2004**, *339*, 2599-2605.

Arafat, A.; Schroën, K.; de Smet, L. C. P. M.; Sudhölter, E. J. R.; Zuilhof, H., Tailor-Made Functionalization of Silicon Nitride Surfaces, *J. Am. Chem. Soc.* **2004**, *126*, 8600-8601.

Sun, Q.-Y.; de Smet, L. C. P. M.; van Lagen, B.; Wright, A.; Zuilhof, H.; Sudhölter, E. J. R., Covalently Attached Monolayers on Hydrogen-Terminated Si(100): Extremely Mild Attachment by Visible Light, *Angew. Chem. Int. Edit.* **2004**, *43*, 1352-1355.

de Smet, L. C. P. M.; Stork, G. A.; Hurenkamp, G. H. F.; Sun, Q.-Y.; Topal, H.; Vronen, P. J. E.; Sieval, A. B.; Wright, A.; Visser, G. M.; Zuilhof, H.; Sudhölter, E. J. R., Covalently Attached Saccharides on Silicon Surfaces, *J. Am. Chem. Soc.* **2003**, *125*, 13916-13917.

Willemen, H. M.; de Smet, L. C. P. M.; Koudijs, A.; Stuart, M. C. A.; Heikamp-de Jong, G. A.; Marcelis, A. T. M.; Sudhölter, E. J. R., Micellization and Anti-Microbial Activity of New Facial Amphiphiles with Three Permanent Ionic Head Groups, *Angew. Chem. Int. Edit.* **2002,** *41*, 4275-4277.

Kaneti, J.; de Smet, L. C. P. M.; Boom, R.; Zuilhof, H.; Sudhölter, E. J. R., Silver(I)-Olefin Complexes: Computational Probes into the Basis of Silver Ion Chromatography, *J. Phys. Chem. A.* **2002**, *106*, 11197-11204.

de Smet, L. C. P. M.; Zuilhof, H.; Sudhölter, E. J. R.; Wittstock, G.; Duerdin, M. S.; Lie, L. H.; Houlton, A.; Horrocks, B. R., Diffusion in Porous Silicon: Effects on the Reactivity of Alkenes and Electrochemistry of Alkylated Porous Silicon, *Electrochim. Acta* **2002**, *47*, 2653-2663.

Refereed Proceeding

Sudhölter, E. J. R.; de Smet, L. C. P. M.; Zuilhof, H., Field Effect Transistors in Precision Agriculture, Proceedings of the 5th European Conference on Precision Agriculture held in Uppsala, Sweden, 9-12 June 2005. Edited by Stafford, J. V., Wageningen Academic Publishers, 17-24.

Manuscripts in Preparation

Achten, R.; de Smet, L. C. P. M.; Giesbers, M.; Zuilhof, H.; Marcelis, A. T. M.; Sudhölter, E. J. R., Covalent Attachment of Banana-Shaped Liquid Crystals to Silicon Surfaces - manuscript in preparation.

Faber, E. J.; de Smet, L. C. P. M.; Thüne, P. C.; Olthuis, W.; Zuilhof, H.; Sudhölter, E. J .R.; Bergveld, P.; van den Berg, A., Covalently Attached 1-Alkynes on Silicon Surfaces Provide Superior Gate-Insulators - manuscript in preparation.

Faber, E. J.; de Smet, L. C. P. M.; Groeneveld, W.; Sparreboom, W.; Olthuis, W.; Zuilhof, H.; Sudhölter, E. J. R.; Bergveld, P.; van den Berg, A., pH-Sensitivity of Alkyl Monolayers on Silicon - manuscript in preparation.

Patent

Method for producing a hybrid organic Group IVA field effect transistor structure. Sudhölter, E. J. R.; Zuilhof, H.; Sieval, A. B.; de Smet, L. C. P. M.; Visser, G. M.; Bergveld, P.; Olthuis, W.; Faber, E. J. (Wageningen University). Eur. Pat. Appl. (2003), 13 pp. Application: EP 2002-76942 20020517. CAN 139:390301 AN 2003:910239.

Dankwoord

Op deze plaats wil ik graag iedereen bedanken die op één of andere manier heeft bijgedragen aan de uitvoering van mijn promotie-onderzoek, het schrijven van dit proefschrift en de plezierige tijd die ik heb gehad. Een aantal mensen wil ik hier in het bijzonder noemen.

Allereerst bedank ik mijn promotor Ernst Sudhölter en co-promotor Han Zuilhof. Ernst, je creativiteit, optimisme en enthousiasme waren van groot belang voor het totstandkomen van dit proefschrift. Ik ben je zeer dankbaar voor de vrijheid bij de invulling van het project en voor het zorgvuldig lezen en verbeteren van de manuscripten, in het bijzonder Hoofdstuk 6.

Han, met veel oog voor zowel de grote lijnen als details zorgde jij voor de dagelijkse begeleiding. Ik ben je daar zeer dankbaar voor. Ik heb veel geleerd van je opbouwende kritiek en heb ook je creativiteit ten aanzien van ideeën, het zoeken naar mogelijkheden voor het gebruik van nieuwe technieken en het opschrijven van de resultaten zeer gewaardeerd.

A major “thank-you!” deserves Qiao-Yu Sun for his contribution and collaboration. Qiao-Yu, you performed experiments with high accuracy and dedication, which promoted the work on visible light enormously. I would also like to thank Ahmed Arafat for his collaboration and support.

Erik Faber (Twente Universiteit) wil ik bedanken voor de prettige en vruchtbare samenwerking. De werelden van de organische chemie en elektrotechniek werden in dit project bij elkaar gebracht en ik heb hier zeer veel van geleerd. Ook Wouter Olthuis, Albert van den Berg en Piet Bergveld wil ik bedanken voor de plezierige samenwerking.

Gedurende het project heb ik heb veel hulp gekregen van studenten. Geert, ik vond het erg leuk om na een hele reeks practica ook nu weer samen te werken. Bedankt voor je inspanningen. Verder wil ik ook Hüseyin, Jan, Johan en Frans bedanken voor alle bijdragen.

Gerben Visser, André Stork, Patrick Vronen en Aliaksei Pukin wil ik bedanken voor de prettige samenwerking aan het project ‘sweet silicon’ en Ric de Vos (PRI) voor de QTOF metingen aan de suikerderivaten.

I would like to thank Ben Horrocks (University of Newcastle upon Tyne) for his day-to-day supervision during my stay in his laboratory.

Na een NWO-bijeenkomst in Lunteren is er een samenwerking ontstaan met de groep van Leo Jenneskens (Utrecht Universiteit). Ik wil hem, Jan van Geldrop en Luc Scheres bedanken voor de prettige samenwerking en de syntheses van diverse ethyleenglycolen.

Verder wil ik alle collega’s van het Laboratorium voor Organische Chemie bedanken voor de leuke werksfeer en ondersteuning. In het bijzonder, Ronald de Bruin voor de chemicaliën,

Beb van Veldhuizen, Barend van Lagen, Marcel Giesbers en Maarten Posthumus voor alle metingen en Arie Koudijs en Ton Marcelis voor tips met betrekking tot organische syntheses.

During my project many Ph.D. students and postdocs were working at the Laboratory of Organic Chemistry, including Marjon, Hendra, Patrick, Yvonne, Frédérique, Tina, Floor, Audrius, Giedrius, Agnes, Cindy, Remko, Ioan, Ganesan, Suzanne, Gregor, Aliaksei, Annemarie, Kishore, Milena, Michel, Jurjen, Luc, Michael, Maud, Ruud and Rosalie. Thank you for the pleasant time in and around the laboratory and for the social events. Remko, de 'bananen op silicium' zijn bijna rijp voor publicatie; bedankt dat je m'n paranimf wilt zijn.

I would like to thank Hermann Drews (Bruker Optics) for IRRAS measurements, Peter Thüne (Eindhoven University) for XPS measurements and Andrew Wright, Richard White and Cees Heijboer (Thermo Electron) for ARXPS measurements. Brain Eves and Greg Lopinski (NRC) are thanked for the STM measurements that were performed during Qiao-Yu's stay in Ottawa and for their further collaboration.

Alex Sieval (Nano-C/Solenne) wil ik bedanken voor zijn hulp en adviezen. Alex, met de bezoeken, telefoontjes en emails heb je me met name in de beginfase van het project wegwijs gemaakt. De leden van de STW gebruikerscommissie wil ik bedanken voor hun betrokkenheid, interesse en adviezen. Met name Marcel Grote Gansey en Henk van Halen (Sentron) bedank ik voor hun inzet omtrent het ontwerp voor de HOSFET.

Remco Fokkink (Fysische Chemie en Kolloïdkunde) wil ik bedanken voor zijn assistentie bij de ellipsometrie- en reflectrometrie-metingen. Willem Norde bedank ik voor zijn interesse in het project en de verhelderde gesprekken die we daarover hebben gehad.

Ook buiten het werk om heb ik veel steun gekregen. Margreet, Judith, Helena, Koen, Marc, Marijn, Huub, Marieke, Floriska: bedankt voor de gezellige uurtjes aan tafel, voor de buis en in de kroeg. Bij jullie kon ik altijd mijn ei kwijt. Dat geldt ook zeker voor jou, Jurgen. Bedankt voor de vele uurtjes in de sportzaal en de kantine en fijn dat je m'n paranimf wilt zijn.

Papa en mama, ik heb me altijd gesteund gevoeld door jullie vertrouwen in mij. Bedankt voor de keuzevrijheid die ik heb gekregen. Philippe, Nathalie, Jan, Maria, Hanneke, David, Stef en Maartje: bedankt voor jullie interesse en betrokkenheid.

De laatste woorden zijn voor jou, Femke. Bedankt voor je relativeringsvermogen, begrip en steun in de afgelopen jaren, je lach en alle dingen die we samen hebben ondernomen.

This thesis was printed by Ponsen & Looijen BV, Wageningen.

The research described in this thesis was carried out in a joint project of the Laboratory of Organic Chemistry of Wageningen University and the Lab-on-a-Chip group of the University of Twente. It was financially supported by the Netherlands Technology Foundation (STW) as project CW/STW 790.35.704.